

The University of Nottingham

Phenolate and Phenylthiolate Ligand Complexes Containing Zn(II), Ni(II) and Cu(II)

Frances Natalie Cowling, MSci

Thesis submitted to the University of Nottingham

for the degree of Doctor of Philosophy

May 2017

Declaration

Except where specific reference is made to other sources, the work presented in this thesis is the original work of the author. It has not been submitted, in whole or in part, for any other degree.

Signed: Frances Natalie Cowling

Date:

Acknowledgements

I would like to thank my supervisors Prof. Martin Schröder and Dr Jonathan McMaster for giving me the opportunity to work with them at the University of Nottingham, and for all of the support and encouragement they have given me over the last 6 years. Thank you also to the University of Nottingham and the EPSRC for funding my research. I would also like to especially thank Dr George Marshall who supported me unwaveringly during my studies and writing and who has been a great friend to me throughout my time at Nottingham.

I would like to thank Dr E. Stephen Davies for all of his invaluable assistance and insight regarding the electrochemical and EPR studies published in this thesis. I am also extremely grateful to Dr Jeremiah Tidey, Dr William Lewis, Dr Stephen Argent and Prof. Sandy Blake for all of their help with my X-ray crystallographic studies. Thanks also to all the technical staff in the School of Chemistry especially Mark Guyler, Graham Coxhill, Dr Mick Cooper, Ben Pointer-Glead-Hill, Kevin Butler, Clive Dixon and all of the chemical stores and workshop staff. I would also like to acknowledge and thank Dr Gemma Skelton for her valuable contribution as my project student, during her undergraduate studies, to this thesis.

I would like to extend a special thank you Prof. Martyn Poliakoff, Prof. Steve Howdle and Dr Darren Walsh who not only supported me during my undergraduate studies but who also gave me the opportunity to work as a research assistant student during my undergraduate summer holidays. I would also like to especially thank Dr Joe Dawson who supervised me during my final undergraduate year and for his constant support, guidance and friendship throughout my PhD.

I would like to thank all of my friends in the School of Chemistry, especially to those who I worked with in C41 including Emma, Bahar, Joe, Ana, George, Ben, Gemma, Jere, Joe^2, Tom, Carlo, Nick and Maggie for all their support, friendship and for all the great and ‘special’ moments we had together.

Finally, my greatest thanks go to my parents, to my science teacher Mary Lynch, who fostered my passion for chemistry and encouraged me to apply to

study chemistry at university, and my friends, Becky and Nathan, for their unwavering support and love throughout. I would also especially like to thank my sister Jenna and the roller girls, who have always kept me going through my darkest times.

Abstract

Chapter 1

Chapter 1 provides an introduction to metalloenzymes and discusses Ni-containing superoxide dismutase (NiSOD), which features Ni-thiolate ligation at the active site, and Cu containing galactose oxidase, which utilises phenoxyl radicals to perform its catalytic function. Studies concerning low molecular weight analogue complexes of each active site are reviewed and their relevance with respect to enzyme structure and function is discussed. Chapter 1 concludes with a description of the aims of this thesis project.

Chapter 2

Chapter 2 discusses of the preparation of a series of Zn(II), Ni(II) and Cu(II) Schiff-base diphenolate complexes incorporating the four novel pentadentate pro-ligands, [$H_2{}^tBuL_O{}^H$], [$H_2{}^tBuL_O{}^{Cl,}$ [$H_2{}^tBuL_O{}^{tBu}$] and [$H_2{}^tBuL_O{}^{OMe}$]. The different pK_a values of the *para*-substituted aryl amines (H, Cl, ^{t}Bu and OMe) appear to modulate the electrochemical properties and redox behaviour of the Zn(II), Ni(II) and Cu(II) diphenolate complexes. Cyclic voltammetric, spectroelectrochemical and EPR spectroscopic studies reveal the first oxidation processes of [Zn($^tBuL_O{}^{OMe}$)] and [Cu($^tBuL_O{}^{OMe}$)] are associated with ligand-based oxidation processes, yielding kinetically inert species possessing phenoxyl radical character. Conversely, the first oxidation process of [Ni($^tBuL_O{}^{OMe}$)] appears to be metal-based.

Chapter 3

Chapter 3 discusses of the syntheses of Schiff-base diphenolate and dithiolate complexes with a diamine bridge that incorporate pendant heterocyclic groups, with the potential to coordinate in an axial position to a metal centre that possess equatorial N_2O_2 or N_2S_2 coordination environments. We targeted the syntheses and characterisations of these complexes as analogues of the active site of NiSOD. Initial attempts to synthesise a diamine incorporating a pendant imidazole donor followed previously established synthetic approaches. The use of protecting groups to protect the NH group of the imidazole ring was unsuccessful. The syntheses of Ni(II) Schiff-base diphenolate and dithiolate complexes was attempted by using the pro-ligands, [$H_2{}^t$BuL$_O{}^{OH}$] and [$H_2{}^t$BuL$_S{}^{OH}$] and a post complexation step that involved a reaction of the OH pendant of the Schiff-base ligand with an aromatic or heterocyclic functionalised acid chloride. Functionalisations of the [Ni(^{t}BuL$_O{}^{OH}$)] and [Ni(^{t}BuL$_S{}^{OH}$)] to incorporate pendant imidazole (Imid), pyridyl (PyN), furan (Fu) and pyrrole (Pyr) yielded crude products and attempts to purify these products proved unsuccessful. [Ni(^{t}BuL$_O{}^{Ph}$)] could be isolated and X-ray crystallographic studies of [Ni(^{t}BuL$_O{}^{R}$)] (R = OH and Ph) and [Ni(^{t}BuL$_S{}^{OH}$)] demonstrate that each centre adopts an approximate square planar geometry. Electrochemical investigations of [Ni(^{t}BuL$_O{}^{R}$)] (R = OH, Ph) and [Ni(^{t}BuL$_S{}^{OH}$)] showed that each exhibit irreversible redox processes and demonstrate that the OH and phenyl ester functionalities pendant to the ligand backbone do not stabilize the products formed following the oxidation of [Ni(^{t}BuL$_O{}^{R}$)] (R = OH, Ph) and [Ni(^{t}BuL$_S{}^{OH}$)].

Chapter 4

Chapter 4 extends the research described in Chapter 3 through the synthesis of [Zn(^{t}BuL$_{O}^{OH}$)] and [Cu(^{t}BuL$_{O}^{OH}$)] and the attempted functionalisation of the OH group in these complexes to incorporate additional pendant heterocyclic groups including imidazole (Imid), pyridyl (PyN), furan (Fu) and pyrrole (Pyr) together with phenyl (Ph). X-ray crystallographic studies show that [Cu(^{t}BuL$_{O}^{OH}$)] possesses an approximately square planar coordination geometry with the metal centre bound by diimine and diphenolate donors. The frozen solution X-band EPR spectra of [Cu(^{t}BuL$_{O}^{R}$)] (R = Ph, PyN, Fu, Pyr and Imid) are similar to one another and confirm each complex possesses a paramagnetic Cu(II) S = ½ d^{9} metal centre. The similarity between each EPR spectrum as R is varied suggests that the functional group pendant to the ligand backbone does not interact greatly with Cu(II) centre in [Cu(^{t}BuL$_{O}^{R}$)]. [Zn(^{t}BuL$_{O}^{OH}$)] was isolated and mass spectrometric data suggested that [Zn(^{t}BuL$_{O}^{R}$)] (R = Ph, PyN, Fu, Pyr and Imid) had formed, however pure products could not be isolated. Electrochemical studies of [Cu(^{t}BuL$_{O}^{R}$)] (R = OH, Ph, PyN, Fu, Pyr and Imid) reveal two irreversible redox processes. [Cu(^{t}BuL$_{O}^{PyN}$)] possesses first and second redox processes that are *ca.* 0.14 V and 0.23V more positive than their [Cu(^{t}BuL$_{O}^{R}$)] (R = OH, Ph, Fu, Pyr and Imid) counterparts. This suggests that the pyridyl functionalization of the pendant arm in [Cu(^{t}BuL$_{O}^{PyN}$)] may stabilize its oxidation product.

Chapter 5

Chapter 5 provides a conclusion to the thesis and draws together the principal themes of each chapter.

Table of Contents

Chapter 1: Introduction 1

1.1 An Introduction to Metalloenzymes 2

1.2 An Introduction to Bioinorganic Chemistry 4

1.3 Ni-Thiolate Ligation in Metalloenzymes 4

1.4 Redox Non-Innocence of Thiolate Ligands 5

1.5 Nickel Superoxide Dismutases Overview 6

1.6 Structure and Redox Chemistry of NiSOD 7

1.7 Redox Chemistry of NiSOD 8

1.8 Synthetic Models of NiSOD

1.9 Galactose Oxidase (GAO) and Phenoxyl Radicals in Biology 18

1.10 Cu(II) Complexes Inspired by GAO Containing Pro-Phenoxyl Radical Ligands 21

1.11 Schiff-Base Complexes and Synthetic Models of CuGAO 22

1.12 Zn(II) and Ni(II) Complexes Containing Pro-Phenoxyl Radical Ligands 23

1.13 Five coordinate M(II) diphenolate [M = Zn(II), Ni(II), and Cu(II)] Schiff base complexes 24

1.14 Aims and Objectives 27

1 .15 References 29

Chapter 2: Synthesis and Characterisation of Schiff-Base Zn(II), Ni(II) and Cu(II)-Diphenolate Complexes 34

2.1 Introduction 35

2.1.1 Previous Work 36

2.1.2 Aims of Chapter 42

2.1.3 Syntheses of [$H_2{}^t$BuL$_O{}^R$] and [M(^{t}BuL$_O{}^R$)] (M = Zn(II), Ni(II) and Cu(II)) and (R = H, Cl, ^{t}Bu, and OMe) 44

2.2 Results and Discussion 46

2.2.1 Syntheses of *para*-functionalised di-nitriles 46

2.2.2 Syntheses of *para*-functionalised di-amine bridges 48

2.2.3 Syntheses of Schiff-base diphenolate ligands [$H_2{}^t$BuL$_O{}^R$] (R = H, Cl, ^{t}Bu or OMe) 50

2.2.4 Attempted Syntheses of Diphenolate Schiff-base complexes containing [M(^{t}BuL$_{O}^{R}$)] (M = Zn(II), Ni(II), Cu(II) and R = H, Cl, ^{t}Bu or OMe) 51
2.2.5 Single Crystal Structures of [Cu(^{t}BuL$_{O}^{H}$)], [Cu(^{t}BuL$_{O}^{OMe}$)] and [Ni(^{t}BuL$_{O}^{OMe}$)] 52
2.2.5.1 Single Crystal Structures of [Cu(^{t}BuL$_{O}^{H}$)] and [Cu(^{t}BuL$_{O}^{OMe}$)] 52
2.2.5.2 Single Crystal Structure of [Ni(^{t}BuL$_{O}^{OMe}$)] 57
2.2.6 EPR Spectroscopy of [Cu(^{t}BuL$_{O}^{R}$)] (R = H, OMe, ^{t}Bu and Cl) 60
2.2.7 Electrochemical Studies of Crude [Zn(^{t}BuL$_{O}^{R}$)] (R = H and ^{t}Bu), [Zn(^{t}BuL$_{O}^{R}$)] (R = Cl and OMe), [M(^{t}BuL$_{O}^{R}$)] (M = Ni(II) and Cu(II) , R = H, OMe, ^{t}Bu and Cl) 63
2.2.7.1 Cyclic Voltammetry of crude [Zn(^{t}BuL$_{O}^{H}$)] and [M(^{t}BuL$_{O}^{H}$)] (M = Ni(II) and Cu(II)) 63
2.2.7.2 Cyclic Voltammetry of [M(^{t}BuL$_{O}^{Cl}$)] (M = Zn(II), Ni(II) and Cu(II)) 65
2.2.7.3 Electrochemical studies of crude [Zn(^{t}BuL$_{O}^{t\text{Bu}}$)] and [M(^{t}BuL$_{O}^{t\text{Bu}}$)] (M = Ni(II) and Cu(II)) 67
2.2.7.4 Electrochemical studies of [M(^{t}BuL$_{O}^{OMe}$)] (M = Zn(II), Ni(II), Cu(II)) 69
2.2.7.5 Summary of the Cyclic Voltammetric data for [M(^{t}BuL$_{O}^{R}$)] M = Zn(II), Ni(II) and Cu(II)) and (R = H, Cl, ^{t}Bu and OMe) 71
2.2.7.6 Cyclic Voltammetry and Coulometry of [Zn(^{t}BuL$_{O}^{OMe}$)] 73
2.2.7.7 Cyclic Voltammetry and Coulometry of [Ni(^{t}BuL$_{O}^{OMe}$)] 77
2.2.7.8 Cyclic Voltammetry and Coulometry of [Cu(^{t}BuL$_{O}^{OMe}$)] 81
2.2.8 UV/Vis Spectroelectrochemistry of [M(^{t}BuL$_{O}^{OMe}$)] (M = Zn, Ni, Cu) 87
2.2.8.1 UV/Vis Spectroelectrochemistry of [Zn(^{t}BuL$_{O}^{OMe}$)] 87
2.2.8.2 UV/Vis Spectroelectrochemistry of [Ni(^{t}BuL$_{O}^{OMe}$)] 89
2.2.8.3 UV/Vis Spectroelectrochemistry of [Cu(^{t}BuL$_{O}^{OMe}$)] 91
2.2.8.4 Summary and assignment of the UV/vis spectroscopic studies of [M(^{t}BuL$_{O}^{OMe}$)]$^{+/0}$ (M = Zn, Ni, Cu) 94
2.2.9 EPR Spectroscopy of [M(^{t}BuL$_{O}^{OMe}$)] (M = Zn, Ni, Cu) 97
2.2.9.1 EPR Spectroscopy of [Zn(^{t}BuL$_{O}^{OMe}$)] 97
2.2.9.2 EPR Spectroscopy of [Ni(^{t}BuL$_{O}^{OMe}$)] 98

2.2.9.3 EPR Spectroscopy of [Cu(^{t}BuL$_{O}^{OMe}$)] 100
2.3 Conclusions 101
2.4 Experimental 104
2.4.1 Synthesis of 3,3'-(phenylazanediyl)dipropanenitrile (R= H) 104
3,3'-(phenylazanediyl)dipropanenitrile 105
2.4.2 3,3'-(4-methoxyphenylazanediyl)dipropanenitrile (R= OMe) 105
2.4.3 3,3'-(4-*tert*-butylphenylazanediyl)dipropanenitrile (R= ^{t}Bu) 105
2.4.4 3,3'-(4-chlorophenylazanediyl)dipropanenitrile (R= Cl) 106
2.4.5 Synthesis of N1-(3-aminopropyl)-N1-phenylpropane-1,3-diamine (R = H) 107
N1-(3-aminopropyl)-N1-phenylpropane-1,3-diamine (R = H) 108
2.4.6 N1-(3-aminopropyl)-N1-(4-methoxyphenyl)propane-1,3-diamine (R = OMe) 108
2.4.7 N1-(3-aminopropyl)-N1-(4-tert-butylphenyl)propane-1,3-diamine (R = ^{t}Bu) 108
2.4.8 N1-(3-aminopropyl)-N1-(4-chlorophenyl)propane-1,3-diamine (R = Cl) 119
2.4.9 Synthesis of the Schiff-base Pro-ligands [H^{t}BuL$_{O}^{R}$] (R = H, OMe, ^{t}Bu, Cl, and Br) 110
2.4.10 [H^{t}BuL$_{O}^{OMe}$] 111
2.4.11 [H^{t}BuL$_{O}^{tBu}$] 111
2.4.12 [H^{t}BuL$_{O}^{Cl}$] 111
2.4.13 Synthesis of the Schiff-base Zn(II), Ni(II) and Cu(II) Diphenolate Complexes [M(^{t}BuL$_{O}^{R}$)] (R = H, OMe, ^{t}Bu, Cl, and Br) 113
Attempted synthesis of [Zn(^{t}BuL$_{O}^{H}$)] 113
2.4.14 [Zn(^{t}BuL$_{O}^{OMe}$)] 114
2.4.15 Attempted synthesis of [Zn(^{t}BuL$_{O}^{tBu}$)] 114
2.4.16 [Zn(^{t}BuL$_{O}^{Cl}$)] 114
2.4.17 [Ni(^{t}BuL$_{O}^{H}$)] 115
2.4.18 [Ni(^{t}BuL$_{O}^{OMe}$)] 115
2.4.19 [Ni(^{t}BuL$_{O}^{tBu}$)] 116
2.4.20 [Ni(^{t}BuL$_{O}^{Cl}$)] 116
2.4.21 [Cu(^{t}BuL$_{O}^{H}$)] 116
2.4.22 [Cu(^{t}BuL$_{O}^{OMe}$] 117

2.4.23 [Cu(^{t}BuL$_{O}^{tBu}$)] 117
2.4.24 [Cu(^{t}BuL$_{O}^{Cl}$)] 117
2.5 References 118
Chapter 3: Synthesis and Characterisation of Schiff-Base Ni(II)-Dithiolate and Diphenolate Complexes 122
3.1.1 Introduction 123
3.1.2 Previous Work 125
3.1.3 Aims of Chapter 131
3.2 Results and Discussion 131
3.2.1 Attempted incorporation of a pendant imidazole functionality into the propane backbone 131
3.2.2 Attempted Synthesis of 2-((5-methyl-1H-imidazol-4-yl)methyl)propane-1,3-diamine (*via* diethyl malonate) 133
3.2.3 Methyl protection: The attempted synthesis of 2-((1-methyl-1H-imidazol-2-yl)methyl)propane-1,3-diamine (*via* diethyl malonate) 136
3.2.4 Trityl Protection: Attempted synthesis of 2-((4-methyl-1-trityl-1H-imidazol-5-yl)methyl)propane-1,3-diamine (*via* diethyl malonate) 138
3.2.5 Attempted synthesis of 2-((4-methyl-1H-imidazol-5-yl)methyl)propane-1,3-diamine (*via* malonitrile) 140
3.2.6 Methyl Protection: Attempted synthesis of 2-((1-methyl-1H-imidazol-2-yl)methyl)propane-1,3-diamine 141
3.2.7 Trityl Protection: Attempted synthesis of 2-((4-methyl-1-trityl-1H-imidazol-5-yl)methyl)propane-1,3-diamine (*via* malonitrile) 142
3.2.8 Proposed syntheses of [H$_2$^{t}BuL$_{O}^{OH}$], [H$_2$^{t}BuL$_{S}^{OH}$], [Ni(^{t}BuL$_{O}^{R}$)] and [Ni(^{t}BuL$_{S}^{R}$)] (R = OH, Ph, PyN, Fu, Pyr and Imid) 144
3.2.9 Syntheses of [H$_2$^{t}BuL$_{O}^{OH}$] and [Ni(^{t}BuL$_{O}^{OH}$)], and the attempted syntheses of [Ni(^{t}BuL$_{O}^{R}$)] (R = Ph, PyN, Fu, Pyr and Imid) 147
3.2.10 Single Crystal Structures of [Ni(^{t}BuL$_{O}^{OH}$)] and [Ni(^{t}BuL$_{O}^{Ph}$)] 149
3.2.11 Electrochemical Studies of [Ni(^{t}BuL$_{O}^{OH}$)] and [Ni(^{t}BuL$_{O}^{Ph}$)] 152
3.3 Synthesis of Dithiolate Ni(II) Complexes 155
3.3.1 Synthesis of 2,4-di-*tert*-butylthiosalicylaldehyde 155
3.3.2 Syntheses of [H$_2$^{t}BuL$_{S}^{OH}$] and [Ni(^{t}BuL$_{S}^{OH}$)], and the attempted syntheses of [Ni(^{t}BuL$_{S}^{R}$)] (R = Ph, PyN, Fu, Pyr and Imid) 157
3.3.3 Single Crystal Structure of [Ni(^{t}BuL$_{S}^{OH}$)] 159

3.3.4 Electrochemical Studies of [Ni(^{t}BuL$_{S}^{OH}$)] 161
3.4 Conclusions 162
3.5 Experimental 164
3.5.1 Synthesis of 5-(chloromethyl)-4-methyl-1H-imidazole 164
3.5.2 Synthesis of diethyl 2-((4-methyl-1H-imidazol-5-yl)methyl)malonate 165
3.5.3 Synthesis of 2-((4-methyl-1H-imidazol-5-yl)methyl)malonamide 166
3.5.4 Attempted synthesis of 2-((4-methyl-1H-imidazol-5-yl)methyl)propane-1,3-diamine *via* reduction with B_2H_6.THF 167
3.5.5 Attempted synthesis of 2-((4-methyl-1H-imidazol-5-yl)methyl)propane-1,3-diamine *via* reduction with $LiAlH_4$ 168
3.5.6 Synthesis of 2-(chloromethyl)-1-methyl-1H-imidazole 169
3.5.7 Attempted synthesis of diethyl 2-((1-methyl-1H-imidazol-5-yl)methyl)malonate 170
3.5.8 Synthesis of diethyl 2-((4-methyl-1-trityl-1H-imidazol-5-yl)methyl)malonate 171
3.5.9 Attempted synthesis of 2-((4-methyl-1-trityl-1H-imidazol-5-yl)methyl)malonamide 172
3.5.10 Attempted synthesis of 2-((5-methyl-1H-imidazol-4-yl)methyl)malononitrile 173
3.5.11 Synthesis of 2-((1-methyl-1H-imidazol-4-yl)methyl)malononitrile 174
3.5.12 Attempted synthesis of 2-((1-methyl-1H-imidazol-4-yl)methyl)propane-1,3-diamine 175
3.5.13 Synthesis of (4-methyl-1-trityl-1H-imidazol-5-yl)methanol 176
3.5.14 Synthesis of 4-(chloromethyl)-5-methyl-1-trityl-1H-imidazole (trtityl protection) 177
3.5.15 Synthesis of 2-((5-methyl-1-trityl-1H-imidazol-4-yl)methyl)malononitrile 178
3.5.16 Attempted synthesis of 2-((5-methyl-1-trityl-1H-imidazol-4-yl)methyl)propane-1,3-diamine 179
3.5.17 Synthesis of [H$_2$^{t}BuL$_{O}^{OH}$] 180
3.5.18 Synthesis of [Ni(^{t}BuL$_{O}^{OH}$)] 181
3.5.19 Attempted Syntheses of [Ni(^{t}BuL$_{O}^{R}$)] (R = Ph, PyN, Fu, Pyr and Imid) 182

3.5.20 [Ni(^{t}BuL$_{O}^{Ph}$)] 183
3.5.21 [Ni(^{t}BuL$_{O}^{PyN}$)] 183
3.5.22 [Ni(^{t}BuL$_{O}^{Fu}$)] 183
3.5.23 [Ni(^{t}BuL$_{O}^{Pyr}$)] 183
3.5.24 [Ni(^{t}BuL$_{O}^{Imid}$)] 183
3.5.25 Synthesis of 1, 3, 5-tri-*tert*-butylbenzene 184
3.5.26 Synthesis of 1-bromo-3, 5-di-*tert*-butylbenzene 185
3.5.27 Synthesis of 1,3-di-*tert*-butylbenzene 186
3.5.28 Synthesis of 1-bromo-2,4-di-*tert*-butylbenzene 187
3.5.29 Synthesis of 2,4-di-*tert*-butylbenzenethiol 188
3.5.30 Synthesis of 2,4-di-*tert*-butylthiosalicylaldehyde 189
3.5.31 Synthesis of [H$_2$^{t}BuL$_{S}^{OH}$] 191
3.5.32 Synthesis of [Ni(^{t}BuL$_{S}^{OH}$)] 192
3.5.33 Attempted syntheses of [Ni(^{t}BuL$_{S}^{R}$)] (R = Ph, PyN, Fu, Pyr and Imid) 193
3.5.34 [Ni(^{t}BuL$_{S}^{Ph}$)] 193
3.5.35 [Ni(^{t}BuL$_{S}^{PyN}$)] 194
3.5.36 [Ni(^{t}BuL$_{S}^{Fu}$)] 194
3.5.37 [Ni(^{t}BuL$_{S}^{Pyr}$)] 194
3.5.38 [Ni(^{t}BuL$_{S}^{Imid}$)] 194
3.6 References 195
Chapter 4: Synthesis and Characterisation of Schiff-Base Zn(II) and Cu(II)-Diphenolate Complexes 199
4.1 Introduction 200
4.1.2 Previous Work 201
4.1.3 Aims 204
4.2 Results and Discussion 206
4.2.1 Proposed syntheses of [H$_2$^{t}BuL$_{O}^{OH}$] and [M(^{t}BuL$_{O}^{R}$)] (M = Cu(II) and Zn(II) and R = Ph, PyN, Fu, Pyr and Imid) 206
4.2.2 X-ray Crystallography of [Cu(^{t}BuL$_{S}^{OH}$)] 208
4.2.3 EPR of [Cu(^{t}BuL$_{O}^{R}$)] (R = OH, Ph, PyN, Fu, Pyr and Imid) 211
4.2.4 Electrochemical Studies of [Zn(^{t}BuL$_{O}^{OH}$)], [Cu(^{t}BuL$_{O}^{OH}$)], and [Cu(^{t}BuL$_{O}^{R}$)] and R = OH, Ph, PyN, Fu, Pyr and Imid) 216
4.2.5 Cyclic Voltammetry of [Zn(^{t}BuL$_{O}^{OH}$)] 216

4.2.6 Cyclic Voltametry of [Cu(^{t}BuL$_{O}^{R}$)] (R = OH, Ph, PyN, Fu, Pyr and Imid) 218
4.3 Conclusions 222
4.4 Experimental 224
4.4.1 Synthesis of [Zn(^{t}BuL$_{O}^{OH}$)] 224
4.4.2 Attempted syntheses of [Zn(^{t}BuL$_{O}^{R}$)] (R = Ph, PyN, Fu, Pyr and Imid) 225
4.4.3 [Zn(^{t}BuL$_{O}^{Ph}$)] 225
4.4.4 [Zn(^{t}BuL$_{O}^{PyN}$)] 226
4.4.5 [Zn(^{t}BuL$_{O}^{Fu}$)] 226
4.4.6 [Zn(^{t}BuL$_{O}^{Pyr}$)] 226
4.4.7 [Zn(^{t}BuL$_{O}^{Imid}$)] 226
4.4.8 Synthesis of [Cu(^{t}BuL$_{O}^{OH}$)] 227
4.4.9 Syntheses of [Cu(^{t}BuL$_{O}^{R}$)] (R = Ph, PyN, Fu, Pyr and Imid) 228
4.4.10[Cu(^{t}BuL$_{O}^{Ph}$)] 228
4.4.11 [Cu(^{t}BuL$_{O}^{PyN}$)] 229
4.4.12 [Cu(^{t}BuL$_{O}^{Fu}$)] 229
4.4.13 [Cu(^{t}BuL$_{O}^{Pyr}$)] 229
4.4.14 [Cu(^{t}BuL$_{O}^{Imid}$)] 229
4.5 References 230
Chapter 5: Conclusions and Future Work **231**
Appendices **241**
Appendix 1: Reagents, Experimental Techniques and Physical Measurements 240
Appendix 2: Single Crystal X-ray Crystallographic Data 244
Appendix 3: Attempted synthesis of the Schiff-base diphenolate ligand [H$_2$^{t}BuL$_{O}^{Br}$] and [M(^{t}BuL$_{O}^{Br}$)] (M = Zn, Ni, Cu) 250
A3.1 Attempted synthesis of 3,3'-((4-bromophenyl)azanediyl)-dipropanenitrile 250
A3.2 Attempted synthesis of N1-(3-aminopropyl)-N1-(4-bromophenyl)propane-1,3-diamine 252
A3.3 Attempted synthesis [H$_2$^{t}BuL$_{O}^{Br}$] and [M(^{t}BuL$_{O}^{Br}$)] (M = Zn, Ni, Cu) 254
A3.4 X-ray Crystallography of [M(^{t}BuL$_{O}^{Br1}$)$_2$] (M = Zn, Ni, Cu) 255

A3.5 Experimental 260
A3.5.1 Attempted synthesis of 3,3'-((4-bromophenyl)azanediyl)-dipropanenitrile 260
A3.5.2 Attempted synthesis of N1-(3-aminopropyl)-N1-(4-bromophenyl)propane-1,3-diamine 260
A3.5.3 Attempted synthesis [$H_2{}^tBuL_O{}^{Br}$] and [M($^tBuL_O{}^{Br}$)] (M = Zn, Ni, Cu) 261
A3.5.4 Attempted synthesis [Zn($^tBuL_O{}^{Br}$)] 261
A3.5.5 Attempted synthesis of [Ni($^tBuL_O{}^{Br}$)] 262
A3.5.6 Attempted synthesis of [Cu($^tBuL_O{}^{Br}$)] 262
A3.6 References 262

Abbreviations

Å	Angstroms (1 Å = 0.1 nm)
A	EPR coupling constant
atm	atmospheres
br	broad
^{t}Bu	*t*-butyl
Cys	cysteine
°	degrees
δ	chemical shift
DFT	density functional theory
dd	doublet of doublets
DMF	*N*,*N*-dimethylformamide
DMSO	dimethylsulfoxide
ε	extinction coefficient
E	redox potential
EC	irreversible electrochemical mechanism
$E_{1/2}$	half-wave potential
E_p^a	peak anodic potential
E_p^c	peak cathodic potential
ENDOR	electron-nuclear double resonance
EPR	electron paramagnetic resonance spectroscopy
ES	electrospray
e.s.d.(s)	estimated standard deviation
Et	ethyl
Fc^+/Fc	ferrocenium/ferrocene
G	Gauss
g_{iso}	isotropic *g*-value
HOMO	highest energy occupied molecular orbital
Hz	Hertz
I	intensity, nuclear spin quantum number or current
K	Kelvin
λ	wavelength
L	ligand
LMCT	ligand to metal charge transfer
LUMO	lowest energy unoccupied molecular orbital

m	multiplet (NMR) or medium (IR)
M	molecular ion or molar
Me	methyl
mg	milligram
MHz	megahertz
MLCT	metal to ligand charge transfer
MS	mass spectrometry
m/z	mass/charge
v	wave number or scan rate
NMR	nuclear magnetic resonance
Ph	phenyl
py	pyridine
q	quartet
R	alkyl group
S	singlet (NMR), strong (IR) or second
S	spin quantum number
SCE	saturated calomel electrode
SOMO	singly occupied molecular orbital
θ	angle of diffraction
t	triplet
T	absolute temperature
tert	tertiary
THF	tetrahydrofuran
TLC	thin layer chromatography
TMEDA	tetramethylethylenediamine
UV/vis	ultraviolet-visible
V	volume or volts
1Z	number of empirical formula in unit cell

Chapter 1: Introduction

1.1 An Introduction to Metalloenzymes

Enzymes are proteins that catalyse biochemical transformations within living organisms, at rates which approach 'catalytic perfection'.[1] This 'catalytic perfection' is facilitated by enzymes lowering the Gibbs free energy of activation ($\Delta G^{\ddagger}$) required to bring about the conversion of a substrate to a product, thus dramatically increasing the rate of a biological reaction (Figure 1.1).[2,3] Enzymes are specifically designed to bind to a single substrate. This substrate is complementary to the geometric and functional features of the enzyme 'active site'.[4] Once the substrate has bound to the enzyme active site it is held in place by the geometric and electronic constraints of the active site, which activates the substrate towards chemical change.[4] After the chemical transformation of the substrate, the product molecule(s) are released leaving the enzyme unchanged by the process and poised for further catalytic cycles. Selective substrate binding and activation are heavily reliant upon the ability of the enzyme to maintain its three dimensional protein structure in order to maintain the geometric and functional features of its active site. As a result of this, enzymes are particularly sensitive to changes in pH and temperature which can lead to change in the protein structure and consequently the properties of the enzyme active site.[5] These changes to the protein tertiary structure and the 'active site' are termed 'denaturation' and are often permanent.[6] The catalytic capability of an enzyme is quantified as the number of molecules of substrate that are converted into product per enzyme molecule per unit of time and is termed the turnover rate.[7]

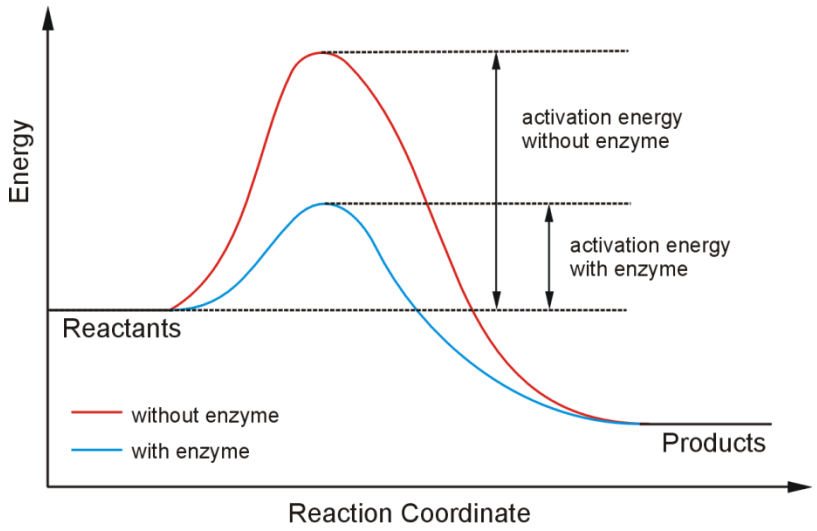


Figure 1.1 Schematic representation of the free energy profile of a hypothetical enzyme catalysed reaction.

Recent advances in spectroscopic techniques and protein crystallography have demonstrated the important role that trace elements such as Fe, Cu and Zn and the ultra-trace elements V, Cr, Mo, Mn, Co and Ni in biology.[2,4,8,9] Metal ion cofactors found within the active sites of metalloenzymes perform structural and/or functional roles whereby geometric and electronic constraints imposed by the supporting ligand field enables the transition metal ions to access a variety of oxidation states thus providing the redox drive essential to the completion of many enzymatic processes. Additionally, the ability of transition metal ions to adopt a variety of coordination geometries through the expansion or contraction of their coordination spheres aids the binding/release of substrate/product molecules essential to catalysis.[5,10–12]

1.2 An Introduction to Bioinorganic Chemistry

Bioinorganic chemistry focuses upon exploring the role of inorganic molecules in biological systems. The study of metalloenzymes and novel metal complexes as catalysts offers us invaluable insight into the uptake, role and fate of metal ions in biological systems. This insight can be used in the development of metal-based complexes which have medicinal applications (*e.g. cis*-platin)[13] and novel bio-inspired catalysts for use in industry[5,8,14] in addition to the crystallographic and spectroscopic investigation of metalloenzymes.

A large amount of information regarding the structure and function of an enzyme active site can be gathered *via* a combination of crystallographic, spectroscopic and theoretical studies. Nevertheless, in addition to this it is often necessary to supplement this information with evidence obtained from studies upon synthetic low molecular weight model complexes that replicate key structural or spectroscopic characteristics of the active site.[10,15] The work presented in this thesis will focus upon the study of two enzymes: nickel superoxide dismutase (NiSOD) and copper galactose oxidase (CuGAO) *via* the synthesis and electrochemical, spectroscopic and crystallographic study of transition metal complexes as analogues of the active sites of these metalloenzymes.

1.3 Ni-Thiolate Ligation in Metalloenzymes

There are many examples of enzymes where Ni is the metal cofactor within the active site including but not limited to: methyl coenzyme M reductase,[16] carbon monoxide dehydrogenase,[17,18] acetyl coenzyme A synthase, [NiFe] hydrogenase[19,20] and Ni-containing superoxide dismutase (NiSOD).[21–23]

Despite Ni being relatively redox inactive it has been suggested that the thiolate ligation contributes to the lowering of the redox potential of the metal unit in these systems and thus enables their unique catalytic capabilities.[23,24] As a consequence of this a huge emphasis has been placed upon the exploration of the redox properties of the Ni-thiolate ligation in these enzymes through analogous synthetic Ni complexes which incorporate thiolate ligands.

1.4 Redox Non-Innocence of Thiolate Ligands

The covalency associated with Ni-SR bonds means that the redox processes occurring simultaneously have an effect on both the Ni centre and the S-ligands, which consequently brings uncertainty in assigning the formal oxidation state of the metal centre.[25] As a consequence of this redox processes which occur at Ni-S(thiolate) centres are defined as hybrids between the thiolate and thiyl-radical resonance extremes (Figure 1.2).[26] A significant contribution from the thiyl-radical leads to a HOMO that possess a significant amount of ligand character and so the redox process cannot solely be assumed to take place at the Ni centre. The metal ligand character of a singly occupied molecular orbital (SOMO) can be assessed by EPR spectroscopy for paramagnetic systems.[27]

$$[M^{(n+1)+}\text{--------}SR]^{n+} \longleftrightarrow [M^{n+}\text{------}\cdot SR]^{n+}$$

Figure 1.2 Representation of the thiolate (left) and thiyl-radical (right) resonance extremes.

The ability of metals and their ligand frameworks to delicately balance redox contributions has been identified as a way to stabilise the organic radical present within these enzymes and has been proven to be vital for biological

catalysis to take place. Free radicals are commonplace at the active sites of many metalloenzymes and the unusual reactivity displayed by these metalloenzymes has often been attributed to the ability of the radical to delocalise across the ligand framework.[28–30] An example of particular relevance to this study is the generation of thiyl radical character within metalloenzymes containing Ni-thiolate ligation.[18–20,23,31] However, for the purpose of this thesis we will focus upon the metalloenzyme, Ni-containing superoxide dismutase (NiSOD), which contains two Ni-S(thiolate) ligands. A brief overview of the NiSOD enzyme will be provided in the following pages.

1.5 Nickel Superoxide Dismutases Overview

Superoxide dismutases (SODs) are metalloenzymes that catalyse the breakdown of the superoxide radical anion ($O_2^{\bullet-}$) in nature.[32,33] This by-product of aerobic metabolism is toxic and can cause significant damage to biological systems if it is not removed. Numerous medical disorders ranging in severity from inflammatory to neurodegenerative diseases have been attributed to the presence of superoxide.[34–36] SODs utilise their one-electron redox-active metal centres to catalyse the dismutation of $O_2^{\bullet-}$, forming hydrogen peroxide and molecular oxygen and ridding the living organism of this toxic by-product (Equation 1.1 - 1.2).[37,38]

Initial research only identified two independent classes of SODs and these were categorised according to the metal content of the active site. This contained either a mononuclear Mn or Fe cofactor at the active site or a binuclear Cu/Zn core.[39,40] However, recently a Ni based SOD metalloenyme has been identified in several *Streptomyces* species and cyanobacteria. The active site of this SOD

enzyme contains a mononuclear nickel centre and was named NiSOD, accordingly.[23,30,40–44]

Equation 1.1 $Ni^{2+} O_2^{\bullet-} + 2H^+ \rightarrow Ni^{3+} + H_2O_2$

Equation 1.2 $Ni^{3+} + O_2^{\bullet-} \rightarrow Ni^{2+} + O_2$

1.6 Structure and Redox Chemistry of NiSOD

Single crystal X-ray diffraction studies of the active site of NiSOD in the oxidised[43] and reduced[45] for were isolated from *Streptomyces seoulensis* were reported in 2004. The homohexameric protein consists of four-helix-bundle subunits with the catalytic centre situated within a nine-residue Ni-hook motif at the N-terminus of the protein. The Ni(II) centre is coordinated by two thiolate ligands derived from Cys2 and Cys6 in a *cis*-arrangement, the deprotonated amide of the Cys2 backbone, and the N-terminal amine group of His1 in a square planar N_2S_2 coordination sphere (Figure 1.3). In the reduced state, the active site contains a monomeric low-spin Ni centre (S = 0).[46]

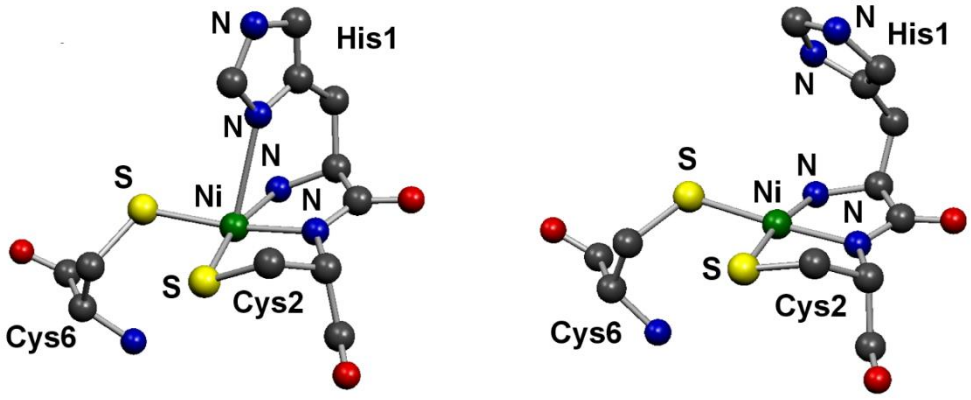


Figure 1.3 Structures of the oxidised (left) and reduced forms (right) of the active site of NiSOD.

Upon oxidation, the metal centre increases its coordination number

through the binding of the axially positioned imidazole group of the His1 residue, to generate a square pyramidal geometry around the Ni(III) centre (Figure 1.3). Barondeau *et al.* proposed that the chemistry performed by the active site of NiSOD proceeds *via* an inner sphere, two-step, 'ping-pong' mechanism involving the Ni centre cycling between the formal Ni(II) and Ni(III) oxidation states (Figure 1.4).[42]

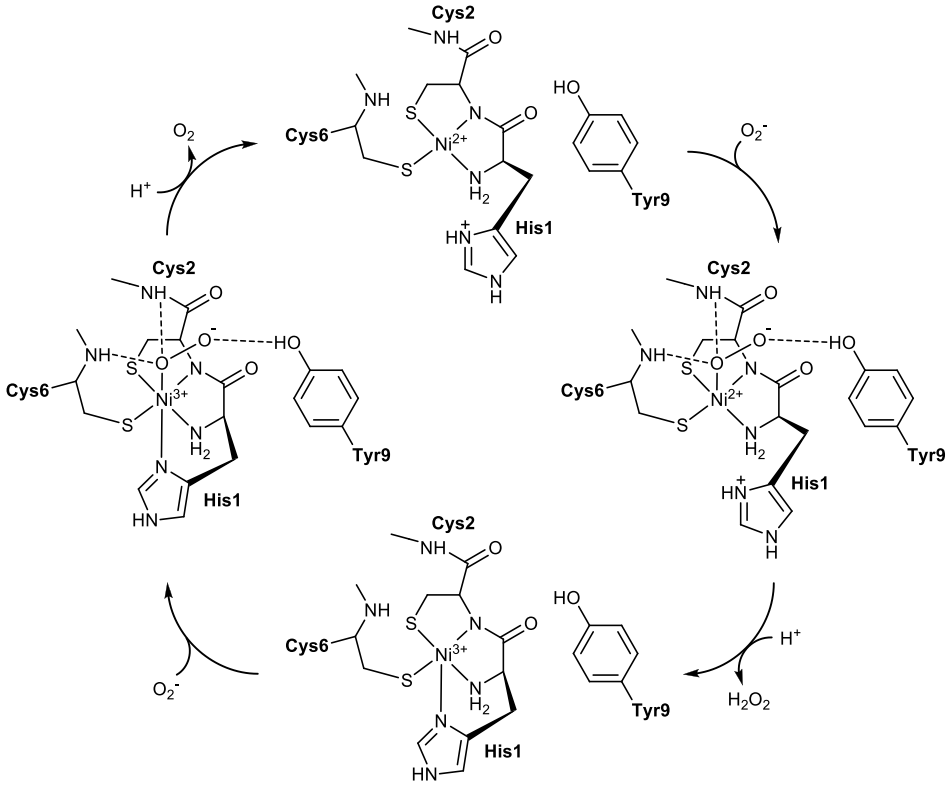


Figure 1.4 Catalytic mechanism of NiSOD proposed by Barondeau *et al.*[42]

1.7 Redox Chemistry of NiSOD

While the occurrence of cysteine-thiolate ligation is commonplace within Ni containing metalloenzymes, its presence within an active site that functions to remove a species that could easily lead to the decomposition of the Ni-thiolate ligation itself, is considered unsual.[47,48] However, detailed spectroscopic studies, supported by theoretical calculations, have revealed that the key bonding

interactions within the Ni-thiolate ligation are essential to the Ni centre for optimal catalytic activity whilst simultaneously actively preventing oxidative decomposition of the thiolate-ligation by its own substrate.[43,46,49,50]

During the catalytic cycle the Ni centre undergoes a change in its coordination sphere with the axial coordination of His1 in the oxidised form of the enzyme which plays a critical role in the enzyme's catalytic mechanism but also prevents decomposition of the enzyme's active site. In the reduced state of NiSOD, the two highest molecular orbitals (HOMOs) reveal strongly covalent π-antibonding interactions between the Ni(π) and π-donor orbitals of the equatorial ligand set, with approximately 30 % metal character and 60 % ligand character. These filled-filled interactions serve to destabilise the Ni(π) orbitals thereby facilitating electron transfer from the Ni(II) centre to the substrate.[46] Prior to the internal rearrangement of the primary coordination sphere, the redox active molecular orbital shifts in favour of a substantially more metal-based SOMO (58 % Ni(xy), 24 % S_6(π) and 10 % N/O(π)).[46] Axial coordination of the imidazole residue from His1 to the Ni(III) centre further stabilises the Ni(III) oxidation state by destabilising the Ni($3d_{z^2}$) orbital consequently forcing the unpaired electron into a SOMO with Ni $3d_{z^2}$ (76 %) character and reduced S (9 %) contributions, thus preventing decomposition *via* oxidation of the Ni-thiolate coordination. Thus, similar to the role assumed by the equatorial ligand set in adjusting the reactivity of the reduced state, the axial imidazole ligand functions to tune the redox properties of the oxidised state towards protecting the potentially vulnerable thiolate donors from oxidative stress, by enforcing the redox active orbital to be predominantly metal-based.[46,51]

1.8 Synthetic Models of NiSOD

Holm *et al.* prepared and studied the amidate-thiolate bound Ni(III/II) complexes $[Ni(ema)]^{2-}$ (ema = *N*,*N*'-ethylenebis(2-(acetylthio)acetamide) and $[Ni(phma)]^{2-}$ (phma = *N*,*N*'-1,2-phenylenebis(2-(acetylthio)acetamide) (Figure 1.5).[52–54] The electrochemical studies showed that these complexes possessed a reversible single electron processes at $E_{1/2}$ = -0.24 and -0.34 V *vs* SCE, respectively. EPR spectroscopic studies upon the electrochemically oxidised solutions demonstrated that the oxidation process involved the formation of a Ni(III) species. On cooling to 243 K the oxidation processes became irreversible and generated EPR silent species. It has been suggested that cooling of the Ni(III) species encouraged the dimerisation of the oxidised products via the formation of a $Ni(\mu\text{-}SR)_2Ni$ bridge, however no crystallographic evidence was provided to support this proposal.

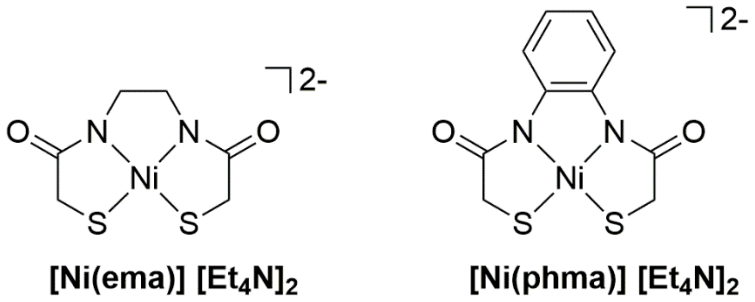
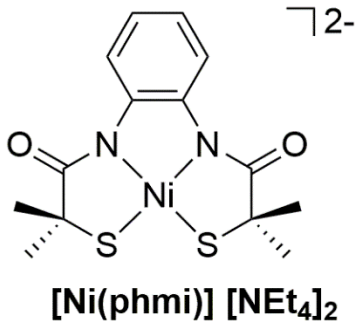


Figure 1.5 Amidate-thiolate Ni(II) complexes, $[Ni(ema)]^{2-}$ (left) and $[Ni(phma)]^{2-}$ (right), reported by Holm *et al*.[52]

Hanss and Krüger incorporated *gem*-dimethyl groups into a $[Ni(phma)]^{2-}$ ligation system, forming $[Ni(phmi)]^{2-}$ (phmi = *N,N'*-1,2-phenylenebis(2-sulfanyl-2-methyl)propionamide) (Figure 1.6).[54] Electrochemical analysis showed that $[Ni(phmi)]^{2-}$ supported a reversible metal-based single electron oxidation process at $E_{1/2}$ = -0.71 V *vs* Fc^+/Fc in MeCN at 293 K. The relative

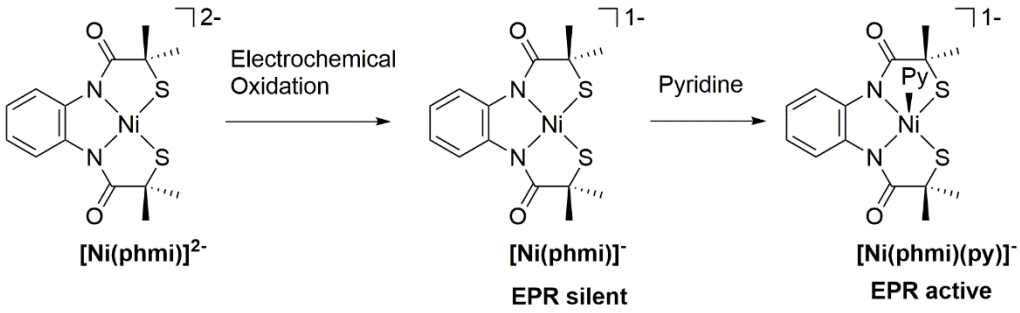
stability of the oxidised species in solution compared to $[Ni(phma)]^{2-}$ enabled crystals suitable for X-ray crystallography to be isolated.



[Ni(phmi)] $[NEt_4]_2$

Figure 1.6 Amidate-thiolate Ni(II) complex $[Ni(phmi)]^{2-}$ reported by Hanss and Krüger.[54]

The addition of excess pyridine to a solution of $[Ni(phmi)]^{-}$ generated a new species that was characterised by EPR spectroscopy. These studies revealed a nearly axial EPR signal (g_{11} = 2.313, g_{22} = 2.281 and g_{33} = 2.000) at 100 K. The splitting of the g_{33} component into three lines of equal intensity due to the superhyperfine coupling (A_{33} = 25 G) of a single N-donor atom (I_N = 1) is consistent with the binding of a single pyridine molecule to the Ni(III) centre, forming the monoadduct $[Ni(phmi)(py)]^{-}$ (Scheme 1.1).[54] Although originally these systems were intended for study as analogues of the active site of [NiFe] hydrogenase, the ability of the $[Ni^{II}N_2S_2]^{2-}$ core of $[Ni(phmi)]^{2-}$ to expand its coordination number upon oxidation through the binding of an additional N-donor has a greater resemblance to the active site of NiSOD, which performs a similar structural change and exhibits a comparable spectroscopic signal upon oxidation.[46,55,56]



Scheme 1.1 Products of the oxidation of $[Ni(phmi)]^{2-}$.[54]

Shearer and co-workers were the first to prepare the only small molecule NiN_2S_2 complex that incorporates mixed amine/amide coordination to the Ni centre and thus represents the closest structural analogue to the active site of NiSOD to date.[36] Electrochemical studies showed that $[Ni^{II}(BEAAM)]$ $[NMe_4]$ possesses a quasi-reversible Ni(III/II) redox couple at 0.12 V *vs* Ag/AgCl, which from an electrochemical perspective fits well between the irreversible oxidation process observed at 0.41 V *vs* Ag/AgCl for the bis-amine analogue ($[Ni^{II}$(bmmp-dmed)]) and the reversible oxidation process exhibited at -0.34 V *vs* Ag/AgCl by the bis-amide analogue ($[Ni^{II}(emi)]$ $[NEt_4]$) (Figure 1.7).[52] Even though the redox potential of $[Ni^{II}(BEAAM)][NMe_4]$ is perfect for SOD activity, ($E_{ox}^{O_2^{\bullet-}}$ = 0.04 V; $E_{red}^{O_2^{\bullet-}}$ = 1.09 V *vs* Ag/Ag^+) the complex was not functional.[57] The inability to dismutate superoxide was suggested to result from either the instability of the Ni(III) adduct, the possible oxidative strain placed upon the thiolate S-donors or the absence of axial ligation to the Ni centre, which may be paramount to SOD catalysis.[36]

Theoretical calculations on models of $[Ni^{II}$(bmmp-dmed)], $[Ni^{II}(emi)]$ $[NEt_4]$ and $[Ni^{II}(BEAAM)]$ $[NMe_4]$ were also used to rationalise the employment of a mixed amine/amide N-donor ligand set at the active site of NiSOD.[50,52,58,59] It was shown that bis-amine coordination increased the sulfur

character in the HOMO, leading to the formation of a predominantly S-based molecular orbital upon oxidation. Bis-amide coordination leads to the activation of the Ni/S(π)* orbitals, which protects the metal thiolate complex towards oxygen. It therefore seems that the mixed amide/amine motif at the active site of NiSOD not only tunes the redox potential of the active site in order to ensure a Ni-centred oxidation process, but also provides the thiolate S-donors protection from oxygenation by O_2.[48]

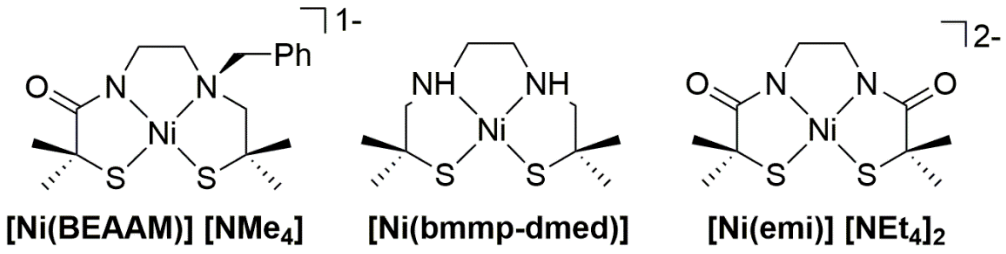


Figure 1.7 [Ni(emi)] $[Et_4N]_2$ (left), [Ni(bmmp-dmed)] (right) and $[Ni^{II}(BEAAM)]^{1-}$ (middle) reported by Shearer *et al.*[48,52]

Shearer and co-workers also prepared and studied a metallopeptide maquette ([Ni(SOD^{M1})]) which incorporated the first 12 residues from the N-terminus of the active site of *Streptomyces coelicolor* NiSOD (H_2N-HCDLPCGVYDPA-COOH). The UV/vis, X-ray absorption and CD spectra of the maquette corresponded well with those of the reduced form of NiSOD. The oxidised form of the maquette [$Ni^{III}(SOD^{M1})$] could not be isolated, however, subsequent electrochemical studies using protein thin-film voltammetry revealed that [Ni(SOD^{M1})] exhibits an appropriate redox potential to act as a SOD (E_p^a = 0.80 V *vs* Ag/Ag^+), and indeed was shown to deliver SOD activity approaching that of native SODs (*c.f.* k_{cat} > 2 x 10^9 M^{-1} s^{-1} for *S. seoulensis* NiSOD).[36,51,60] The second generation maquettes [Ni(SOD^{M2})] (SOD^{M2}: H_2N-

HCDLPCG) and [Ni(SOD^{M2}H(1)A)] (SOD^{M2}H(1)A: H_2N-ACDLPCG) were prepared in order to assess the influence of axial ligation within the active site of NiSOD (Figure 1.8).[51] Electrochemical studies highlighted the presence of the imidazole group to stabilise the production of the Ni(III) state enabling the maquette to oxidise at a more cathodic potential ([Ni(SOD^{M2})]: 0.52 V *vs* Ag/Ag^+; [Ni(SOD^{M2}H(1)A)]: 0.62 V *vs* Ag/Ag^+) and also to cause a significant increase in the peak-to-peak separation of the redox couple concurrent with the axial ligand provided by the N-terminal residue coordinating and un-coordinating from the Ni centre upon oxidation/reduction. The presence of the imidazole residue was also identified to improve the activity of the SOD maquette.

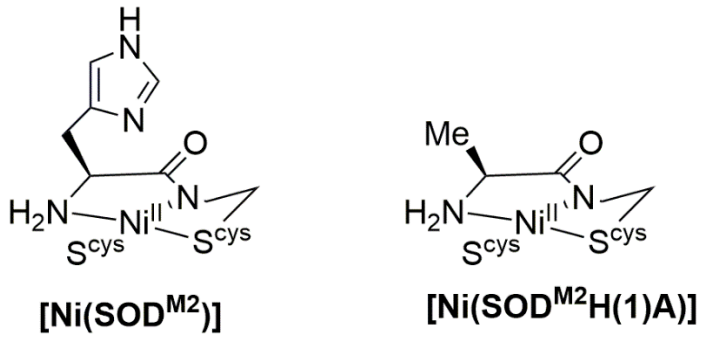


Figure 1.8 Metallopeptide maquettes, [Ni(SOD^{M2})] (left) and [Ni(SOD^{M2}H(1)A)] (right) reported by Shearer *et al.*[36,51]

Stenson *et al*. isolated a range of Ni(III/II) Schiff-base dithiolate complexes (Figure 1.9). These diamagnetic, mononuclear $Ni^{II}N_2S_2$ complexes utilised four donor atoms (two S-thiolate and two N-imine) to support the Ni centre within a slightly distorted square planar coordination environment.[61,62] The incorporation of multiple *tert*-butyl groups within the ligand system permitted electrochemical investigation in non-polar solvents. Subsequent electrochemical studies at 293 K revealed that [Ni(^{t}BuL$_S^1$)] and [Ni(^{t}BuL$_S^2$)]

underwent reversible one-electron oxidation processes at $E_{1/2}$ = 0.16 V and 0.10 V *vs* Fc^+/Fc, respectively. EPR and UV/vis spectroscopies showed that the SOMOs of the one-electron oxidised species possess thiyl radical character. Theoretical calculations (DFT) supported predominantly ligand-based oxidation processes. Upon cooling (< 253 K) these complexes followed a similar behaviour to that expressed by the systems studied by Holm *et al.*, which produced irreversible oxidation processes to generate EPR silent species.[52] Single crystal X-ray diffraction demonstrated that this irreversibility results from the dimerisation of two monomeric units on oxidation at low temperature through the formation of an S-S disulfide bridge.

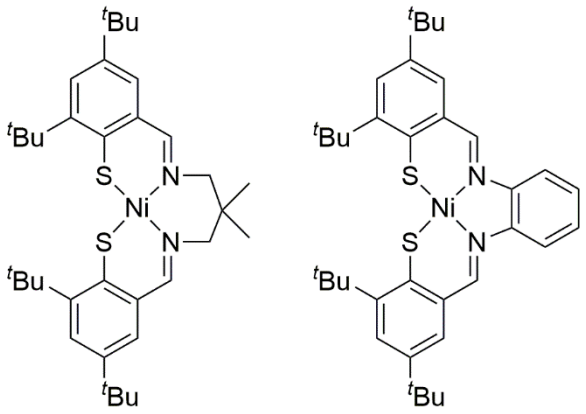


Figure 1.9 Schiff-base Ni(II) complexes**,** [Ni(^{t}BuL$_S^1$)] (left) and [Ni(^{t}BuL$_S^2$)] (right), reported by Stenson *et al.*[62]

In addition to the temperature dependent nature of these oxidation processes a solvent dependence was also identified. EPR spectroscopic studies and DFT calculations revealed that oxidation in neat CH_2Cl_2 showed a predominantly ligand-based orbital with the SOMO containing *ca.* 40% S-character. The addition of the coordinating solvent pyridine to chemically oxidised samples of [Ni(^{t}BuL$_S^1$)]$^+$ and [Ni(^{t}BuL$_S^2$)]$^+$ caused a shift in the nature

of this oxidation process. The EPR spectra of these adducts are typical of Ni(III) centres possessing a d_{z^2} ground state. These observations emphasise the ability of exogenous N-donors to drive a metal-centred oxidation.[61,62]

Franks *et al.*[63] synthesised a range of dithiosalicylidenediamine Ni(II) complexes that built upon the previous work conducted by Stenson *et al.*[61,62] with the aim to incorporate N-donors into the original [N_2S_2] ligand framework (Figure 1.10) with the goal of synthesising complexes that more accurately reproduced the structural, spectroscopic and functional properties of the active site of NiSOD.

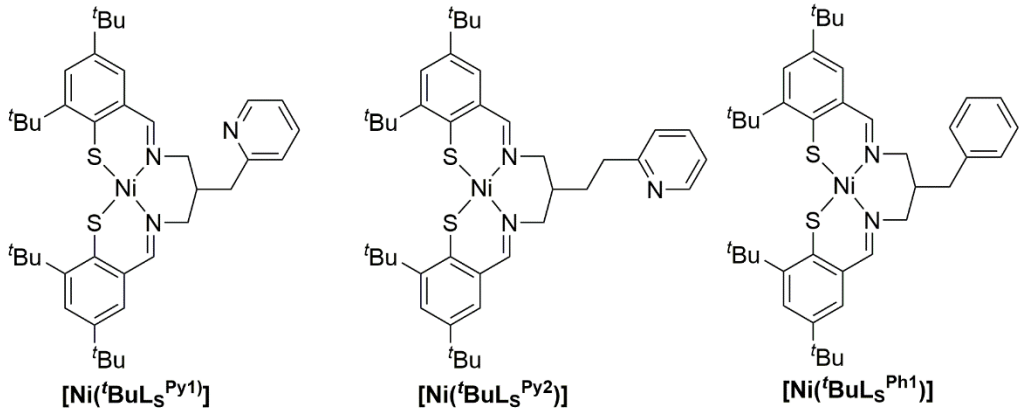


Figure 1.10 Schiff-base Ni(II) complexes, [Ni(^{t}BuL$_S^{Py1}$)], [Ni(^{t}BuL$_S^{Py2}$)] and [Ni(^{t}BuL$_S^{Ph1}$)].[63]

Electrochemical investigations demonstrated that [Ni(^{t}BuL$_S^{Ph1}$)] possessed an electrochemically reversible single-electron oxidation process (E_p^a = 0.18 and E_p^c = 0.11 V *vs* Fc^+/Fc) at a similar potential to that reported by Stenson *et al.* for the analogous dithiosalicylidenediamine Ni(II) complexes [Ni(^{t}BuL$_S^1$)] and [Ni(^{t}BuL$_S^2$)] (Figure 1.10).[61,62]

The position of the pyridyl group relative to the metal centre appeared to have an impact upon the redox properties of the complex [Ni(^{t}BuL$_S^{Py1}$)]. Analysis of the electrochemical properties of [Ni(^{t}BuL$_S^{Py1}$)] revealed the 2-pyridyl group lowered the potential of the first oxidation process of

[Ni(^{t}BuL$_S^{Py1}$)] by *ca.* 0.08 V relative to that for [Ni(^{t}BuL$_S^{Ph1}$)] and [Ni(^{t}BuL$_S^{Py2}$)]. The first oxidation couple of [Ni(^{t}BuL$_S^{Py1}$)] (E_p^a = 0.10 and E_p^c = 0.00 V *vs* Fc^+/Fc) also displayed a peak-to-peak separation that was larger than that of a couple controlled by heterogeneous electron transfer, and provided support for an internal rearrangement that may take place upon oxidation and reduction. This was supported by X-band EPR spectroscopic studies upon [Ni(^{t}BuL$_S^{Py1}$)]$^+$ which showed that the oxidised species possessed a rhombic EPR spectrum (g_{11} = 2.282, g_{22} = 2.200, g_{33} = 2.016) consistent with a metal-centred SOMO. The well-defined three-line superhyperfine coupling to a single ^{14}N (I=1) nuclei in the g_{33} region inferred that the proposed intramolecular rearrangement, which occurred upon oxidation, involved axial coordination of the 2-pyridyl group to the Ni(III) centre.

Electrochemical studies revealed that [Ni(^{t}BuL$_S^{Py2}$)] (E_p^a = 0.18 and E_p^c = 0.11 V *vs* Fc^+/Fc) was oxidised at the same potential as [Ni(^{t}BuL$_S^{Ph1}$)], which suggested that the pyridyl group of [Ni(^{t}BuL$_S^{Py2}$)] was too distant from the redox active centre of the molecule to stabilise the product formed upon oxidation. Fluid solution X-band EPR spectroscopy showed that the EPR spectrum of the species initially formed upon electrochemical and chemical oxidation of [Ni(^{t}BuL$_S^{Py2}$)] possessed an isotropic feature at g_{iso} = 2.071 with a Gaussian linewidth of 18 G, consistent with the generation of a species possessing substantial thiyl radical character (*c.f.* [Ni(^{t}BuL$_S^{Ph1}$)]$^+$).

The binding of the 2-pyridyl group to the Ni(III) centre on oxidation of [Ni(^{t}BuL$_S^{Py1}$)] generated a SOMO possessing substantial metal character. A similar internal rearrangement of the coordination sphere takes place at the Ni centre of the active site of NiSOD, where the axial imidazole group of the His1

residue binds to the metal centre upon oxidation (Figure 1.10). The chemistry of [Ni(^{t}BuL$_S^{Py1}$)] emphasises the importance of the role of the axial imidazole ligand at the active site of NiSOD, which may tune the redox properties of the oxidised state of the enzyme and protect the thiolate donors of Cys1 and Cys6 from oxidative stress by ensuring that the redox active orbitals of the active site are predominantly metal-based.

1.9 Galactose Oxidase (GAO) and Phenoxyl Radicals in Biology

Galactose oxidase (GAO) is an extracellular fungal enzyme containing a copper cofactor. The enzyme catalyses the two-electron oxidation of an extensive range of primary alcohols to form their corresponding aldehydes alongside the reduction of molecular oxygen to form hydrogen peroxide (Equation 1.3).[64–66]

Equation 1.3 $RCH_2OH + O_2 \rightarrow RCHO + H_2O_2$

Single crystal X-ray diffraction studies have shown that the active site of GAO is composed of a mononuclear copper atom coordinated by two histidine imidazoles (His496 and His581), a tyrosine phenolate (Tyr272), and an acetate ion (replacing the substrate) located within the equatorial plane, and a second tyrosine phenolate (Tyr495) resides in the axial position with a long Cu-O distance (2.7 Å).[67–71] This forms a distorted N_2O_3 square-based pyramidal coordination geometry (Figure 1.13). [69,72,73]

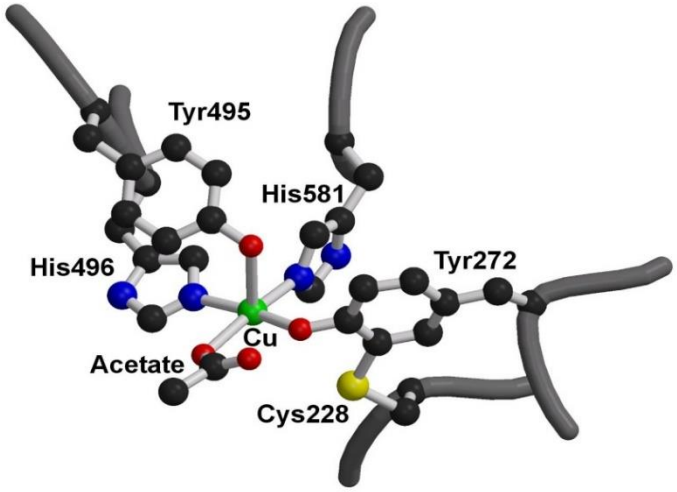


Figure 1.13 The single x-ray crystal structure of GAO.[74, 75]

The mononuclear copper cofactor has the ability to exist in three redox forms, however, only the fully oxidised or fully reduced forms have been identified as catalytically active.[74,75] Originally, the two-electron oxidation processes carried out by the GAO active site was thought to be solely metal-based redox processes [Cu(I), Cu(II) and Cu(III)].[75] However, through a combination of spectroscopic and crystallographic studies the fully oxidised active site was identified as a Cu(II) ion coordinated to a tyrosyl radical (Tyr272$^{\bullet}$) instead of the originally proposed Cu(III) species. Therefore, it has been concluded that it is a combination of two redox active units: [Cu(I)/Cu(II) and tyrosinate/tyrosyl radical] that drives the two-electron oxidative chemistry at the active site of GAO.[66,76]

It has been observed that the radical cofactor, Tyr272 that is involved in the oxidative chemistry at the GAO active site is cross-linked at the *ortho*-position of its phenolic side chain to the sulfur atom of Cys228.[69] This feature is extremely uncommon and has only been observed in one other enzyme, glyoxal oxidase.[77] This thioether bond is known to structurally increase the rigidity of

the active site, but is also responsible for lowering the redox potential of the side chain of Tyr272, making it easier to oxidise and thus facilitating oxidation at the enzyme active site.[66,78]

The GAO enzyme functions using a two-step 'ping-pong' mechanism whereby the substrate molecule, galactose, coordinates to the metal centre in a vacant equatorial position (in the native enzyme this position is occupied by a molecule of water). The basic Tyr495 residue then deprotonates the alcohol followed by the rate determining step whereby the H-atom removed by the O-atom of the coordinated radical, Tyr272•. The oxidative phase of the enzyme's catalytic mechanism is then completed by an intramolcular electron transfer from the ketyl radical anion to the Cu(II) centre leading to loss of the aldehyde product and generation of the reduced form, Cu(I), of the enzyme. The second stage of the enzymatic mechanism involves oxidation of the active site by molecular oxygen to regenerate the active form of the enzyme, Cu(II), and generate hydrogen peroxide using the protons that were made available previously from the galactose substrate. A schematic of the mechanism performed by GAO is shown in Figure 1.14, which demonstrates the presence and role of the phenoxyl radical within the catalytic mechanism of GAO.[28,64,66,79]

Tyrosyl phenoxyl radicals play a key role in several important biological processes, including DNA biosynthesis and photosynthesis. However, the most relevant biological example to the work presented in this thesis was the identification of the tyrosyl phenoxyl radical at the active site of galactose oxidase (GAO).[72,80,81] A selection of the synthetic complexes inspired by the chemistry performed by GAO are reviewed in the following pages to introduce the work presented in this thesis.

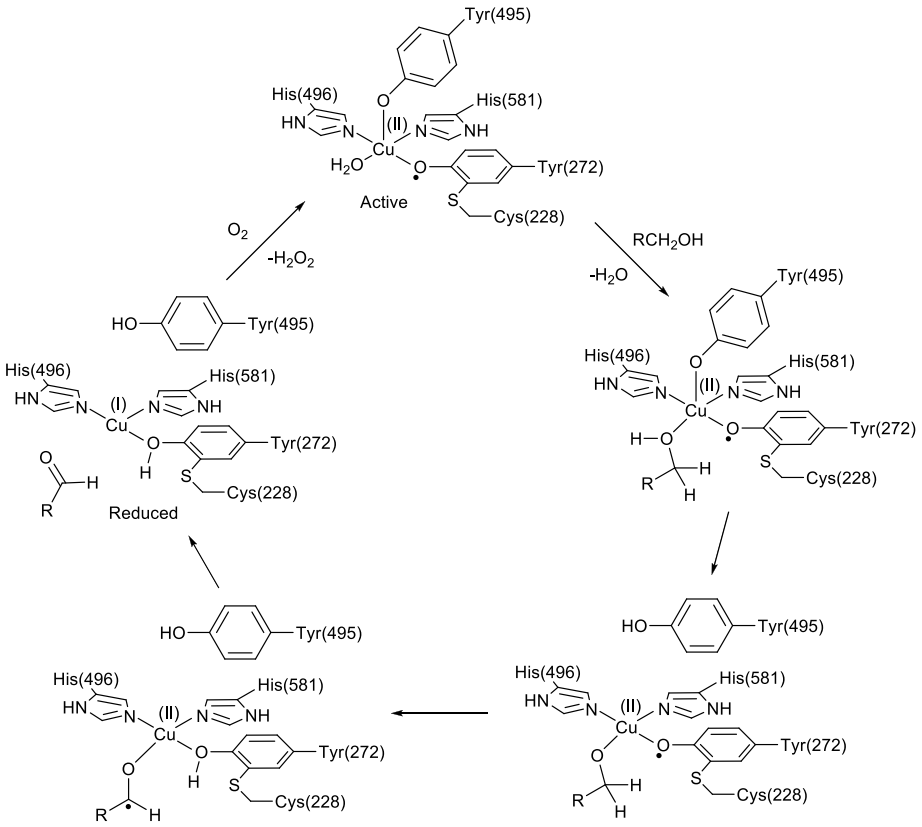


Figure 1.14 Catalytic mechanism performed by GAO.[66]

1.10 Cu(II) Complexes Inspired by GAO Containing Pro-Phenoxyl Radical Ligands

A wide number of Cu(II) complexes possessing pro-phenoxyl radical ligands containing sterically bulky substituents at the *ortho*- and *para*- positions of each phenol have been reported. A summary of three of the more pertinent classes of Cu(II) complexes containing pro-phenoxyl ligation are discussed below.

1.11 Schiff-Base Complexes and Synthetic Models of CuGAO

McMaster *et al*. has previously reported the synthesis and study of a range of Cu(II) complexes formed from the *N*,*O*-bidentate, Schiff-base phenol-imidazole pro-ligands shown in Figure 1.15. The Cu(II) complexes, $[Cu(^{t}BuL_o^{1})_2]$ ($H^{t}BuL_o^{1}$ = 2-(4,6-di-*tert*-butylhydroxyphenyl)-4,5-diphenyl imidazole),[82] $[Cu(^{t}BuL_o^{2})_2]$ ($^{t}BuL_o^{2}$ = 4,5-di-*p*-methoxyphenyl substituted imidazole)[83] and $[Cu(^{t}BuL_o^{3})_2]$ ($H\,^{t}BuL_o^{3}$ = *o*,*p*-di-*tert*-butyl-substituted phenol covalently bonded to a benzimidazole)[83] were shown to contain CuN_2O_2 centres possessing distorted square planar coordination geometries.[82,84] The UV/vis spectra of $[Cu(^{t}BuL_o^{1\text{-}3})_2]$ in CH_2Cl_2 exhibit a phenolate-to-Cu(II) charge transfer transition and a lower energy ligand field transition (e.g. for $[Cu(^{t}BuL_o^{1})_2]$: λ_{max} = 508 (ε = 750 $M^{-1}cm^{-1}$) and 694 nm (ε = 550 $M^{-1}cm^{-1}$)). X-band EPR spectra of $[Cu(^{t}BuL_o^{1\text{-}3})_2]$ in CH_2Cl_2-DMF (9:1) solution at 77 K are typical of a Cu(II) complex possessing a $(d_{x^2-y^2})^1$ ground state (S = 1/2) with $g_{zz} > g_{yy} \approx g_{xx}$. Electrochemical studies have shown that $[Cu(^{t}BuL_o^{1\text{-}3})_2]$ possess two reversible one-electron oxidation processes in the region 0.11 – 0.58 V *vs* Fc^+/Fc consistent with each process being ligand-based, with $[Cu(^{t}BuL_o^{1\text{-}3})(^{t}BuL_o^{1\text{-}3})^{\bullet}]^+$ produced initially and then $[Cu(^{t}BuL_o^{1\text{-}3})^{\bullet}_2]^{2+}$. The UV/vis spectra of the mono cations exhibit an intense absorption feature at *ca.* 410 nm and a less intense broad absorption between 500 and 900 nm that are assigned to the π-π^* transitions of the coordinated phenoxyl radical ligand. All of the Cu(II)-mono-phenoxyl radical complexes are essentially EPR silent as a result of the antiferromagnetic coupling between the S = 1/2 Cu(II) centre and the S = 1/2 coordinated radical ligand. The nature of $[Cu(^{t}BuL_o^{1})(^{t}BuL_o^{3})^{\bullet}]^+$ has also been confirmed by X-ray crystallographic studies of $[Cu(^{t}BuL_o^{1})_2][BF_4]$ which

identified the cation as one phenoxyl radical and one phenoxide ligand coordinated to a Cu(II) centre.[82,84,85]

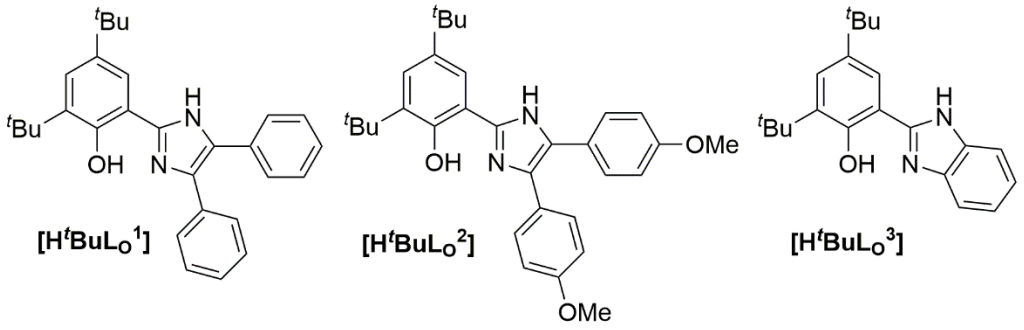


Figure 1.15 *N,O*-bidentate, Schiff-base phenol-imidazole pro-ligands reported by McMaster *et al.*[82,84,85]

1.12 Zn(II) and Ni(II) Complexes Containing Pro-Phenoxyl Radical Ligands

Zn(II) complexes containing phenolate ligands capable of supporting phenoxyl radical character have also been prepared and extensively studied.[82,83,86–88] The redox inactive nature of the Zn(II) cation over a wide potential range ensures that the redox processes in the cyclic voltammograms of Zn(II)-phenolate complexes may be assigned exclusively to ligand-based processes associated with the phenoxyl/phenolate redox couple.[88] Zn(II)-phenoxyl radical complexes can be paramagnetic and may exhibit EPR spectra typical of phenoxyl radicals (e.g. for $[Zn(^{t}BuL_{O}^{2})_2]$: g = 2.004, (Figure 1.15)).[83] The UV/vis spectra of Zn(II)-phenoxyl radical complexes exhibit similar characteristics to their corresponding Cu(II) analogues, for example $[Zn(^{t}BuL_{O}^{2})_2]^{\bullet+}$ exhibits bands at λ_{max} = 410 (ε = 11300 $M^{-1}cm^{-1}$) and 792 nm (ε = 5900 $M^{-1}cm^{-1}$), which are associated with the π-π^{*} transitions associated with a phenoxyl radical ligand.[83]

In contrast to Cu(II) and Zn(II) complexes containing phenoxyl radical ligands, far fewer scientific investigations have been completed on the analogous Ni(II) complexes. Ni complexes containing phenolate ligands may undergo either metal or ligand based oxidation processes due to the ligand- and metal-based frontier orbitals lying close in energy.[89] As a result, the nature of the one-electron oxidation processes of Ni(II)-phenolate complexes may reside somewhere between the two redox extremes involving either metal centred (Ni(III)-phenolate) or ligand centred (Ni(II)-phenoxyl radical) oxidation.[90–92]

1.13 Five coordinate M(II) diphenolate [M = Zn(II), Ni(II), and Cu(II)] Schiff base complexes

Franks *et al.*[93] prepared a range of Zn(II), Ni(II) and Cu(II) Schiff-base diphenolate complexes utilising novel N_3O_2 pro-ligands ([$H_2{}^tBuL_O{}^{C3N}$] and [$H_2{}^tBuL_O{}^{NMe}$]) (Figure 1.16) that incorporated an additional N-donor in to the ligand back bone within the structures of the M(II) complexes (M = Cu, Ni, Zn).

The pro-ligands, [$H_2{}^tBuL_O{}^{NMe}$] and [$H_2{}^tBuL_O{}^{C3N}$], form monomeric trigonal bipyramidal complexes with the Zn(II) cations to form [Zn($^tBuL_O{}^{NMe}$)] and [Zn($^tBuL_O{}^{C3N}$)] (Figure 1.16). Whereas single X-ray crystallography studies showed for Ni(II) there is a conformational change to yield two paramagnetic distorted square-based pyramidal complexes, [Ni($^tBuL_O{}^{NMe}$)] and [Ni($^tBuL_O{}^{C3N}$)]. The analogous paramagnetic Cu(II) Schiff-base diphenolate complexes, [Cu($^tBuL_O{}^{NMe}$)] and [Cu($^tBuL_O{}^{C3N}$)], adopt similar distorted square-based pyramidal coordination geometries to their Ni(II) counterparts.

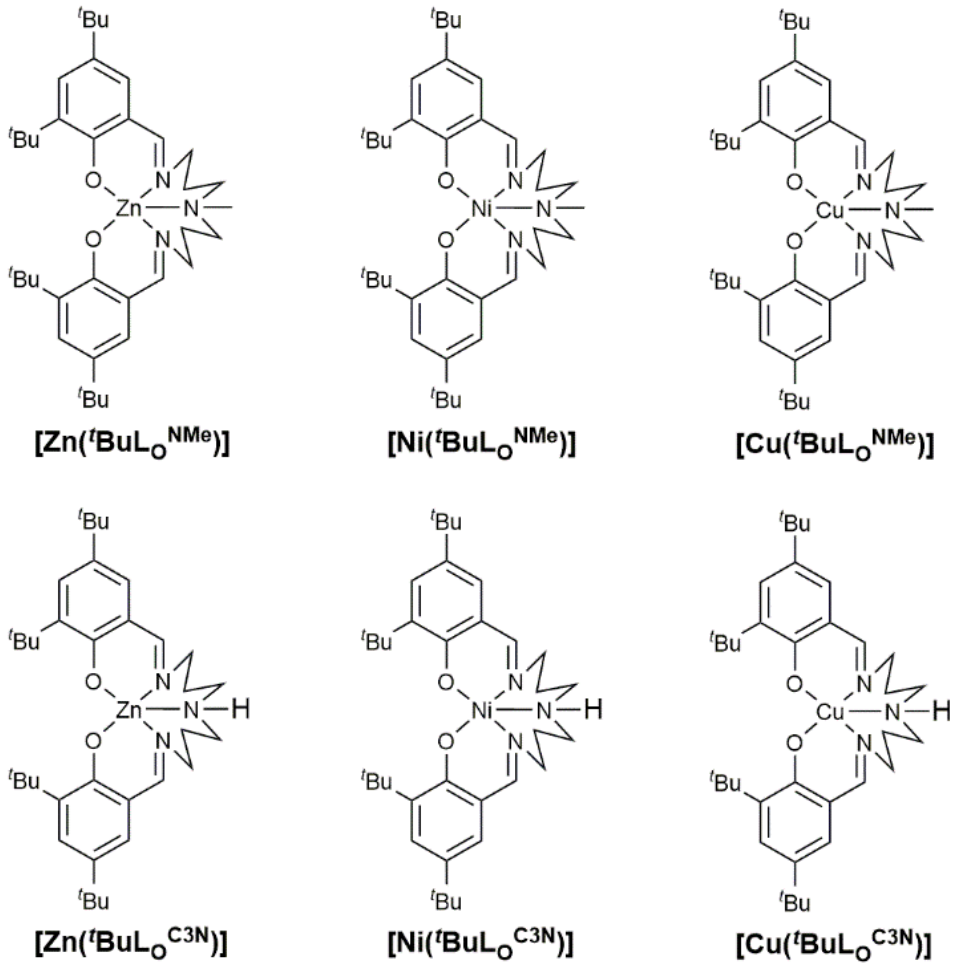


Figure 1.16 Schematic representation of the Zn(II), Ni(II) and Cu(II) Schiff-base diphenolate complexes synthesised by Franks *et al.*[63,93]

Electrochemical studies showed [M(^{t}BuL$_O^{NMe}$)] and [M(^{t}BuL$_O^{C3N}$)] (M = Zn(II), Ni(II) and Cu(II)) all support two single-electron electrochemically reversible oxidation processes. UV/vis and EPR spectroscopic studies confirmed the first oxidation processes of the d^{10} [Zn(^{t}BuL$_O^{NMe}$)] and [Zn(^{t}BuL$_O^{C3N}$)] metal complexes to be ligand-based, generating stable phenoxyl radical species similar to that observed in GAO. The second oxidation processes of [Zn(^{t}BuL$_O^{NMe}$)] and [Zn(^{t}BuL$_O^{C3N}$)] were not chemically reversible however these processes were also assigned as ligand-based processes leading to the formation of bisphenoxyl radical species. Similar experiments showed that [Cu(^{t}BuL$_O^{NMe}$)] and [Cu(^{t}BuL$_O^{C3N}$)] support two successive reversible ligand-based oxidation

processes generating kinetically inert bisphenoxyl radical species.[63,93] In contrast, the first oxidation processes of [Ni(^{t}BuL$_O^{NMe}$)] and [Ni(^{t}BuL$_O^{C3N}$)] were metal-based yielding a formal Ni(III) centre with the second oxidation process generating, [Ni(^{t}BuL$_O^{NMe}$)]$^{2+}$ and [Ni(^{t}BuL$_O^{C3N}$)]$^{2+}$, being ligand-based and exhibiting phenoxyl radical character.[63,93]

1.14 Aims and Objectives

This thesis aims to provide a detailed study of the factors controlling the nature of the oxidation processes for complexes containing Ni(II)-S(thiolate) ligation and how the nature of this coordination controls the chemistry at the active sites of NiSOD via a ligand donor metal based Ni(II)/Ni(III) couple. Additionally, for comparison, we will also focus upon the role that ligand based radicals play within metalloenzymes' catalytic mechanism with particular focus upon the nature of the phenoxyl radical in M(II) diphenolate complexes in relation to the CuGAO active site.

Chapter 2 builds upon work previously set out by Frank *et al.*[63,93] which aims to synthesise five coordinate M(II) diphenolate [M = Zn(II), Ni(II), and Cu(II)] Schiff-base complexes with a series of electron donating and electron withdrawing groups pendant to the bridging N donor to in order to probe the effect of the basicity of the bridging N donor upon modulating the redox processes of the complexes. This will offer insight into the phenoxyl radical stability of the Zn(II) and Cu(II) diphenolate complexes, the metal based oxidation stability in the Ni(II) diphenolate complexes, and the tyrosinate /tyrosyl radical within the CuGAO active site and the role it plays in the catalytic mechanism at the enzyme active site.

Chapter 3 builds upon the previous work set out by Stenson *et al.*[61,62] and Franks *et al.*[63,94] and aims to synthesise analogous Ni(II) diphenolate and dithiolate complexes that incorporate a pendant imidazole into the ligand framework. This chemistry bears significance to the Ni centre within the active site of NiSOD. The oxidised form of NiSOD binds to an imidazole group and this rearrangement is believed to protect the active site from oxidative stress by

ensuring a metal-based redox active orbital. The synthesis and characterisation of dithiolate and diphenolate complexes that incorporate an imidazole donor group, similar to that featured at the active site of NiSOD will further our understanding of the Ni(II)-thiolate and Ni(II)-phenolate interaction, with particular emphasis placed upon how the incorporation of N-donor functionalities in addition to the N_2S_2 and N_2O_2 coordination sphere effect the redox chemistry of dithiolate and diphenolate Ni(II) complexes.

Phenoxyl radicals can display enhanced stability and longer lifetimes when compared to their phenylthiyl analogues.[95] In order to provide a direct comparison between the relative stabilities of the two radical species we aim to synthesise the analogous Ni(II) Schiff-base diphenolate complexes for comparison with their diphenylthiolate Ni(II) counterparts.

Additionally, Chapter 4 will focus upon the synthesis of analogous Zn(II) and Cu(II) diphenolate complexes utilising the diphenolate pro-ligands synthesised in Chapter 3. Taken together these studies will develop the coordination chemistry of complexes containing phenylthiolate and phenolate donors with a view to providing insight into how these redox active ligands assist the chemistry of enzymatic active sites that feature cysteinate and tyrosinate ligation.

1 .15 References

(1) Bugg, T. *An Introduction to Enzyme and Coenzyme Chemistry*, **1997**.

(2) Wilkins, P. C.; Wilkins, R. G. *Inorganic Chemistry in Biology*, **1997**.

(3) Cowan, J. A. *Inorganic Biochemistry: An Introduction*; **1996**.

(4) Fenton, D. E. *Biocoordination Chemistry*, Oxford University Press, Oxford, **1995**.

(5) Kaim, W.; Schwederski, B. *Bioinorganic Chemistry: Inorganic Elements in the Chemistry of Life*, **1995**.

(6) Frausto da Silva, J. J. R.; Williams, R. J. P. *The Biological Chemistry of the Elements: The Inorganic Chemistry of Life*, Second.; Oxford University Press: Oxford, **2001.**

(7) Merz, K. M.; Hoffmann, R.; Dewar, M. J. S. *J. Am. Chem. Soc.* **1989**, *111*, 5636–5649.

(8) Crichton, R. R. *Biological Inorganic Chemistry*, Elsevier, **2008**

(9) Slep, L. D.; Neese, F. *Angew. Chem. Int. Ed. Engl.* **2003**, *42*, 2942–2945.

(10) Holm, R. H.; Kennepohl, P.; Solomon, E. I. *Chem. Rev.* **1996**, *96*, 2239–2314.

(11) Shriver, D. F.; Atkins, P. W. *Inorganic Chemistry*, Third edn., **1999**.

(12) Lippard, S. J.; Berg, J. M. *Principles of Bioinorganic Chemistry*, **1994**.

(13) Richards, A. D.; Rodger, A. *Chem. Soc. Rev.* **2007,** *36*, 471–483.

(14) Bertini, I.; Rosato, A. *Proc. Natl. Acad. Sci. U. S. A.* **2003**, *100*, 3601–3604.

(15) Groysman, S.; Holm, R. H. *Biochemistry* **2009**, *48*, 2310–2320.

(16) Ermler, U. *Science.* **1997**, *278*, 1457–1462.

(17) Drennan, C. L.; Heo, J.; Sintchak, M. D.; Schreiter, E.; Ludden, P. W. *Proc. Natl. Acad. Sci. U. S. A.* **2001**, *98*, 11973–11978.

(18) Dobbek, H.; Svetlitchnyi, V.; Gremer, L.; Huber, R.; Meyer, O. *Science* **2001**, *293*, 1281–1285.

(19) Doukov, T. I.; Iverson, T. M.; Seravalli, J.; Ragsdale, S. W.; Drennan, C. L. *Science* **2002**, *298*, 567–572.

(20) Svetlitchnyi, V.; Dobbek, H.; Meyer-Klaucke, W.; Meins, T.; Thiele, B.; Römer, P.; Huber, R.; Meyer, O. *Proc. Natl. Acad. Sci. U. S. A.* **2004**, *101*, 446–451.

(21) Neupane, K. P.; Shearer, J. *Inorg. Chem.* **2006**, *45*, 10552–10566.

(22) Kieber-Emmons, M. T.; Riordan, C. G. *Acc. Chem. Res.* **2007**, *40*, 618–625.

(23) Wuerges, J.; Lee, J.-W.; Yim, Y.-I.; Yim, H.-S.; Kang, S.-O.; Djinovic Carugo, K. *Proc. Natl. Acad. Sci. U. S. A.* **2004**, *101*, 8569–8574.

(24) Marr, A. *Coord. Chem. Rev.* **2001**, *219-221*, 1055–1074.

(25) Kumar, D. N.; Garg, B. S. *Spectrochim. Acta - Part A Mol. Biomol. Spectrosc.* **2006**, *64*, 141–147.

(26) Ghosh, P.; Begum, A.; Bill, E.; Weyhermüller, T.; Wieghardt, K. *Inorg. Chem.* **2003**, *42*, 3208–3215.

(27) Mabbs, F. E.; Collison, D. *Electron Paramagnetic Resonance of d Transition Metal Compounds* **1992**.

(28) Krüger, H. *Angew. Chem Int.Ed.* **1999**, *38*, 627–631.

(29) Branscombe, N. D. J.; Atkins, A. J.; Marin-Becerra, A.; McInnes, E. J. L.; Mabbs, F. E.; McMaster, J.; Schröder, M. *Chem. Commun.* **2003**, 1098–1099.

(30) Lee, J.; Roe, J.; Kang, S. *Superoxide Dismutase*, **2002,** *349*, 90–101.

(31) Volbeda, A.; Charon, M. H.; Piras, C.; Hatchikian, E. C.; Frey, M.; Fontecilla-Camps, J. C. *Nature* **1995**, *373*, 580–587.

(32) Finkel, T.; Holbrook, N. J. *Nature* **2000**, *408*, 239–247.

(33) Droge, W. *Physiol. Rev.* **2002**, *82*, 47–95.

(34) McCord, J. M. *Superoxide Dismutase*; Methods in Enzymology; Elsevier, 2002; Vol. 349.

(35) Miao, L.; St Clair, D. K. *Free Radic. Biol. Med.* **2009**, *47*, 344–356.

(36) Shearer, J.; Zhao, N. *Inorg. Chem.* **2006**, *45*, 9637–9639.

(37) Nakane, D.; Kuwasako, S.; Tsuge, M.; Kubo, M.; Funahashi, Y.; Ozawa, T.; Ogura, T.; Masuda, H. *Chem. Commun. (Camb).* **2010**, *46* , 2142–2144.

(38) Wuerges, J.; Lee, J. W.; Kang, S.O.; Carugo, K. D. *Acta Crystallogr., Sect. D: Biological Crystallogr.*, **2002**, *58*, 1220–1223.

(39) Valko, M.; Leibfritz, D.; Moncol, J.; Cronin, M. T. D.; Mazur, M.; Telser, J. *Int. J. Biochem. Cell Biol.* **2007**, *39*, 44–84.

(40) Youn, H.; Kim, E.; Roe, J.; Hah, Y.; Kang, S. *Biochem. J.* **1996**, *318*, 889–896.

(41) Youn, H. D.; Youn, H.; Lee, J. W.; Yim, Y. I.; Lee, J. K.; Hah, Y. C.; Kang, S. O. *Arch. Biochem. Biophys.* **1996**, *334*, 341–348.

(42) Barondeau, D.; Kassman, C.; Bruns, C.; Tainer, J.; Getzoff, E. *Protein Sci.* **2004**, *13*, 192–192.

(43) Bryngelson, P. A.; Arobo, S. E.; Pinkham, J. L.; Cabelli, D. E.; Maroney, M. J. *J. Am. Chem. Soc.* **2004**, *126*, 460–461.

(44) Palenik, B.; Brahamsha, B.; Larimer, F. W.; Land, M.; Hauser, L.;

Chain, P.; Lamerdin, J.; Regala, W.; Allen, E. E.; McCarren, J.; Paulsen, I.; Dufresne, A.; Partensky, F.; Webb, E. A.; Waterbury, J. *Nature* **2003**, *424*, 1037–1042.

(45) Kieber-Emmons, M. T.; Riordan, C. G. *Acc. Chem. Res.* **2007**, *40*, 618–625.

(46) Fiedler, A. T.; Bryngelson, P. A.; Maroney, M. J.; Brunold, T. C. *J. Am. Chem. Soc.* **2005**, *127*, 5449–5462.

(47) Herbst, R. W.; Guce, A.; Bryngelson, P. A.; Higgins, K. A.; Ryan, K. C.; Cabelli, D. E.; Garman, S. C.; Maroney, M. J. *Biochemistry* **2009**, *48*, 3354–3369.

(48) Shearer, J.; Dehestani, A.; Abanda, F. *Inorg. Chem.* **2008**, *47*, 2649–2660.

(49) Fiedler, A. T.; Brunold, T. C. *Inorg. Chem.* **2007**, *46*, 8511–8523.

(50) Mullins, C. S.; Grapperhaus, C. A.; Kozlowski, P. M. *JBIC J. Biol. Inorg. Chem.* **2006**, *11*, 617–625.

(51) Neupane, K. P.; Gearty, K.; Francis, A.; Shearer, J. *J. Am. Chem. Soc.* **2007**, *129*, 14605–14618.

(52) Krüger, H. J.; Peng, G.; Holm, R. H. *Inorg. Chem.* **1991**, *30*, 734–742.

(53) Krüger, H.; Holm, R. *Inorg. Chem.* **1987**, *26*, 3645–3647.

(54) Hanss, J.; Krüger, H. *Angew. Chem Int.Ed.* **1998**, *37*, 360–363.

(55) Halfen, J. A.; Jazdzewski, B. A.; Mahapatra, S.; Berreau, L. M.; Wilkinson, E. C.; Que, L.; Tolman, W. B. *J. Am. Chem. Soc.* **1997**, *119*, 8217–8227.

(56) Bryngelson, P. A.; Arobo, S. E.; Pinkham, J. L.; Cabelli, D. E.; Maroney, M. J. *J. Am. Chem. Soc.* **2004**, *126*, 460–461.

(57) Shearer, J.; Long, L. M. *Inorg. Chem.* **2006**, *45*, 2358–2360.

(58) Grapperhaus, C. A.; Mullins, C. S.; Kozlowski, P. M.; Mashuta, M. S. *Inorg. Chem.* **2004**, *43*, 2859–2866.

(59) Rao, P.; Bhaduri, S.; Jiang, J.; Holm, R. *Inorg. Chem.* **2004**, *43*, 5833–5849.

(60) Choudhury, S. B.; Lee, J. W.; Davidson, G.; Yim, Y. I.; Bose, K.; Sharma, M. L.; Kang, S. O.; Cabelli, D. E.; Maroney, M. J. *Biochemistry* **1999**, *38*, 3744–3752.

(61) Stenson, P. Transition Metal Thiolate Complexes: Modelling the Active Sites of Sulfur-Ligated Metalloenzymes, The University of Nottingham, 2005.

(62) Stenson, P. A.; Board, A.; Marin-Becerra, A.; Blake, A. J.; Davies, E. S.; Wilson, C.; McMaster, J.; Schröder, M. *Chem. Eur. J.* **2008**, *14*, 2564–2576.

(63) Franks, M. Transition Metal Complexes Containing Phenylthiolate and Phenolate Ligands, University of Nottingham, 2011.

(64) Whittaker, J. W. *Chem. Rev.* **2003**, *103*, 2347–2363.

(65) Borman, C.; Saysell, C.; Sokolowski, A.; Twitchett, M.; Wright, C.; Sykes, A. *Coord. Chem. Rev.* **1999**, *192*, 771–779.

(66) Jazdzewski, B. a.; Tolman, W. B. *Coord. Chem. Rev.* **2000**, *200-202*, 633–685.

(67) Kasumov, V. T.; Medjidov, A. A.; Yayli, N.; Zeren, Y. *Spectrochim. Acta. A. Mol. Biomol. Spectrosc.* **2004**, *60*, 3037–3047.

(68) Stubbe, J.; Nocera, D. G.; Yee, C. S.; Chang, M. C. Y. *Chem. Rev.* **2003**, *103*, 2167–2201.

(69) Ito, N.; Phillips, S. E.; Stevens, C.; Ogel, Z. B.; McPherson, M. J.; Keen, J. N.; Yadav, K. D.; Knowles, P. F. *Nature* **1991**, *350*, 87–90.

(70) Whittaker, M.; Whittaker, J. *J. Biol. Chem.* **1988**, *263*, 6074–6080.

(71) Whittaker, M. M.; Ekberg, C. A.; Peterson, J.; Sendova, M. S.; Day, E. P.; Whittaker, J. W. *J. Mol. Catal. B Enzym.* **2000**, *8*, 3–15.

(72) Whittaker, J. W. *Arch. Biochem. Biophys.* **2005**, *433*, 227–239.

(73) Ito, N.; Phillips, S.; Yadav, K.; Knowles, P. *J. Mol. Biol.* **1994**, *238*, 794–814.

(74) Whittaker, M. M.; Ballou, D. P.; Whittaker, J. W. *Biochemistry* **1998**, *37*, 8426–8436.

(75) Knowles, P. F.; Brown, R. D.; Koenig, S. H.; Wang, S.; Scott, R. A.; McGuirl, M. A.; Brown, D. E.; Dooley, D. M. *Inorg. Chem.* **1995**, *34*, 3895–3902.

(76) Nairn, A. K.; Archibald, S. J.; Bhalla, R.; Gilbert, B. C.; Maclean, E. J.; Teat, S. J.; Walton, P. H. *Dalton Trans.* **2006**, No. 1, 172–176.

(77) Whittaker, M.; Kersten, P.; Nakamura, N.; SandersLoehr, J.; Schweizer, E.; Whittaker, J. *J. Biol. Chem.* **1996**, *271*, 681–687.

(78) Whittaker, J. W. *Adv. Protein Chem.* **2002**, *60*, 1–49.

(79) Zueva, E.; Walton, P. H.; McGrady, J. E. *Dalton Trans.* **2006**, No. 1, 159–167.

(80) Stubbe, J.; van der Donk, W. A. *Chem. Rev.* **1998**, *98*, 705–762.

(81) Rogers, M. *Curr. Opin. Chem. Biol.* **2003**, *7*, 189–196.

(82) Benisvy, L.; Blake, A. J.; Collison, D.; Stephen Davies, E.; David Garner, C.; McInnes, E. J. L.; McMaster, J.; Whittaker, G.; Wilson, C.; *Dalton Trans.* **2003**, No. 5, 1975–1985.

(83) Benisvy, L.; Bill, E.; Blake, A. J.; Collison, D.; Davies, E. S.; Garner, C. D.; McArdle, G.; McInnes, E. J. L.; McMaster, J.; Ross, S. H. K.;

Wilson, C. *Dalton Trans.* **2006**, No. 1, 258–267.

(84) Benisvy, L.; Bill, E.; Blake, A. J.; Collison, D.; Davies, E. S.; Garner, C. D.; Guindy, C. I.; McInnes, E. J. L.; McArdle, G.; McMaster, J.; Wilson, C.; Wolowska, J. *Dalton. Trans.* **2004**, No. 21, 3647.

(85) Benisvy, L.; Blake, A J.; Collison, D.; Davies, E. S.; Garner, C. D.; McInnes, E. J.; McMaster, J.; Whittaker, G.; Wilson, C. *Chem. Commun.* **2001**, 1824–1825.

(86) Arora, H.; Philouze, C.; Jarjayes, O.; Thomas, F. *Dalton Trans.* **2010**, *39*, 10088–10098.

(87) Orio, M.; Philouze, C.; Jarjayes, O.; Neese, F.; Thomas, F. *Inorg. Chem.* **2010**, *49*, 646–658.

(88) Sokolowski, A.; Leutbecher, H.; Weyhermüller, T.; Schnepf, R.; Bothe, E.; Bill, E.; Hildebrandt, P.; Wieghardt, K. *J. Biol. Inorg. Chem.* **1997**, *2*, 444–453.

(89) Fontecilla-Camps, J. C.; Volbeda, A.; Cavazza, C.; Nicolet, Y. *Chem. Rev.* **2007**, *107*, 4273–4303.

(90) Müller, J.; Kikuchi, A.; Bill, E.; Weyhermüller, T.; Hildebrandt, P.; Ould-Moussa, L.; Wieghardt, K. *Inorganica Chim. Acta* **2000**, *29*, 265–277.

(91) Shimazaki, Y.; Tani, F.; Fukui, K.; Naruta, Y.; Yamauchi, O. *J. Am. Chem. Soc* **2003**, *125*, 10512–10513.

(92) Shimazaki, Y.; Huth, S.; Karasawa, S.; Hirota, S.; Naruta, Y.; Yamauchi, O. *Inorg. Chem.* **2004**, *43*, 7816–7822.

(93) Franks, M.; Gadzhieva, A.; Ghandhi, L.; Murrell, D.; Blake, A. J.; Davies, E. S.; Lewis, W.; Moro, F.; McMaster, J.; Schröder, M. *Inorg. Chem.* **2013**, *52*, 660–670.

(94) Komen, C. M. D.; Bickelhaupt, F. *Synth. Commun.* **1996**, *26*, 1693–1697.

(95) Kimura, S.; Bill, E.; Bothe, E.; Weyhermüller, T.; Wieghardt, K. *J. Am. Chem. Soc.* **2001**, *123*, 6025–6039.

Chapter 2: Synthesis and Characterisation of Schiff-Base Zn(II), Ni(II) and Cu(II)-Diphenolate Complexes

2.1 Introduction

The ability of the amino acid tyrosine residue to undergo redox processes, transitioning between the tyrosinate and tyrosyl radical forms, is essential for the catalytic activity of a wide number of important enzymes found in nature. These include cytochrome *c* oxidase,[1,2] ribonucleotide reductase,[3,4] prostaglandin H synthase[5] and photosystem II.[6] The common occurrence of these tyrosinate/tyrosyl radical units in enzymes has prompted the synthesis of small molecule metal-containing analogues containing metal-phenolate centres that are capable of being oxidised to form phenoxyl-metal centres for in-depth study and comparison to these enzyme systems.[6–10] These studies seek to provide further insight into the structural and electronic factors that control the chemistry of these systems.

Galactose oxidase (GAO) is an enzyme that catalyses the two-electron oxidation of a wide range of primary alcohols forming the corresponding aldehydes. This process also serves to reduce molecular oxygen to form hydrogen peroxide. GAO performs chemistry utilising an active site containing a monomeric Cu(II) centre within a N_2O_2 coordination sphere that also incorporates a tyrosine residue, which forms a tyrosyl radical during the catalytic cycle. The coordinated tyrosyl radical/tyrosinate ligand enables GAO to catalyse a multi-electron redox reaction despite the enzyme only containing a monomeric Cu(II) centre in its fully oxidised form.[6,7,9–12]

2.1.1 Previous Work

Several systems have been developed at Nottingham that employ a range of bidentate (NO) and tridentate (N_2O) ligand architectures in an attempt to model the behaviour of and provide insight into the GAO active centre (Figure 2.1).[11,13,14]

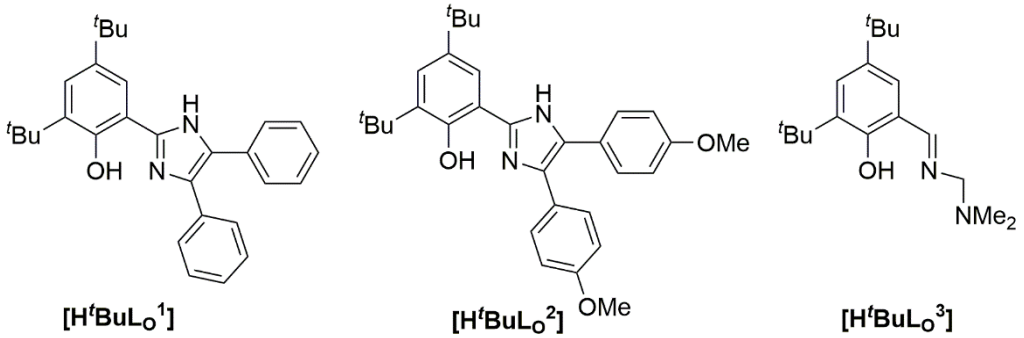


Figure 2.1 Diagram of the previous ligands studied by McMaster *et al.*[11,13,15]

The phenol-imidazole pro-ligand, [H^{t}BuL$_O$^{1}], shown (Figure 2.1) supports a single-electron, electrochemically reversible oxidation process at $E_{1/2}$ = 0.43 V *vs* Fc^+/Fc.[17] Additionally, high-field EPR spectroscopy and DFT calculations showed that the reversibility of this process is associated with the presence of an intramolecular hydrogen bond formed between the phenoxyl radical and the imidazolium cation (Figure 2.2).[17, 18]

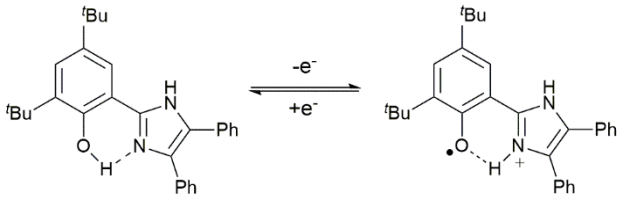


Figure 2.2 The intramolecular hydrogen bond in [H^{t}BuL$_O$^{1}].

The bidentate phenolate-imidazole pro-ligands [H^{t}BuL$_O$^{1}] and [H^{t}BuL$_O$^{2}] have been coordinated to a variety of transition metal ions (Zn^{2+}, Cu^{2+} and Ni^{2+})

and have yielded complexes that are capable of undergoing two reversible, ligand-based oxidation processes involving the formation of phenoxyl radicals.[14,17,19] However, whilst the chemistry of Cu(II) and Zn(II) complexes containing ligands capable of supporting phenoxyl radical character has been extensively studied, the analogous Ni complexes have been studied less.

Studies have shown that Ni complexes containing phenolate ligands may undergo metal or ligand-based oxidation processes because the ligand-based and metal-based redox-active orbitals lie close in energy to one another. Consequently, the nature of the one-electron oxidation processes of Ni(II)-phenolate complexes may reside somewhere between the two redox extremes involving either metal centred (Ni(III)-phenolate) or ligand centred (Ni(II)-phenoxyl radical) oxidation processes.[16–20]

Studies of Ni complexes containing phenolate ligands have shown that the nature of the oxidation processes of low-spin nickel complexes containing tetradentate Schiff-base ligation are solvent dependent.[12,16,20–22] The oxidation processes are predominantly ligand-based in non-coordinating solvents and in the presence of exogenous pyridine, axial coordination of two pyridine units to the metal centre may drive the formation of pseudo-octahedral Ni(III)-phenolate complexes upon the oxidation of the Ni(II) species.[8,12,16,22–28] The expansion of the denticity of the ligand framework to create Ni(II)-diphenolate complexes with octahedral coordination spheres removes the effect of solvent-dependent redox-tautomerism and leads to systems that demonstrate a subtle balance between the generation of either a high-spin Ni(II) centre coordinated to a

phenoxyl radical or a Ni(III) species coordinated by a phenolate ligand upon oxidation.[13,18,22,29] Weighardt *et al.* have reported an octahedral Ni(II)-phenolate complex, [Ni(L_O^5)(Bu_2acac)] (L_O^5 = 1,4-dimethyl-7-(3-*tert*-butyl-5-methoxy-2-hydroxybenzyl)-1,4,7-triazacyclononane and Bu_2acac = 1,3-di-*tert*-butyl-1,3-dionate) (Figure 5.3), which affords a Ni(II)-phenoxyl species upon oxidation in which the radical is ferromagnetically coupled to a high-spin Ni(II) centre (S_{total} = 3/2).[20] Thomas *et al.* demonstrated that oxidation of an octahedral Ni(II)-phenolate complex, [Ni(L_O^6)$_2$] (Figure 2.3), synthesised from two asymmetric tridentate (N_2O) Schiff-base ligands generates a Ni(II)-phenoxyl species upon oxidation in which the radical is anti-ferromagnetically coupled to a high-spin Ni(II) centre (S_{total} = 1/2),[26] while Parker *et al.* utilised the tridentate salicylidiminato (N_2O) pro-ligand, [H^{t}BuL_O^4] (Figure 2.3), the resulting distorted octahedral Ni(II) complex (Figure 5.3) supports a reversible Ni(III/II) couple.[13]

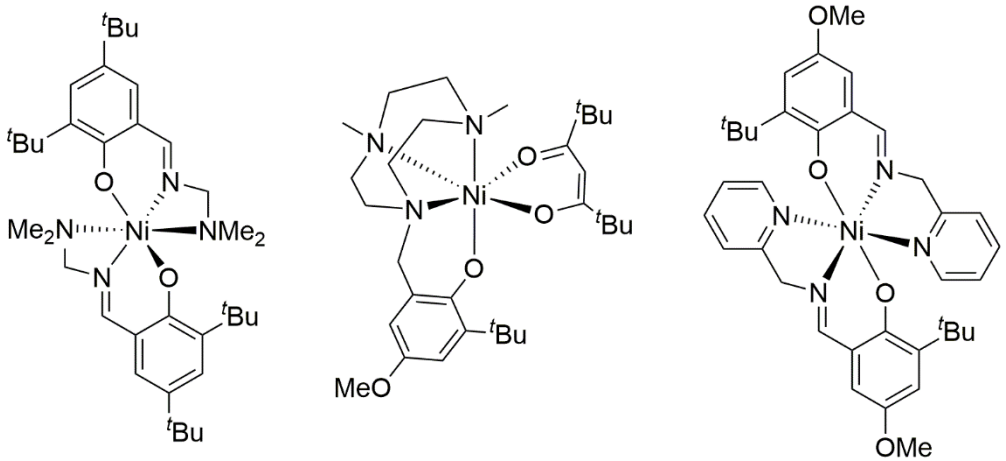


Figure 2.3 Previously reported Ni(II) phenolate complexes [Ni(^{t}BuL_O^4)$_2$] (left), [Ni(L_O^5)(Bu_2acac)] (middle) and [Ni(L_O^6)$_2$] (right).

Franks *et al.*[30] prepared a range of Zn(II), Ni(II) and Cu(II) Schiff-base diphenolate complexes (Figure 2.4) utilising novel N_3O_2 pro-ligands ([$H_2{}^tBuL_O{}^{C3N}$] and [$H_2{}^tBuL_O{}^{NMe}$]) that incorporate an additional N-donor in to the ligand back bone within the structures of the M(II) complexes (M = Cu, Ni, Zn).

The pro-ligands, [$H_2{}^tBuL_O{}^{NMe}$] and [$H_2{}^tBuL_O{}^{C3N}$], form monomeric trigonal bipyramidal complexes with the Zn(II) cation to form [Zn($^tBuL_O{}^{NMe}$)] and [Zn($^tBuL_O{}^{C3N}$)] (Figure 2.4). Transmetallation afforded the analogous Ni(II) [Ni($^tBuL_O{}^{NMe}$)] and [Ni($^tBuL_O{}^{C3N}$)] and Cu(II) Schiff-base diphenolate complexes [Cu($^tBuL_O{}^{NMe}$)] and [Cu($^tBuL_O{}^{C3N}$)]. X-ray crystallographic studies showed that the substitution of Zn(II) for Ni(II) is accompanied by a conformational change to yield two paramagnetic distorted square-based pyramidal complexes, [Ni($^tBuL_O{}^{NMe}$)] and [Ni($^tBuL_O{}^{C3N}$)]. The analogous paramagnetic Cu(II) Schiff-base diphenolate complexes, [Cu($^tBuL_O{}^{NMe}$)] and [Cu($^tBuL_O{}^{C3N}$)], adopt similar distorted square-based pyramidal coordination geometries to their Ni(II) counterparts.

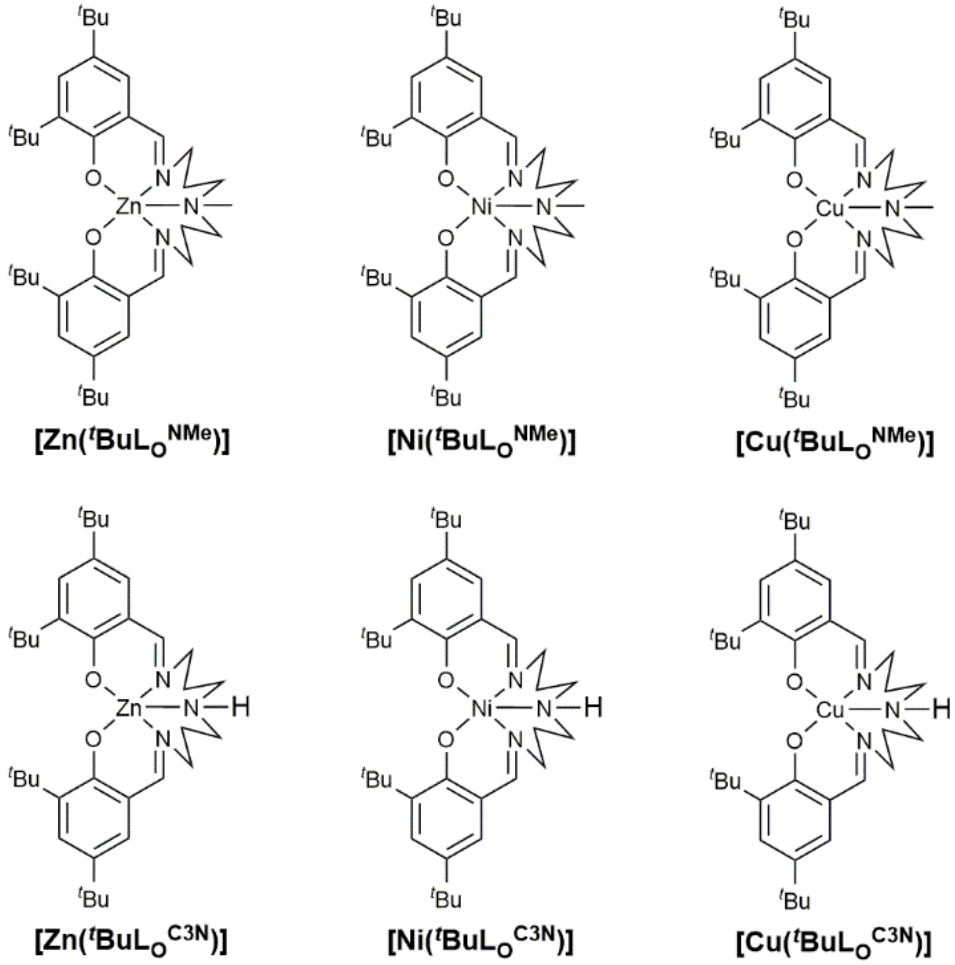


Figure 2.4 Schematic representation of the Zn(II), Ni(II) and Cu(II) Schiff-base diphenolate complexes synthesised by Franks *et al.*[30,31]

[M(^{t}BuL$_O^{NMe}$)] and [M(^{t}BuL$_O^{C3N}$)] (M = Zn(II), Ni(II) and Cu(II)) all support two single-electron electrochemically reversible oxidation processes which are summarised in Table 2.1.

Table 2.1 Summary of $E_{½}^1$ and $E_{½}^2$ potentials at scan rate 100mVs^{-1} for [M(^{t}BuL$_O^{NMe}$)] and [M(^{t}BuL$_O^{C3N}$)] [M = Zn(II), Ni(II), Cu(II)].[31]

Complex	$E_{½}^1$ *vs* Fc^+/Fc (V)	$E_{½}^2$ *vs* Fc^+/Fc (V)
[Zn(^{t}BuL$_O^{NMe}$)]	0.30	0.54
[Zn(^{t}BuL$_O^{C3N}$)]	0.29	0.50
[Ni(^{t}BuL$_O^{NMe}$)]	0.13	0.57
[Ni(^{t}BuL$_O^{C3N}$)]	0.09	0.50
[Cu(^{t}BuL$_O^{NMe}$)]	0.24	0.57
[Cu(^{t}BuL$_O^{C3N}$)]	0.15	0.54

UV/vis and EPR spectroscopic studies confirmed the first oxidation processes of the d^{10} [Zn(^{t}BuL$_O^{NMe}$)] and [Zn(^{t}BuL$_O^{C3N}$)] metal complexes to be ligand-based, generating stable phenoxyl radical species similar to that observed in GAO. The second oxidation processes of [Zn(^{t}BuL$_O^{NMe}$)] and [Zn(^{t}BuL$_O^{C3N}$)] were not chemically reversible however these processes were also assigned as ligand-based processes leading to the formation of bisphenoxyl radical species. Similar experiments showed that [Cu(^{t}BuL$_O^{NMe}$)] and [Cu(^{t}BuL$_O^{C3N}$)] support two successive reversible ligand-based oxidation processes generating kinetically inert bisphenoxyl radical species.[30,31]

In contrast, the first oxidation processes of [Ni(^{t}BuL$_O^{NMe}$)] and [Ni(^{t}BuL$_O^{C3N}$)] are metal-based yielding a formal Ni(III) centre with the second oxidation process generating, [Ni(^{t}BuL$_O^{NMe}$)]$^{2+}$ and [Ni(^{t}BuL$_O^{C3N}$)]$^{2+}$, being ligand-based and exhibiting phenoxyl radical character.

2.1.2 Aims of Chapter

This study aims to extend our knowledge of the redox chemistry of transition metal Schiff-base diphenolate complexes through the preparation of a range of Zn(II), Ni(II) and Cu(II) Schiff-base diphenolate complexes incorporating pentadentate (N_3O_2) pro-ligands that utilise the design features that build upon the Schiff-base dithiolate complexes previously reported by Franks *et al*.[30,31] The work in this chapter will focus on the incorporation of a series of electron donating and electron withdrawing groups pendant to the bridging N donor to in order to probe the effect of the basicity of the bridging N donor to modulate the redox processes. This could provide greater insight into the role of the coordination sphere in controlling the chemistry of redox active transition metal diphenolate complexes relevant for understanding the catalytic properties GAO.

The properties of the Schiff-base diphenolate systems will be probed using a combination of electrochemical, EPR and UV/vis spectroscopic methods, and by X-ray crystallography. This approach will enable the relative stabilities of transition metal - phenoxyl radical systems incorporating analogous ligand backbone structures to be directly compared.

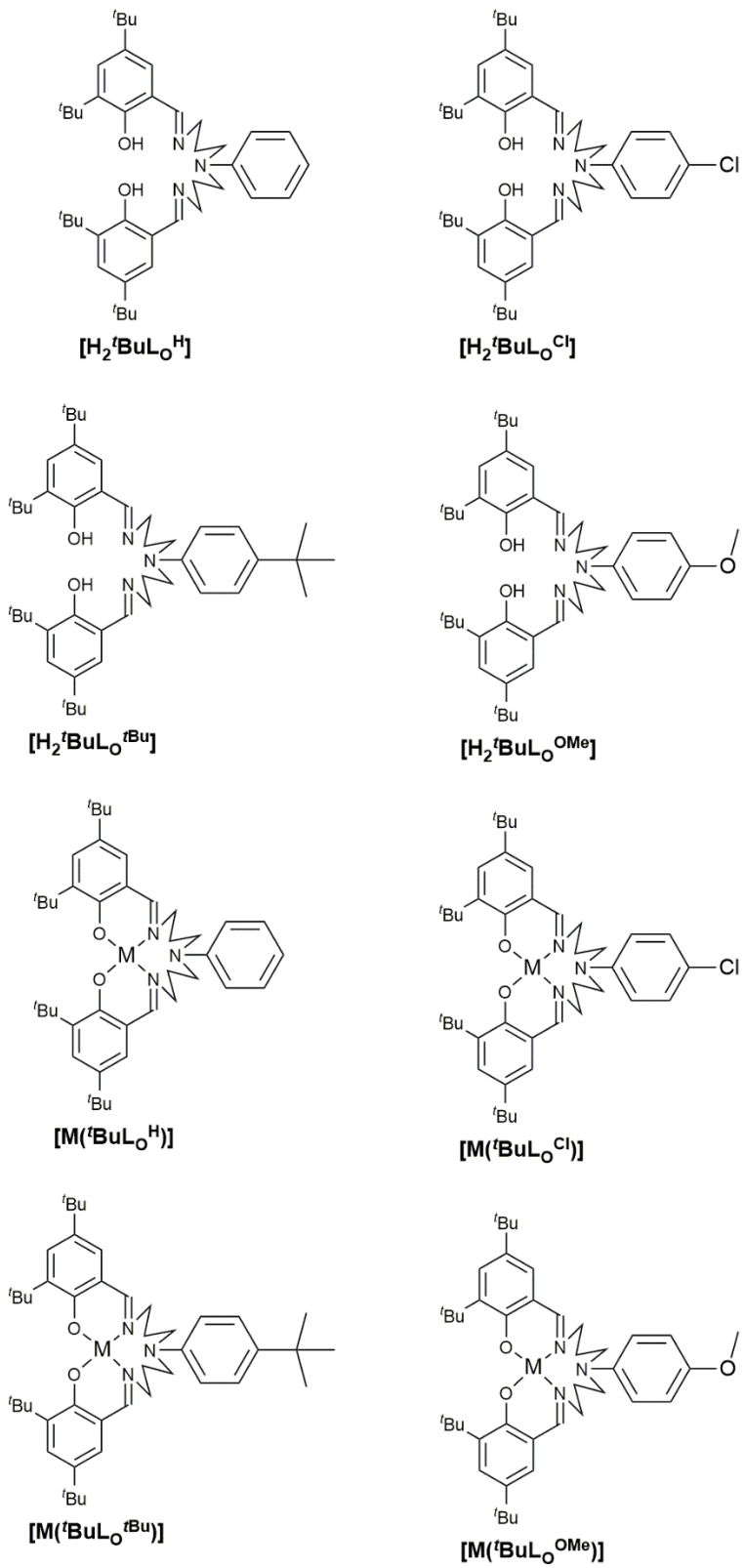
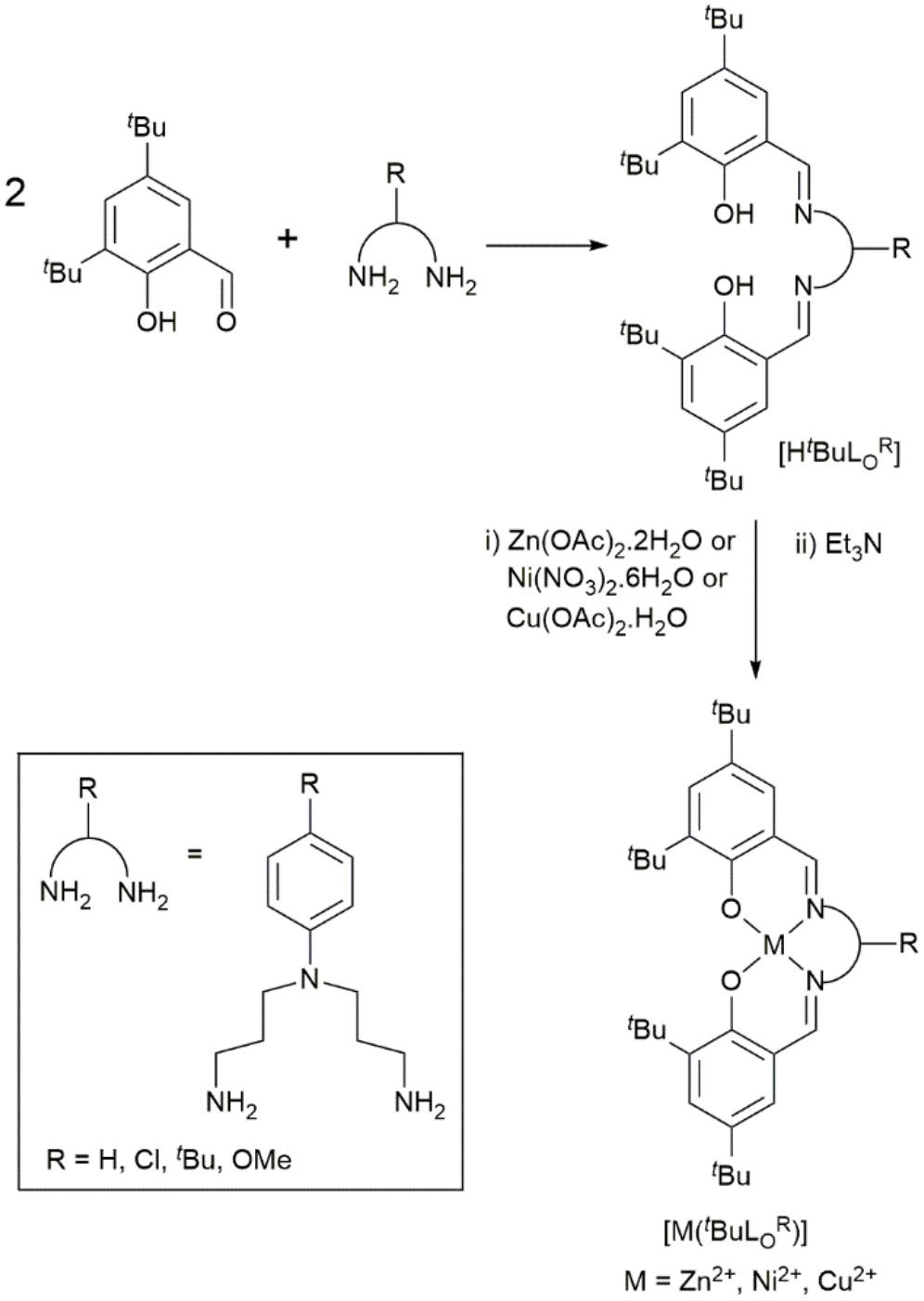


Figure 2.5 Schematic representation of the Zn(II), Ni(II) and Cu(II) Schiff-base diphenolate complexes discussed in this Chapter.

2.1.3 Syntheses of [$H_2{}^tBuL_O{}^R$] and [$M({}^tBuL_O{}^R)$] (M = Zn(II), Ni(II) and Cu(II)) and (R = H, Cl, ^{t}Bu, and OMe)

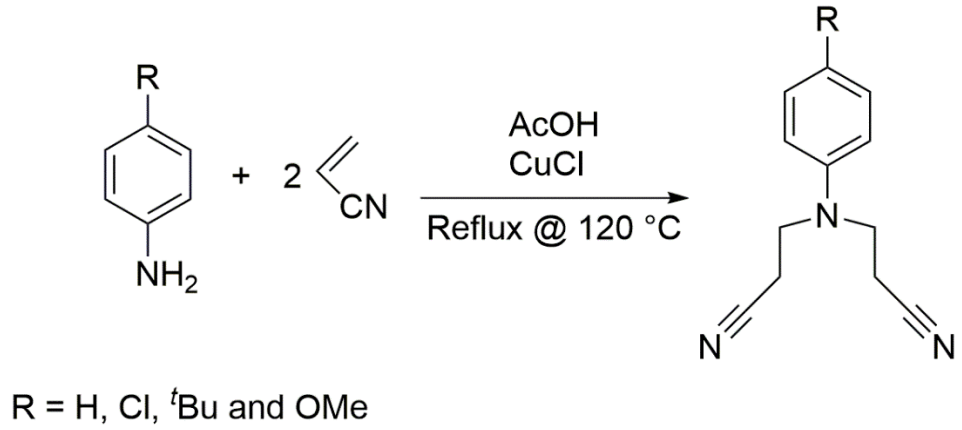
Synthetic methodologies for the preparation of Schiff-base diphenolate complexes that incorporate *2,4-tert*-butyl substitution on the phenolate rings are well documented[12,16,30,32] and have been adapted for attempts at the syntheses of the targets [$H_2{}^tBuL_O{}^R$] (R = H, Cl, ^{t}Bu, and OMe) (Figure 2.5) and their corresponding Zn(II), Ni(II) and Cu(II) Schiff-base diphenolate complexes, respectively. The general syntheses are shown in Scheme 2.2 and the target complexes [$M({}^tBuL_O{}^R)$] (M = Zn(II), Ni(II) and Cu(II)) and (R = H, Cl, ^{t}Bu, and OMe) are shown in Figure 2.5. In the following sections the attempted syntheses of these pro-ligands and metal complexes are discussed in detail.



Scheme 2.2 Attempted syntheses of $[H_2{}^tBuL_O{}^R]$ and $[M({}^tBuL_O{}^R)]$ (M = Zn(II), Ni(II) and Cu(II)) and (R = H, Cl, ^{t}Bu, and OMe).

2.2 Results and Discussion

2.2.1 Syntheses of *para*-functionalised di-nitriles



R = H, Cl, ^{t}Bu and OMe

Scheme 2.3 *General Scheme*: Synthesis of *para*-functionalised di-nitrile.

General Procedure: The syntheses of the *para*-functionalised di-nitrile compounds employed approaches that have been reported previously.[33] The appropriate aniline was dissolved in glacial acetic acid and acrylonitrile was then added to the reaction mixture drop-wise in the presence of CuCl powder. CuCl was incorporated to prevent the explosive polymerisation of acrylonitrile, which may occur during the reaction.[34,35] The reaction mixture was extracted with dichloromethane and the combined organic phases washed with an aqueous sodium hydroxide solution, dried over magnesium sulfate and reduced *in vacuo* to yield a crystalline solid. This brown solid was purified by re-crystallisation from ethanol. The synthesis of N1-(3-aminopropyl)-N1-phenylpropane-1,3-diamine was confirmed by ^{1}H-NMR, ^{13}C-NMR spectroscopies and mass spectrometry.

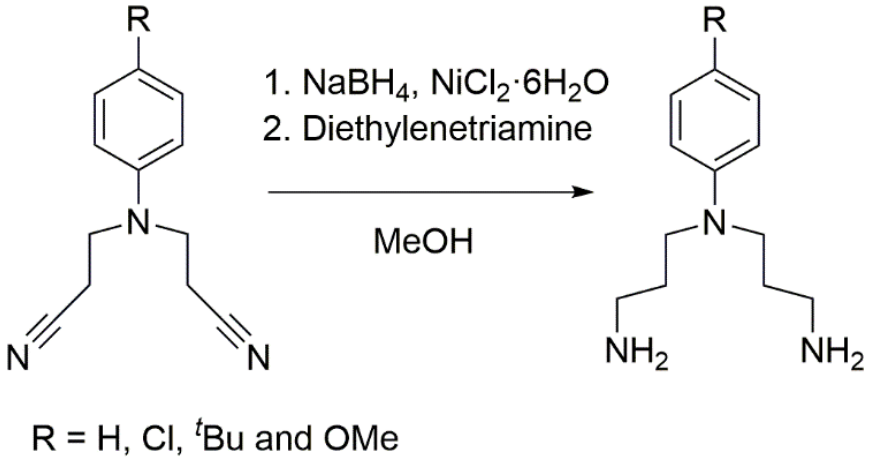
The synthetic yields of the *para*-functionalised di-nitrile are summarised in Table 2.2. It should be noted that the yields for each di-nitrile in some instances appeared to vary with respect to electron withdrawing or electron

donating properties of the *para*-functionalised aniline, which can be quantified *via* the p*K*a.[36]

Table 2.2 Synthetic yields of *para*-functionalised di-nitrile.

Nitrile	**Yield %**	**p*K*a**
3,3'-(phenylazanediyl)dipropanenitrile (H)	49	4.87
3,3'-[(4-chlorophenyl)azanediyl]dipropanenitrile (Cl)	22	3.98
3,3'-[(4-(tert-butyl)phenyl)azanediyl]dipropanenitrile (^{t}Bu)	32	4.93
3,3'-[(4-methoxyphenyl)azanediyl]dipropanenitrile (OMe)	51	5.36

2.2.2 Syntheses of *para*-functionalised di-amine bridges



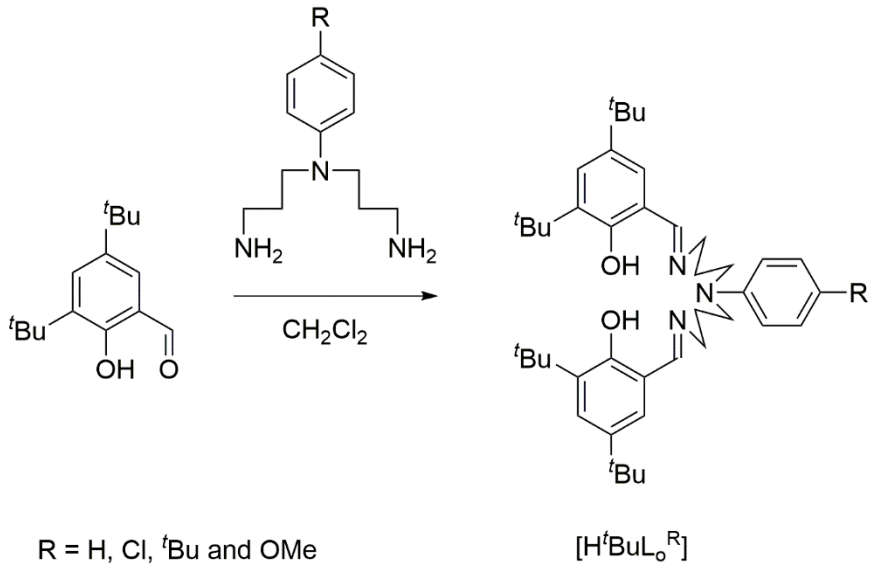
Scheme 2.4 *General Scheme*: Synthesis of *para*-functionalised di-amine bridges.

The syntheses of the *para*-functionalised di-propane amine compounds was achieved by the reduction of the dipropanenitrile compounds with sodium borohydride and used procedures which were adapted from the literature.[37] The progress of each reaction was followed via thin layer chromatography and a second addition of Ni(II) chloride and sodium borohydride was shown to improve the final yields of the reactions. The synthesis of each compound was confirmed via ^{1}H-NMR and ^{13}C-NMR spectroscopies, and by mass spectrometry. The synthetic yields of each compound are shown in Table 2.3.

Table 2.3 Synthetic yields of *para*-functionalised di-amine bridges

Nitrile	Yield %
N1-(3-aminopropyl)-N1-phenylpropane-1,3-diamine (H)	49
N1-(3-aminopropyl)-N1-(4-chlorophenyl)propane-1,3-diamine (Cl)	37
N1-(3-aminopropyl)-N1-(4-(tert-butyl)phenyl)propane-1,3-diamine (^{t}Bu)	70
N1-(3-aminopropyl)-N1-(4-methoxyphenyl)propane-1,3-diamine (OMe)	75

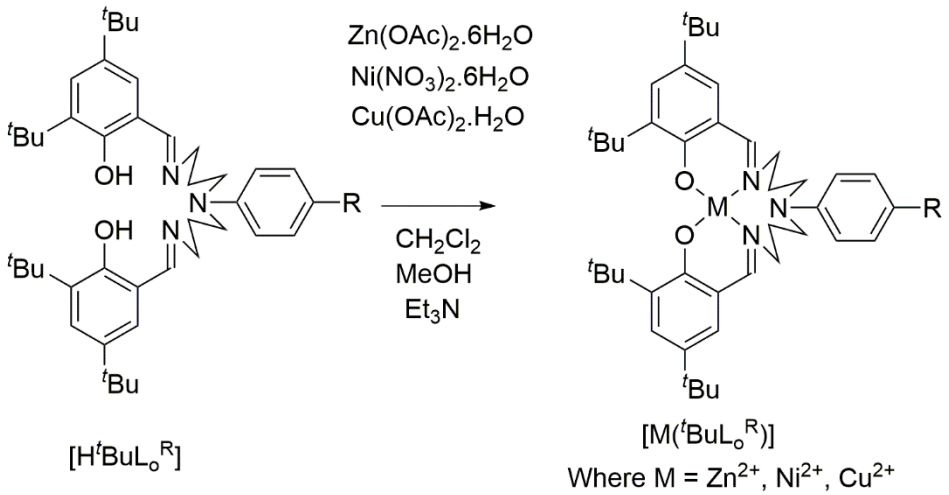
2.2.3 Syntheses of Schiff-base diphenolate ligands [$H_2{}^tBuL_O{}^R$] (R = H, Cl, ^{t}Bu or OMe)



Scheme 2.5 Synthesis of Schiff-base diphenolate ligands [$H_2{}^tBuL_O{}^R$] (R = H, Cl, ^{t}Bu or OMe)

The Schiff-base diphenolate ligands [$H_2{}^tBuL_O{}^R$], (R = H, Cl, ^{t}Bu or OMe), were synthesised by a condensation reaction between di-*tert*-butyl-2-hydroxybenzaldehyde and the previously synthesised functionalised di-amine (R = H, Cl, ^{t}Bu or OMe) in dichloromethane at room temperature for 2 hours (Scheme 2.5). The crude products were isolated as yellow oils and the formation of each [$H_2{}^tBuL_O{}^R$] (R = H, Cl, ^{t}Bu or OMe) was supported by ^{1}H NMR spectroscopy and by mass spectrometry. ^{1}H NMR spectroscopy identified the principal contaminant in each product as unreacted di-*tert*-butyl-2-hydroxybenzaldehyde. The crude pro-ligands were used in the attempted syntheses of [M(^{t}BuL$_O{}^R$)] (M = Zn(II), Ni(II), Cu(II) and R = H, Cl, ^{t}Bu or OMe) without further purification.

2.2.4 Attempted Syntheses of Diphenolate Schiff-base complexes containing [M(^{t}BuL$_O^R$)] (M = Zn(II), Ni(II), Cu(II) and R = H, Cl, ^{t}Bu or OMe)



Scheme 2.6 Attempted syntheses of diphenolate Schiff-base complexes containing [M(^{t}BuL$_O^H$)] (M = Zn(II), Ni(II), Cu(II))

Attempts to synthesise [M(^{t}BuL$_O^R$)] (M = Zn(II), Ni(II), Cu(II)) from crude [H$_2$^{t}BuL$_O^R$] (R = H, Cl, ^{t}Bu or OMe), triethylamine and the corresponding M(II) acetate or nitrate salt in dichloromethane (Scheme 2.6) were made. The reaction mixtures were heated at reflux for 24 hours and the solvent removed *in vacuo* to produce coloured powders. Attempts were made to purify each complex by recrystallisation from methanol and the formation of [M(^{t}BuL$_O^R$)] (M = Zn(II), R = Cl or OMe) and [M(^{t}BuL$_O^R$)] (M = Ni(II), Cu(II), R = H, Cl, ^{t}Bu or OMe) was confirmed by IR, and ^{1}H NMR spectroscopies, by mass spectrometry and by elemental analysis as appropriate. Overall yields ranged from *ca.* 28 – 66 %. Attempts to obtain pure [M(^{t}BuL$_O^R$)] (M = Zn(II), R = H or ^{t}Bu) were unsuccessful.

2.2.5 Single Crystal Structures of [Cu(^{t}BuLO^H)], [Cu(^{t}BuLO^{OMe})] and [Ni(^{t}BuLO^{OMe})]

Single crystals suitable for X-ray diffraction were obtained for [Cu(^{t}BuLO^H)], [Cu(^{t}BuLO^{OMe})] and [Ni(^{t}BuLO^{OMe})], and the structures of these compounds were determined by X-ray crystallography. Details of the structure solution and refinement are provided in Appendix 2.

2.2.5.1 Single Crystal Structures of [Cu(^{t}BuLO^H)] and [Cu(^{t}BuLO^{OMe})]

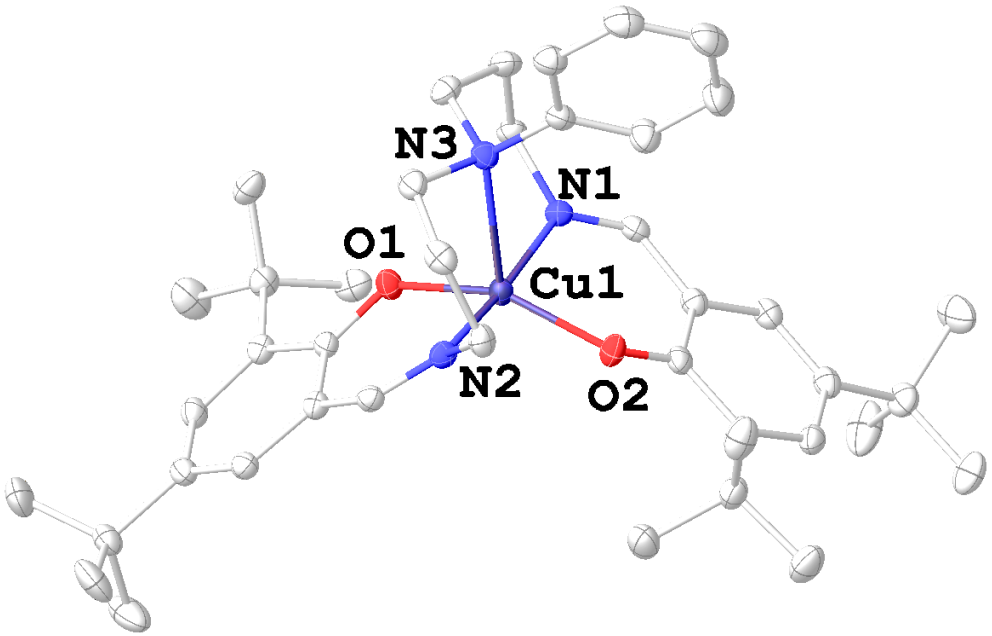


Figure 2.5 View of the x-ray crystal structure of [Cu(^{t}BuLO^H)] with H atoms omitted for clarity.

Table 2.4 Selected bond lengths (Å) and angles (°) with e.s.d.s for [Cu(^{t}BuL$_O^H$)].

[Cu(^{t}BuL$_O^H$)]	Bond lengths / Å	[Cu(^{t}BuL$_O^H$)]	Bond angles / °
Cu(1)-N(1)	1.9504(17)	N(1)-Cu(1)-N(2)	171.69(10)
Cu(1)-N(2)	1.9408(19)	N(1)-Cu(1)-N(3)	87.80(9)
Cu(1)-N(3)	2.579(2)	N(2)-Cu(1)-N(3)	83.92(7)
Cu(1)-O(1)	1.9389(16)	N(1)-Cu(1)-O(1)	91.65(8)
Cu(1)-O(2)	1.9419(14)	N(2)-Cu(1)-O(1)	90.43(7)
N(1)-C(1)	1.285(3)	N(3)-Cu(1)-O(1)	99.79(7)
N(1)-C(3)	1.470(3)	N(1)-Cu(1)-O(2)	91.35(7)
N(2)-C(2)	1.281(3)	N(2)-Cu(1)-O(2)	90.63(7)
N(2)-C(4)	1.472(3)	N(3)-Cu(1)-O(2)	108.46(8)
O(1)-C(16)	1.312(3)	O(1)-Cu(1)-O(2)	151.69(9)
O(2)-C(15)	1.307(3)	-	-

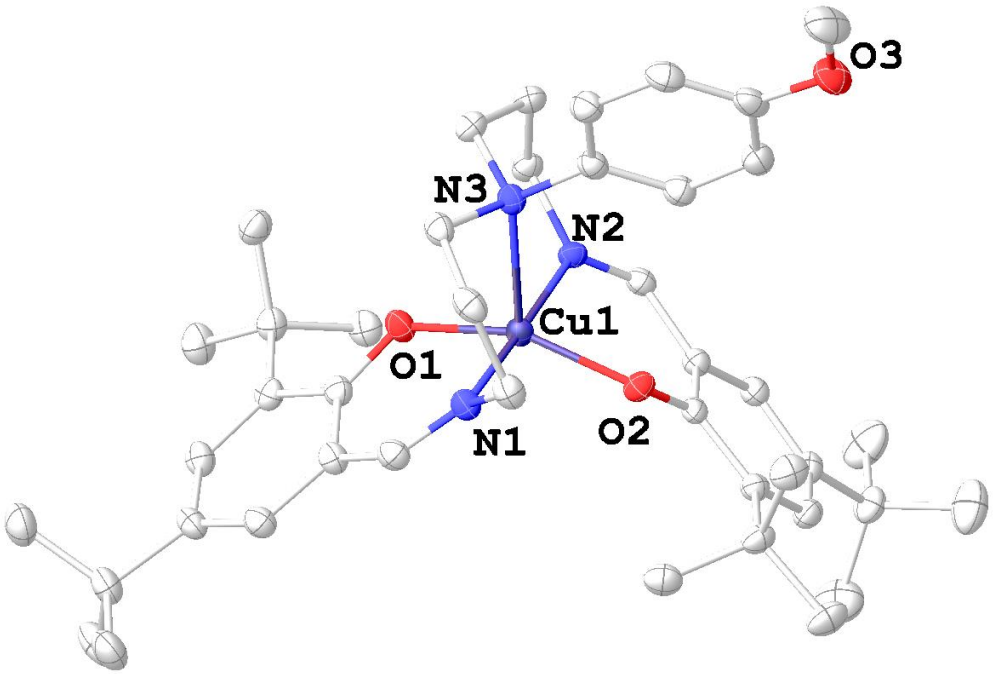


Figure 2.6 View of the X-ray crystal structure of [Cu(^{t}BuL$_O^{OMe}$)] with H atoms omitted for clarity.

Table 2.5 Selected bond lengths (Å) and angles (°) with e.s.d.s for [Cu(^{t}BuL$_O^{OMe}$)].

[Cu(^{t}BuL$_O^{OMe}$)]	Bond lengths / Å	[Cu(^{t}BuL$_O^{OMe}$)]	Bond angles / °
Cu(1)-N(1)	1.9593(16)	N(1)-Cu(1)-N(2)	177.77(7)
Cu(1)-N(2)	1.9565(17)	N(1)-Cu(1)-N(3)	90.68(6)
Cu(1)-N(3)	2.4511(17)	N(2)-Cu(1)-N(3)	87.11(6)
Cu(1)-O(1)	1.9376(14)	N(1)-Cu(1)-O(1)	90.00(6)
Cu(1)-O(2)	1.9399(14)	N(2)-Cu(1)-O(1)	90.85(6)
N(1)-C(1)	1.282(3)	N(3)-Cu(1)-O(1)	105.31(6)
N(1)-C(3)	1.467(2)	N(1)-Cu(1)-O(2)	90.60(6)
N(2)-C(2)	1.286(3)	N(2)-Cu(1)-O(2)	89.55(6)
N(2)-C(4)	1.461(3)	N(3)-Cu(1)-O(2)	101.08(6)
O(1)-C(16)	1.307(2)	O(1)-Cu(1)-O(2)	153.59(6)
O(2)-C(17)	1.307(2)	-	-

The Cu(II) centres in [Cu(^{t}BuL$_O^H$)] and [Cu(^{t}BuL$_O^{OMe}$)] (Figures 2.5 and 2.6) are coordinated by pentadentate dianionic ligands in a distorted square-based pyramidal coordination geometry, which was confirmed by their τ values, 0.33 and 0.39 respectively. The bond angles α and β, the two largest angles in the coordination sphere, determine the τ parameter (τ = (β-α)/60). The τ parameter[38] describes the degree of trigonality within the metal coordination sphere ranging from trigonal bipyramidal to square-based pyramidal. A τ = 0 corresponds to perfect square-based pyramidal geometry and a τ = 1 corresponds to perfect trigonal-bipyramidal geometry. Within the structures of [Cu(^{t}BuL$_O^H$)] and [Cu(^{t}BuL$_O^{OMe}$)] the four equatorial sites are occupied by two phenolate O-donors and two imine N-donors arranged in a *trans* configuration. The apical coordination site is occupied by the amine N-donor. The Cu(II)-O(phenolate) (*ca.* 1.94 Å) and Cu(II)-N(imine) (*ca.* 1.96 Å) bond distances are comparable to

those recorded for the analogous pentadentate N_3O_2 coordinated Cu(II) complexes [Cu(^{t}BuL$_O^{NMe}$)] and [Cu(^{t}BuL$_O^{C3N}$)] (Cu(II)-O(phenolate) = *ca.* 1.96 Å and Cu(II)-N(imine) = *ca.* 1.97 Å) and [Cu(salenN3)] (salenN3 = 2-({[3-(methyl{3-[(2-hydroxybenzylidene)amino]propyl}-amino)propyl]imino}-methyl)phenol) (Cu(II)-O(phenolate) = *ca.* 1.95 Å and Cu(II)-N(imine) = *ca.* 1.96 Å).[30,39]

The amine N-donor coordination, Cu(1)-N(3), for [Cu(^{t}BuL$_O^{OMe}$)] (2.4511(17) Å) is significantly shorter than the distance reported for [Cu(^{t}BuL$_O^{H}$)] (2.579(2) Å). This may be rationalised in terms of the differences in basicity of the amine N-donor in each compound that would be expected to follow the pK_a values of the parent substituted phenylamine compounds. The N-OMe donor in [Cu(^{t}BuL$_O^{OMe}$)] (pK_a of 4-methoxyphenylamine = 5.36) is a stronger base than that of the N-H donor in [Cu(^{t}BuL$_O^{H}$)] (p*K*a of phenylamine = 4.87). The stronger the base the stronger the bonding interaction between the N-donor and the metal centre hence the shorter M-N(3) distance in [Cu(^{t}BuL$_O^{OMe}$)] relative to that in [Cu(^{t}BuL$_O^{H}$)]. However, in comparison these bond lengths are significantly longer than the bond distances recorded for previous analogous pentadentate N_3O_2 Cu(II) complexes: [Cu(salenN3)] (salenN3 = 2-({[3-(methyl{3-[(2-hydroxybenzylidene)amino]-propyl}-amino)propyl]imino}methyl)phenol) (2.27(5) Å), [Cu(^{t}BuL$_O^{NMe}$)] and [Cu(^{t}BuL$_O^{C3N}$)], (2.34(11) Å and 2.26(3) Å). The difference in the Cu-N(3) bond lengths for [Cu(^{t}BuL$_O^{H}$)] and [Cu(^{t}BuL$_O^{OMe}$)] in comparison to [Cu(salenN3)], [Cu(^{t}BuL$_O^{NMe}$)] and [Cu(^{t}BuL$_O^{C3N}$)] can be attributed to the pK_a of the N-donor of the bridges. For [Cu(salenN3)] and [Cu(^{t}BuL$_O^{NMe}$)] (diethylamine pK_a =

10.75)[36] and for [Cu(^{t}BuL$_{O}^{C3N}$)] (triethylamine pK_a of 10.84)[36] in comparison to [Cu(^{t}BuL$_{O}^{H}$)] and [Cu(^{t}BuL$_{O}^{OMe}$)] (aniline pK_a = 4.87 and 4-methoxyaniline pK_a = 5.36). It appears that the difference in the pK_a is significant enough to have an impact of the Cu-N interaction and consequently the length of the Cu-N(3) bond; in [Cu(^{t}BuL$_{O}^{NMe}$)] and [Cu(^{t}BuL$_{O}^{C3N}$)], the M-N(3) bond length increases by *ca.* 0.08 Å, from 2.34(11) Å and 2.26(3) Å upon changing the N-donor from a secondary to a tertiary amine.

2.2.5.2 Single Crystal Structure of [Ni(^{t}BuLo^{OMe})]

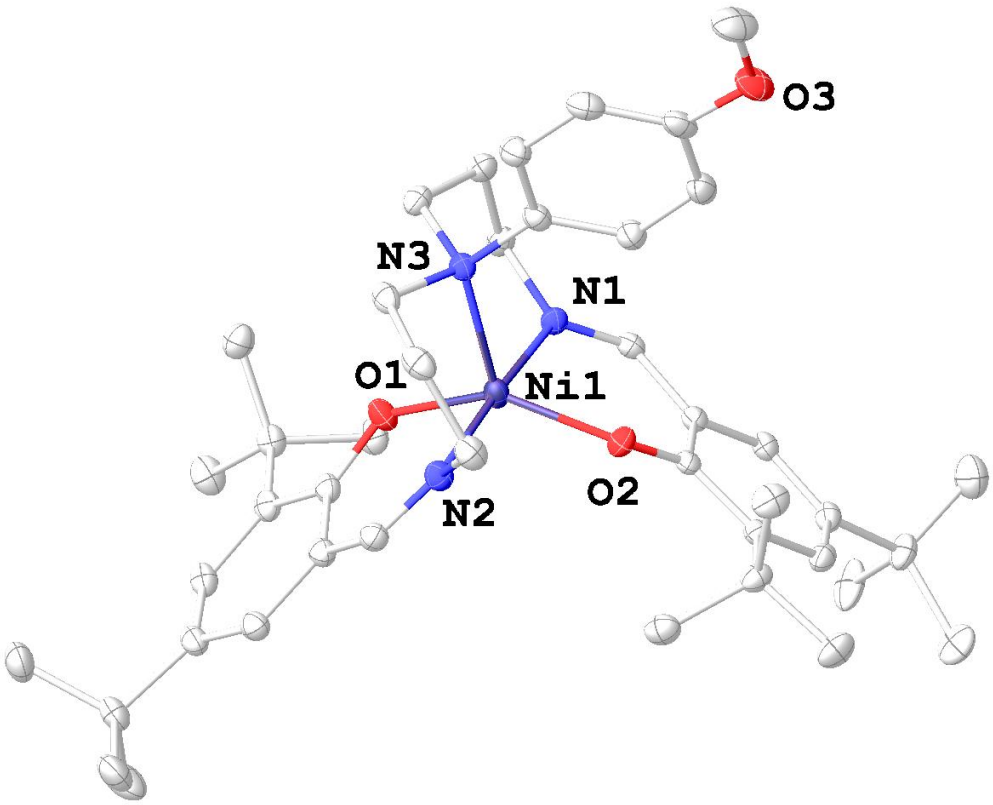


Figure 2.7 Views of the molecular structures of [Ni(^{t}BuLo^{OMe})] with H atoms omitted for clarity.

Table 2.6 Selected bond lengths (Å) and angles (°) with e.s.d.s for [Ni(^{t}BuLo^{OMe})].

[Ni(^{t}BuLo^{OMe})]	Bond lengths / Å	[Ni/.(^{t}BuLo^{OMe})]	Bond angles / °
Ni(1)-N(1)	1.9955(12)	N(1)-Ni(1)-N(2)	174.74(5)
Ni(1)-N(2)	1.9959(11)	N(1)-Ni(1)-N(3)	91.14(4)
Ni(1)-N(3)	2.1905(11)	N(2)-Ni(1)-N(3)	94.04(4)
Ni(1)-O(1)	1.9727(10)	N(1)-Ni(1)-O(1)	87.91(4)
Ni(1)-O(2)	1.9596(9)	N(2)-Ni(1)-O(1)	89.93(4)
N(1)-C(1)	1.2824(18)	N(3)-Ni(1)-O(1)	104.04(4)
N(1)-C(3)	1.4583(17)	N(1)-Ni(1)-O(2)	90.04(4)
N(2)-C(2)	1.2859(17)	N(2)-Ni(1)-O(2)	88.94(4)
N(2)-C(4)	1.4617(16)	N(3)-Ni(1)-O(2)	111.37(4)
O(1)-C(16)	1.3043(16)	O(1)-Ni(1)-O(2)	144.56(4)
O(2)-C(17)	1.3049(16)	-	-

[Ni(^{t}BuL$_{O}^{OMe}$)] (Figure 2.7 and Table 2.6) contains a five-coordinate monomeric Ni(II) centre coordinated by a N_3O_2 donor set derived from two phenolate O-donors, two imine N-donors and a tertiary amine N-donor, which is located on the N1-(3-aminopropyl)-N1-(4-methoxyphenyl)propane-1,3-diamine bridge. The bond angles (Table 2.6) show that the NiN_3O_2 core in [Ni(^{t}BuL$_{O}^{OMe}$)] adopts a distorted square-based pyramidal coordination geometry (τ = 0.55) in which the axial position is occupied by the N(amine) donor and the equatorial plane is occupied by the remaining two N(imine) and two O(phenolate) donors.

The Ni(II)-O(phenolate) (1.97(10) and 1.95(9) Å) and Ni(II)-N(imine) (1.99(12) and 1.99(11) Å) bond distances are comparable to those in [Ni(^{t}BuL$_{O}^{C3N}$)] and [Ni(^{t}BuL$_{O}^{NMe}$)], (Ni(II)-O(phenolate)= *ca.* 1.98 Å and 2.00 Å, respectively, and Ni(II)-N(imine) = 1.98 Å and 1.99 Å, respectively).[30,31] [Ni(Saldipa)] (Saldipa = bis(salicylidene-γ-iminopropyl)amine), [Ni(SalMeDPT)] (SalMeDPT = bis(salicylidene-γ-iminopropyl)methylamine) and [Ni(Me-sal)$_2$DPT] (Me-sal)$_2$DPT = *N*,*N*-bis(α-methylsalicylidene)dipropylenetriamine) also contain a Ni(II) centre within an N_3O_2 coordination sphere and possess Ni(II)-O(phenolate) and Ni(II)-N(imine) distances of *ca.* 1.93 - 2.02 Å and *ca.* 2.01 - 2.03 Å,respectively.[30,40–44]

The Ni(1)-N(3) distance [Ni(^{t}BuL$_{O}^{OMe}$)] (2.19 (11) Å) is longer than that found in [Ni(^{t}BuL$_{O}^{NMe}$)] and [Ni(^{t}BuL$_{O}^{3CN}$)] [Ni(1)-N(3) = 2.09(4) and 2.052(3) Å, respectively). This difference can be rationalised in terms of the pK_a values for the parent amines for each N(3) amine. For [Ni(^{t}BuL$_{O}^{NMe}$)] (diethylamine

pK_a = 10.75)[36] and for [Ni(^{t}BuL$_O^{C3N}$)] (triethylamine pK_a = 10.84)[36] in comparison to [Ni(^{t}BuL$_O^{OMe}$)] (4-methoxyaniline pK_a = 5.36).

The difference in M-N(3) bond length between [Ni(^{t}BuL$_O^{OMe}$)] (2.1905(11) Å) and [Cu(^{t}BuL$_O^{OMe}$)] (2.4511(17) Å) and [Cu(^{t}BuL$_O^{H}$)] (2.579(2) Å) might reflect a Jahn-Teller distortion that usually accompanies the coordination of ligands at the apical positions of a Cu(II) centre.[30,39]

2.2.6 EPR Spectroscopy of [Cu(^{t}BuL$_O^R$)] (R = H, OMe, ^{t}Bu and Cl)

X-band EPR spectra of [Cu(^{t}BuL$_{O}^{R}$)] (R = H, OMe, *t*Bu and Cl) as CH_2Cl_2 frozen solutions containing 0.4 M [N^{n}Bu$_4$][BF$_4$] were recorded at 77 K.

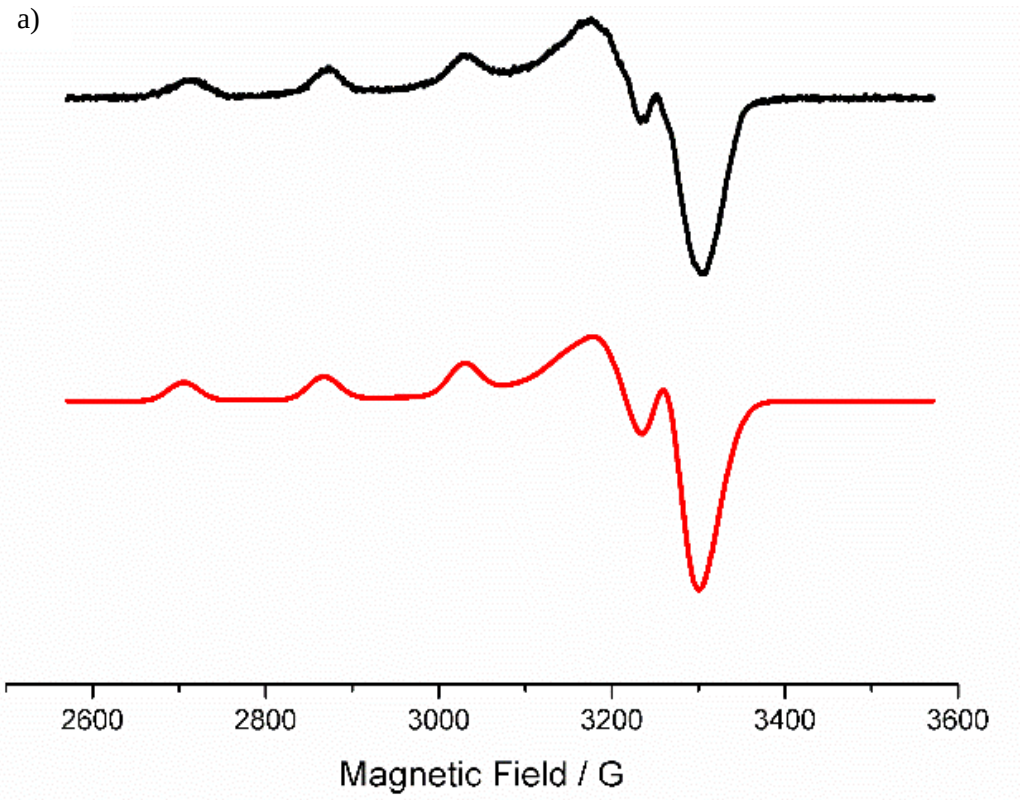
[Cu(^{t}BuL$_{O}^{R}$)] (R = H, OMe, *t*Bu and Cl) all exhibit rhombic S = ½ spectra with four features resolved in the low field region, which are assigned to hyperfine coupling of the unpaired electron with the ^{63,65}Cu (I = 3/2) nuclei. The experimental and simulated frozen solution X-band EPR spectra of [Cu(^{t}BuL$_{O}^{R}$)] R = H, OMe, *t*Bu and Cl) and are shown in Figure 2.8, and the spin Hamiltonian parameters derived from spectral simulation are shown in Table 2.7.

Table 2.7 EPR spin Hamiltonian parameters for [Cu(^{t}BuL$_{O}^{R}$)] R = H, OMe, *t*Bu and Cl).

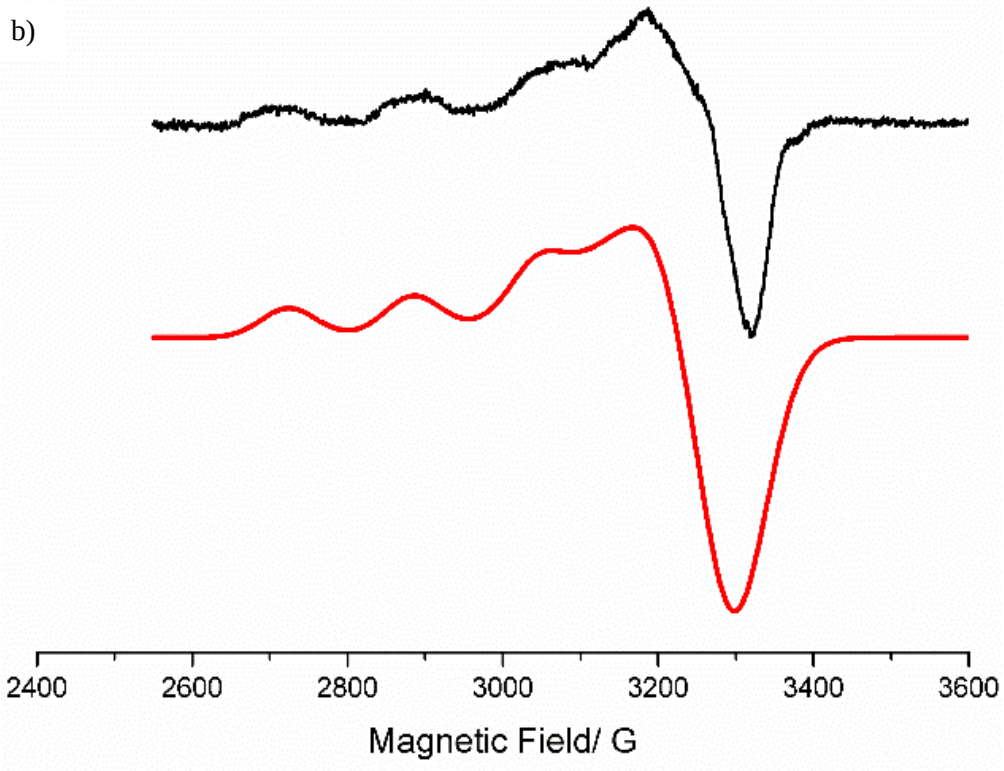
Complex	g_{11}	g_{22}	g_{33}	A_{11} / G	A_{22} / G	A_{33} / G
[Cu(^{t}BuL$_{O}^{H}$)]	2.050	2.060	2.238	40	15	160
[Cu(^{t}BuL$_{O}^{Cl}$)]	2.050	2.060	2.250	40	15	160
[Cu(^{t}BuL$_{O}^{tBu}$)]	2.050	2.060	2.250	42	18	162
[Cu(^{t}BuL$_{O}^{OMe}$)]	2.050	2.060	2.250	40	15	160

The spin Hamiltonian parameters reported for [Cu(^{t}BuL$_{O}^{R}$)] R = H, OMe, *t*Bu and Cl are similar to those recorded for the structurally analogous five coordinate square-based pyramidal Cu(II) complexes reported by Wieghardt *et al.* and Franks *et al*.[30] These parameters suggest that the N_3O_2 coordination spheres of [Cu(^{t}BuL$_{O}^{R}$)] R = H, OMe, *t*Bu and Cl are retained in solution.[7,30]

a)


2600
2800
3000
3200
3400
3600
Magnetic Field / G

b)


2400
2600
2800
3000
3200
3400
3600
Magnetic Field/ G

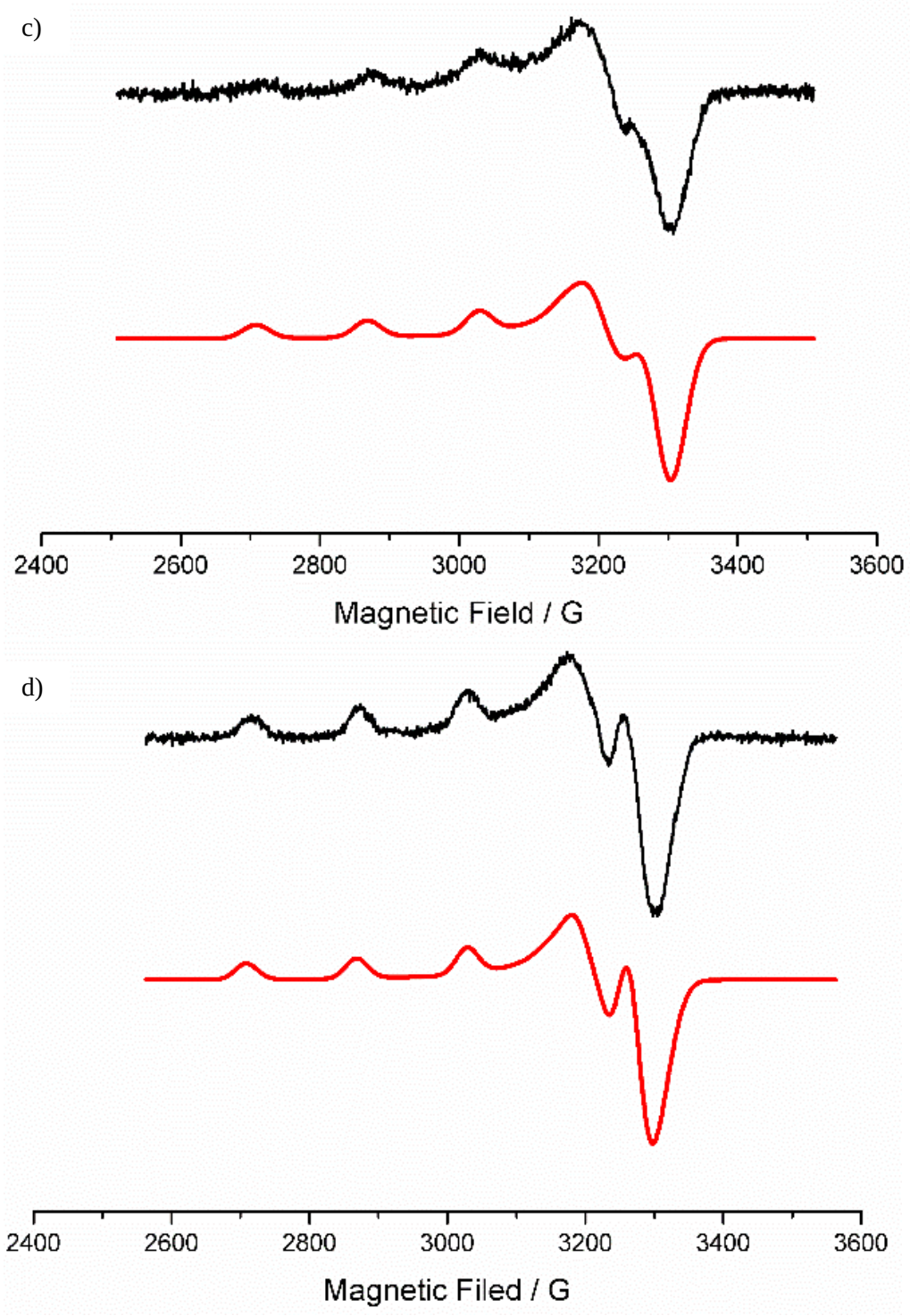


Figure 2.8 The frozen solution EPR spectra [Cu(^{t}BuL$_{O}^{R}$)] R = H, OMe, *t*Bu and Cl) (black) in CH_2Cl_2 at 77 K and simulated spectra (red). [Cu(^{t}BuL$_{O}^{H}$)] (a), [Cu(^{t}BuL$_{O}^{Cl}$)] (b), [Cu(^{t}BuL$_{O}^{tBu}$)] (c), and [Cu(^{t}BuL$_{O}^{OMe}$)] (d).

2.2.7 Electrochemical Studies of Crude [Zn(^{t}BuLO^R)] (R = H and ^{t}Bu), [Zn(^{t}BuLO^R)] (R = Cl and OMe), [M(^{t}BuLO^R)] (M = Ni(II) and Cu(II) , R = H, OMe, ^{t}Bu and Cl)

The cyclic voltammograms (CVs) of 1 mM solutions of crude [Zn(^{t}BuLO^R)] (R = H and ^{t}Bu), [Zn(^{t}BuLO^R)] (R = Cl and OMe) and [M(^{t}BuLO^R)] (M = Ni(II) and Cu(II), R = H, Cl, ^{t}Bu and OMe) in CH_2Cl_2 containing 0.4 M [N^{n}Bu$_4$][BF$_4$] as supporting electrolyte were recorded at 293K under an argon atmosphere. [M(^{t}BuLO^R)] show electrochemical processes between the ranges of 0.0 – 1.5 V *vs* Fc/Fc$^+$.

2.2.7.1 Cyclic Voltammetry of crude [Zn(^{t}BuLO^H)] and [M(^{t}BuLO^H)] (M = Ni(II) and Cu(II))

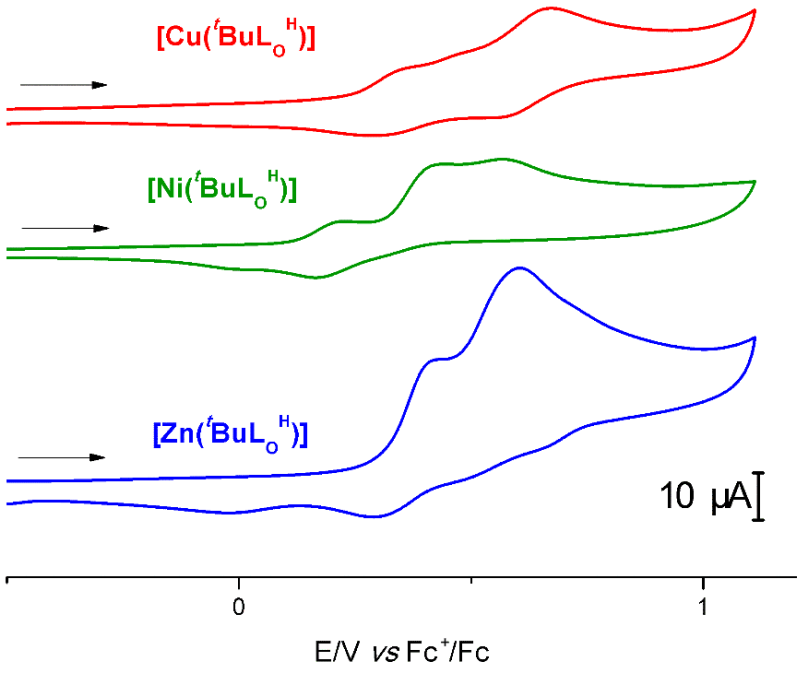


Figure 2.9 CVs of crude [Zn(^{t}BuLO^H)] and [M(^{t}BuLO^H)] (M = Ni(II), Cu(II)) (1 mM) at 293 K in CH_2Cl_2 containing 0.4 M [N^{n}Bu$_4$][BF$_4$] as supporting electrolyte at 100 mVs^{-1}.

Table 2.8 Summary of anodic and cathodic peak potentials at scan rate 100mVs^{-1} for [M(^{t}BuL$_{O}^{H}$)] [M = Zn(II)*, Ni(II), Cu(II)]. *electrochemical experiments were carried out on crude [Zn(^{t}BuL$_{O}^{H}$)] for comparative purposes.

Complex	Ep_a^1 *vs* Fc^+/Fc (V)	Ep_c^1 *vs* Fc^+/Fc (V)	Ep_a^2 *vs* Fc^+/Fc (V)	Ep_c^2 *vs* Fc^+/Fc (V)	Ep_a^3 *vs* Fc^+/Fc (V)	Ep_c^3 *vs* Fc^+/Fc (V)
[Zn(^{t}BuL$_{O}^{H}$)]*	0.43	0.28	0.58	-	-	-
[Ni(^{t}BuL$_{O}^{H}$)]	0.22	0.17	0.43	-	0.57	-
[Cu(^{t}BuL$_{O}^{H}$)]	0.37	0.28	0.67	0.57	-	-

The cyclic voltammetric data recorded for crude [Zn(^{t}BuL$_{O}^{H}$)] is poorly resolved (Figure 2.9). Two redox processes are apparent but because of the lack of separation between these processes they could not be studied separately. Consequently, for [Zn(^{t}BuL$_{O}^{H}$)] it is not possible to assign the oxidation peaks to the corresponding reduction peaks.

For [Ni(^{t}BuL$_{O}^{H}$)] the first redox process occurs at Ep_a^1 = 0.22 V with an associated return wave at Ep_c^1 = 0.17 V *vs* Fc/Fc^+ and there are two additional two oxidation peaks at Ep_a^2 = 0.43 V and Ep_a^3 = 0.57 V *vs* Fc/Fc^+ with no associated return waves (Figure 2.9). The first redox process occurs at a lower potential of Ep_a^1 = 0.22 V *vs* Fc^+/Fc relative to those for crude [Zn(^{t}BuL$_{O}^{H}$)] and [Cu(^{t}BuL$_{O}^{H}$)] (Ep_a^1 = 0.43 and 0.33 V *vs* Fc^+/Fc, respectively). The third oxidation peak at Ep_a^3 = 0.57 V *vs* Fc/Fc^+ for [Ni(^{t}BuL$_{O}^{H}$)] is only apparent at scan rates $\leq$ 100 mVs^{-1} and is not observed at scan rates $\geq$ 100 mVs^{-1}.

For [Cu(^{t}BuL$_{O}^{H}$)] the first oxidation process occurs at Ep_a^1 = 0.37 V with an associated return wave at Ep_c^1 = 0.28 V *vs* Fc/Fc^+ and the second at Ep_a^2 = 0.67 V with an associated return wave at Ep_c^2 = 0.57 V *vs* Fc/Fc^+ (Figure 2.9). These processes are not electrochemically reversible and suggest that the

oxidation products of [Cu(^{t}BuL$_O^H$)] are unstable over the timescale of the electrochemical experiments.

2.2.7.2 Cyclic Voltammetry of [M(^{t}BuL$_O^{Cl}$)] (M = Zn(II), Ni(II) and Cu(II))

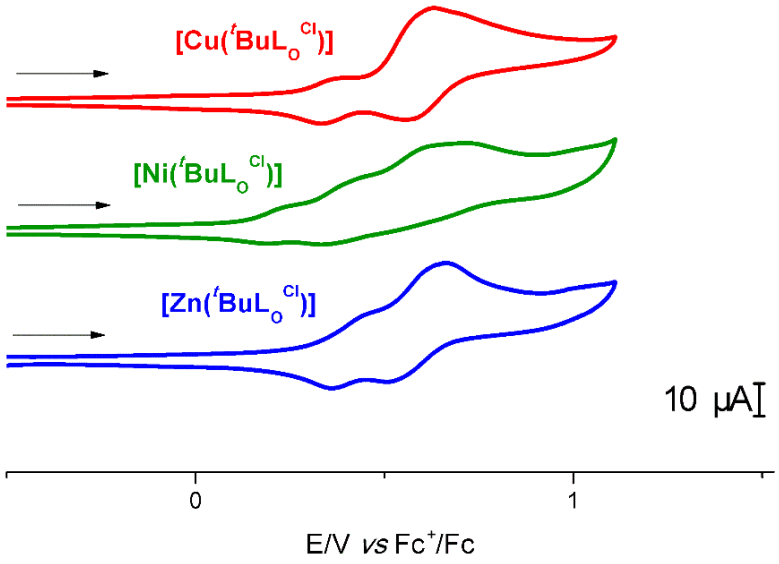


Figure 2.10 CVs of [M(^{t}BuL$_O^{Cl}$)] (M = Zn(II), Ni(II), Cu(II)) (1 mM) at 293 K in CH_2Cl_2 containing 0.4 M [N^{n}Bu$_4$][BF$_4$] as supporting electrolyte at 100 mVs^{-1}.

Table 2.9 Summary of anodic and cathodic peak potentials at scan rate 100mVs^{-1} for [M(^{t}BuL$_O^{Cl}$)] (M = Zn(II), Ni(II), Cu(II)).

Complex	Ep_a^1 *vs* Fc^+/Fc (V)	Ep_c^1 *vs* Fc^+/Fc (V)	Ep_a^2 *vs* Fc^+/Fc (V)	Ep_c^2 *vs* Fc^+/Fc (V)
[Zn(^{t}BuL$_O^{Cl}$)]	0.45	0.35	0.66	0.50
[Ni(^{t}BuL$_O^{Cl}$)]	0.23	0.17	0.69	0.37
[Cu(^{t}BuL$_O^{Cl}$)]	0.37	0.33	0.63	0.55

The cyclic voltammogram of [Zn(^{t}BuL$_O^{Cl}$)] possesses two irreversible redox processes at Ep_a^1 = 0.45V and Ep_c^1 = 0.35 *vs* Fc/Fc^+ and a second at Ep_a^2 = 0.66 and Ep_c^2 = 0.50 *vs* Fc/Fc^+ (Figure 2.10 and Table 2.9). The second redox process of [Zn(^{t}BuL$_O^{Cl}$)] loses its return reduction peak, Ep_c^2 = 0.50 *vs* Fc/Fc^+, at slower scan rates $\leq$ 100 mVs^{-1} and at faster scan rates the reduction peak begins to re-appear $\geq$ 100 mVs^{-1}. This suggests that the oxidation product decomposes over the timescale of the experiment. At higher scan rates the timescale of the reaction is short compared to the lifetime of the oxidised compound and the CV resembles that of a reversible process. However, at slower scan rates the oxidised species decomposes before the return sweep is complete and no return reduction peak is observed.

The cyclic voltammograms of [Ni(^{t}BuL$_O^{Cl}$)] and [Cu(^{t}BuL$_O^{Cl}$)] (Figure 2.10) show two irreversible redox processes. For [Ni(^{t}BuL$_O^{Cl}$)] these occur at Ep_a^1 = 0.23 V and Ep_c^1 = 0.17 V *vs* Fc/Fc^+ and at Ep_a^2 = 0.69 V and Ep_c^2 = 0.37 V *vs* Fc/Fc^+, respectively. For [Cu(^{t}BuL$_O^{Cl}$)] these processes occur at Ep_a^1 = 0.37 V, and Ep_c^1 = 0.33 V *vs* Fc/Fc^+ and at Ep_a^2 = 0.63 V and Ep_c^2 = 0.55 V *vs* $Fc/Fc^{+\cdot}$ For [Ni(^{t}BuL$_O^{Cl}$)] and [Cu(^{t}BuL$_O^{Cl}$)] the reduction peaks for the irreversible processes, Ep_c^1 and Ep_c^2, disappear at slower scan rates $\leq$ 100 mVs^{-1} and at faster scan rates $\geq$ 100 mVs^{-1} the reduction peaks to re-appear. Thus, the electrochemical data for [Ni(^{t}BuL$_O^{Cl}$)] and [Cu(^{t}BuL$_O^{Cl}$)] suggest that the oxidation products for both complexes are unstable over the timescale of the electrochemical experiment.

2.2.7.3 Electrochemical studies of crude [Zn(^{t}BuLO^{tBu})] and [M(^{t}BuLO^{tBu})] (M = Ni(II) and Cu(II))

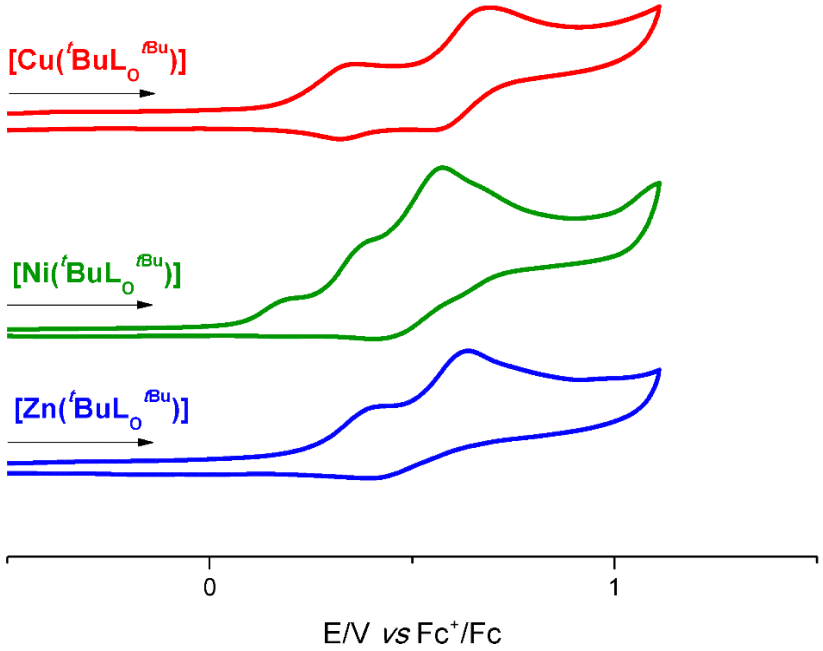


Figure 2.11 CVs of crude [Zn(^{t}BuLO^{tBu})] and [M(^{t}BuLO^{tBu})] (M = Ni(II), Cu(II)) (1 mM) at 293 K in CH_2Cl_2 containing 0.4 M [N^{n}Bu$_4$][BF_4] as supporting electrolyte at 100 mVs^{-1}

Table 2.10 Summary of anodic and cathodic peak potentials at scan rate 100mVs-1 for [M(^{t}BuLO^{tBu})] (M = Zn(II)*, Ni(II), Cu(II)). *electrochemical experiments were carried out on crude [Zn(^{t}BuLO^{tBu})] for comparative purposes.

Complex	Ep_a^1 *vs* Fc^+/Fc (V)	Ep_c^1 *vs* Fc^+/Fc (V)	Ep_a^2 *vs* Fc^+/Fc (V)	Ep_c^2 *vs* Fc^+/Fc (V)	Ep_a^3 *vs* Fc^+/Fc (V)	Ep_c^3 *vs* Fc^+/Fc (V)
[Zn(^{t}BuLO^{tBu})]*	0.41	0.39	0.63	-	-	-
[Ni(^{t}BuLO^{tBu})]	0.18	-	0.38	-	0.57	0.42
[Cu(^{t}BuLO^{tBu})]	0.35	0.32	0.69	0.54	-	-

The cyclic voltammogram of crude [Zn(^{t}BuLO^{tBu})] possesses two irreversible redox processes at Ep_a^1 = 0.41V and Ep_c^1 = 0.39 *vs* Fc/Fc$^+$ (Figure 2.11 and Table 2.10). The first redox process losses its reduction peak, Ep_c^1 = 0.39 *vs* Fc/Fc$^+$, at slower scan rates ≤ 100 mVs^{-1} and then at faster scan rates ≥

100 mVs^{-1} the reduction peak begins to re-appear. This redox behaviour is consistent with the oxidation products of crude [Zn($^{t}BuL_{O}^{tBu}$) being unstable over the timescale of the electrochemical experiment.

The cyclic voltammogram of [Ni($^{t}BuL_{O}^{tBu}$)] (Figure 2.11) shows oxidation peaks at Ep_a^1 = 018 V, Ep_a^2 = 0.38 V and Ep_a^3 = 0.57 V *vs* Fc/Fc^+ and a reduction peak at Ep_c^1 = 0.42 V *vs* Fc/Fc^+. The cyclic voltammogram of [Cu($^{t}BuL_{O}^{tBu}$)] (Figure 2.11) shows two irreversible redox processes at Ep_a^1 = 0.35 V and Ep_c^1 = 0.32 V *vs* Fc/Fc^+ and the second at Ep_a^2 = 0.69 V and Ep_c^2 = 0.54 V *vs* Fc/Fc^+. For [Ni($^{t}BuL_{O}^{tBu}$)] and [Cu($^{t}BuL_{O}^{tBu}$)] the reduction peaks for the irreversible processes, Ep_c^1 and Ep_c^2, disappear at slower scan rates $\leq$ 100 mVs^{-1} and at higher scan rates $\geq$ 100 mVs^{-1} the reduction peaks re-appear. Thus, the electrochemical data for [Ni($^{t}BuL_{O}^{tBu}$)] and [Cu($^{t}BuL_{O}^{tBu}$)] suggests that both complexes follow an EC mechanism on oxidation.

2.2.7.4 Electrochemical studies of [M(^{t}BuL$_O^{OMe}$)] (M = Zn(II), Ni(II), Cu(II))

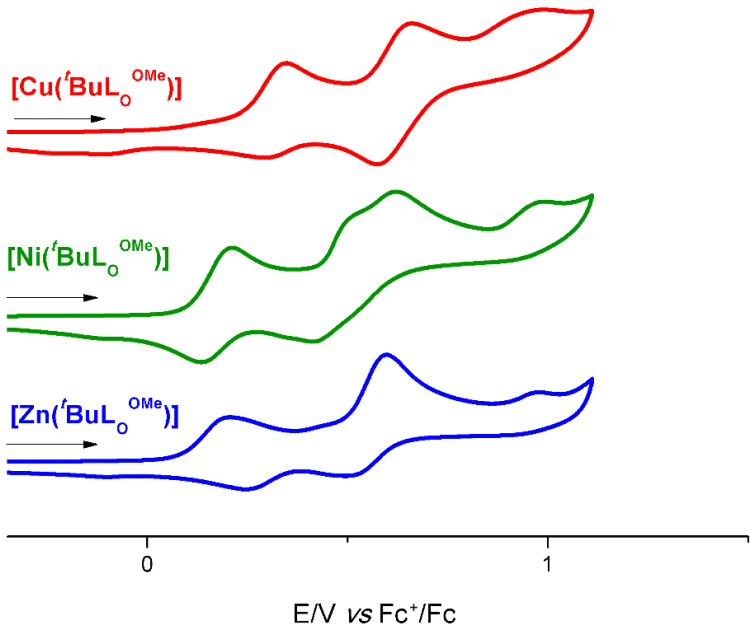


Figure 2.12 CVs of [M(^{t}BuL$_O^{OMe}$)] (M = Zn(II), Ni(II), Cu(II)) (1 mM) at 293 K in CH_2Cl_2 containing 0.4 M [N^{n}Bu$_4$][BF$_4$] as supporting electrolyte at 100 mVs^{-1}

The cyclic voltammograms of (1 mM) solutions of [M(^{t}BuL$_O^{OMe}$)] (M = Zn(II), Ni(II) and Cu(II)) in CH_2Cl_2 containing 0.4 M [N^{n}Bu$_4$][BF$_4$] as supporting electrolyte were recorded at 293K under Ar (Figure 2.12 and Table 2.11).

Table 2.11 Summary of anodic and cathodic peak potentials at scan rate 100mVs-1 for [M(^{t}BuL$_O^{OMe}$)] (M = Zn(II), Ni(II), Cu(II))

Complex	Ep_a^1 *vs* Fc^+/Fc (V)	Ep_c^1 *vs* Fc^+/Fc (V)	$E_{½}^1$ *vs* Fc^+/Fc (V)	Ep_a^2 *vs* Fc^+/Fc (V)	Ep_c^2 *vs* Fc^+/Fc (V)	$E_{½}^2$ *vs* Fc^+/Fc (V)
[Zn(^{t}BuL$_O^{OMe}$)]	0.20	0.12	0.16	0.59	0.50	-
[Ni(^{t}BuL$_O^{OMe}$)]	0.20	0.13	0.17	0.63	0.44	-
[Cu(^{t}BuL$_O^{OMe}$)]	0.34	0.26	0.30	0.66	0.57	0.62

The cyclic voltammograms of [Zn(^{t}BuL$_O^{OMe}$)] showed two redox processes. The first redox process of [Zn(^{t}BuL$_O^{OMe}$)] demonstrated electrochemical reversibility, $E_{½}^1$ = 0.16 V *vs* Fc/Fc$^+$, whereas the second redox process, Ep_a^2 = 0.59 V and Ep_a^2 = 0.50 V *vs* Fc/Fc$^+$, was irreversible and demonstrated an EC mechanism.

The cyclic voltammograms of [Ni(^{t}BuL$_O^{OMe}$)] and [Cu(^{t}BuL$_O^{OMe}$)] show two redox processes (Figure 2.12). As for [Zn(^{t}BuL$_O^{OMe}$)] the first redox process of [Ni(^{t}BuL$_O^{OMe}$)] demonstrated electrochemical reversibility, $E_{½}^1$ = 0.17 V *vs* Fc/Fc$^+$, whereas the second redox process was irreversible, Ep_a^2 = 0.63 V and Ep_c^2 = 0.44 V *vs* Fc/Fc$^+$, and demonstrated an EC mechanism. However, for [Cu(^{t}BuL$_O^{OMe}$)] both redox processes observed were both electrochemically reversible occurring at $E_{½}^1$ = 0.30 V and $E_{½}^2$ = 0.62V *vs* Fc/Fc$^+$ respectively.

The processes that demonstrated electrochemical reversibility will now be further investigated during the remainder of this chapter.

2.2.7.5 Summary of the Cyclic Voltammetric data for [M(^{t}BuL$_O^R$)] M = Zn(II), Ni(II) and Cu(II)) and (R = H, Cl, ^{t}Bu and OMe)

Investigations into the electrochemical properties of crude [Zn(^{t}BuL$_O^R$)] (R = H, ^{t}Bu), [Zn(^{t}BuL$_O^R$)] (R = Cl, OMe) and [M(^{t}BuL$_O^R$)] (M = Ni(II) and Cu(II), R = H, Cl, ^{t}Bu and OMe) in CH_2Cl_2 by cyclic voltammetric methods show that these compounds support at least two oxidation processes between 0.04 V and 0.70 V *vs* Fc^+/Fc. For all complexes except [M(^{t}BuL$_O^{OMe}$)] (M = Zn(II), Ni(II) and Cu(II)) the electrochemistry observed is irreversible. For [M(^{t}BuL$_O^{OMe}$)] (M = Zn(II), Ni(II) and Cu(II)) the first oxidation processes (and second for [Cu(^{t}BuL$_O^{OMe}$)]) are electrochemically reversible. These complexes will be further investigated for the remainder of the chapter.

The range of observed redox potentials for [M(^{t}BuL$_O^R$)] can be attributed to the *para*-functionality of the benzene ring and its impact on the donating abilities of the bridging N-donor amine. The pK_a of the parent amine used to synthesise the ligand provides an indication of the availability of the lone pair of the pendant amine to bind to the metal centre. We suggest the higher the pK_a, the stronger the potential bond between this amine donor and the metal centre. In addition the greater the electron donation from the amine group to the metal centre the more electron rich the metal centre becomes which manifests as a lower oxidation potential for the metal complex.

This trend was observed for the Zn(II) and Ni(II) complexes with oxidation potentials decreasing with decreasing pK_a values. However, this trend was not observed for the [Cu(^{t}BuL$_O^R$)] complexes (R = H, Cl, ^{t}Bu and OMe) whose redox potentials remained essentially invariant despite changing the *para*-

substituted functionality upon the *N*-donor bridge. This can be attributed to the M(1)-N(3) bond due to the Jahn-Teller distortion that usually accompanies the coordination of ligands at the apical positions of a Cu(II) centre and which has been confirmed in the crystal structures of [Cu(^{t}BuL$_O^H$)] and [Cu(^{t}BuL$_O^{OMe}$)] (Section 2.2.5). [30,39] Here the bonding interaction between the M(1)-N(3) will be inherently weaker and thus there will be reduced modulation of electron density at the metal centre by the pendant bridge.

In comparison to the analogous metal complexes, [M(^{t}BuL$_O^R$)] (M = Zn(II), Ni(II) and Cu(II)) and (R = NMe and C3N), synthesised by Franks *et al.* the redox potentials observed for [M(^{t}BuL$_O^R$)] (M = Ni(II), Cu(II), R = H, Cl, ^{t}Bu and OMe), are higher.[30,31] This can be attributed to the lower pK_a values of the bridging N-donor amines in [M(^{t}BuL$_O^R$)] (M = Zn(II), Ni(II) and Cu(II), R = NMe and C3N)[30,31] than those of the bridging N-donor amines discussed in this chapter (R = H, Cl, ^{t}Bu and OMe).

The redox potentials for [Cu(^{t}BuL$_O^{OMe}$)] are higher than those of its Ni(II) and Zn(II) counterparts that may be associated with the anticipated antiferromagnetic coupling between the unpaired electrons of the d^9 Cu(II) centre and those of the pendant phenoxyl radicals that are generated following oxidation of the [Cu(^{t}BuL$_O^{OMe}$)] complex.[45]

2.2.7.6 Cyclic Voltammetry and Coulometry of [Zn(^{t}BuL$_O^{OMe}$)]

The first redox process of [Zn(^{t}BuL$_O^{OMe}$)] occurs at 0.16 V *vs* Fc/Fc$^+$ (Figure 2.13). The values of ΔE_1 for the first oxidation process of [Zn(^{t}BuL$_O^{OMe}$)] are to those of the Fc$^+$/Fc couple recorded under the same conditions (Table 2.12) . The variations of $I_p^{a/c}$ with √(scan rate for the first process are shown below and demonstrate that $I_p^{a/c}$ is proportional to √(scan rate (Figure 2.14). These tests, when considered in combination, indicate that the [Zn(^{t}BuL$_O^{OMe}$)]$^{+/0}$ couple is an electrochemically reversible redox process.

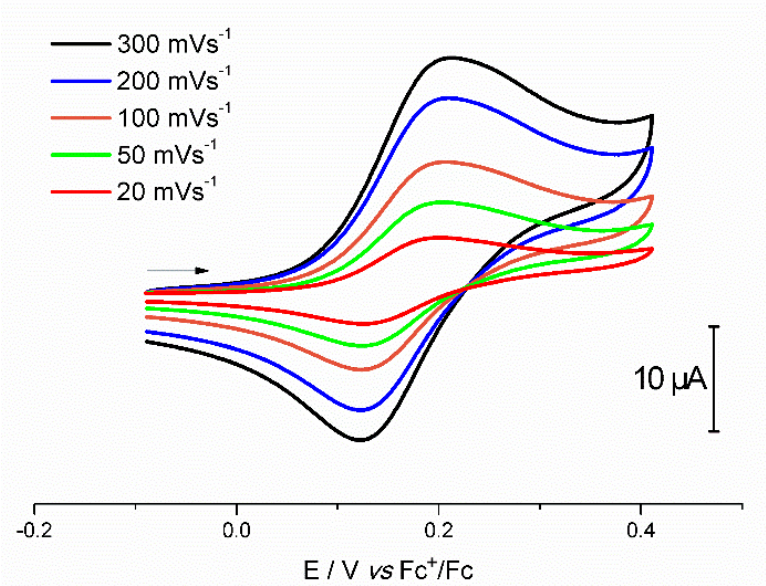


Figure 2.13 Cyclic Voltammograms of the first oxidation process recorded for [Zn(^{t}BuL$_O^{OMe}$)] (1 mM) at 293 K in CH_2Cl_2 containing 0.4 M [N^{n}Bu$_4$][BF$_4$] as supporting electrolyte at multiple scan rates.

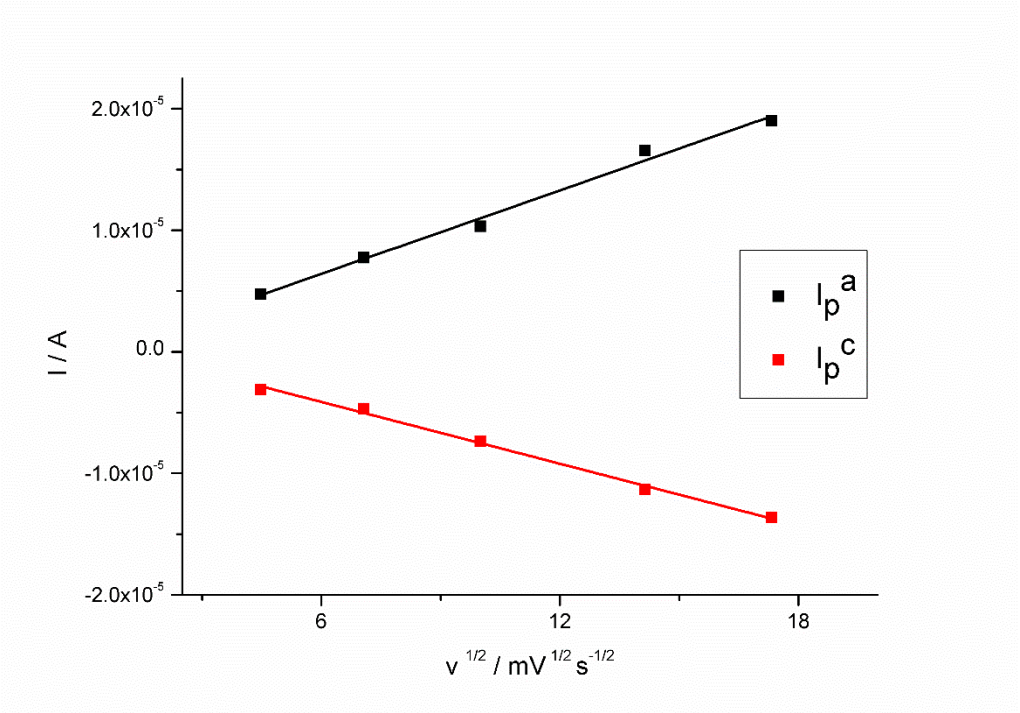


Figure 2.14 Variation of the I_p^a and I_p^c with √(scan rate) for the $[Zn(^tBuL_O^{OMe})]^{+/0}$ couple at 293 K

Table 2.12 Variation of ΔE with scan rate for Fc^+/Fc and for the $[Zn(^tBuL_O^{OMe})]^{+/0}$ couple at 293 K.

Scan Rate / mVs^{-1}	**$[Zn(^tBuLO^{OMe})]$ ΔE_1 / mV**	**Fc^+/Fc ΔE / mV**
20	70	70
50	70	70
100	80	80
200	90	80
300	100	90

Coulombic measurements for the first redox process of [Zn(^{t}BuL$_{O}^{OMe}$)] were recorded at a potential of 0.40 V *vs* Fc/Fc^{+} (Figure 2.15). This measurement confirmed that the first oxidation process is a single electron process as the observed Q = 0.48 C value was the same as the theoretical value of Q for a one-electron process.

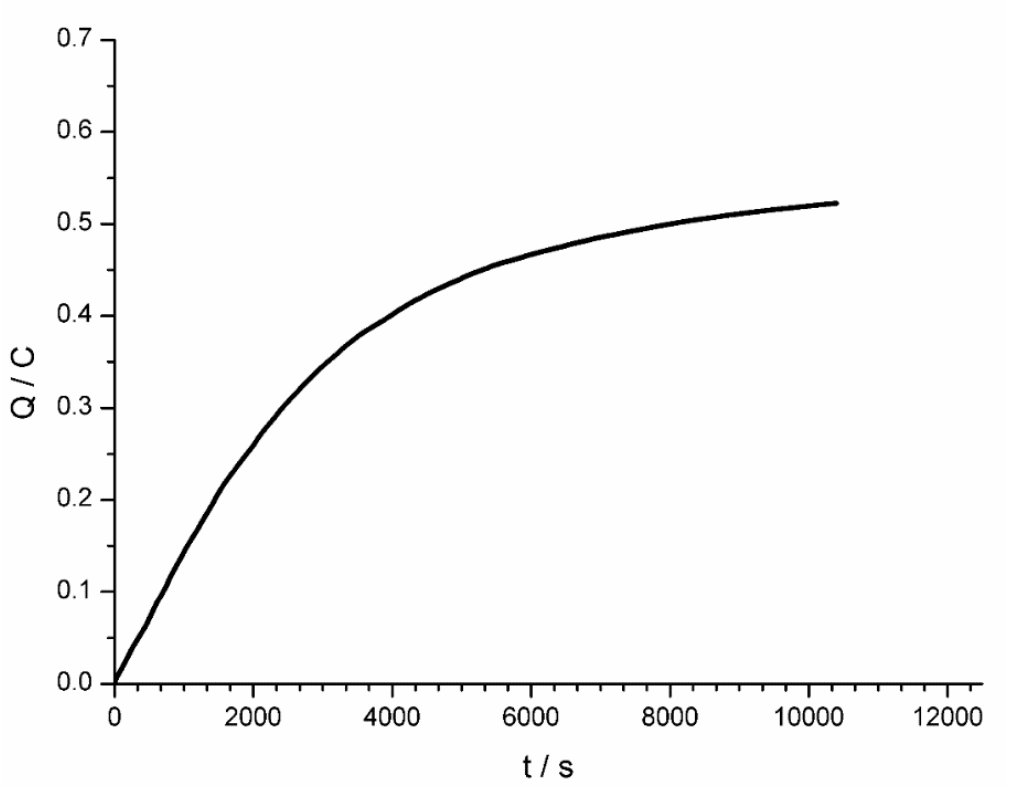


Figure 2.15 Controlled potential electrolysis of [Zn(^{t}BuL$_{O}^{OMe}$)] to [Zn(^{t}BuL$_{O}^{OMe}$)]$^{+}$ at 0.40 V *vs* Fc^{+}/Fc (1 mM) at 253 K in CH_2Cl_2 containing 0.4 M [N^{n}Bu$_4$][BF$_4$] as supporting electrolyte. Theoretical value of Q for a one-electron process = 0.48 C.

The previously reported Zn(II)-diphenolate complexes [Zn(^{t}BuL$_{O}^{C3N}$)], [Zn(^{t}BuL$_{O}^{NMe}$)] (Figure 2.2) and [Zn(^{t}BuL$_{O}^{1}$)$_2$] (H^{t}BuL$_{O}^{1}$ = 2'-(4',6'-di-*tert*-butylhydroxyphenyl)-4,5-diphenyl imidazole), (Figure 2.1), all exhibit two reversible one-electron oxidation processes at 0.29 and 0.50, 0.30 and 0.54, and 0.23 and 0.49 V *vs* Fc^{+}/Fc respectively.[30,31,46] These redox processes have been

assigned as ligand-based given the redox inactive nature of the d^{10} metal centre over the potential range used within the experiment. The redox processes are associated with the successive one-electron oxidation of each coordinated phenolate donor, leading to the formation of $[Zn(L^{\bullet})(L)]^{+}$ and $[Zn(L^{\bullet})_2]^{2+}$ (L is a phenolate donor).[31]

$$[Zn(L)_2] \underset{+1e^-}{\overset{-1e^-}{\rightleftharpoons}} [Zn(L)^{\bullet}(L)]^{+} \underset{+1e^-}{\overset{-1e^-}{\rightleftharpoons}} [Zn(L)_2^{\bullet}]^{2+}$$

Thus, we propose that the first $[Zn(^{t}BuL_O^{OMe})]^{+/0}$ process is ligand-based and results in the generation of a phenoxyl radical unit bound to the Zn(II) centre.[11,30,45–48] The oxidation of $[Zn(^{t}BuL_O^{OMe})]^{+}$ to $[Zn(^{t}BuL_O^{OMe})]^{2+}$ is associated with an irreversible redox process and we propose that oxidation of $[Zn(^{t}BuL_O^{OMe})]^{+}$ generates a species containing two phenoxyl radical ligands that decomposes on the timescale of the electrochemical experiment.

2.2.7.7 Cyclic Voltammetry and Coulometry of [Ni(^{t}BuL$_O^{OMe}$)]

The first redox process of [Ni(^{t}BuL$_O^{OMe}$)] occurs at 0.17 V *vs* Fc/Fc$^+$ (Figure 2.16). The values of ΔE at different scan rates for this first oxidation process are similar to those of the Fc$^+$/Fc couple (Table 2.13). The variation of $I_p^{a/c}$ with √(scan rate) and demonstrate that $I_p^{a/c}$ is proportional to √(scan rate) (Figure 2.17). These tests are indicative of an electrochemically reversible redox process for [Ni(^{t}BuL$_O^{OMe}$)]$^{+/0}$.

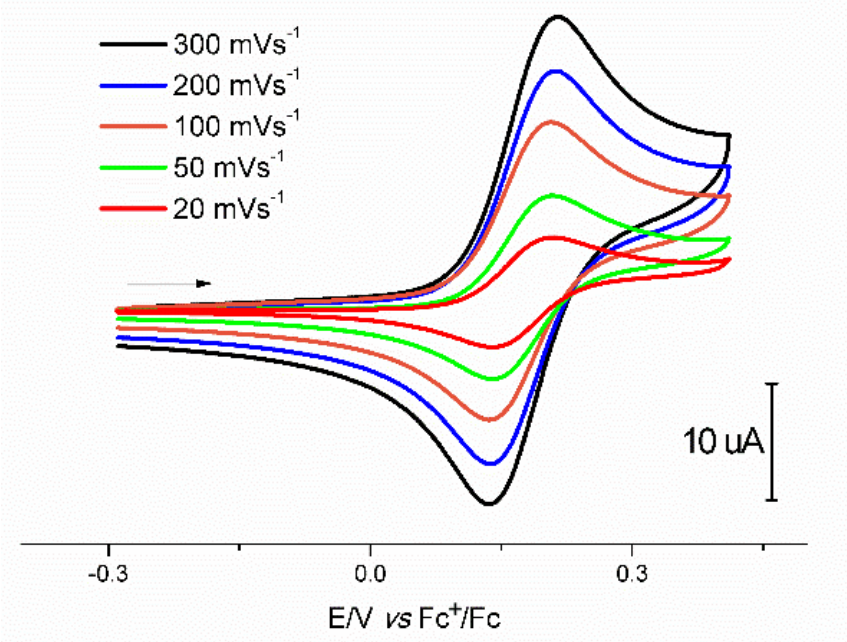


Figure 2.16 Cyclic voltammograms of the first oxidation process recorded for [Ni(^{t}BuL$_O^{OMe}$)] (1 mM) at 293 K in CH_2Cl_2 containing 0.4 M [N^{n}Bu$_4$][BF$_4$] as supporting electrolyte at multiple scan rates.

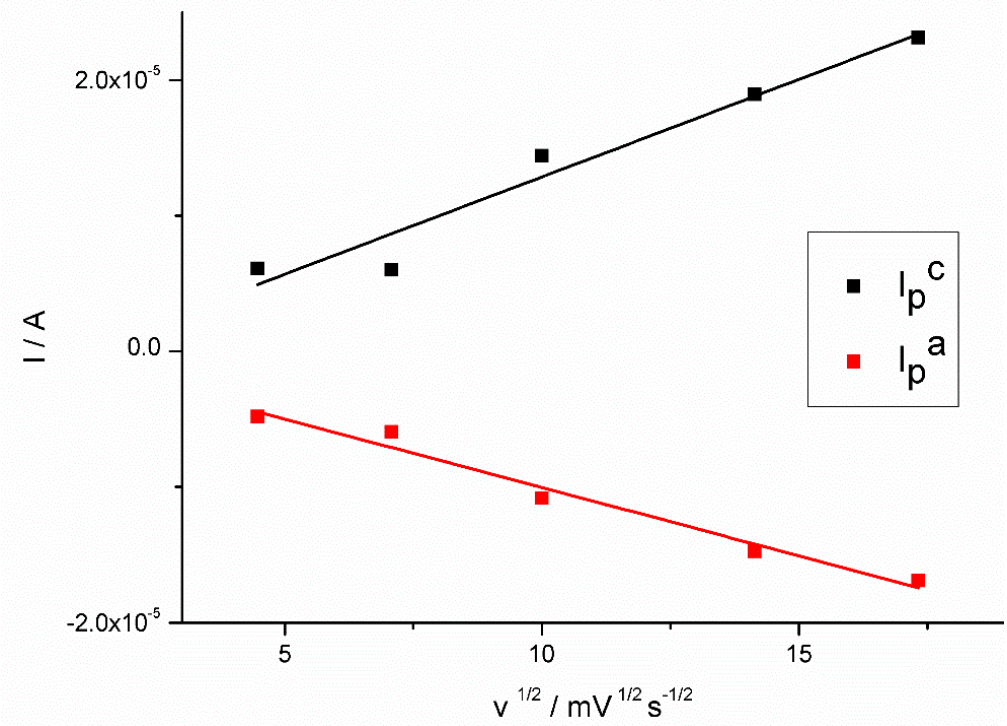


Figure 2.17 Variation of the I_p^a and I_p^c with √(scan rate) for the $[Ni(^tBuL_O^{OMe})]^{+/0}$ couple at 293 K.

Table 2.13 Variation of ΔE with scan rate for the Fc^+/Fc and the $[Ni(^tBuL_O^{OMe})]^{+/0}$ couples at 293 K.

Scan Rate / mVs^{-1}	**$[Zn(^tBuLO^{OMe})]$ ΔE_1 / mV**	**Fc+/Fc ΔE / mV**
20	70	70
50	70	70
100	80	80
200	90	80
300	100	90

Coulombic measurements for the first redox process for [Ni(^{t}BuL$_{O}^{OMe}$)] were recorded at potential of 0.41 V *vs* Fc/Fc^{+} (Figure 2.18). This measurement confirmed that the first oxidation process is a single electron process as the observed Q = 0.48 C value is similar to the theoretical value of Q for a one-electron process.

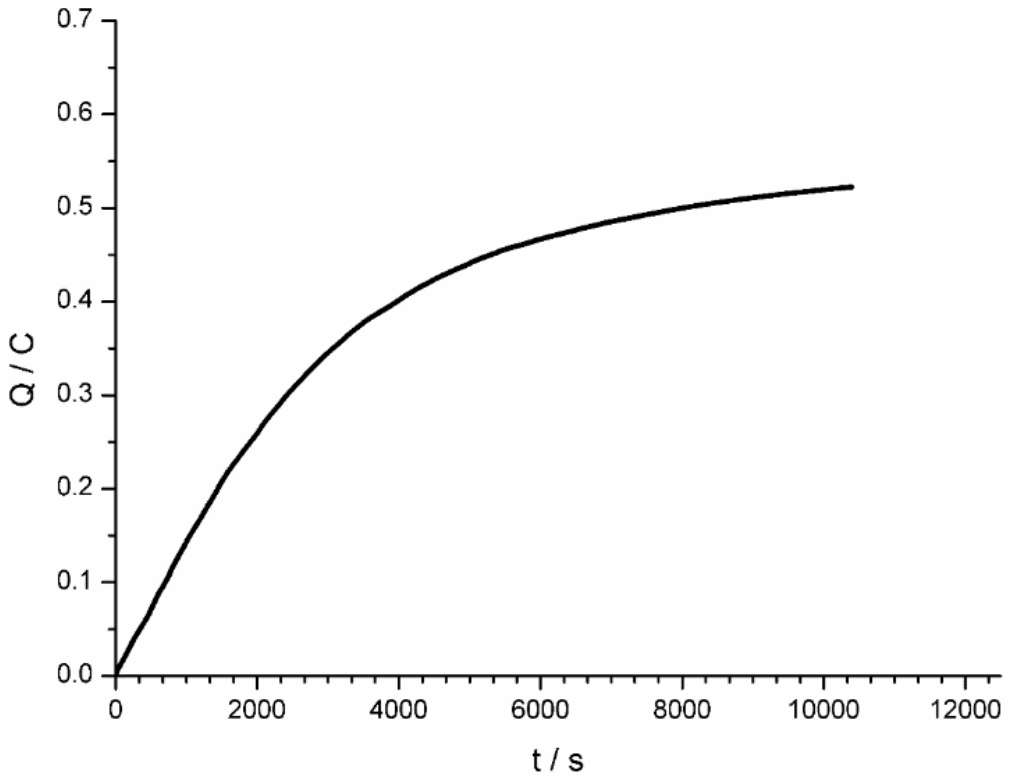


Figure 2.18 Controlled potential electrolysis of [Ni(^{t}BuL$_{O}^{OMe}$)] to [Ni(^{t}BuL$_{O}^{OMe}$)]$^{+}$ at 0.40 V *vs* Fc^{+}/Fc (1 mM) at 253 K in CH_2Cl_2 containing 0.4 M [N^{n}Bu$_4$][BF$_4$] as supporting electrolyte. Theoretical value of Q for a one-electron process = 0.49 C.

Ni phenolate complexes containing phenolate ligands within their coordination sphere have been observed to undergo either metal or ligand based oxidation processes due to the ligand- and metal-based frontier orbitals lying close in energy to one another.[12] The nature of the one-electron oxidation processes of Ni(II)-phenolate complexes may reside somewhere between the

two redox extremes involving either metal centred (Ni(III)-phenolate) or ligand centred (Ni(II)-phenoxyl radical) oxidation.[8,12,16–18,21–24,26–28] The first oxidation processes of [Ni(^{t}BuL$_O^{NMe}$)] and [Ni(^{t}BuL$_O^{C3N}$)] have been assigned by spectroelectrochemistry and EPR spectroscopy as metal-based oxidation processes resulting in the formation of a Ni(III) centre.[30,31] In contrast the spectrochemical and EPR spectroscopic measurements are consistent with the second oxidation process being ligand-based with the generation of a phenoxyl radical centre.[30,31] Given that [Ni(^{t}BuL$_O^{NMe}$)], [Ni(^{t}BuL$_O^{C3N}$)] and [Ni(^{t}BuL$_O^{OMe}$)] possess similar coordination spheres, we propose that the first oxidation of [Ni(^{t}BuL$_O^{OMe}$)] is formally metal-based. Future spectroelectrochemical and EPR spectroscopic studies will be undertaken to confirm this assignment.

2.2.7.8 Cyclic Voltammetry and Coulometry of [Cu(^{t}BuL$_O^{OMe}$)]

The first redox process of [Cu(^{t}BuL$_O^{OMe}$)] occurs at 0.30 V *vs* Fc/Fc$^+$ and a second redox process occurs at 0.62 V *vs* Fc/Fc$^+$. The values of ΔE for the first and second oxidation processes of [Cu(^{t}BuL$_O^{OMe}$)] (Figures 2.19 and 2.20, Tables 2.14 and 2.15) are similar to those for the Fc$^+$/Fc couple. The variation of $I_p^{a/c}$ with √(scan rate) for the first process (Figure 2.21) and second process (Figure 2.22) demonstrates that $I_p^{a/c}$ is proportional to √(scan rate). These tests are indicative of an electrochemically reversible redox processes.

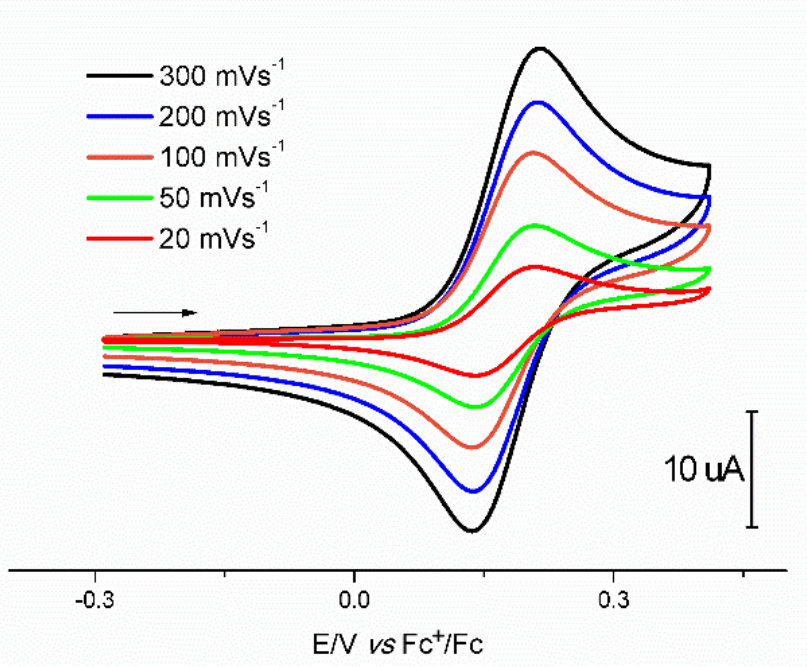


Figure 2.19 Cyclic Voltammograms of the first oxidation processes recorded for [Cu(^{t}BuL$_O^{OMe}$)] (1 mM) at 293 K in CH_2Cl_2 containing 0.4 M [N^{n}Bu$_4$][BF$_4$] as supporting electrolyte at multiple scan rates.

Table 2.14 Variation of ΔE with scan rate for the Fc^{+}/Fc and the $[Cu(^{t}BuL_{O}^{OMe})]^{+/0}$ couples at 293 K,

Scan Rate / mVs^{-1}	$[Cu(^{t}BuLO^{OMe})]$ ΔE_1 / mV	Fc+/Fc ΔE / mV
20	70	70
50	70	70
100	80	80
200	80	80
300	90	90

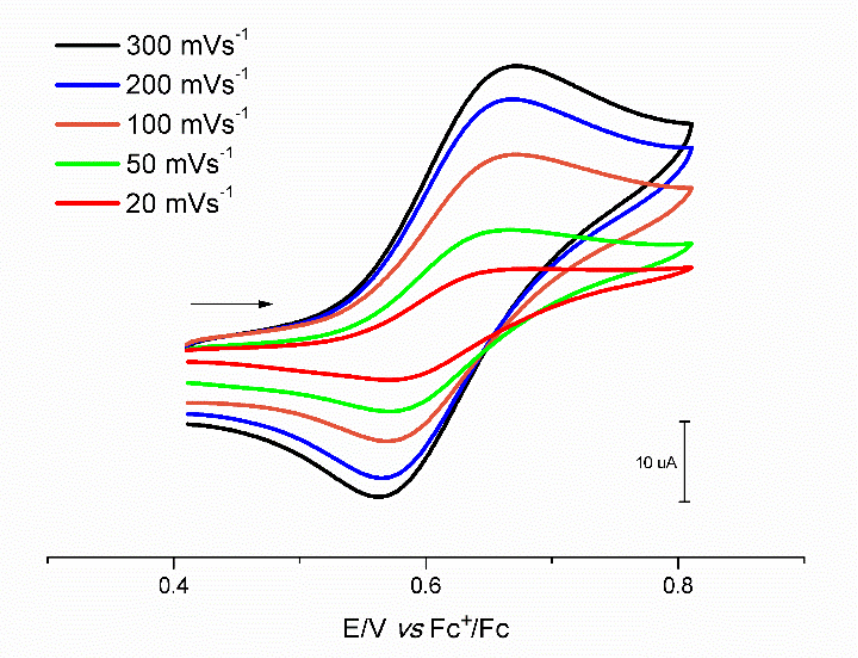


Figure 2.20 Cyclic Voltammograms of the second oxidation processes recorded for $[Cu(^{t}BuL_{O}^{OMe})]$ (1 mM) at 293 K in CH_2Cl_2 containing 0.4 M $[N^{n}Bu_4][BF_4]$ as supporting electrolyte at multiple scan rates.

Table 2.15 Variation of ΔE with scan rate for the Fc^{+}/Fc and the $[Cu(^{t}BuL_{O}^{OMe})]^{2+/+}$ couples at 293 K.

Scan Rate / mVs^{-1}	**$[Cu(^{t}BuLO^{OMe})]$ ΔE_2 / mV**	**Fc+/Fc ΔE / mV**
20	70	70
50	70	70
100	80	80
200	90	80
300	100	90

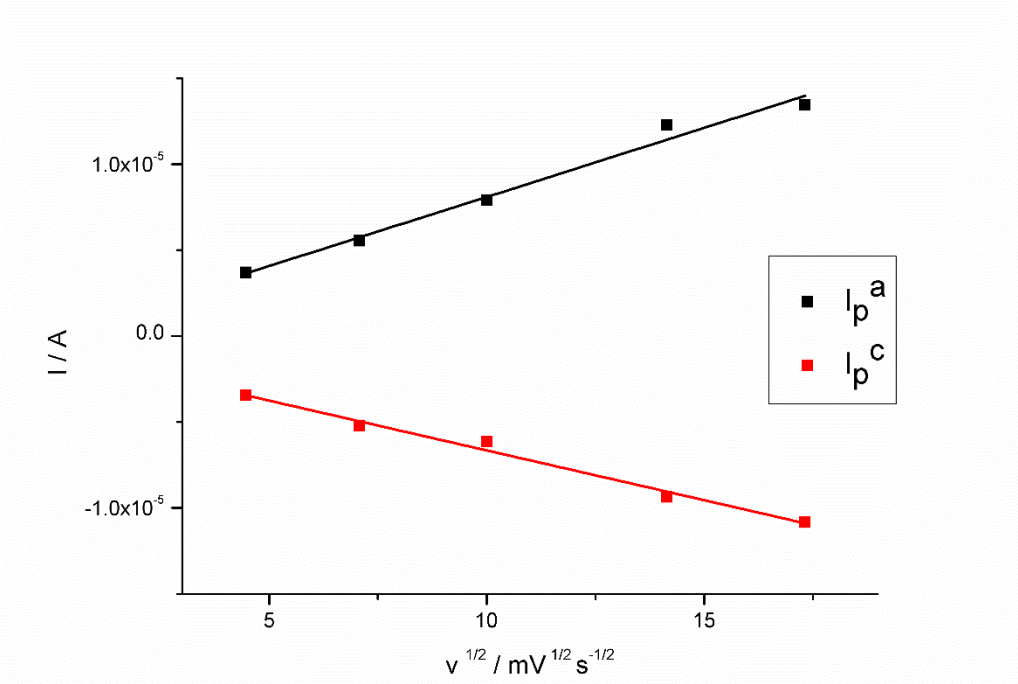


Figure 2.21 Variation of the I_p^a and I_p^c with √(scan rate) for the $[Cu(^{t}BuL_{O}^{OMe})]^{+/0}$ couple at 293 K

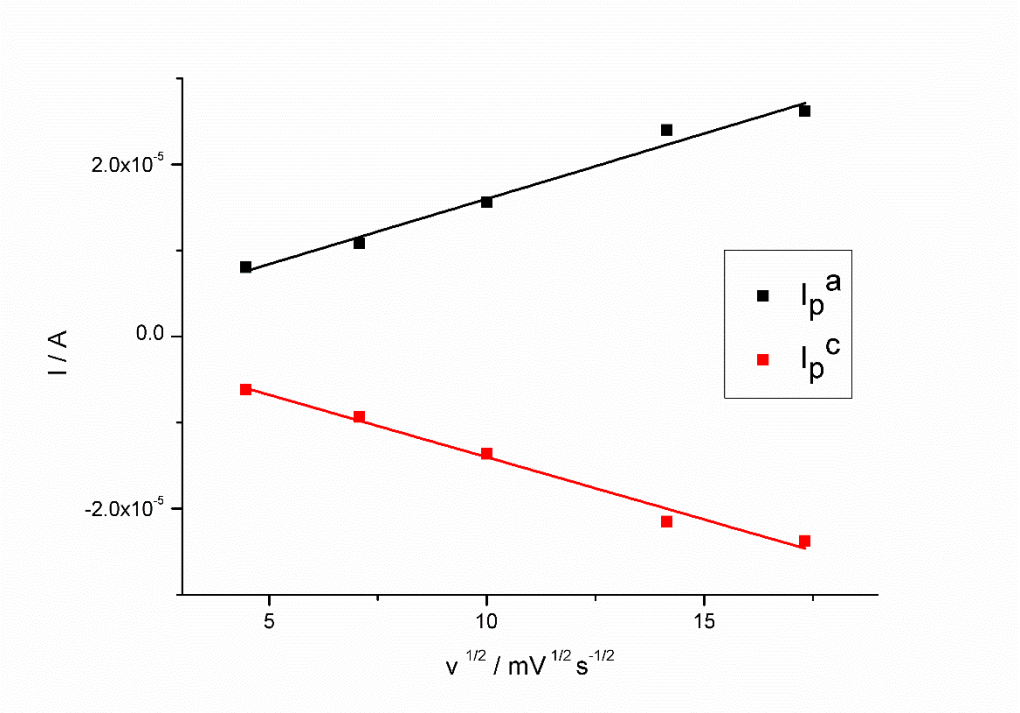


Figure 2.22 Variation of the I_p^a and I_p^c with √(scan rate) for the $[Cu(^tBuL_O^{OMe})]^{2+/+}$ couple at 293 K.

Controlled potential electrolysis (Figure 2.23) of a solution of $[Cu(^tBuL_O^{OMe})]$ at an applied potential of 0.40 *vs* Fc^+/Fc at 253 K in CH_2Cl_2 containing 0.4 M $[N^nBu_4][BF_4]$ as supporting electrolyte afforded dark green solutions of the one-electron oxidised species $[Cu(^tBuL_O^{OMe})]^+$. This measurement confirmed that the first oxidation process of $[Cu(^tBuL_O^{OMe})]^{0/+}$ is a single electron process as the observed Q = 0.48 C value was essentially the same as the theoretical value of Q for a one-electron process.

The controlled potential electrolysis of $[Cu(^tBuL_O^{OMe})]^+$ was not investigated because the second redox process involving $[Cu(^tBuL_O^{OMe})]^{+/2+}$ is chemically irreversible, as demonstrated by spectroeletrochemical studies (Section 2.2.8), in which $[Cu(^tBuL_O^{OMe})]^{2+}$ decomposes over the timescale of

the experiment. This is further discussed in the next section which details spectroelectrochemical studies of the redox processes of [Cu(^{t}BuL$_O^{OMe}$)].

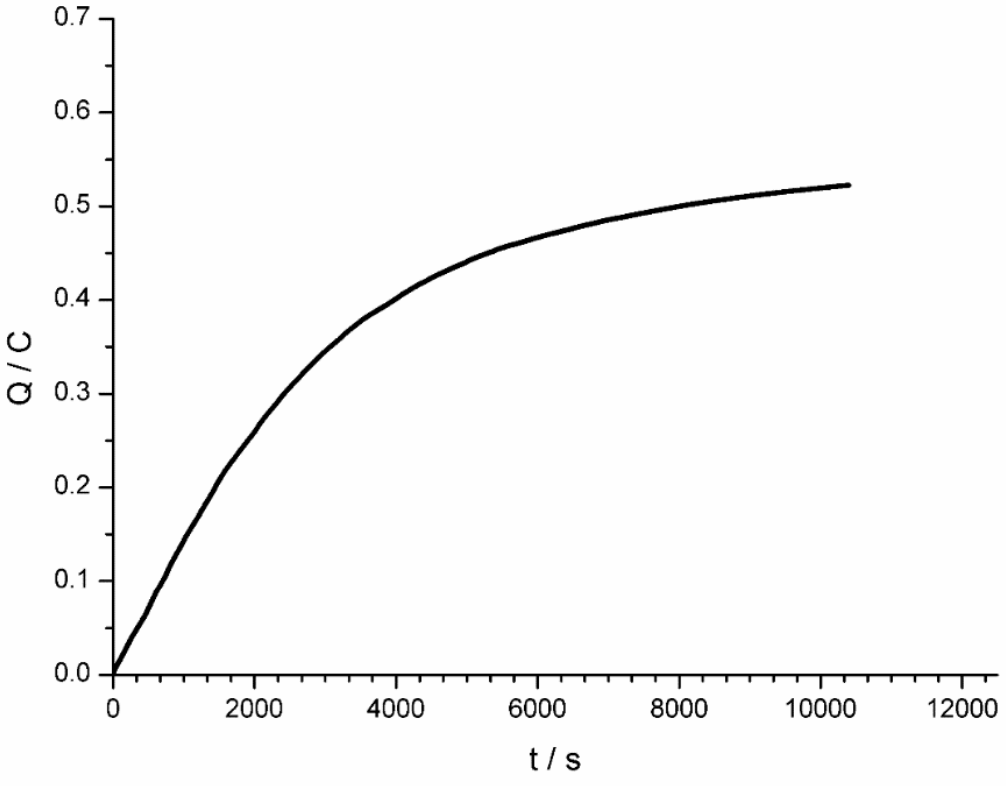


Figure 2.23 Controlled potential electrolysis of [Cu(^{t}BuL$_O^{OMe}$)] to [Cu(^{t}BuL$_O^{OMe}$)]$^+$ at 0.40 V *vs* Fc^+/Fc (1 mM) at 253 K in CH_2Cl_2 containing 0.4 M [N^{n}Bu$_4$][BF_4] as supporting electrolyte. Theoretical value of Q for a one-electron process = 0.49 C.

For the previously reported Cu(II)-diphenolate complexes [Cu(^{t}BuL$_O^{C3N}$)], [Cu(^{t}BuL$_O^{NMe}$)][30,31] and [Cu(^{t}BuL$_O^1$)$_2$] (H^{t}BuL$_O^1$ = 2'-(4',6'-di-*tert*-butylhydroxyphenyl)-4,5-diphenyl imidazole)[46] the redox processes are ligand-based oxidation processes generating kinetically inert biphenoxyl radical species. We also propose that [Cu(^{t}BuL$_O^{OMe}$)] shows similar behaviour. The redox processes occurring for similar Cu(II)-diphenolate complexes has been attributed to the successive one electron oxidation of each coordinated phenolate

donor, leading to the formation of $[Cu(L^{\bullet})(L)]^{+}$ and $[Cu(L^{\bullet})_2]^{2+}$ (L = phenolate donor and $L^{\bullet}$ = phenoxyl radical donor).[31] However, the oxidation of $[Cu(^{t}BuL_{O}^{OMe})]^{+}$ to $[Cu(^{t}BuL_{O}^{OMe})]^{2+}$ is associated with a chemically irreversible redox process and we propose that oxidation of $[Cu(^{t}BuL_{O}^{OMe})]^{+}$ generates a species containing two phenoxyl radical ligands that decomposes over the longer experimental timescales associated with the spectoelectrochemical experiments.

2.2.8. UV/Vis Spectroelectrochemistry of [M(^{t}BuL$_O^{OMe}$)] (M = Zn, Ni, Cu)

2.2.8.1 UV/Vis Spectroelectrochemistry of [Zn(^{t}BuL$_O^{OMe}$)]

The nature of the first redox processes of [M(^{t}BuL$_O^{OMe}$)] (M = Zn, Ni and Cu) and the second redox process for [Cu(^{t}BuL$_O^{OMe}$)] were probed spectroelectrochemically at 243K.

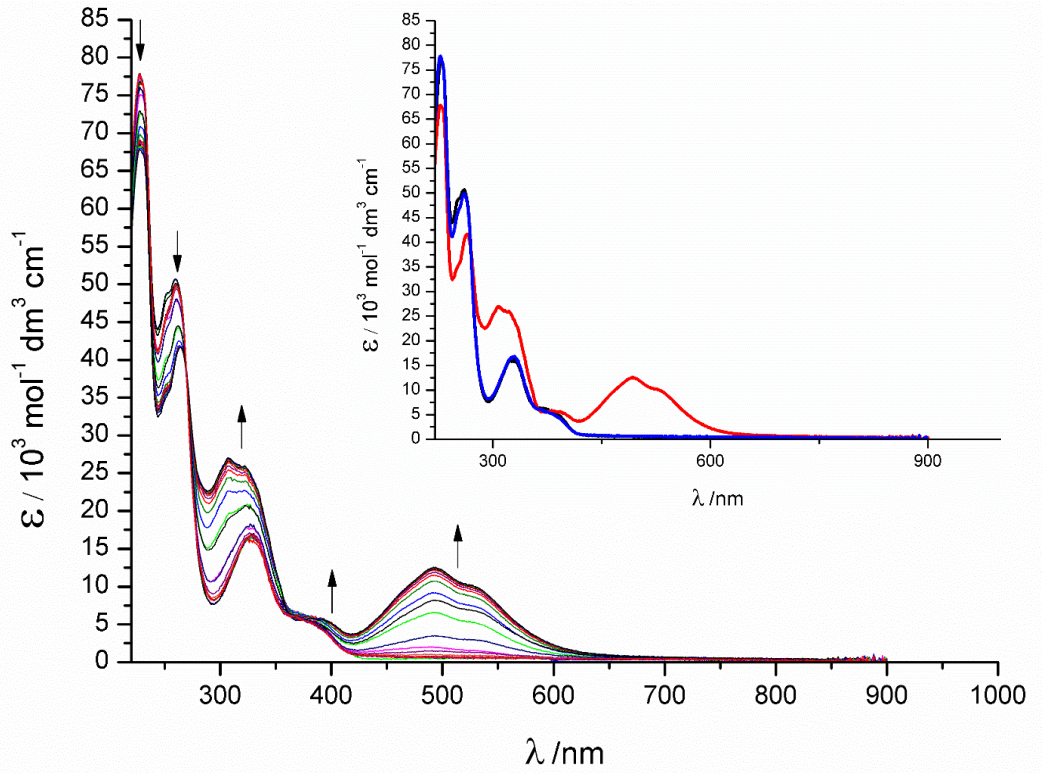


Figure 2.24 The sequential UV/vis spectra taken during the one electron oxidation of [Zn(^{t}BuL$_O^{OMe}$)] (0.183 mM) at 243 K in CH_2Cl_2 containing 0.4 M [N^{n}Bu$_4$][BF$_4$] identifying the bands formed and lost upon oxidation. (Inset): [Zn(^{t}BuL$_O^{OMe}$)] (black) [Zn(^{t}BuL$_O^{OMe}$)]$^+$ (red) and [Zn(^{t}BuL$_O^{OMe}$)] (blue) spectra.

Table 2.16 Absorptions observed in the UV/Vis spectra of the products of the one electron oxidation of [Zn(^{t}BuL$_O^{OMe}$)] at 293 K in an OTE (optically transparent electrode) cell for a solution of compound (ca. 1 mM) in CH_2Cl_2 containing [N^{n}Bu$_4$][BF$_4$] (0.4 M).

Compound	λ_{max} (nm) ε (M^{-1} cm^{-1})	Isobestic point / nm
[Zn(^{t}BuL$_O^{OMe}$)]	227 (77500), 260 (50100), 328 (16800), 391 (4450)	
[Zn(^{t}BuL$_O^{OMe}$)]$^+$	228 (67500), 264 (41600), 306 (269700), 323 (25700), 394 (5490), 492 (12500), 532 (9740)	373, 361, 269, 236

Figure 2.24 and Table 2.16 show the changes observed in the electronic spectrum of [Zn(^{t}BuL$_O^{OMe}$)] during the one electron oxidation of [Zn(^{t}BuL$_O^{OMe}$)] to [Zn(^{t}BuL$_O^{OMe}$)]$^+$ at an applied potential of 0.40 V *vs* Fc^+/Fc. The electrochemical reduction of [Zn(^{t}BuL$_O^{OMe}$)]$^+$ at an applied potential of 0.00 V *vs* Fc^+/Fc returned the UV/vis spectrum to the original profile of [Zn(^{t}BuL$_O^{OMe}$)] confirming chemical reversibility of the first oxidation processes under the conditions of the experiment (Figure 2.24 (inset)). The second oxidation of [Zn(^{t}BuL$_O^{OMe}$)] to [Zn(^{t}BuL$_O^{OMe}$)]$^{2+}$ was not investigated electrochemically by UV/vis spectroelectrochemistry as this did not demonstrate electrochemical reversibility during the initial electrochemical investigations.

2.2.8.2 UV/Vis Spectroelectrochemistry of [Ni(^{t}BuLo^{OMe})]

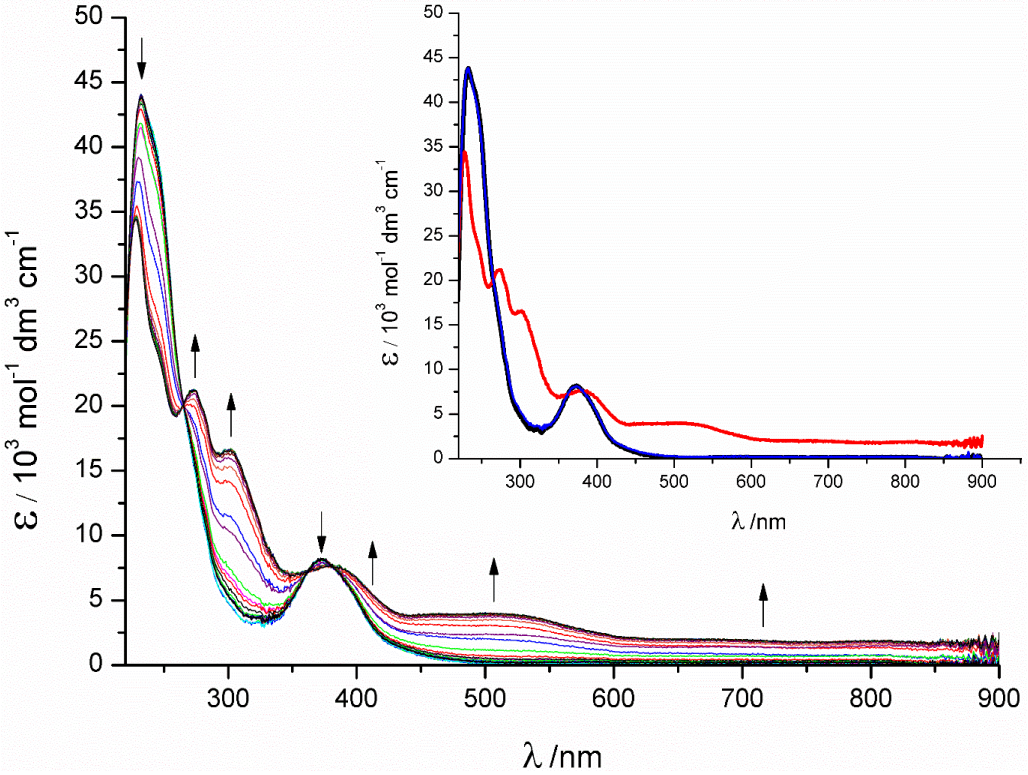


Figure 2.25 The sequential UV/vis spectra taken during the one electron oxidation of [Ni(^{t}BuLo^{OMe})], 1.83 x 10^{-4} mol dm^{-3} at 243 K in CH_2Cl_2 containing 0.4 M [N^{n}Bu$_4$][BF_4] identifying the bands formed and lost upon oxidation. (Inset): [Ni(^{t}BuLo^{OMe})] (black) [Ni(^{t}BuLo^{OMe})]$^+$ (red) and [Ni(^{t}BuLo^{OMe})] (blue) spectra.

Table 2.17 Absorptions observed in the UV/Vis spectra of the products of the one electron oxidation of [Ni(^{t}BuLo^{OMe})] at 293 K in an OTE cell for a solution of compound (ca. 1 mM) in CH_2Cl_2 containing [N^{n}Bu$_4$][BF_4] (0.4 M).

Compound	λ_{max} (nm) ε (M^{-1} cm^{-1})	Isosbestic point / nm
[Ni(^{t}BuLo^{OMe})]	232 (43800), 373 (8210)	
[Ni(^{t}BuLo^{OMe})]$^+$	226 (34400), 273 (21200), 321 (16500), 386 (7610), 518 (4030)	265, 361, 380

Figure 2.25 and Table 2.17 show the changes observed in the electronic spectrum of [Ni(^{t}BuL$_O^{OMe}$)] during the one electron oxidation of [Ni(^{t}BuL$_O^{OMe}$)] to [Ni(^{t}BuL$_O^{OMe}$)]$^+$ at an applied potential of 0.41 V *vs* Fc^+/Fc. The electrochemical reduction of [Ni(^{t}BuL$_O^{OMe}$)]$^+$ at an applied potential of 0.00 V *vs* Fc^+/Fc returned the UV/vis spectrum to the original profile of [Ni(^{t}BuL$_O^{OMe}$)] confirming electrochemical reversibility of the first oxidation process (Figure 2.25 (inset)). The oxidation of [Ni(^{t}BuL$_O^{OMe}$)] to [Ni(^{t}BuL$_O^{OMe}$)]$^{2+}$ was not investigated electrochemically by UV/vis spectroscopy as this did not demonstrate electrochemical reversibility during the initial electrochemical investigations.

2.2.8.3 UV/Vis Spectroelectrochemistry of [Cu(^{t}BuL$_O^{OMe}$)]

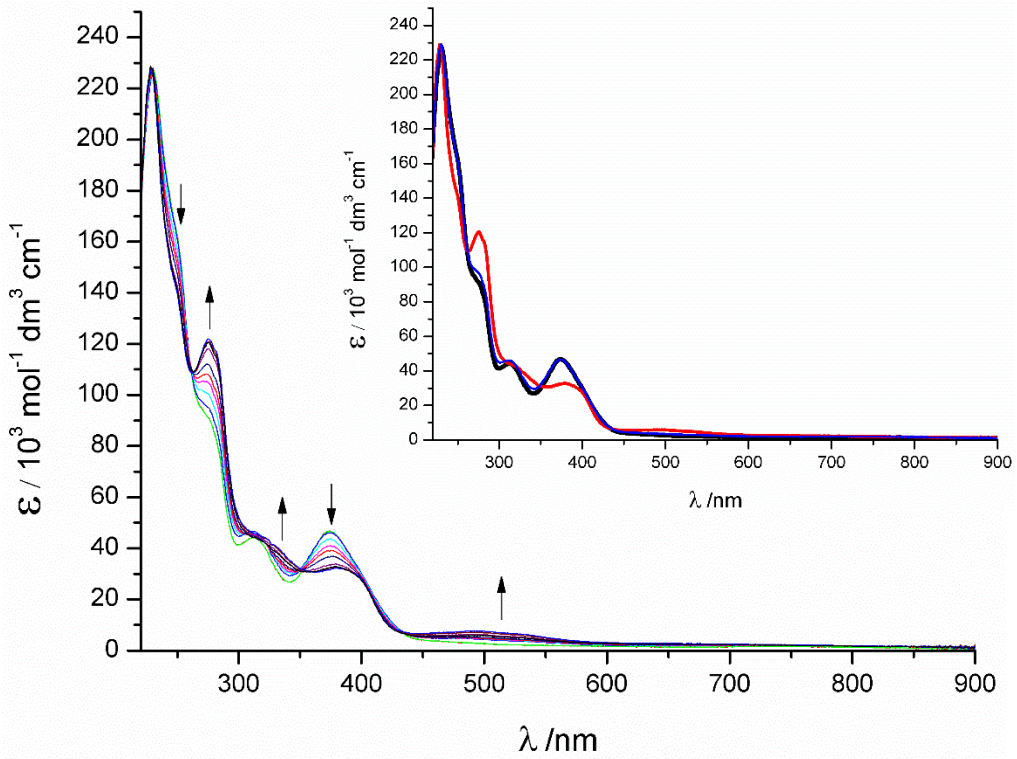


Figure 2.26 The sequential UV/vis spectra taken during the one electron oxidation of [Cu(^{t}BuL$_O^{OMe}$)], 1.83 x 10^{-4} mol dm^{-3} at 243 K in CH_2Cl_2 containing 0.4 M [N^{n}Bu$_4$][BF$_4$] identifying the bands formed and lost upon oxidation. (Inset): [Cu(^{t}BuL$_O^{OMe}$)] (black) [Cu(^{t}BuL$_O^{OMe}$)]$^+$ (red) and [Cu(^{t}BuL$_O^{OMe}$)] (blue) spectra.

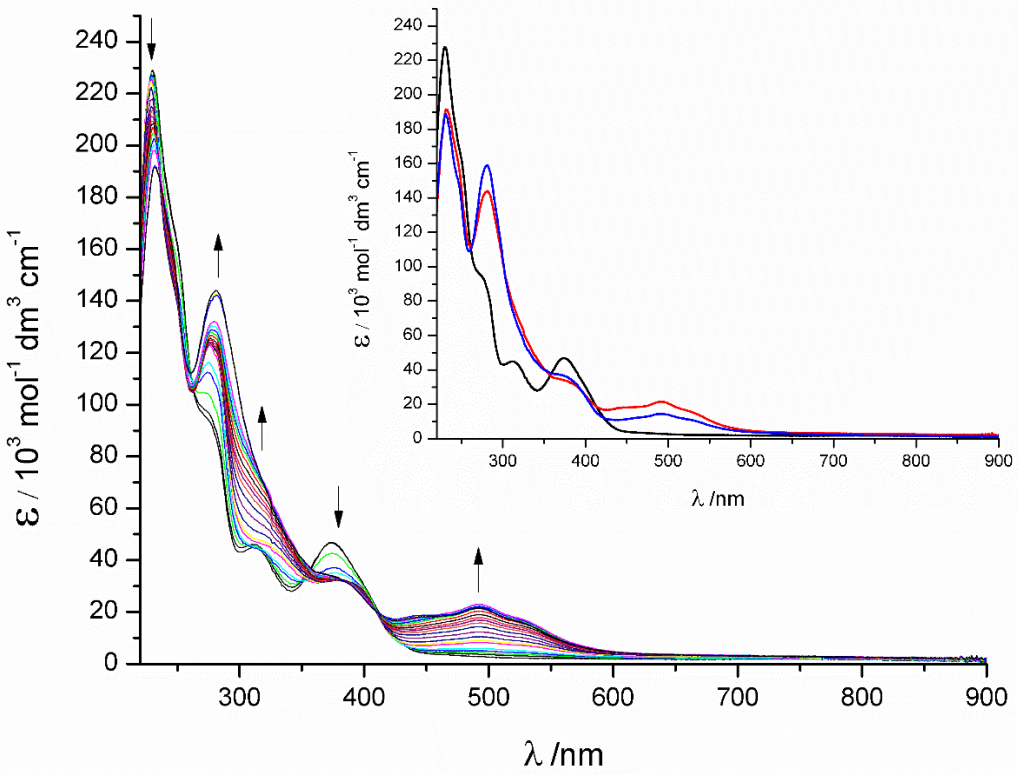


Figure 2.27 The sequential UV/vis spectra taken during the one electron oxidation of [Cu(^{t}BuL$_O^{OMe}$)]$^+$, 1.83 x 10^{-4} mol dm^{-3} at 243 K in CH_2Cl_2 containing 0.4 M [N^{n}Bu$_4$][BF$_4$] identifying the bands formed and lost upon oxidation. (Inset): [Cu(^{t}BuL$_O^{OMe}$)]$^{+1}$ (black) [Cu(^{t}BuL$_O^{OMe}$)]$^{2+}$ (red) and decomposed [Cu(^{t}BuL$_O^{OMe}$)]$^{+2}$ (blue) spectra.

Table 2.18 Absorptions observed in the UV/Vis spectra of the products of one and two electron oxidation of [Cu(^{t}BuL$_O^{OMe}$)] at 293 K in an OTE cell for a solution of compound (ca. 1 mM) in CH_2Cl_2 containing [N^{n}Bu$_4$][BF$_4$] (0.4 M).

Compound	λ_{max} (nm) ε (M^{-1} cm^{-1})	Isosbestic point / nm
[Cu(^{t}BuL$_O^{OMe}$)]	229 (227000), 274 (91500), 313 (44500), 380 (32500), 504 (5850)	
[Cu(^{t}BuL$_O^{OMe}$)]$^+$	229 (48600), 277 (24900), 323 (15800), 376 (9530), 502 (4060), 607 (19400)	262, 350, 433
[Cu(^{t}BuL$_O^{OMe}$)]$^{2+}$	231 (190000), 282 (144000, 373 (34400), 443 (17800), 492 (22100), 526 (15900)	260, 357, 414

The chemical natures of the first and second oxidation processes of [Cu(^{t}BuL$_O^{OMe}$)] was monitored spectroelectrochemically at 243K (Figures 2.26 and 2.27). A summary of the absorption spectra of [Cu(^{t}BuL$_O^{OMe}$)], [Cu(^{t}BuL$_O^{OMe}$)]$^+$ and [Cu(^{t}BuL$_O^{OMe}$)]$^{2+}$ are shown in Table 2.18. While the second oxidation process associated with the [Cu(^{t}BuL$_O^{OMe}$)]$^{2+/+}$ couple demonstrates electrochemical reversibility, reduction of the [Cu(^{t}BuL$_O^{OMe}$)]$^{2+}$ species to [Cu(^{t}BuL$_O^{OMe}$)] did not return the UV/vis profile to that of [Cu(^{t}BuL$_O^{OMe}$)]. Consequently the [Cu(^{t}BuL$_O^{OMe}$)]$^{2+/+}$ couple does not appear to be chemically reversible under the conditions of the experiment and was not investigated further.

2.2.8.4 Summary and assignment of the UV/vis spectroscopic studies of $[M(^{t}BuL_{O}^{OMe})]^{+/0}$ (M = Zn, Ni, Cu)

The absorption spectrum of $[Zn(^{t}BuL_{O}^{OMe})]^{+}$ contains features at 264 and 323 nm which are associated with π-π* type transitions involving the molecular orbitals located on the phenolate chromophore[49] and the features of 391 and 394 nm in $[Zn(^{t}BuL_{O}^{OMe})]$ and $[Zn(^{t}BuL_{O}^{OMe})]^{+}$ respectively are assigned to intraligand n-π* type transitions based on the C=N chromophore.[49] The additional features observed at 492 and 532 in the UV/vis spectrum of $[Zn(^{t}BuL_{O}^{OMe})]^{+}$ are assigned to π-π*transitions associated with a phenxoyl radical ligand.[19,49] The features observed in the UV/vis spectrum of $[Zn(^{t}BuL_{O}^{OMe})]^{+}$ generated electrochemically are similar to those observed for $[Zn(^{t}BuL_{O}^{C3N})]^{+}$ and $[Zn(^{t}BuL_{O}^{NMe})]^{+}$ [30,31] and $[Zn(^{t}BuL_{O}^{1})_2]^{+}$ ($H^{t}BuL_{O}^{1}$ = 2'-(4',6'-di-*tert*-butylhydroxyphenyl)-4,5-diphenyl imidazole).[46] The UV/vis spectrum of $[Zn(^{t}BuL_{O}^{OMe})]^{+}$ is also similar to other five-coordinate N_3O_2 monomeric Zn(II) centres in which the first redox process has been assigned as phenoxyl radical bassed.[19,32]

The absorption spectra of $[Ni(^{t}BuL_{O}^{OMe})]^{+}$ exhibits a band at 226 nm, which is associated with a phenoxide $\pi \rightarrow \pi^{*}$ transition, bands at 321 and 386 nm which are associated with LMCT transitions, and at 518 nm that may arise from LMCT and/or d → d transitions.[30,31] Similar transitions have been observed previously for $[Ni(^{t}BuL_{O}^{C3N})]^{+}$, $[Ni(^{t}BuL_{O}^{NMe})]^{+}$ [30,31], $[Ni(II)L]^{+}$ ([H(2)L = 2,2'-[2,2']bipyridinyl-6-yl-bis-4,6-di-tert-butylphenol],[20] $[Ni(^{t}bu\text{-}salcn)]^{+}$ ($H_2{}^{t}bu$-salcn) = *N*,*N*´-bis(3´,5´-di-*tert*-butylsalicylidene)- 1,2-cyclohexanediamine,[16] and $[Ni(1)_2]^{+}$ (1) = 3,5-di-t-butyl-N-(dimethylaminoethyl) salicylideneamine.[13] Despite the similarities between the UV/vis spectra of $[Ni(^{t}BuL_{O}^{OMe})]^{+}$,

[Ni(^{t}BuL$_O^{C3N}$)]$^+$ and [Ni(^{t}BuL$_O^{NMe}$)]$^+$ [30] the intense feature at 390 nm, which occurs in [Ni(^{t}BuL$_O^{OMe}$)]$^+$, [Ni(^{t}BuL$_O^{C3N}$)]$^+$ and [Ni(^{t}BuL$_O^{NMe}$)]$^+$, may mask the characteristic bands that are associated with the $\pi \rightarrow \pi^*$ transitions of a phenoxyl radical. Therefore an assignment of the nature of the redox process for the [Ni(^{t}BuL$_O^{OMe}$)]$^{0/+}$ couple i.e. whether it is ligand- or metal-based oxidation cannot be made on the basis of the UV/vis spectroscopic data alone.

The absorption spectrum of [Cu(^{t}BuL$_O^{OMe}$)]$^+$ possess bands at wavelengths that are comparable to those reported for [Cu(^{t}BuL$_O^{NMe}$)]$^+$ and [Cu(^{t}BuL$_O^{C3N}$)]$^+$ [30] and to those of other Cu(II)-phenolate complexes including *N*-benzyl-*N',N''*-di-*tert*-butyl-disalicyl-triaminocyclohexane Cu(II).[9] Thus, we assign the bands at 229 and 274 nm in the UV/vis spectrum of [Cu(^{t}BuL$_O^{OMe}$)]$^+$ to phenoxide $\pi \rightarrow \pi^*$ charge transfer transitions and the band at 380 nm to LMCT involving the phenolate and Cu(II) metal centre.[7,39,50–52] The generation of a ligand-based phenoxyl radical is supported by the appearance of a broad absorption at 504 nm; the other absorption characteristic of the production of a phenoxyl radical should be observed around 410 nm, however this may be masked by the strong band at 380 nm and thus further study is required in order to determine whether the oxidation is phenoxyl radical based.[45]

The second oxidation process was also investigated spectroelectrochemically. [Cu(^{t}BuL$_O^{OMe}$)]$^{2+}$ possess bands at wavelengths that are comparable to those reported for [Cu(^{t}BuL$_O^{NMe}$)]$^{2+}$ and [Cu(^{t}BuL$_O^{C3N}$)]$^{2+}$ [30] and to those of other Cu(II)-phenolate complexes including *N*-benzyl-*N',N''*-di-*tert*-butyl-disalicyl-triaminocyclohexane copper (II).[9] Electrochemical reduction did not return the UV/vis spectra to the UV/vis profile for [Cu(^{t}BuL$_O^{OMe}$)]$^+$.

Thus, the second oxidation process of [Cu(^{t}BuL$_{O}^{OMe}$)] appears to be chemically irreversible under the conditions of the experiment. The absorption spectra of [Cu(^{t}BuL$_{O}^{NMe}$)]$^{2+}$ and [Cu(^{t}BuL$_{O}^{C3N}$)]$^{2+}$ show the development of new bands at 433, 492 and 526 nm all of which are associated with $\pi \rightarrow \pi^{*}$ transitions of a bisphenoxyl radical species.[7,50]

2.2.9 EPR Spectroscopy of [M(^{t}BuL$_O^{OMe}$)] (M = Zn, Ni, Cu)

2.2.9.1 EPR Spectroscopy of [Zn(^{t}BuL$_O^{OMe}$)]

Controlled potential electrolysis of [Zn(^{t}BuL$_O^{OMe}$)] at an applied potential of 0.40 V *vs* Fc/Fc$^+$ at 253 K in CH_2Cl_2 containing 0.4 M [N^{n}Bu$_4$][BF$_4$] as supporting electrolyte afforded a pink solution of the one electron oxidised species, [Zn(^{t}BuL$_O^{OMe}$)]$^+$. The EPR spectrum of [Zn(^{t}BuL$_O^{OMe}$)]$^+$ at 77 K possess a single isotropic signal with g_{iso} = 2.0040 with no hyperfine coupling (Figure 2.28). The S = ½ EPR signals obtained for [Zn(^{t}BuL$_O^{OMe}$)]$^+$ are typical for ligand-based phenoxyl radical species and compare to the *g*-values of those reported for analogous Zn(II)-phenoxyl radical complexes: [Zn(^{t}BuL$_O^{C3N}$)] and [Zn(^{t}BuL$_O^{NMe}$)] g_{iso} = 2.0046 and 2.0044,[30,31] respectively and [Zn(L)$_2$] (LH) = 2-(4,6-di-*tert*-butylhydroxyphenyl)-4,5-diphenyl imidazole g_{iso} = 2.0047.[46]

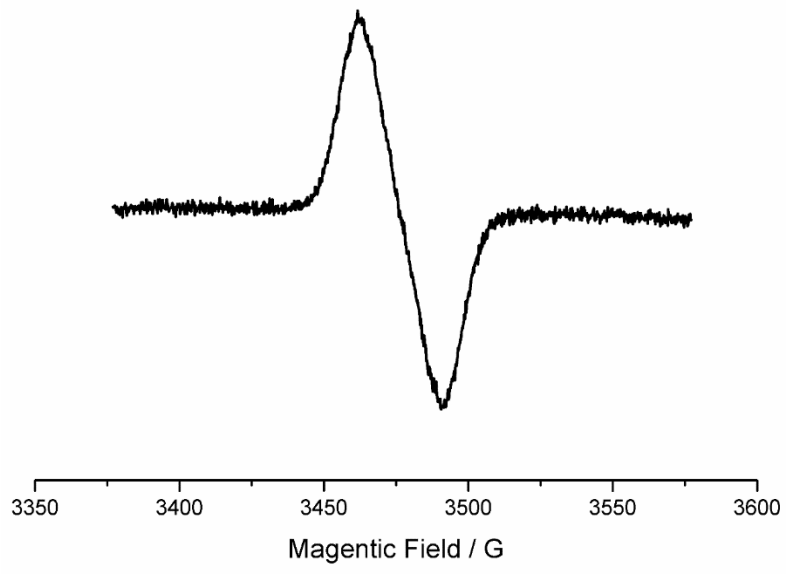


Figure 2.28 X-band EPR spectra of electrochemically generated [Zn(^{t}BuL$_O^{OMe}$)]$^+$ in CH_2Cl_2 containing 0.4 M [N^{n}Bu$_4$][BF$_4$] as supporting electrolyte at 77 K.

2.2.9.2 EPR Spectroscopy of [Ni(^{t}BuL$_O^{OMe}$)]

For the neutral species of [Ni(^{t}BuL$_O^{OMe}$)], no EPR signal was observed in the X-band EPR spectra in CH_2Cl_2 at 77K. High-spin Ni(II) complexes usually exhibit zero-field splitting parameters that are larger than the X-band quantum (0.3 cm^{-1}) and are thus not detected by conventional X-band EPR spectroscopy.[53–55]

Controlled potential electrolysis of [Ni(^{t}BuL$_O^{OMe}$)] at an applied potential of 0.41 V *vs* Fc/Fc^+ afforded a dark green solution of the one electron oxidised species of [Ni(^{t}BuL$_O^{OMe}$)]$^+$ and EPR spectroscopy identified the sample as EPR-active at 77 K. the EPR spectrum of [Ni(^{t}BuL$_O^{OMe}$)]$^+$ possesses rhombic symmetry with a g-tensor anisotropy, g_{11} = 2.520, g_{22} = 2.085, g_{33} = 1.990 and Gaussian linewidths of W_{11} = 51.0, W_{22} = 30.0 and W_{33} = 30.0 G as determined by EPR simulation.

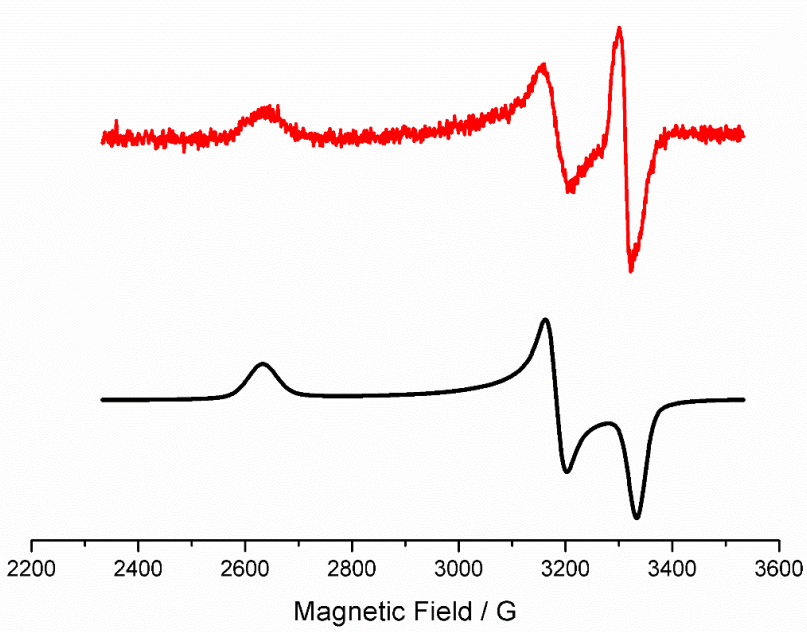


Figure 2.29 X-band EPR spectra of electrochemically generated [Ni(^{t}BuL$_O^{OMe}$)]$^+$ (red) in frozen CH_2Cl_2 solution at 77 K and simulation [Ni(^{t}BuL$_O^{OMe}$)]$^+$ (black). Spin Hamiltonian parameters g_{11} = 2.520, g_{22} = 2.085, g_{33} = 1.990, Gaussian linewidths of W_{11} = 51.0, W_{22} = 30.0 and W_{33} = 30.0 G.

The *g*-values are substantially larger than typical values observed for phenoxyl radicals (2.002 – 2.009) and indicate that the SOMO of $[Ni(^{t}BuL_{O}^{OMe})]^{+}$ possesses significant metal-character. This lends support to the $[Ni(^{t}BuL_{O}^{OMe})]^{+/0}$ couple being formally metal-based and being assigned to a Ni(III)/Ni(II) couple. A formally metal-based Ni(III)/Ni(II) redox process has also been observed in other Ni-phenolate complexes including $[Ni(^{t}BuL_{O}^{C3N})]$ and $[Ni(^{t}BuL_{O}^{NMe})]$,[30,31] [Ni(tbu-salcn)] (H_2tbu-salcn) = *N*,*N*'-bis(3',5'-di-*tert*-butylsalicylidene)-1,2-cyclohexanediamine,[7] and [Ni(salen)] and its derivatives.[56] The extra feature in the frozen solution X-band EPR spectrum of $[Ni(^{t}BuL_{O}^{OMe})]^{+}$ at *ca.* 3300 G (Figure 2.29) may be associated with a radical species, which might result from the decomposition of $[Ni(^{t}BuL_{O}^{OMe})]^{+}$ under the conditions of this experiment.

2.2.9.3 EPR Spectroscopy of [Cu(^{t}BuL$_O^{OMe}$)]

Controlled potential electrolysis of solutions of [Cu(^{t}BuL$_O^{OMe}$)] at an applied potential of 0.55 *vs* Fc^+/Fc at 253 K in CH_2Cl_2 containing 0.4 M [N^{n}Bu$_4$][BF$_4$] as supporting electrolyte afforded dark green solutions of the one-electron oxidised species [Cu(^{t}BuL$_O^{OMe}$)]$^+$. Solutions of this oxidised species are EPR silent. The absence of an EPR signal for [Cu(^{t}BuL$_O^{OMe}$)]$^+$ is consistent with this species possessing an S = 0 or S = 1 ground state, as a result of the magnetic coupling between the S = 1/2 Cu(II) centre and an S = 1/2 coordinated phenoxyl radical ligand. This observation lends support for the first oxidation process of [Cu(^{t}BuL$_O^{OMe}$)] being phenoxyl radical based.[4,17-30]

2.3 Conclusions

A range of Zn(II), Ni(II) and Cu(II) Schiff-base diphenolate complexes [M(^{t}BuL$_O^R$)] have been prepared using four novel N_3O_2 pro-ligands ([H$_2$^{t}BuL$_O^R$] (R = H, Cl, ^{t}Bu, and OMe). For M = Zn(II) and R = H and ^{t}Bu only crude material could be isolated. The X-ray crystal structures of [Cu(^{t}BuL$_O^H$)], [Cu(^{t}BuL$_O^{OMe}$)] and [Ni(^{t}BuL$_O^{OMe}$)] show these complexes possess metal centres in a five-coordinate distorted square-based pyramidal coordination sphere.

The metal to amine N-donor distance, M(1)-N(3) for [Cu(^{t}BuL$_O^{OMe}$)] (2.4511(17) Å) is significantly shorter than the distance reported for [Cu(^{t}BuL$_O^H$)] (2.579(2) Å). This may be rationalised in terms of the differences in basicity of the amine N-donor in each compound. The N donor in [Cu(^{t}BuL$_O^{OMe}$)] is a stronger base (4-methoxyphenylamine pK_a = 5.36) than that of the N-H donor (phenylamine pK_a = 4.87) in [Cu(^{t}BuL$_O^H$)]. The M-N(3) distance in [Ni(^{t}BuL$_O^{OMe}$)] (2.19(11) Å) is shorter than that in [Cu(^{t}BuL$_O^H$)] and [Cu(^{t}BuL$_O^{OMe}$)]. The difference in the M-N(3) distance in [Ni(^{t}BuL$_O^{OMe}$)] and [Cu(^{t}BuL$_O^{OMe}$)] and [Cu(^{t}BuL$_O^H$)] can be rationalised in terms of the Jahn-Teller distortion that usually accompanies the coordination of ligands at the apical positions of a Cu(II) centres. [30,39] The M(II)-O(phenolate) and M(II)-N(imine) bond distances in [Cu(^{t}BuL$_O^H$)], [Cu(^{t}BuL$_O^{OMe}$)] and [Ni(^{t}BuL$_O^{OMe}$)] are comparable to those previously reported for the analogous complexes [Cu(^{t}BuL$_O^{C3N}$)] and [Cu(^{t}BuL$_O^{NMe}$)], and [Ni(^{t}BuL$_O^{C3N}$)] and [Ni(^{t}BuL$_O^{NMe}$)] respectively. However, a difference in the M-N(3) bond lengths for [Cu(^{t}BuL$_O^H$)], [Cu(^{t}BuL$_O^{OMe}$)] and [Ni(^{t}BuL$_O^{OMe}$)] was observed in comparison to those in [M(^{t}BuL$_O^{NMe}$)] and [M(^{t}BuL$_O^{C3N}$)]. The difference in the pK_a is

sufficiently significant to impact the M-N bonding interaction and consequently the length of the M-N(3) bond.

Crude [Zn(^{t}BuL$_O^R$)] (R = H, ^{t}Bu), [Zn(^{t}BuL$_O^R$)] (R = Cl, OMe) and [M(^{t}BuL$_O^R$)] (M = Ni(II) and Cu(II), R = H, Cl, ^{t}Bu and OMe) possess at least two oxidation processes between 0.11 V and 0.61 V *vs* Fc^+/Fc. In comparison to the analogous metal complexes, [M(^{t}BuL$_O^R$)] (M = Zn(II), Ni(II) and Cu(II)) and (R = NMe and C3N), synthesised by Franks *et al.* the potentials observed for crude [Zn(^{t}BuL$_O^R$)] (R = H, ^{t}Bu), [Zn(^{t}BuL$_O^R$)] (R = Cl, OMe) and [M(^{t}BuL$_O^R$)] (M = Ni(II) and Cu(II), R = H, Cl, ^{t}Bu and OMe) are higher. This can be attributed to the lower pK_a values of the bridging N-donor amines (R = NMe and C3N) in [M(^{t}BuL$_O^R$)] (M = Zn(II), Ni(II) and Cu(II)) and (R = NMe and C3N) than those of the bridging N-donor amines discussed in this chapter (R = H, Cl, ^{t}Bu and OMe).

Only the first oxidation processes of [M(^{t}BuL$_O^{OMe}$)] (M = Zn(II), Ni(II) and Cu(II)) and the second oxidation process of [Cu(^{t}BuL$_O^{OMe}$)] were electrochemically reversible. UV/vis spectra electrochemical studies also confirmed the chemical reversibility of the first oxidation processes of [M(^{t}BuL$_O^{OMe}$)]. Importantly, these results indicate that an electron donating substituent on the pendant aryl ring appears to be necessary to support the reversible redox chemistry of these systems. Thus, in comparison to [M(^{t}BuL$_O^R$)] (M = Zn(II), Ni(II) and Cu(II), R = NMe and C3N) (Figure 2.3)[30,31] a decrease in electron donation from the bridging amine unit as a result of the change from tertiary amine to aryl amine group in [M(^{t}BuL$_O^R$)] (M = Zn(II), Ni(II), Cu(II), R = H, Cl, ^{t}Bu) results in the loss of electrochemical reversibility.

Reversibility is maintained where the substituent R = OMe is present because the OMe substituent is relatively electron donating.

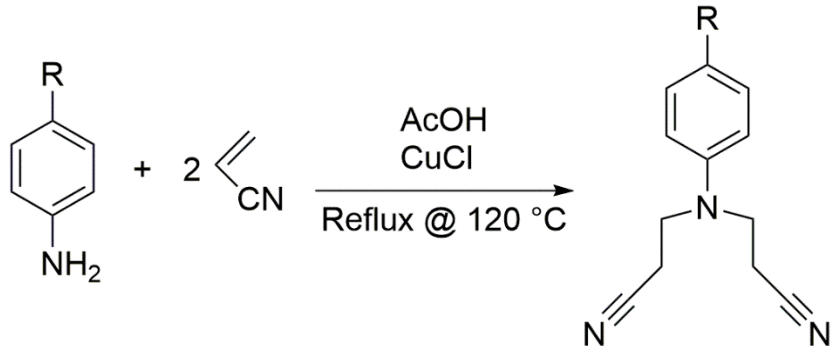
EPR spectroscopic studies on [Zn(^{t}BuL$_O^{OMe}$)] and [Cu(^{t}BuL$_O^{OMe}$)] suggest that the first oxidation processes associated with the oxidation of a phenolate unit bound to the metal centre to form a ligand-based phenoxyl radical ligand in [Zn(^{t}BuL$_O^{OMe}$)]$^+$ and [Cu(^{t}BuL$_O^{OMe}$)]$^+$. For [Ni(^{t}BuL$_O^{OMe}$)] EPR spectroscopy suggests that the first oxidation process is metal-based so that [Ni(^{t}BuL$_O^{OMe}$)]$^+$ is best described as a Ni(III) centre.

In summary we have shown that the introducing various *para*-substituted aryl amines into the ligand manifold can modulate the reduction potentials in [Zn(^{t}BuL$_O^R$)] and [Ni(^{t}BuL$_O^R$)] (R = H, Cl, ^{t}Bu and OMe) complexes but not in [Cu(^{t}BuL$_O^R$)] (R = H, Cl, ^{t}Bu and OMe). Here the Jahn-Teller distortion appears to disrupt the effect of the subsituent due the elongation of the Cu(1)-N(3) bond length with a concomitant weakening of the Cu(1)-N(3) interaction.

In future studies we suggest that our approach of modulating the basicity of amine to control reduction potential may be viable, however electron withdrawing/donating substituents directly at the amine N donor or through a linker which is not based upon an aromatic ring such that a higher overall basicity is maintained should be considered.

2.4 Experimental

2.4.1 Synthesis of 3,3'-(phenylazanediyl)dipropanenitrile (R= H)



R = H, Cl, ^{t}Bu and OMe

Typical procedure: Aniline (9.3 g, 0.10 mol) was added to a solution of CuCl (1.00 g, 0.01 mol) in glacial acetic acid (20.0 ml) after which acrylonitrile (20.0 ml, 3.10 mol) was added to the reaction mixture drop-wise over a period of 10 mins. The solution was then heated to reflux at 120 °C for 24 h. After cooling to room temperature the reaction mixture was extracted with CH_2Cl_2 (2 x 100 ml), the organic phase was washed with 2 M NaOH (2 x 75.0 ml) and dried over $MgSO_4$. The mixture was filtered and reduced *in vacuo.* The crude product was re-crystallised twice from hot ethanol to give crystalline solid.

3,3'-(phenylazanediyl)dipropanenitrile

The reaction to prepare 3,3'-(phenylazanediyl)dipropanenitrile followed the typical procedure described in 2.4.1 and used aniline (9.32 g 0.10 mol), to give 3,3'-(phenylazanediyl)dipropanenitrile as a white crystalline solid (9.75 g, 4.90 mmol, 49 %).

^{1}H NMR (270 MHz, $CDCl_3$, 298 K): δ_H 7.32 (2H, t, *J* 7.4, Ar<u>H</u>), 6.89 (1H, m, Ar<u>H</u>), 6.74 (2H, d, *J* 7.4, Ar<u>H</u>), 3.78 (4H, t, *J* 6.7, C<u>H</u>$_2$), 2.64 (4H, t, *J* 6.7, C<u>H</u>$_2$). ^{13}C NMR (270 MHz, $CDCl_3$, 298 K): δ_C 145.0 (Ar<u>C</u>-N), 130.0 (Ar<u>C</u>), 119.6 (Ar<u>C</u>), 118.3 (<u>C</u>N), 113.4 (Ar<u>C</u>), 48.3 (<u>C</u>H$_2$), 16.3 (<u>C</u>H$_2$). MS (ES+, m/z): 222.1007 [M+Na].

2.4.2 3,3'-(4-methoxyphenylazanediyl)dipropanenitrile (R= OMe)

The reaction to prepare 3,3'-(4-methoxyphenylazanediyl)dipropanenitrile followed the typical procedure described in 2.4.1 and used 4-methoxyaniline (12.30 g 0.10 mol), to give 3,3'-(4-methoxyphenylazanediyl)dipropanenitrile as a white crystalline solid (11.6 g, 5.10 mmol, 51 %).

^{1}H NMR (270 MHz, $CDCl_3$, 298 K): δ_H 6.88 (2H, d, *J* 6.8, Ar<u>H</u>), 6.86 (2H, d, *J* 6.8, Ar<u>H</u>), 3.79 (3H, s, C<u>H</u>$_3$), 3.59 (4H, t, *J* 7.2, C<u>H</u>$_2$), 2.52 (4H, t, *J* 7.2, C<u>H</u>$_2$). ^{13}C NMR (67 MHz, $CDCl_3$, 298 K): δ_C 154.7 (Ar<u>C</u>-O), 138.9 (Ar<u>C</u>-N), 119.1 (Ar<u>C</u>), 118.3 (<u>C</u>N), 115.3 (Ar<u>C</u>), 55.6 (O<u>C</u>H$_3$), 49.6 (<u>C</u>H$_3$), 16.62 (<u>C</u>H$_2$). MS (ES+, m/z): 252.1113 [M+Na].

2.4.3 3,3'-(4-*tert*-butylphenylazanediyl)dipropanenitrile (R= ^{t}Bu)

The reaction to prepare 3,3'-(4-*tert*-butylphenylazanediyl)dipropanenitrile followed the typical procedure described in 2.4.1 and used 4-(*tert*-butyl)aniline (14.90 g 0.10 mol), to give 3,3'-(4-*tert*-butylphenylazanediyl)dipropanenitrile as a white crystalline solid (8.24 g, 0.32 mmol, 32 %).

^{1}H NMR (270 MHz, $CDCl_3$, 298 K): δ_H 6.88 (2H, d, *J* 6.8, Ar<u>H</u>), 6.84 (2H, d, *J* 6.8, Ar<u>H</u>), 3.79 (9H, s, C(C<u>H</u>$_3$)$_3$), 3.59 (4H, t, *J* 6.2, C<u>H</u>$_2$), 2.52 (4H, t, *J* 6.2, C<u>H</u>$_2$). ^{13}C NMR (67 MHz, $CDCl_3$, 298 K): δ_C 146.5 (Ar<u>C</u>-N), 142.1 (Ar<u>C</u>-

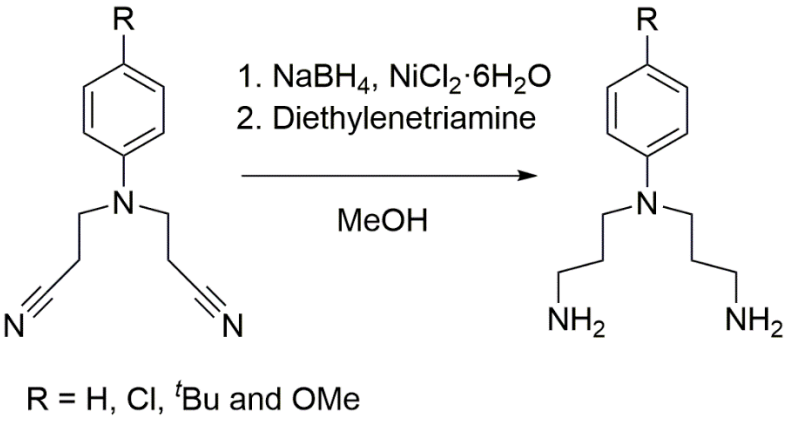
$C(CH_3)_3$), 126.6 (Ar<u>C</u>), 119.3 (<u>C</u>N), 113.3 (Ar<u>C</u>), 48.0 (N-<u>C</u>H_2), 33.8 (<u>C</u>$(CH_3)_3$), 31.31 (<u>C</u>H_3), 16.3 (<u>C</u>H_2). MS (ES+, m/z): 278.1633 [M+Na].

2.4.4 3,3'-(4-chlorophenylazanediyl)dipropanenitrile (R= Cl)

The reaction to prepare 3,3'-(4-chlorophenylazanediyl)dipropanenitrile followed the typical procedure described in 2.4.1 and used chloroaniline (14.9 g 0.10 mmol), to give 3,3'-(4-chlorophenylazanediyl)dipropanenitrile as a white crystalline solid (5.17 g, 2.20 mol, 22 %).

^{1}H NMR (270 MHz, $CDCl_3$, 298 K): δ_H 7.29 (2H, d, *J* 6.8, Ar<u>H</u>), 6.60 (2H, d, *J* 6.8, Ar<u>H</u>), 3.77 (4H, t, *J* 6.7, C<u>H</u>$_2$), 2.63 (4H, t, *J* 6.7, C<u>H</u>$_2$). ^{13}C NMR (67 MHz, $CDCl_3$, 298 K): δ_C 147.0 (Ar<u>C</u>-N), 130.2 (Ar<u>C</u>), 127.8 (Ar<u>C</u>-Cl), 118.1 (<u>C</u>N), 115.4 (Ar<u>C</u>), 48.6 (<u>C</u>H_2), 16.6 (<u>C</u>H_2). MS (ES+, m/z): 234.07 [M+H] 256.0617 [M+Na].

2.4.5 Synthesis of N1-(3-aminopropyl)-N1-phenylpropane-1,3-diamine (R = H)



Typical procedure: To a solution of 3,3'-(phenylazanediyl)dipropanenitrile (0.50 g, 2.50 mmol) in anhydrous methanol (100 ml) was added $NiCl_2 \cdot 6H_2O$ (0.48 g, 0.20 mmol). Then over a period of 30 min $NaBH_4$ (0.53 g, 14.0 mmol) was added in small portions to the reaction solution. After the addition was complete the reaction mixture was stirred for 48 h at room temperature. After this time diethylenetriamine (1.00 ml, 8.72 mmol) was added to the reaction mixture and was left to stir for a further 30 min and the reaction mixture was then reduced *in vacuo.* The resulting residue was dissolved in EtOAc and washed with a saturated $NaHCO_3$ solution (2 x 50.0 ml). The mixture was then dried with $MgSO_4$ and reduced *in vacuo* to give a brown oil.

N1-(3-aminopropyl)-N1-phenylpropane-1,3-diamine (R = H)

The reaction to prepare N1-(3-aminopropyl)-N1-phenylpropane-1,3-diamine followed the typical procedure described in 2.4.5 and used 3,3'-(phenylazanediyl)dipropanenitrile (0.50 g, 2.50 mmol), to give N1-(3-

aminopropyl)-N1-phenylpropane-1,3-diamine as a brown oil (0.25 g, 1.21 mmol, 49 %).

^{1}H NMR (270 MHz, $CDCl_3$, 298 K): δ_H 7.29 (1H, t, *J* 7.4, Ar<u>H</u>), 6.88 (2H, m, Ar<u>H</u>), 6.73 (2H, d, *J* 7.4, Ar<u>H</u>), 3.77 (4H, t, *J* 6.7, C<u>H</u>$_2$), 3.64 (4H, m, C<u>H</u>$_2$), 2.65 (4H, t, *J* 6.7, C<u>H</u>$_2$). ^{13}C NMR (270 MHz, $CDCl_3$, 298 K): δ_C 145.0 (Ar<u>C</u>-N), 130.0 (Ar<u>C</u>), 119.6 (Ar<u>C</u>), 113.4 (Ar<u>C</u>), 48.3 (<u>C</u>H$_2$), 38.3 (<u>C</u>-NH$_2$), 29.4 (<u>C</u>H$_2$). MS (ES+, m/z): 208.1735 [M+H].

2.4.6 N1-(3-aminopropyl)-N1-(4-methoxyphenyl)propane-1,3-diamine (R = OMe)

The reaction to prepare N1-(3-aminopropyl)-N1-(4-methoxyphenyl)propane-1,3-diamine followed the typical procedure described in 2.4.5 and used 3,3'-((4-methoxyphenyl)azanediyl)dipropanenitrile (2.00 g, 10.0 mmol), to give N1-(3-aminopropyl)-N1-phenylpropane-1,3-diamine as a brown oil (1.36 g, 5.75 mmol, 66 %).

^{1}H NMR (270 MHz, $CDCl_3$, 298 K): δ_H 6.88 (2H, d, *J* 6.8, Ar<u>H</u>), 6.82 (2H, d, *J* 6.8, Ar<u>H</u>), 3.81 (3H, s, C<u>H</u>$_3$), 3.72 (4H, t, *J* 7.2, C<u>H</u>$_2$), 3.56 (4H, m, C<u>H</u>$_2$), 2.59 (4H, t, *J* 7.2, C<u>H</u>$_2$). ^{13}C NMR (67 MHz, $CDCl_3$, 298 K): δ_C 155.0 (Ar<u>C</u>-O), 139.2 (Ar<u>C</u>-N), 119.4 (Ar<u>C</u>), 115.3 (Ar<u>C</u>), 55.3 (O-<u>C</u>H$_3$), 49.9 (<u>C</u>H$_2$), 39.7 (<u>C</u>-NH$_2$) 29.3 (<u>C</u>H$_2$). MS (ES+, m/z): 238.1841 [M+H].

2.4.7 N1-(3-aminopropyl)-N1-(4-tert-butylphenyl)propane-1,3-diamine (R = ^{t}Bu)

The reaction to prepare N1-(3-aminopropyl)-N1-(4-*tert*-butylphenyl)propane-1,3-diamine followed the typical procedure described in 2.4.5 and used 3,3'-((4-

(*t*-butyl)phenyl)azanediyl)dipropanenitrile (2.00 g, 10.0 mmol), to give N1-(3-aminopropyl)-N1-(4-*tert*-butylphenyl)propane-1,3-diamine as a brown oil (1.54 g, 5.85 mmol, 75 %).

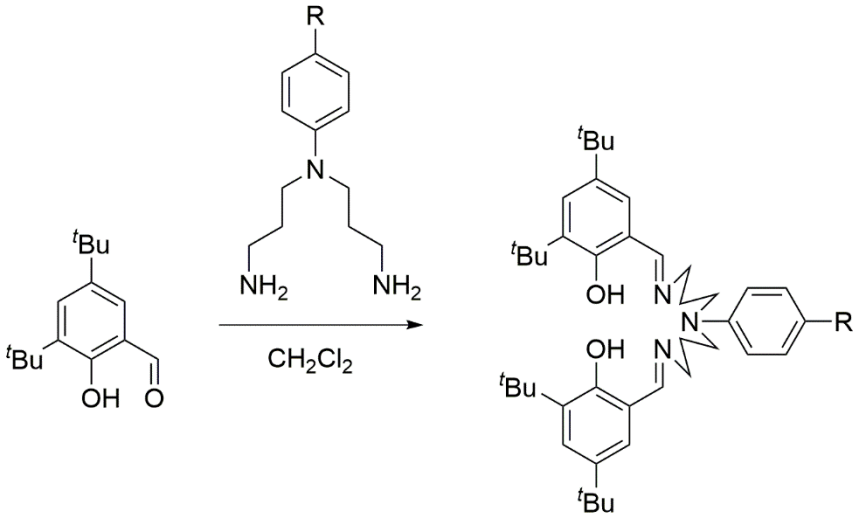
^{1}H NMR (270 MHz, $CDCl_3$, 298 K): δ_H 6.87 (2H, d, *J* 6.7, Ar<u>H</u>), 6.78 (2H, d, *J* 6.7, Ar<u>H</u>), 3.82 (9H, s, C(C<u>H</u>$_3$)$_3$), 3.69 (4H, t, *J* 6.2, C<u>H</u>$_2$), 3.58 (4H, m, C<u>H</u>$_2$), 2.2 (4H, t, *J* 6.2, C<u>H</u>$_2$). ^{13}C NMR (67 MHz, $CDCl_3$, 298 K): δ_C 146.2 (Ar<u>C</u>-N), 142.8 (Ar<u>C</u>- C$(CH_3)_3$), 126.7 (Ar<u>C</u>), 113.4 (Ar<u>C</u>), 48.0 (N-<u>C</u>H$_2$), 39.8 (<u>C</u>-NH$_2$), 34.8 (<u>C</u>$(CH_3)_3$), 31.4 (<u>C</u>H$_3$) , 29.8 (<u>C</u>H$_2$). MS (ES+, m/z): 264.2361 [M+H].

2.4.8 N1-(3-aminopropyl)-N1-(4-chlorophenyl)propane-1,3-diamine (R = Cl)

The reaction to prepare N1-(3-aminopropyl)-N1-(4-chlorophenyl)propane-1,3-diamine followed the typical procedure described in 2.4.5 and used 3,3'-((4-chlorophenyl)azanediyl)dipropanenitrile (2.00 g, 10.0 mmol), to give N1-(3-aminopropyl)-N1-(4-chlorophenyl)propane-1,3-diamine as a brown oil (1.32 g, 5.47 mmol, 63 %).

^{1}H NMR (270 MHz, $CDCl_3$, 298 K): δ_H 7.12 (2H, d, *J* 6.9, Ar<u>H</u>), 6.68 (2H, d, *J* 6.9, Ar<u>H</u>), 3.33 (4H, t, *J* 6.8, C<u>H</u>$_2$), 2.75 (4H, m, C<u>H</u>$_2$) 1.71 (4H, t, *J* 6.8, C<u>H</u>$_2$). ^{13}C NMR (67 MHz, $CDCl_3$, 298 K): δ_C 146.3 (Ar<u>C</u>-N), 130.2 (Ar<u>C</u>), 128.6 (Ar<u>C</u>-Cl), 113.4 (Ar<u>C</u>), 48.4 (<u>C</u>H$_2$), 39.5 (<u>C</u>-NH$_2$) 30.6 (<u>C</u>H$_2$). MS (ES+, m/z): 242.1346 [M+H].

2.4.9 Synthesis of the Schiff-base Pro-ligands [H^{t}BuL$_O^R$] (R = H, OMe, ^{t}Bu, Cl, and Br)



Typical procedure: A solution of *N*1-(3-aminopropyl)-N1-phenylpropane-1,3-diamine (1.50 g, 7.24 mmol) in CH_2Cl_2 (25.0 ml) was added drop-wise to a solution of 3,5-di-*tert*-butyl-2-hydroxybenzaldehyde (3.39 g, 14.5 mmol) in CH_2Cl_2 (25 ml). The reaction mixture was stirred at room temperature for 2 h. The solvent was removed *in vacuo* to give a yellow oil which was used without further purification.

[H^{t}BuL$_O^H$]

[H^{t}BuL$_O^H$] was prepared following the typical procedure described in 2.4.9 using N1-(3-aminopropyl)-N1-phenylpropane-1,3-diamine (1.50 g, 7.24 mmol), to give [H^{t}BuL$_O^H$] as a crude yellow oil (4.46 g, 7.81 mmol, 96 %). The ^{1}H NMR spectrum of the crude product contains features that may be assigned to [H^{t}BuL$_O^H$]. ^{1}H NMR (400 MHz, $CDCl_3$, 298 K): δ_H 8.38 (2H, s, N=C<u>H</u>), 7.41 (2H, d, *J* 2.4, Ar<u>H</u>), 7.26 – 7.19 (3H, m, Ar<u>H</u>), 7.10 (2H, d, *J* 2.4, Ar<u>H</u>), 6.66-

6.78 (2H, m, ArH), 3.66 (4H, t, *J* 7.2, C$\underline{H}_2$), 3.49 (4H, t, *J* 7.2, C$\underline{H}_2$), 2.08 – 2.00 (4H, m, C$\underline{H}_2$), 1.44 (18H, s, C(C$\underline{H}_3$)$_3$), 1.34 (18H, s, C(C$\underline{H}_3$)$_3$). MS (ES+, m/z): 644.5077 [M+H].

2.4.10 [H^{t}BuL$_O^{OMe}$]

The reaction to prepare [H^{t}BuL$_O^{OMe}$] followed the typical procedure described in 2.4.9 and used N1-(3-aminopropyl)-N1-(4-methoxyphenyl)propane-1,3-diamine (1.72 g, 7.24 mmol), to give [H^{t}BuL$_O^{OMe}$] as a crude yellow oil (4.80 g, 7.18 mmol, 99 %). ^{1}H NMR (400 MHz, $CDCl_3$, 298 K): δ_H 8.34 (2H, s, N=C$\underline{H}$), 7.41 (2H, d, *J* 2.3, Ar$\underline{H}$), 7.09 (2H, d, *J* 6.8, Ar$\underline{H}$), 6.94 - 6.75 (4H, m, Ar$\underline{H}$), 3.63 – 3.68 (4H, m, *J* 7.1, C$\underline{H}_2$), 3.54 (4H, t, *J* 7.1, C$\underline{H}_2$), 3.43 (3H, s, OC$\underline{H}_3$), 2.05 - 2.00 (4H, m, C$\underline{H}_2$), 1.46 (18H, s, C(C$\underline{H}_3$)$_3$), 1.31 (18H, s, C(C$\underline{H}_3$)$_3$). MS (ES+, m/z): 674.5182 [M+H].

2.4.11 [H^{t}BuL$_O^{tBu}$]

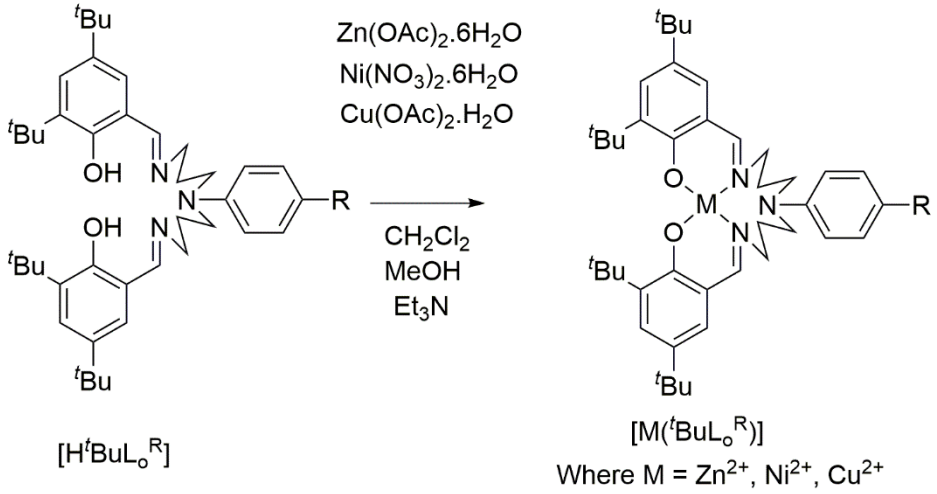
The reaction to prepare [H^{t}BuL$_O^{tBu}$] followed the typical procedure described in 2.4.9 and used N1-(3-aminopropyl)-N1-(4-(*tert*-butyl)phenyl)propane-1,3-diamine (1.91 g, 7.24 mmol), to give [H^{t}BuL$_O^{tBu}$] as a crude yellow oil (4.99 g, 7.18 mmol, 99 %). The ^{1}H NMR spectrum of the crude product could not be assigned reliably because of overlapping features associated with the putative product and byproducts. The positive ion electrospray mass spectrum provided some evidence that the target compound had been synthesised. MS (ES+, m/z): 700.5703 [M+H].

2.4.12 [H^{t}BuL$_O^{Cl}$]

The reaction to prepare [H^{t}BuL$_O^{Cl}$] followed the typical procedure described in 2.4.9 and used N1-(3-aminopropyl)-N1-(4-chlorophenyl)propane-1,3-diamine

(1.74 g, 7.24 mmol), to give [H^{t}BuL$_O^{Cl}$] as a yellow oil (4.71 g, 6.99 mmol, 97 %). ^{1}H NMR (400 MHz, $CDCl_3$, 298 K): δ_H 8.38 (2H, s, N=C<u>H</u>), 7.43 (2H, d, *J* 2.5, Ar<u>H</u>), 7.14 (2H, d, *J* 9.2 Ar<u>H</u>), 7.10 (2H, d, *J* 2.5, Ar<u>H</u>), 6.65 (2H, d, *J* 9.2, Ar<u>H</u>), 3.68 (4H, t, *J* 6.4, C<u>H</u>$_2$), 3.43 (4H, t, *J* 6.4, C<u>H</u>$_2$), 2.06 – 2.00 (4H, m, C<u>H</u>$_2$), 1.49 (18H, s, C(C<u>H</u>$_3$)$_3$), 1.34 (18H, s, C(C<u>H</u>$_3$)$_3$). MS (ES+, m/z): 678.4687 [M+H].

2.4.13 Synthesis of the Schiff-base Zn(II), Ni(II) and Cu(II) Diphenolate Complexes [M(^{t}BuL$_O^R$)] (R = H, OMe, ^{t}Bu, Cl, and Br)



Typical procedure: $Zn(OAc)_2{\cdot}2H_2O$ (0.17 g, 0.78 mmol) in methanol (3.00 ml) was added drop-wise to a solution of crude [H^{t}BuL$_O^H$] (0.50 g, 0.78 mmol) in CH_2Cl_2 (20.0 ml). The mixture was left to stir for 5 min before Et_3N (0.11 ml, 0.78 mmol) was added. After this time the reaction mixture was left to stir for 24 h at reflux. The volume of the solvent was then reduced to *ca.* 5 ml *in vacuo* and a yellow solid was precipitated following the addition of hexane (30 ml) and collected by filtration.

Attempted synthesis of [Zn(^{t}BuL$_O^H$)]

[Zn(^{t}BuL$_O^H$)] was prepared using the general procedure described in 2.4.13 and used [H^{t}BuL$_O^H$] (0.50 g, 0.78 mmol) to give [Zn(^{t}BuL$_O^H$)] as a crude yellow powder (0.32 g, 0.51 mmol, 66 %). Attempts to purify this material by recrystallization from CH_2Cl_2 / hexane mixtures were unsuccessful. FTIR ν / cm^{-1} (ATR): 2957 (m), 2859 (m), 1620 (m), 1599 (m), 1435 (w), 1290 (s), 1214 (w), 1102 (m), 1022 (m), 835 (w) 765 (s) 732 (m), 718 (m) 527 (w). MS (ES+, m/z): 704.4055 [M+H].

2.4.14 [Zn(^{t}BuL$_O^{OMe}$)]

[Zn(^{t}BuL$_O^{OMe}$)] was prepared using the general procedure described in 2.4.13 and used [H^{t}BuL$_O^{OMe}$] (0.51 g, 0.78 mmol) to give [Zn(^{t}BuL$_O^{OMe}$)] as a yellow powder (0.378 g, 0.52 mmol, 68 %). ^{1}H NMR (400 MHz, $CDCl_3$, 298 K): δ_H 8.35 (2H, s, N=C<u>H</u>), 7.39 (2H, d, *J* 2.3, Ar<u>H</u>), 7.07 (2H, d, *J* 2.3, Ar<u>H</u>), 6.81 (2H, d, *J* 9.2, Ar<u>H</u>), 6.76 (2H, d, *J* 9.2, Ar<u>H</u>), 3.62 (4H, t, *J* 6.5, C<u>H</u>$_2$), 3.34 (4H, t, *J* 6.5 C<u>H</u>$_2$), 3.78 (3H, s, C<u>H</u>$_3$), 1.97 – 1.94 (4H, m, C<u>H</u>$_2$), 1.46 (18H, s, C(C<u>H</u>$_3$)$_3$), 1.32 (18H, s, C(C<u>H</u>$_3$)$_3$). FTIR ν / cm^{-1} (ATR): 2955 (m), 2862 (m), 1628 (m), 1503 (m), 1456 (s), 1309 (s), 1250 (s), 1164 (m), 1027 (m), 834 (m) 789 (s) 689(m), 620 (m) 534 (m). MS (ES+, m/z): 734.4161 [M+H]. Elemental analysis: found (calculated for $ZnC_{43}H_{61}N_3O_3$): C 70.45 (70.43), H 8.41 (8.38), N 5.75 (5.73).

2.4.15 Attempted synthesis of [Zn(^{t}BuL$_O^{tBu}$)]

[Zn(^{t}BuL$_O^{tBu}$)] was prepared using the general procedure described in 2.4.13 and used [H^{t}BuL$_O^{tBu}$] (0.52 g, 0.78 mmol) to give [Zn(^{t}BuL$_O^{OMe}$)] as a crude yellow powder (0.35 g, 0.46 mmol, 62 %). Attempts to purify this material by recrystallization from CH_2Cl_2 / hexane mixtures were unsuccessful. FTIR ν / cm^{-1} (ATR): 2958 (m), 2865 (m), 2166 (m), 1963 (m) 1612 (s), 1519 (s), 1459 (m), 1437(m), 1360 (m), 1254 (s), 1163 (s), 1028 (m), 951 (w) 874 (s), 534 (m). MS (ES+, m/z): 760.4681 [M+H].

2.4.16 [Zn(^{t}BuL$_O^{Cl}$)]

[Zn(^{t}BuL$_O^{Cl}$)] was prepared using the general procedure described in 2.4.13 and used [H^{t}BuL$_O^{Cl}$] (0.51 g, 0.78 mmol) to give [Zn(^{t}BuL$_O^{Cl}$)] as a yellow powder (0.18 g, 0.25 mmol, 34 %). ^{1}H NMR (400 MHz, $CDCl_3$, 298 K): δ_H 8.36 (2H,

s, N=C<u>H</u>), 7.42 (2H, d, *J* 2.5, Ar<u>H</u>), 7.14 (2H, d, *J* 9.2, Ar<u>H</u>), 7.10 (2H, d, *J* 2.4, Ar<u>H</u>), 6.64 (2H, d, *J* 9.2, Ar<u>H</u>), 3.63 (4H, t, *J* 6.2, C<u>H</u>$_2$), 3.27 (4H, t, *J* 6.2 C<u>H</u>$_2$), 2.03 – 1.94 (4H, m, C<u>H</u>$_2$), 1.32 (18H, s, C(C<u>H</u>$_3$)$_3$), 1.29 (18H, s, C(C<u>H</u>$_3$)$_3$). FTIR ν / cm^{-1} (ATR): 2957 (m), 2864 (m), 1621 (s), 1591 (s), 1459 (s), 1322 (s), 1255 (s), 1164 (m), 1043 (m), 836 (m) 798 (s) 747 (m), 671 (m) 632 (m). MS (ES+, m/z): 738.3666 [M+H]. Elemental analysis: found (calculated for $ZnC_{42}H_{58}N_3O_2Cl$): C 68.39 (68.38), H 7.90 (7.92), N 5.68 (5.70).

2.4.17 [Ni(^{t}BuLo^H)]

[Ni(^{t}BuL$_O^H$)] was prepared using the general procedure above from [H^{t}BuL$_O^H$] (0.50 g, 0.75 mmol). [Ni(^{t}BuL$_O^H$)] was isolated as a light green powder (0.27 g, 0.40 mmol, 53 %). FTIR ν / cm^{-1} (ATR): 2957 (m), 2859 (m), 1620 (m), 1597 (m), 1504 (m), 1435 (w), 1390 (s), 1214 (w), 1103 (m), 1022 (s), 835 (w) 765 (s) 731 (m), 718 (m). MS (ES+, m/z): 697.64 [M+H]. Elemental analysis: found (calculated for $C_{42}H_{59}N_3NiO_2$): C 72.43 (72.41), H 8.60 (8.54), N 6.03 (6.03). Yield = 53 %

2.4.18 [Ni(^{t}BuLo^{OMe})]

[Ni(^{t}BuL$_O^{OMe}$)] was prepared using the general procedure above from [H^{t}BuL$_O^{OMe}$] (0.50 g, 0.75 mmol). [Ni(^{t}BuL$_O^{OMe}$)] was isolated as a light green powder (0.32 g, 0.44 mmol, 59 %). FTIR ν / cm^{-1} (ATR): 2955 (m), 2862 (m), 1629 (m), 1504 (m), 1456 (s), 1309 (s), 1251 (s), 1164 (m), 1027 (m), 837 (m) 789 (s) 689(m), 620 (m) 535 (m). MS (ES+, m/z): 652.57 [M+H]. Elemental analysis: found (calculated for $C_{43}H_{61}N_3NiO_3$): C 71.08 (71.07), H 8.42 (8.46), N 5.78 (5.78).

2.4.19 [Ni(^{t}BuL$_{O}^{tBu}$)]

[Ni(^{t}BuL$_{O}^{tBu}$)] was prepared using the general procedure above from [H^{t}BuL$_{O}^{tBu}$] (0.50 g, 0.72 mmol). [Ni(^{t}BuL$_{O}^{OMe}$)] was isolated as a green powder (0.26 g, 0.35 mmol, 49 %). FTIR ν / cm^{-1} (ATR): 2958 (m), 2865 (m), 1614 (s), 1519 (s), 1456 (m), 1436 (m), 1361 (m), 1322 (s), 1270 (s), 1255 (s), 1199 (s), 1167 (s), 1131 (m), 1113 (m), 1044 (m), 971 (w) 813 (s), 514 (m). MS (ES+, m/z): 652.57 [M+H]. Elemental analysis: found (calculated for $C_{46}H_{67}N_3NiO_2$): C 73.41 (73.40), H 8.97 (8.97), N 5.56 (5.58).

2.4.20 [Ni(^{t}BuL$_{O}^{Cl}$)]

[Ni(^{t}BuL$_{O}^{Cl}$)] was prepared using the general procedure above from [H^{t}BuL$_{O}^{Cl}$] (0.50 g, 0.74 mmol). [Ni(^{t}BuL$_{O}^{Cl}$)] was isolated as a dark green powder (0.18 g, 0.25 mmol, 34 %). FTIR ν / cm^{-1} (ATR): 2959 (m), 2864 (m), 1621 (s), 1591 (s), 1458 (s), 1322 (s), 1256 (s), 1164 (m), 1043 (m), 838 (m) 798 (s) 747 (m), 671 (m) 632 (m). MS (ES+, m/z): 730.35 [M+H]. Elemental analysis: found (calculated for $C_{42}H_{58}ClN_3NiO_2$): C 68.98 (69.00), H 7.95 (8.00), N 5.80 (5.75).

2.4.21 [Cu(^{t}BuL$_{O}^{H}$)]

[Cu(^{t}BuL$_{O}^{H}$)] was prepared using the general procedure above from [H^{t}BuL$_{O}^{H}$] (0.50 g, 0.75 mmol). [Cu(^{t}BuL$_{O}^{H}$)] was isolated as a light brown powder (0.28 g, 0.40 mmol, 54 %). (ATR): 2957 (m), 2859 (m), 1618 (m), 1597 (m), 1504 (s), 1459 (s), 1434 (w), 1411(s), 1385 (s), 1359 (s), 1318 (s), 1255 (w), 1234 (w), 1200 (w), 1102 (m), 1022 (m), 837 (w) 765 (s) 732 (m), 719 (m) 526 (w). MS (ES+, m/z): 701.39 [M+H]. Elemental analysis: found (calculated for $C_{42}H_{59}CuN_3O_2$): C 71.92 (71.91), H 8.45 (8.48), N 5.97 (5.99).

2.4.22 [Cu(^{t}BuL$_{O}^{OMe}$]

[Cu(^{t}BuL$_{O}^{OMe}$)] was prepared using the general procedure above from [H^{t}BuL$_{O}^{OMe}$] (0.50 g, 0.75 mmol). [Cu(^{t}BuL$_{O}^{OMe}$)] was isolated as a dark brown powder (0.34 g, 0.47 mmol, 62 %). FTIR ν / cm^{-1} (ATR): 2955 (m), 2863 (m), 1628 (m), 1503 (m), 1456 (s), 1359 (s), 1322 (m), 1309 (s), 1250 (s), 1165 (m), 1027 (m), 835 (m) 787 (s) 681 (m), 625 (m) 534 (m) 489 (m). MS (ES+, m/z): 731.40 [M+H]. Elemental analysis: found (calculated for $C_{43}H_{61}CuN_3O_3$): C 70.62 (70.60), H 8.43 (8.41), N 5.76 (5.74).

2.4.23 [Cu(^{t}BuL$_{O}^{tBu}$)]

[Cu(^{t}BuL$_{O}^{tBu}$)] was prepared using the general procedure above from [H^{t}BuL$_{O}^{tBu}$] (0.50 g, 0.72 mmol). [Cu(^{t}BuL$_{O}^{tBu}$)] was isolated as a dark brown powder (0.21 g, 0.29 mmol, 41 %). FTIR ν / cm^{-1} (ATR): 2959 (m), 2865 (m), 2167 (m), 1964 (m) 1614 (s), 1562 (4 (m), 964 (w) 836 (s), 770 (s), 711 (s), 534 (m). MS (ES+, m/z): 731.40 [M+H]. Elemental analysis: found (calculated for $C_{46}H_{67}CuN_3O_2$): C 72.93 (72.93), H 8.89 (8.91), N 5.55 (5.55).

2.4.24 [Cu(^{t}BuL$_{O}^{Cl}$)]

[Cu(^{t}BuL$_{O}^{Cl}$)] was prepared using the general procedure above from [H^{t}BuL$_{O}^{Cl}$] (0.50 g, 0.74 mmol). [Cu(^{t}BuL$_{O}^{Cl}$)] was isolated as a dark borwn powder (0.15 g, 0.20 mmol, 28 %). FTIR ν / cm^{-1} (ATR): 2956 (m), 2864 (m), 1623 (s), 1592 (s), 1459 (s), 1321 (s), 1255 (s), 1166 (m), 1041 (m), 836 (m) 798 (s) 747 (m), 671 (m) 638 (m). MS (ES+, m/z): 735.35 [M+H]. Elemental analysis: found (calculated for $C_{42}H_{58}ClCuN_3O_2$): C 68.55 (68.55), H 7.92 (7.94), N 5.75 (5.71).

2.5 References

(1) Rogers, M. *Curr. Opin. Chem. Biol.* **2003**, *7*, 189–196.

(2) Cappuccio, J. A.; Ayala, I.; Elliott, G. I.; Szundi, I.; Lewis, J.; Konopelski, J. P.; Barry, B. A.; Einarsdóttir, Ó. *J. Am. Chem. Soc.* **2002**, *124*, 1750–1760.

(3) Stubbe, J.; van der Donk, W. A. *Chem. Rev.* **1998**, *98*, 705–762.

(4) Stubbe, J.; Nocera, D. G.; Yee, C. S.; Chang, M. C. Y. *Chem. Rev.* **2003**, *103*, 2167–2201.

(5) Dorlet, P.; Seibold, S. A.; Babcock, G. T.; Gerfen, G. J.; Smith, W. L.; Tsai, A. L.; Un, S. *Biochemistry*, **2002**, *41*, 6107-6114.

(6) Wang, Y.; Stack, T. D. P. *J. Am. Chem. Soc.* **1996**, *118*, 13097–13098.

(7) Sokolowski, A.; Leutbecher, H.; Weyhermüller, T.; Schnepf, R.; Bothe, E.; Bill, E.; Hildebrandt, P.; Wieghardt, K. *J. Biol. Inorg. Chem.* **1997**, *2*, 444–453.

(8) Rotthaus, O.; Thomas, F.; Jarjayes, O.; Philouze, C.; Saint-Aman, E.; Pierre, J. L. *Chem. Eur. J.* **2006**, *12*, 6953–6962.

(9) Nairn, A. K.; Archibald, S. J.; Bhalla, R.; Gilbert, B. C.; Maclean, E. J.; Teat, S. J.; Walton, P. H. *Dalton Trans.* **2006**, *1*, 172–176.

(10) Jazdzewski, B. A.; Tolman, W. B.; *Coord. Chem. Rev.* **2000**, 200, 633-685.

(11) Benisvy, L.; Blake, A. J.; Collison, D.; Davies, E. S.; Garner, C. D.; McInnes, E. J.; McMaster, J.; Whittaker, G.; Wilson, C. *Chem. Commun.* **2001**, *18*, 1824–1825.

(12) Rotthaus, O.; Jarjayes, O.; Perez Del Valle, C.; Philouze, C.; Thomas, F. *Chem. Commun.* **2007**, *43*, 4462–4464.

(13) Parker, D.; Davies, E. S.; Wilson, C.; McMaster, J. *Inorg. Chim. Acta.* **2007**, *360*, 203–211.

(14) Benisvy L.; Bill E.; Blake A. J.; Collison D.; Davies E. S.; Garner C. D.; Guindy C. I.; McInnes E. J. L.; McArdle G.; McMaster J.; Wilson C.; Wolowska J., *Dalton Trans.* **2004**, 3647-3653.

(15) L. Benisvy, A. J. Blake, D. Collison, E. S. Davies, C. D. Garner, E. J. L. McInnes, J. McMaster, G. Whittaker and C. Wilson, *Dalton Trans.* **2003**, 1975-1985.

(16) Shimazaki, Y.; Tani, F.; Fukui, K.; Naruta, Y.; Yamauchi, O. *J. Am. Chem. Soc* **2003**, *125*, 10512–10513.

(17) Shimazaki, Y.; Huth, S.; Karasawa, S.; Hirota, S.; Naruta, Y.; Yamauchi, O. *Inorg. Chem.* **2004**, *43*, 7816–7822.

(18) Müller, J.; Kikuchi, A.; Bill, E.; Weyhermüller, T.; Hildebrandt, P.; Ould-Moussa, L.; Wieghardt, K. *Inorg. Chim. Acta.* **2000**, *297*, 265–277.

(19) Orio, M.; Philouze, C.; Jarjayes, O.; Neese, F.; Thomas, F. *Inorg. Chem.* **2010**, *49*, 646–658.

(20) Arora, H.; Philouze, C.; Jarjayes, O.; Thomas, F. *Dalton Trans.* **2010**, *39*, 10088–10098.

(21) Rotthaus, O.; Jarjayes, O.; Philouze, C.; Del Valle, C. P.; Thomas, F. *Dalton Trans.* **2009**, 1792–1800.

(22) Rotthaus, O.; Labet, V.; Philouze, C.; Jarjayes, O.; Thomas, F. *Eur. J. Inorg. Chem.* **2008**, *2008*, 4215–4224.

(23) Rotthaus, O.; Thomas, F.; Jarjayes, O.; Philouze, C.; Saint-Aman, E.; Pierre, J. L.; *Chem. Eur. J.* **2006**, *12*, 6953-6962.

(24) Benisvy, L.; Kannappan, R.; Song, Y.-F.; Milikisyants, S.; Huber, M.; Mutikainen, I.; Turpeinen, U.; Gamez, P.; Bernasconi, L.; Baerends, E. J.; Hartl, F.; Reedijk, J. *Eur. J. Inorg. Chem.* **2007**, 637–642.

(25) Freire, C.; de Castro, B. *J. Chem. Soc., Dalton Trans.* **1998**, 1491-1497.

(26) Glaser, T.; Heidemeier, M.; Fröhlich, R.; Hildebrandt, P.; Bothe, E.; Bill, E. *Inorg. Chem.* **2005**, *44*, 5467–5482.

(27) Shimazaki, Y.; Yajima, T.; Tani, F.; Karasawa, S.; Fukui, K.; Naruta, Y.; Yamauchi, O. *J. Am. Chem. Soc.* **2007**, *129*, 2559–2568.

(28) Storr, T.; Wasinger, E. C.; Pratt, R. C.; Stack, T. D. P. *Angew. Chem. Int. Ed. Engl.* **2007**, *46*, 5198–5201.

(29) Bencini, A.; Carbonera, C.; Dei, A.; Vaz, M. G. F. *Dalton Trans.* **2003**, 1701–1706.

(30) Franks, M.; Gadzhieva, A.; Ghandhi, L.; Murrell, D.; Blake, A. J.; Davies, E. S.; Lewis, W.; Moro, F.; McMaster, J.; Schröder, M. *Inorg. Chem.* **2013**, *52*, 660–670.

(31) Franks, M. Transition Metal Complexes Containing Phenylthiolate and Phenolate Ligands, University of Nottingham, 2011.

(32) Sokolowski, A.; Müller, J.; Weyhermüller, T.; Schnepf, R.; Hildebrandt, P.; Hildenbrand, K.; Bothe, E.; Wieghardt, K. *J. Am. Chem. Soc.* **1997**, *119*, 8889–8900.

(33) Pittelkow, M.; Nielsen, C. B.; Kadziola, A.; Christensen, J. B. *J. Incl. Phenom. Macrocycl. Chem.* **2008**, *63*, 257–266.

(34) Johnson J. W.; Potter W.; Rose P. G.; Scott G.; *Polym. Int.* **1972**, *6*, 527–540

(35) Bengough, W. I.; Fairservice, W. H. *Trans. Faraday Soc.* **1967**, *63*, 382.

(36) pK_a table http://sites.chem.colostate.edu/diverdi/all_courses/CRC reference data/dissociation constants of organic acids and bases.pdf (accessed Apr 4, 2015).

(37) Caddick, S.; Judd, D. B.; Lewis, A. K. d. K.; Reich, M. T.; Williams, M. R., *Tetrahedron* **2003**, *59*, 5417–5423.

(38) Addison A. W.; Rao T. N.; Reedijk J.; Vanrijn J.; Verschoor G. C., *J. Chem. Soc., Dalton Trans.*, **1984**, 1349-1356.

(39) Yilmaz, V. T.; Degirmencioglu, I.; Andac, O.; Karabocek, S.; Slawin, A. M. Z. *J. Mol. Struct.* **2003**, *654*, 125–129.

(40) Seleborg, M.; Holt, S.; Post, B. *Inorg. Chem.* **1971**, *10*, 1501.

(41) Orioli, P. L.; Di Vaira, M.; Sacconi, L. *Chem. Commun.* **1966**, *10*, 300.

(42) Healy, P. C.; Mockler, G. M.; Freyberg, D. P.; Sinn, E. *J. Chem. Soc. Dalton Trans.* **1975**, *8*, 691.

(43) Divaira, M.; Sacconi, L.; Oriloi, P. *Inorg. Chem.* **1971**, *10*, 553.

(44) Amirnasr, M.; Schenk, K. J.; Meghdadi, S.; Morshedi, M. *Polyhedron* **2006**, *25*, 671–677.

(45) Benisvy, L.; Bill, E.; Blake, A. J.; Collison, D.; Davies, E. S.; Garner, C. D.; McArdle, G.; McInnes, E. J. L.; McMaster, J.; Ross, S. H. K.; Wilson, C. *Dalton Trans.* **2006**, *1*, 258–267.

(46) Benisvy, L.; Blake, A. J.; Collison, D.; Davies, E. S.; David, C.; Mcinnes, E. J. L.; Mcmaster, J.; Wilson, C. *Dalton Trans.*, **2003**, 1975–1985.

(47) Benisvy, L.; Blake, A. J.; Collison, D.; Stephen Davies, E.; David Garner, C.; McInnes, E. J. L.; McMaster, J.; Whittaker, G.; Wilson, C. *Dalton Trans.*, **2003**, *10*, 1975.

(48) Bill, E.; Müller, J.; Weyhermüller, T.; Wieghardt, K. *Inorg. Chem.* **1999**, *38*, 5795–5802.

(49) Kumar, D. N.; Garg, B. S. *Spectrochim. Acta - Part A Mol. Biomol. Spectrosc.* **2006**, *64*, 141–147.

(50) Halfen, J. A.; Jazdzewski, B. A.; Mahapatra, S.; Berreau, L. M.; Wilkinson, E. C.; Que, L.; Tolman, W. B. *J. Am. Chem. Soc.* **1997**, *119*, 8217–8227.

(51) Amundsen, A. R.; Whelan, J.; Bosnich, B. *J. Am. Chem. Soc.* **1977**, *99*, 6730–6739.

(52) Kasumov, V. T.; Medjidov, A. A.; Yayli, N.; Zeren, Y. *Spectrochim. Acta. A. Mol. Biomol. Spectrosc.* **2004**, *60*, 3037–3047.

(53) Rogez, G.; Rebilly, J. N.; Barra, A. L.; Sorace, L.; Blondin, G.;

Kirchner, N.; Duran, M.; Van Slageren, J.; Parsons, S.; Ricard, L.; Marvilliers, A.; Mallah, T. *Angew. Chemie - Int. Ed.* **2005**, *44*, 1876–1879.1876–1879.

(54) Krzystek, J.; Park, J. H.; Meisel, M. W.; Hitchma, M. A.; Stratemeier, H.; Brunel, L. C.; Telser, J. *Inorg. Chem.* **2002**, *41*, 4478–4487.

(55) Collison, D.; Helliwell, M.; Jones, V. M.; Mabbs, F. E.; McInnes, E. J. L.; Riedi, P. C.; Smith, G. M.; Pritchard, R. G.; Cross, W. I. *J. Chem. Soc. Faraday Trans.* **1998**, *94*, 3019–3025.

(56) Freire, C.; de Castro B. *Polyhedron*, **1998**, *17*, 4227-4235

Chapter 3: Synthesis and Characterisation of Schiff-Base Ni(II)-Dithiolate and Diphenolate Complexes

3.1.1 Introduction

Cysteine thiolate ligation occurs regularly at the active sites of Ni-containing metalloenzymes. Ni-containing enzymes with cysteine thiolate ligation include: methyl coenzyme M reductase,[1] carbon monoxide dehydrogenase,[2,3] acetyl coenzyme A synthase,[4,5] [NiFe] hydrogenase[6,7] and Ni-containing superoxide dismutase (NiSOD).[8–10] This observation has driven the synthesis and characterisation of low molecular weight complexes incorporating thiolate-bound Ni(II) centres.[11–13] These investigations focus on the role of this ligation in controlling the chemistry of the active sites of these Ni-containing enzymes. Of particular interest is the role of the thiolate co-ordination in tuning the formal Ni(III/II) redox couple.[14,15] The redox non-innocent nature of the thiolate ligation and the high degree of covalency that may be associated with the Ni-S(thiolate) bond means that oxidation processes that occur at the active sites of Ni-containing enzymes may lie between the metal-based [Ni(III)] and ligand-based (thiyl radical) redox extremes.[16–18]

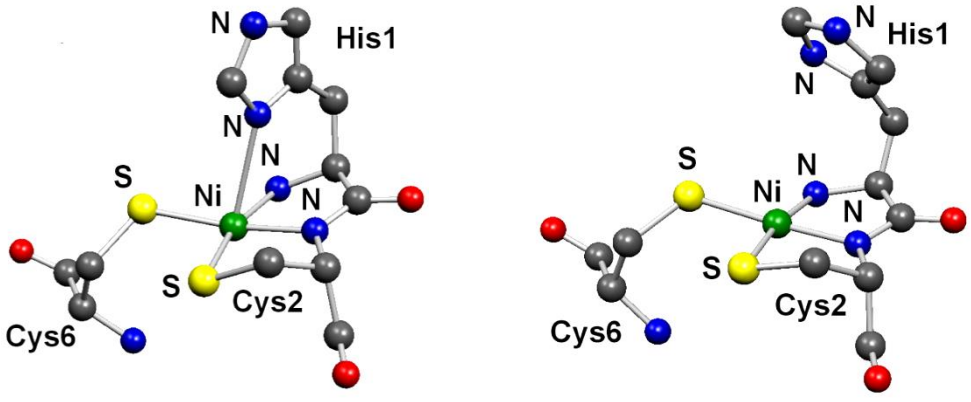


Figure 3.1 (Figure 1.3) Structures of the oxidised (left) and reduced forms (right) of the active site of NiSOD.

The active site of NiSOD (Figure 3.1) has received significant attention from inorganic chemists following X-ray diffraction studies on the NiSOD from *Streptomyces seoulensis*, which show the active site of this enzyme contains an unusual monomeric Ni(II) centre.[10,19] Although cysteine thiolate ligation is common within Ni-containing metalloenzymes, its presence at an active site primed to catalyse the dismutation of the biologically toxic oxidant, $O_2^{\bullet-}$ appeared unusual considering the potential vulnerability of thiolate donors towards oxidation.[20,21] This observation has prompted the preparation and study of low molecular weight thiolate-coordinated Ni(II) complexes to provide insight into how the coordination sphere at the active site of NiSOD primes the centre for optimal catalytic activity, whilst avoiding oxidative decomposition by its own substrate.

3.1.2 Previous Work

Two Ni(II) Schiff-base dithiolate complexes (Figure 3.2) have been reported by Stenson *et al.*[12,22] These complexes contain diamagnetic, mononuclear $Ni^{II}N_2S_2$ centres with four donor atoms (two S-thiolate and two N-imine) that bind to the Ni centre to give a distorted square planar coordination sphere. Cyclic voltammetry and coulombic measurements at 293 K in CH_2Cl_2 show reversible single-electron oxidation processes at $E_{1/2}$ = 0.16 V and 0.10 V *vs* Fc^+/Fc, for [Ni(^{t}BuL$_S^1$)] and [Ni(^{t}BuL$_S^2$)], respectively. Additionally, upon cooling (< 253 K) the oxidation processes become irreversible and are associated with the generation of EPR-silent species. X-ray crystallography showed that [Ni(^{t}BuL$_S^2$)]$^+$ decomposes to form a diamagnetic Ni(μ-SR)$_2$Ni dimer at low temperatures *via* the formation of a S-S disulfide bridge.[12,22]

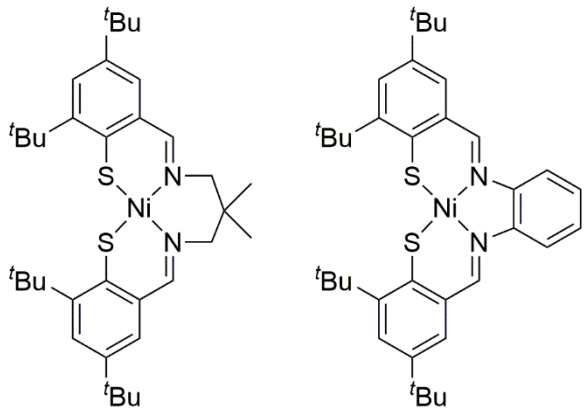


Figure 3.2 Schiff-base Ni(II) complexes, [Ni(^{t}BuL$_S^1$)] (left), [Ni(^{t}BuL$_S^2$)].[22]

The oxidation processes are also solvent dependent in addition to being dependent upon temperature.[12,22] EPR and UV/vis spectroscopic studies and supporting theoretical DFT calculations revealed that the oxidation of [Ni(^{t}BuL$_S^1$)] and [Ni(^{t}BuL$_S^2$)] in neat CH_2Cl_2 produce [Ni(^{t}BuL$_S^1$)]$^+$ and

$[Ni(^tBuL_S{}^2)]^+$, respectively, which possess SOMOs with substantial thiyl radical character (*ca.* 40% s-character). However, the addition of small coordinating molecules, such as pyridine, generates species that possess a metal-based, $d_z{}^2$ SOMO that suggests the addition of exogenous N-donors can drive a metal-centred oxidation process.[12,22]

Franks *et al.*[23] synthesised a range of dithiosalicylidenediamine Ni(II) complexes that built upon the previous work conducted by Stenson *et al.*.[12,22] Additional N-donor residues were incorporated into the original $[N_2S_2]$ ligand framework (Figure 3.3) with the goal of synthesising complexes that more accurately reproduced the structural, spectroscopic and functional properties of the active site of NiSOD.

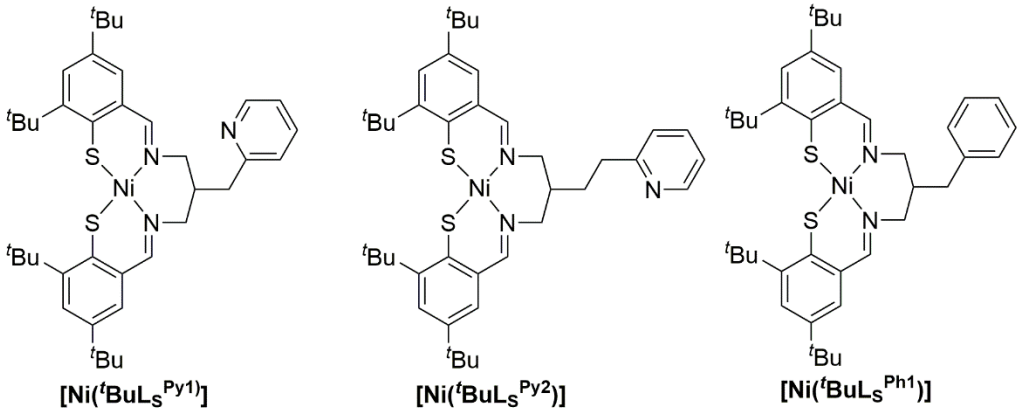


Figure 3.3 Schiff-base Ni(II) complexes, $[Ni(^tBuL_S{}^{Py1})]$, $[Ni(^tBuL_S{}^{Py2})]$ and $[Ni(^tBuL_S{}^{Ph1})]$.[23]

Electrochemical investigations show that $[Ni(^tBuL_S{}^{Ph1})]$ possesses an electrochemically reversible single-electron oxidation process ($E_p{}^a$ = 0.18 and $E_p{}^c$ = 0.11 V *vs* Fc^+/Fc) at a similar potential to those reported by Stenson *et al.*

for the analogous dithiosalicylidenediamine Ni(II) complexes [Ni(^{t}BuL$_S^1$)] and [Ni(^{t}BuL$_S^2$)] (Figure 3.2).[12,22] In contrast, electrochemical and spectroscopic studies show that [Ni(^{t}BuL$_S^{Py1}$)] and [Ni(^{t}BuL$_S^{Py2}$)] form singly oxidised species that are susceptible to a further oxidation by one redox equivalent. Electrochemical studies revealed that [Ni(^{t}BuL$_S^{Py2}$)] (E_p^a = 0.18 and E_p^c = 0.11 V *vs* Fc^+/Fc) is oxidised at the same potential as [Ni(^{t}BuL$_S^{Ph1}$)], which suggests that the pyridyl group of [Ni(^{t}BuL$_S^{Py2}$)] is too distant from the redox active centre of the molecule to stabilise the product formed upon oxidation. Fluid solution X-band EPR spectroscopy showed that the EPR spectrum of the species initially formed upon electrochemical and chemical oxidation of [Ni(^{t}BuL$_S^{Py2}$)] possesses an isotropic feature at g_{iso} = 2.071 with a Gaussian linewidth of 18 G, consistent with the generation of a species possessing substantial thiyl radical character (*c.f.* [Ni(^{t}BuL$_S^{Ph1}$)]$^+$).[23]

The position of the pyridyl group relative to the metal centre appears to have an impact upon the redox properties of the complex. Analysis of the electrochemical properties of [Ni(^{t}BuL$_S^{Py1}$)] revealed that the closer proximity of the 2-pyridyl group lowers the potential of the first oxidation process of [Ni(^{t}BuL$_S^{Py1}$)] by *ca.* 0.08 V relative to that for [Ni(^{t}BuL$_S^{Ph1}$)] and [Ni(^{t}BuL$_S^{Py2}$)]. The first oxidation couple of [Ni(^{t}BuL$_S^{Py1}$)] (E_p^a = 0.10 and E_p^c = 0.00 V *vs* Fc^+/Fc) also displayed a peak-to-peak separation that was larger than that of a couple controlled by heterogeneous electron transfer, which provides support for an internal rearrangement that may take place upon oxidation and reduction. This was supported by X-band EPR spectroscopic studies upon [Ni(^{t}BuL$_S^{Py1}$)]$^+$ which showed that the oxidised species possesses a rhombic

EPR spectrum (g_{11} = 2.282, g_{22} = 2.200, g_{33} = 2.016) consistent with a metal-centred SOMO. The well-defined three-line super hyperfine coupling to a single ^{14}N (I=1) nucleus in the g_{33} region suggests that the intramolecular rearrangement, which occurs upon oxidation, involves the axial coordination of the 2-pyridyl group to the Ni(III) centre. The binding of the 2-pyridyl group to the Ni(III) centre on oxidation of [Ni(^{t}BuL$_S^{Py1}$)] generates a SOMO possessing substantial metal character. A similar internal rearrangement of the coordination sphere takes place at the Ni centre of the active site of NiSOD, where the axial imidazole group of the His1 residue binds to the metal centre upon oxidation (Figure 3.1). The chemistry of [Ni(^{t}BuL$_S^{Py1}$)] emphasises the importance of the role of the axial imidazole ligand at the active site of NiSOD, which may tune the redox properties of the oxidised state of the enzyme and protect the thiolate donors of Cys1 and Cys6 from oxidative stress by ensuring that the redox active orbitals of the active site are predominantly metal-based.

The incorporation of 2,4-di-*tert*-butyl substitution into the thiophenol ring within Ni(II) Schiff-base dithiolate complexes has previously been shown to be important for the stabilisation of thiyl radical character that may be generated upon oxidation of the complex. The ability of the 2-pyridyl group to promote a metal-based oxidation process within [Ni(^{t}BuL$_S^{Py1}$)] raises the question as to whether 2,4-di-*tert*-butyl substitution of the thiophenolate ring remains a requirement within these systems for the stabilisation of the products of the oxidation process.

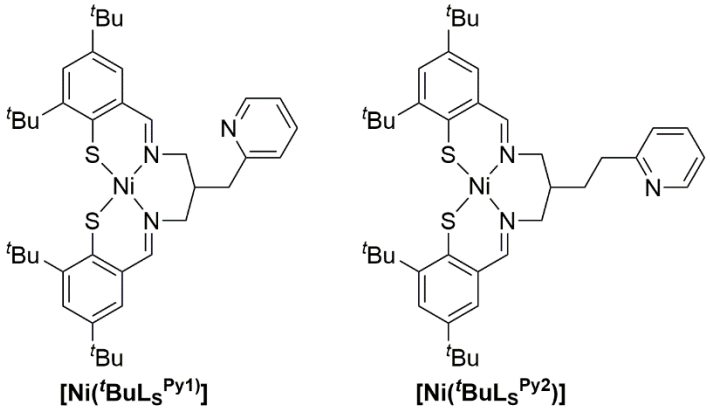


Figure 3.4 Schiff-base Ni(II) complexes, [Ni(^{t}BuL$_O^{Py1}$)] and [Ni(^{t}BuL$_S^{Py2}$)]. [23]

Franks *et al.*[23] also studied the analogous diphenolate [Ni(^{t}BuL$_O^{Py1}$)] and [Ni(^{t}BuL$_O^{Py2}$)] complexes (Figure 3.4). Electrochemical studies revealed that small changes in the composition of the ligand framework lead to a significant effect on the kinetic inertness of the oxidised species. Whilst the two overlapping one-electron oxidation processes of [Ni(^{t}BuL$_O^{Py1}$)] are chemically reversible, the two oxidation processes of [Ni(^{t}BuL$_O^{Py2}$)] yield species that readily decompose. This has been attributed to the pyridyl group being unable to bind to the metal centre upon oxidation and thus stabilise the [Ni(^{t}BuL$_O^{Py2}$)]$^+$ species.[23] The relative separation between the two sequential oxidation processes of [Ni(^{t}BuL$_O^{Py1}$)] meant that the two oxidation processes of [Ni(^{t}BuL$_O^{Py1}$)] could not be investigated individually using UV/vis spectroscopy, however absorption bands consistent with the generation of phenoxyl radical character were observed on the oxidation of [Ni(^{t}BuL$_O^{Py1}$)]. Attempts to electrochemically generate the one-electron oxidised product of [Ni(^{t}BuL$_O^{Py1}$)] yielded a species that was shown by X-band EPR spectroscopy to be consistent with the formation of a centre possessing substantial phenoxyl radical character. Cooling the sample to 77 K generated an EPR spectrum that could not be simulated as a single

species and that may result from redox tautomers of $[Ni(^{t}BuL_{O}^{Py1})]^{+}$. However, the predominant features within the spectrum appeared to be associated with a species possessing a SOMO with substantial metal character. It was proposed that the binding of the pyridyl group to the metal centre of $[Ni(^{t}BuL_{O}^{Py1})]^{+}$ may account for the proposed redox-tautomerism on cooling. X-band EPR spectroscopic studies upon solutions containing the doubly oxidised species of $[Ni(^{t}BuL_{O}^{Py1})]$ produced a rhombic EPR signal (g_{av} = 2.054). It was proposed that the signal is associated with an oxidised species that contains two equivalent non-interacting phenoxyl radical centres, however further measurements are required in order to define more precisely the nature of this species.

3.1.3 Aims of Chapter

This study aims to extend our knowledge of the previous work that has been completed at Nottingham through the synthesis of a range of [Ni(tsalen)] derived complexes that incorporate *ortho*- and *para*-*tert*-butyl substituents about the phenylthiolate aromatic rings. This work seeks to expand the original N_2S_2 ligand set through the incorporation of additional N-donor functionalities.

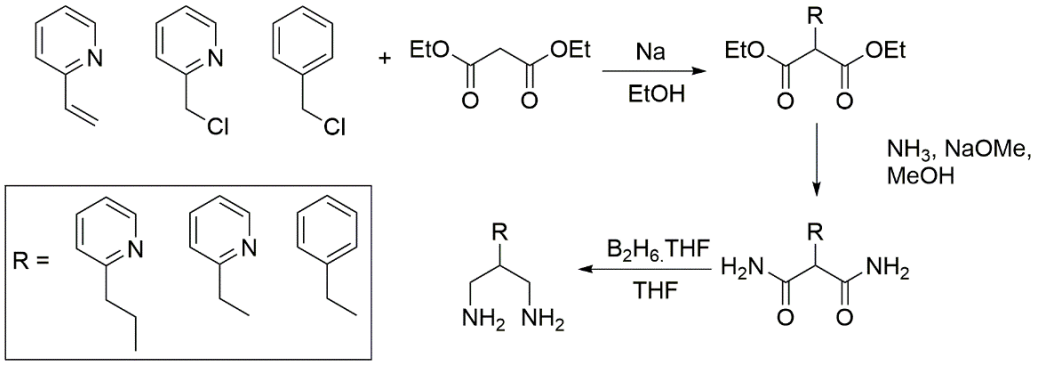
In previous work by Franks *et al.*[24] a pyridine donor group incorporated into the ligand framework binds to the coordinated Ni centre upon oxidation. The primary aim of the research described in this chapter is the synthesis and characterisation of dithiolate and diphenolate complexes that incorporate an imidazole donor group, similar to that featured at the active site of NiSOD (Figure 3.1). Our aim is to further our understanding of the Ni(II)-thiolate and Ni(II)-phenolate interaction, with particular emphasis placed upon how the incorporation of N-donor functionalities in addition to the N_2S_2 and N_2O_2 coordination sphere effect the redox chemistry of dithiolate and diphenolate Ni(II) complexes.

3.2 Results and Discussion

3.2.1 Attempted incorporation of a pendant imidazole functionality into the propane backbone

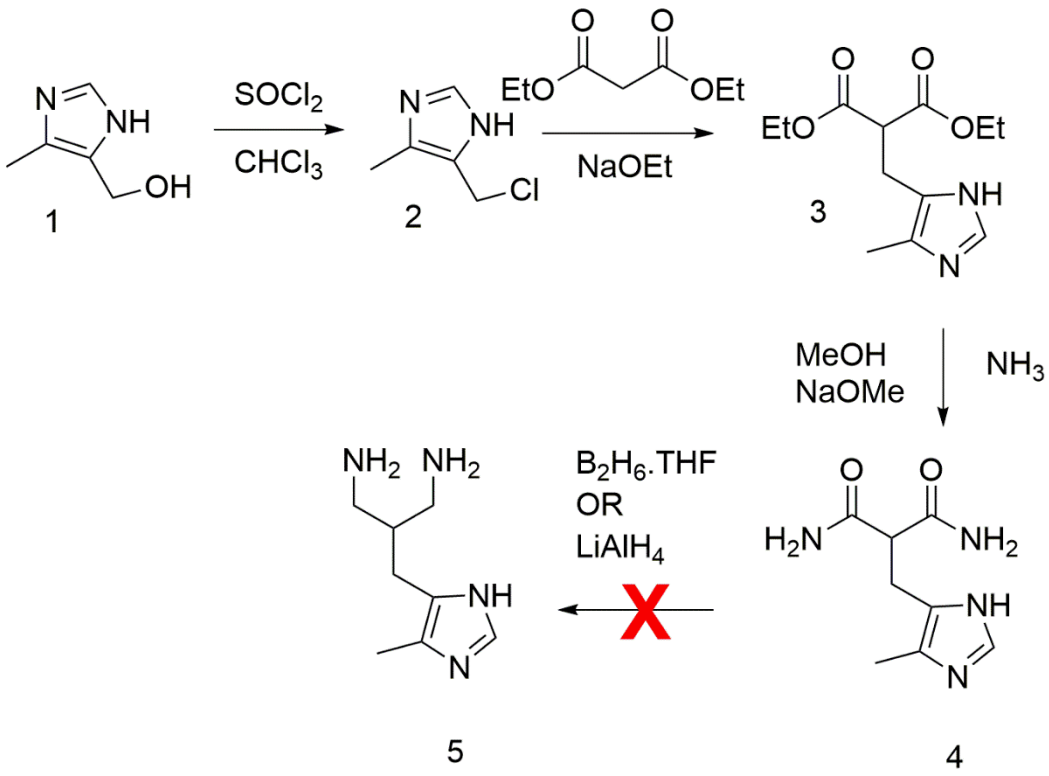
The synthesis of 2-((4-methyl-1H-imidazol-5-yl)methyl)propane-1,3-diamine, an imidazole analogue of the phenol and pyridine bridges used by Franks *et al.*[23], was initially attempted via synthetic techniques that had been outlined in the literature (Scheme 3.1).[25–28] However, the final reduction of the di-amine 2-((5-methyl-1H-imidazol-4-yl)methyl)malonamide was unsuccessful

and the target di-amine 2-((5-methyl-1H-imidazol-4-yl)methyl)propane-1,3-diamine could not be isolated. As a consequence alternative synthetic routes outlined in the literature were investigated in order to isolate the target molecule 2-((4-methyl-1H-imidazol-5-yl)methyl)propane-1,3-diamine. These synthetic approaches will be discussed in the following sections.



Scheme 3.1 Schematic representation of the syntheses of 2-benzyl-1,3-propanediamine, 2-(2-pyridylethyl)-1,3-propanediamine and 2-(2-pyridylmethyl)-1,3-propanediamine used by Franks *et al.*[23]

3.2.2 Attempted Synthesis of 2-((5-methyl-1H-imidazol-4-yl)methyl)propane-1,3-diamine (*via* diethyl malonate)



Scheme 3.2 Attempted synthesis of 2-((4-methyl-1H-imidazol-5-yl)methyl)propane-1,3-diamine (**5**).

The attempted synthesis of 2-((4-methyl-1H-imidazol-5-yl)methyl)propane-1,3-diamine (**5**) (Scheme 3.2) utilised the same synthetic route used proposed by Franks *et al.*[23] to synthesise 2-benzylpropane-1,3-diamine, 2-(pyridin-2-ylmethyl)propane-1,3-diamine and 2-(2-(pyridin-2-yl)ethyl)propane-1,3-diamine, respectively (Scheme 3.1).[25–28] The synthesis of diethyl 2-((4-methyl-1H-imidazol-5-yl)methyl)malonate (**3**) has also been outlined in the literature by Matziari *et al.*[29]

The synthesis of 2-((4-methyl-1H-imidazol-5-yl)methyl)propane-1,3-diamine (**5**) was attempted using the four step procedure outlined in Scheme 3.2.

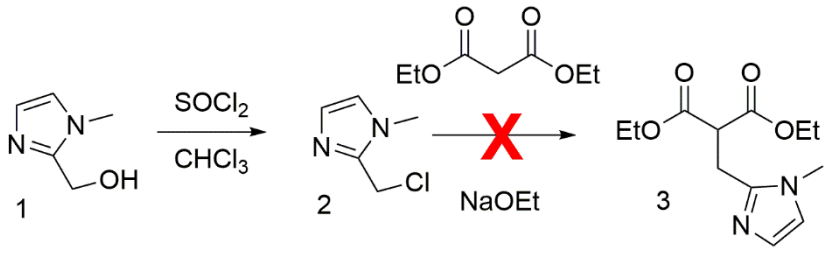
The first step involved the preparation of 5-(chloromethyl)-4-methyl-1H-imidazole (**2**) by the addition of (4-methyl-1H-imidazol-5-yl)methanol to thionyl chloride and after stirring for 1 hour the product, 5-(chloromethyl)-4-methyl-1H-imidazole, precipitated as a cream powder with an overall yield of 88%. The second step involved the preparation of diethyl 2-((4-methyl-1H-imidazol-5-yl)methyl)malonate (**3**) from the reaction between diethyl malonate and 5-(chloromethyl)-4-methyl-1H-imidazole (**2**) in the presence of an excess of sodium ethoxide and at reflux for 24 hours. The product was isolated as a bright orange oil with an overall 88 % yield.[29] The third step involved the conversion of (**3**) into the corresponding diamide, 2-((4-methyl-1H-imidazol-5-yl)methyl)malonamide (**4**). A solution of anhydrous methanol, diethyl 2-((4-methyl-1H-imidazol-5-yl)methyl)malonate and sodium methoxide was saturated with gaseous ammonia and the product precipitated from the reaction mixture as a white crystalline solid over 48 h in an overall yield of 92 %. The final step in the synthesis involved the reduction of 2-((4-methyl-1H-imidazol-5-yl)methyl)malonamide to form the corresponding diamine, 2-((4-methyl-1H-imidazol-5-yl)methyl)propane-1,3-diamine (**5**). This was attempted using excess diborane-tetrahydrofuran complex in tetrahydrofuran as had been used by Franks *et al.*[23] for the synthesis of 2-benzylpropane-1,3-diamine, 2-(pyridin-2-ylmethyl)propane-1,3-diamine and 2-(2-(pyridin-2-yl)ethyl)propane-1,3-diamine, respectively (Scheme 3.1).[25–28] However, the desired product, 2-((4-methyl-1H-imidazol-5-yl)methyl)propane-1,3-diamine (**5**), could not could not be identified in the reaction mixture by ^{1}H-NMR, ^{13}C-NMR spectroscopies and by mass spectrometry. In addition, unreacted 2-((4-methyl-1H-imidazol-5-

yl)methyl)malonamide (**4**) could not be identified by ^{1}H-NMR, ^{13}C-NMR spectroscopies and by mass spectrometry either. This suggests that the reaction conditions employed in this reaction leads to a range of undesired and unidentified products. Further attempts to reduce 2-((4-methyl-1H-imidazol-5-yl)methyl)malonamide (**4**) to 2-((4-methyl-1H-imidazol-5-yl)methyl)propane-1,3-diamine (**5**) utilised lithium aluminium hydride,[30] as an alternative reducing agent, however, this reaction was also unsuccessful.

Borane tetrahydrofuran complex is commonly used for the reduction of amides to their corresponding amines in the presence of other functional groups due to its chemoselectivity[31] and sensitivity in the presence of other functional groups. However, the reduction of (**4)** to (**5**) using a borane tetrahydrofuran complex was unsuccessful. The previous literature methods that had used borane tetrahydrofuran to reduce an amide to an amine had not been undertaken in the presence of an imidazole functional group. It has been well documented that excess di-borane, in the presence of imidazole, can catalyse the formation of an imidazole-borane polymer.[32] This competing reaction could prevent the desired reduction of the di-amide to the corresponding di-amine and could also destroy the initial starting material (**4**) thereby preventing the formation of 2-((4-methyl-1H-imidazol-5-yl)methyl)propane-1,3-diamine (**5**).

In order to attempt to synthesise the target compound, 2-((4-methyl-1H-imidazol-5-yl)methyl)propane-1,3-diamine (**5**), we investigated of the use of protecting groups for the protection of the imidazole N atoms. These approaches will be discussed in the following sections.

3.2.3 Methyl protection: The attempted synthesis of 2-((1-methyl-1H-imidazol-2-yl)methyl)propane-1,3-diamine (*via* diethyl malonate)



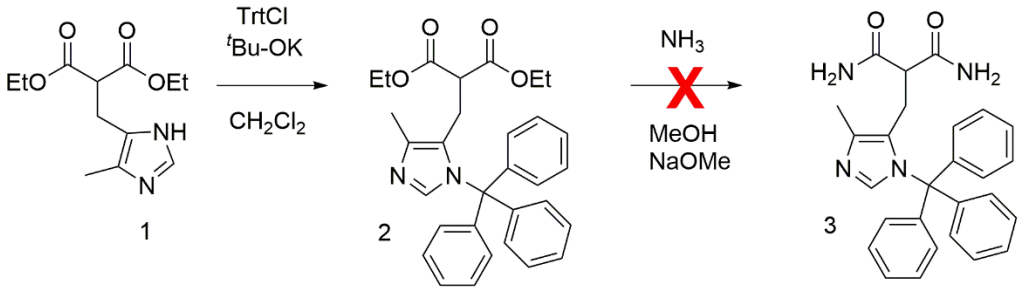
Scheme 3.3 The attempted synthesis of diethyl 2-((1-methyl-1H-imidazol-2-yl)methyl)malonate.

The starting material (1-methyl-1H-imidazol-2-yl)methanol (**1**) is available commercially. The use of a methyl group was considered ideal as it is a small and sterically non-demanding protection group that would not inhibit the imidazole N-donor from binding to the metal centre upon oxidation.

The synthesis of 2-((1-methyl-1H-imidazol-2-yl)methyl)propane-1,3-diamine was attempted using the four step procedure outlined in Scheme 3.3. The first step involved the preparation of 2-(chloromethyl)-1-methyl-1H-imidazole (**2**) by the reaction of (1-methyl-1H-imidazol-2-yl)methanol (**1**) with thionyl chloride in dichloromethane at reflux for 15 minutes.[33] The product, 2-(chloromethyl)-1-methyl-1H-imidazole (**2**), was recrystallised from ethanol as a light brown solid with a yield of 54%. The second step involved the preparation of diethyl 2-((1-methyl-1H-imidazol-2-yl)methyl)malonate (**3**) from the reaction between diethyl malonate and 5-(chloromethyl)-4-methyl-1H-imidazole (**2**) in the presence of an excess of sodium ethoxide and heated to reflux for 24 hours as described previously for 2-((4-methyl-1H-imidazol-5-yl)methyl)malonamide (**4**) (Section 3.2.2).[17–20] However, neither diethyl malonate, 5-(chloromethyl)-4-

methyl-1H-imidazole (**2**) or diethyl 2-((1-methyl-1H-imidazol-2-yl)methyl)malonate (**3**) could be identified by ^{1}H-NMR, ^{13}C-NMR spectroscopies and mass spectrometry from the final reaction mixture. It is likely that the reaction conditions lead to the decomposition of the protection group.[34]

3.2.4 Trityl Protection: Attempted synthesis of 2-((4-methyl-1-trityl-1H-imidazol-5-yl)methyl)propane-1,3-diamine (*via* diethyl malonate)



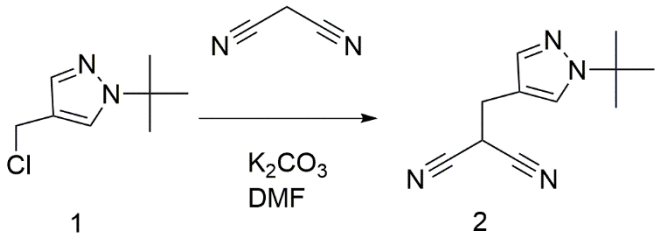
Scheme 3.4 The attempted synthesis of 2-((4-methyl-1-trityl-1H-imidazol-5-yl)methyl)malonamide.

We also attempted to protect the imidazole unit with a trityl group. This unit has been used previously to protect 2-((4-methyl-1H-imidazol-5-yl)methyl)malonamide (**1**) (Scheme 3.4).[29] The trityl group can also be removed easily by treatment with trifluoroacetic acid in dichloromethane.[35]

The synthesis of 2-((4-methyl-1-trityl-1H-imidazol-5-yl)methyl)propane-1,3-diamine was attempted using the three step procedure outlined in Scheme 3.4. The first step involved the preparation of diethyl 2-((4-methyl-1H-imidazol-5-yl)methyl)malonate (**1**), which is discussed in Section 3.2.2. The second step involved the preparation diethyl 2-((4-methyl-1-trityl-1H-imidazol-5-yl)methyl)malonate (**2**) by the addition of trityl chloride to diethyl 2-((4-methyl-1H-imidazol-5-yl)methyl)malonate which produced an orange oil with an overall yield of 90%.[29] The third step involved the reduction of the trityl protected diethyl 2-((4-methyl-1-trityl-1H-imidazol-5-yl)methyl)malonate (**2**) to the corresponding amide 2-((4-methyl-1-trityl-1H-imidazol-5-yl)methyl)malonamide (**3**) by reaction with ammonia and sodium methoxide.[25–

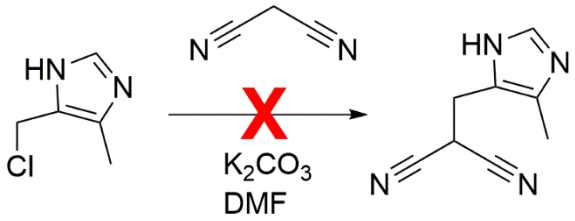
[28] However, ^{1}H-NMR, ^{13}C-NMR spectroscopies and mass spectrometry indicated that the desired product, 2-((4-methyl-1-trityl-1H-imidazol-5-yl)methyl)malonamide (**3**), had not formed and any remaining starting material, diethyl 2-((4-methyl-1-trityl-1H-imidazol-5-yl)methyl)malonate (**2**) could not be identified either. It is likely that the reaction conditions lead to the decomposition of the protection group.[34]

3.2.5 Attempted synthesis of 2-((4-methyl-1H-imidazol-5-yl)methyl)propane-1,3-diamine (*via* malonitrile)



Scheme 3.5 Attempted synthesis of of 2-((1-(tert-butyl)-1H-pyrazol-4-yl)methyl)malononitrile.

A literature search identified a route to 2-((1-(tert-butyl)-1H-pyrazol-4-yl)methyl)malononitrile (**2**) (Scheme 3.5) which we identified as a potential route for the synthesis of the target imidazole di-amine bridged compound *via* the reduction of the corresponding malonitrile (**2**) (Scheme 3.6). [36,37]

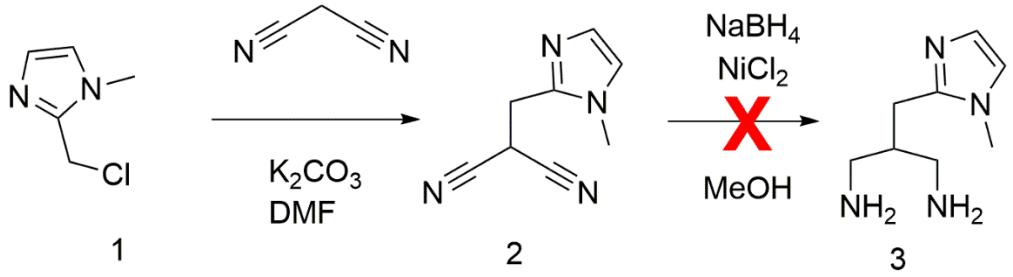


Scheme 3.6 Attempted synthesis of 2-((4-methyl-1H-imidazol-5-yl)methyl)malononitrile.

The attempted synthesis of 2-((1-methyl-1H-imidazol-2-yl)methyl)propane-1,3-diamine was attempted following the two-step synthetic procedure outlined in Scheme 3.6. The first step involved the preparation of 5-(chloromethyl)-4-methyl-1H-imidazole (**1**) (Section 3.2.3).[33] The second step involved the preparation of 2-((4-methyl-1H-imidazol-5-yl)methyl)malononitrile (**2**) by the addition of 5-(chloromethyl)-4-methyl-1H-imidazole (**1**) to malonitrile in the presence of potassium carbonate. However,

we were unable to identify the desired product, 2-((4-methyl-1H-imidazol-5-yl)methyl)malononitrile (**2**), or starting material, 5-(chloromethyl)-4-methyl-1H-imidazole (**1**), by ^{1}H-NMR, ^{13}C-NMR spectroscopies and mass spectrometry of the final reaction mixture. We therefore attempted analogous reactions using 1-methyl- and 1-trityl-subsituted protected imidazole species.

3.2.6 Methyl Protection: Attempted synthesis of 2-((1-methyl-1H-imidazol-2-yl)methyl)propane-1,3-diamine

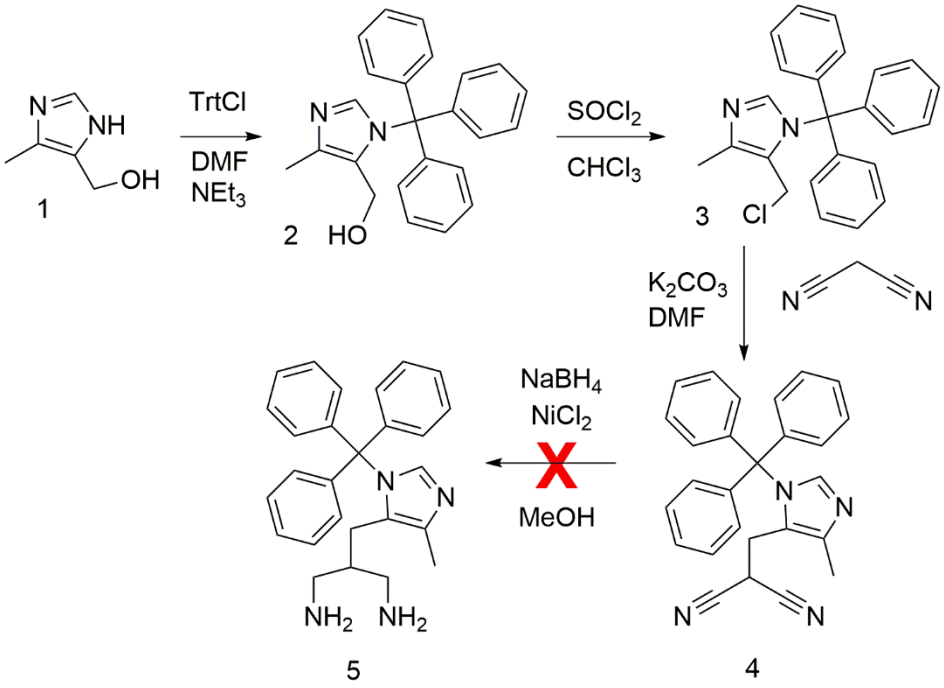


Scheme 3.7 Attempted synthesis of 2-((1-methyl-1H-imidazol-2-yl)methyl)propane-1,3-diamine.

The synthesis of 2-((1-methyl-1H-imidazol-2-yl)methyl)propane-1,3-diamine (**3**) was attempted following the two-step synthetic procedure outlined in Scheme 3.7. The first step involved the preparation of 2-(chloromethyl)-1-methyl-1H-imidazole (**1**) (Section 3.2.3).[33] The second step involved the preparation of 2-((1-methyl-1H-imidazol-2-yl)methyl)malononitrile (**2**) by the addition of 2-(chloromethyl)-1-methyl-1H-imidazole (**1**) to malonitrile in the presence of potassium carbonate which produced a brown oil with an overall yield of 67%.[37] The final step required the reduction of 2-((1-methyl-1H-imidazol-2-yl)methyl)malononitrile (**2**) to 2-((1-methyl-1H-imidazol-2-yl)methyl)propane-1,3-diamine (**3**) using $NaBH_4$ and $NiCl_2$. However, ^{1}H-

NMR, ^{13}C-NMR spectroscopies and mass spectrometry from the final reaction mixture showed that the desired product had not formed and any remaining starting materials could not be identified either.

3.2.7 Trityl Protection: Attempted synthesis of 2-((4-methyl-1-trityl-1H-imidazol-5-yl)methyl)propane-1,3-diamine (*via* malonitrile)



Scheme 3.8 The attempted synthesis of 2-((1-methyl-1H-imidazol-2-yl)methyl)malononitrile.

We attempted the synthesis of 2-((4-methyl-1-trityl-1H-imidazol-5-yl)methyl)propane-1,3-diamine (**5**), using trityl functionalisation of the imidazole unit. This synthesis was attempted by the four step route outlined in Scheme 3.8. The first step involved the preparation of (4-methyl-1-trityl-1H-imidazol-5-yl)methanol (**2**).[38,39] The product precipitated as a white fluffy solid in an overall yield of 62%. The second step involved the preparation of 5-(chloromethyl)-4-methyl-1-trityl-1H-imidazole (**3**) from the reaction of (**2**) with

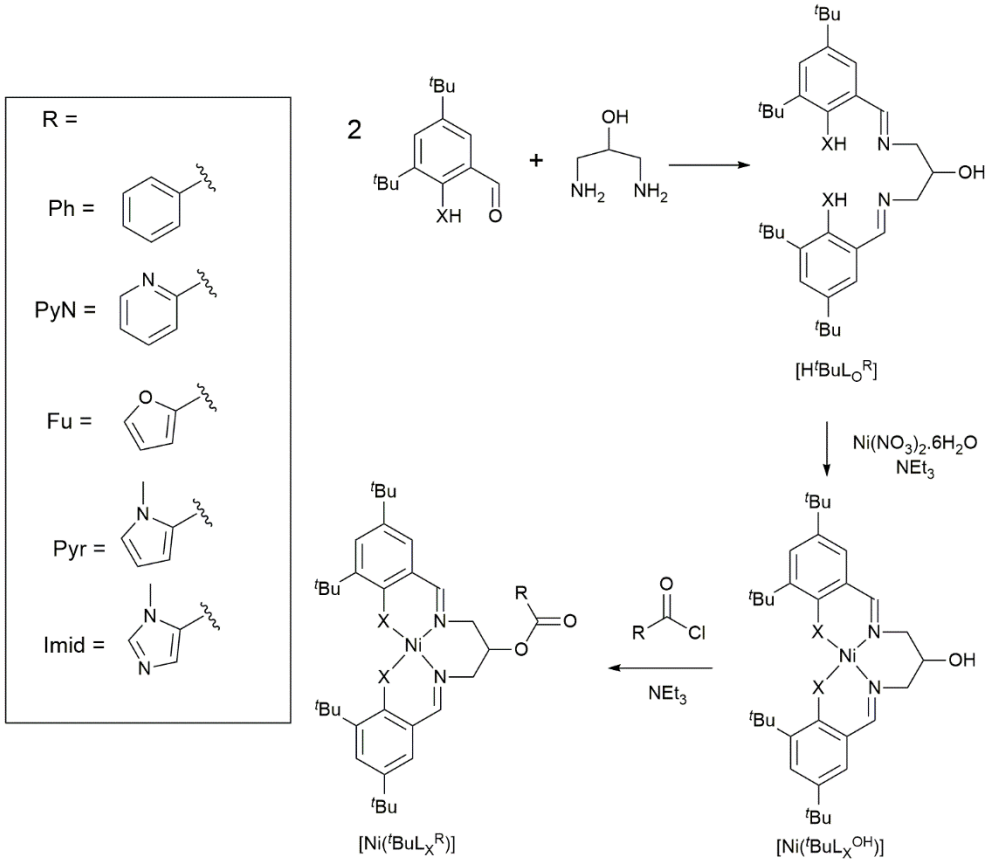
thionyl chloride in dichloromethane. This reaction produced a yellow oil in an overall yield of 90%.[38,39] The third step involved the preparation of 2-((1-methyl-1H-imidazol-2-yl)methyl)malononitrile (**4**) by the addition of 2-(chloromethyl)-1-methyl-1H-imidazole (**3**) to malonitrile in the presence of potassium carbonate.[37] The product was isolated as a brown oil in a yield of 47%. The final step involved the reduction of 2-((1-methyl-1H-imidazol-2-yl)methyl)malononitrile (**4**) to 2-((4-methyl-1-trityl-1H-imidazol-5-yl)methyl)propane-1,3-diamine (**5**) using sodium borohydride and nickel chloride. However, ^{1}H-NMR, ^{13}C-NMR spectroscopies and mass spectrometry indicated that the desired product had not formed and any remaining starting materials could not be identified either.

Attempts to synthesise and isolate 2-((5-methyl-1-trityl-1H-imidazol-4-yl)methyl)propane-1,3-diamine (**5**) (Scheme 3.2) with methyl and trityl group functionalisation were unsuccessful. We note that the conditions employed for the attempted reduction of the relevant diamide or dinitrile to the corresponding diamine are basic. The imidazole ring is susceptible to decomposition *via* a ring opening mechanism under basic conditions.[40] Thus, despite the use of methyl and trityl functionalisation of the imidazole group it is possible that the imidazole ring containing starting materials undergo decomposition under the conditions of the reduction reactions and fail to form the desired product.

Alternative synthetic routes that enable the functionalisation of the diamine bridge with heterocylic donors using approaches developed by Dawson *et al.*[41] were investigated and will be discussed in the next section.

3.2.8 Proposed syntheses of [$H_2{}^tBuL_O{}^{OH}$], [$H_2{}^tBuL_S{}^{OH}$], [Ni($^tBuL_O{}^R$)] and [Ni($^tBuL_S{}^R$)] (R = OH, Ph, PyN, Fu, Pyr and Imid)

Synthetic methodologies for the preparation of Schiff-base diphenolate and dithiolate metal complexes that incorporate *2,4-tert*-butyl substitution on the phenolate and thiolate rings are well documented and have been adapted for the synthesis of [$H_2{}^tBuL_O{}^{OH}$] and [$H_2{}^tBuL_S{}^{OH}$], which contain an OH functionality upon the propane backbone of [$H_2{}^tBuL_O{}^{OH}$] and [$H_2{}^tBuL_S{}^{OH}$].[22,23,42]



Scheme 3.9 Synthesis of [$H_2{}^tBuL_X{}^{OH}$], [Ni($^tBuL_X{}^{OH}$)] and attempted syntheses of [Ni($^tBuL_X{}^R$)] (R = Ph, PyN, Fu, Pyr and Imid, X = O or S).

The [$H_2{}^tBuL_O{}^{OH}$] and [$H_2{}^tBuL_S{}^{OH}$] pro-ligands were reacted directly with $Ni(NO_3)_2.6H_2O$ to form the Ni(II) Schiff-base diphenolate and dithiolate complexes, [Ni($^tBuL_O{}^{OH}$)] and [Ni($^tBuL_S{}^{OH}$)]. Further reaction of these

complexes with the appropriate acid chloride was attempted to attempt to incorporate the desired bridging moiety: phenyl (Ph), pyridyl (PyN), furan (Fu), pyrrole (Pyr) and imidazole (Imid) (R = Ph, PyN, Fu, Pyr and Imid), respectively (Scheme 3.9). Schematic structures of [Ni(^{t}BuL$_{O}^{R}$)] and [Ni(^{t}BuL$_{S}^{R}$)] (R = OH, Ph, PyN, Fu, Pyr and Imid) are shown in Figure 3.7. In the following sections we will discuss in detail the syntheses of these pro-ligands and the attempted syntheses of the Ni(II) complexes in detail.

The synthesis of 2,4-di-tert-butylthiosalicylaldehyde was achieved via a six step synthesis previously outlined by Stenson *et al*.[22,23]

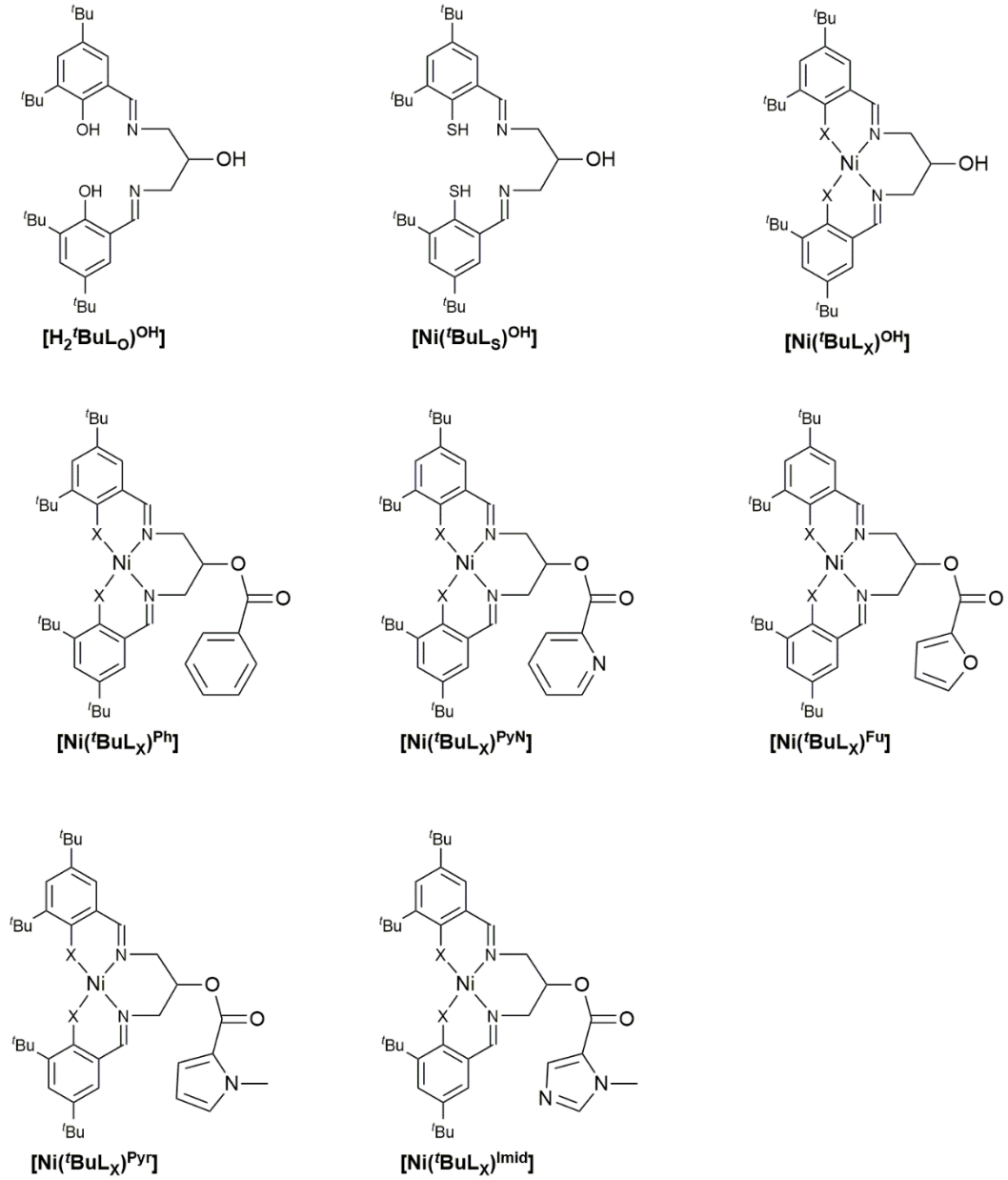
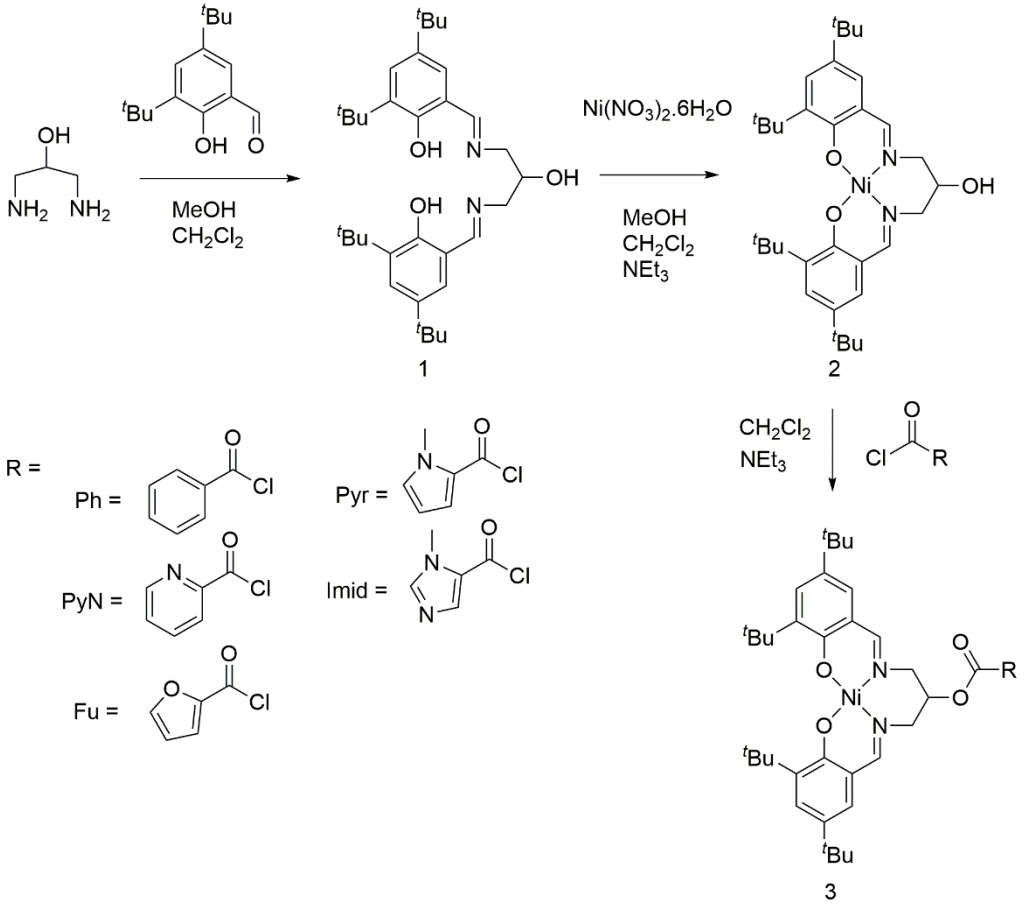


Figure 3.7. Schematic representation of the Ni(II) diphenolate and dithiolate Schiff-base complexes discussed in this Chapter (X = S or O).

3.2.9 Syntheses of [$H_2{}^tBuL_O{}^{OH}$] and [Ni($^tBuL_O{}^{OH}$)], and the attempted syntheses of [Ni($^tBuL_O{}^{R}$)] (R = Ph, PyN, Fu, Pyr and Imid)



Scheme 3.10 Synthesis of [$H_2{}^tBuL_O{}^{OH}$], [Ni($^tBuL_O{}^{OH}$)] and [Ni($^tBuL_O{}^{R}$)] (R = Ph, PyN, Fu, Pyr and Imid).

The synthesis of crude [$H_2{}^tBuL_O{}^{OH}$] was achieved by the Schiff-base condensation reaction between di-*tert*-butyl-2-hydroxybenzaldehyde and 1,3-diaminopropan-2-ol in methanol. $Ni(NO_3)_2.6H_2O$ was then added as a solution in methanol to crude [$H_2{}^tBuL_O{}^{OH}$] as a solution in dichloromethane, and the mixture heated to reflux for 24 hours. The product, [Ni($^tBuL_O{}^{OH}$)], was isolated as a dark brown powder and purified via column chromatography on silica gel

using dichloromethane and pentane (3:2 v/v) as eluent with an overall yield of 69%.

Attempts were then made to functionalise the hydroxyl moiety of the metal complex [Ni(^{t}BuL$_{O}^{OH}$)] using a range of functionalised acid chloride starting materials. The reaction between [Ni(^{t}BuL$_{O}^{OH}$)] and the acid chlorides were attempted in anhydrous conditions under an Ar atmosphere. Each reaction mixture was stirred for 24 hours at room temperature and attempts were made to purify the products by column chromatography on silica gel using dichloromethane and pentane (3:2 v/v) as eluent. Only [Ni(^{t}BuL$_{O}^{Ph}$)] could be isolated following recrystallization from the column fractions.

3.2.10 Single Crystal Structures of [Ni(^{t}BuLo^{OH})] and [Ni(^{t}BuLo^{Ph})]

Single crystal structures were obtained for [Ni(^{t}BuL$_O{}^{OH}$)] and [Ni(^{t}BuL$_O{}^{Ph}$)] by X-ray crystallography. The molecular structures of [Ni(^{t}BuL$_O{}^{OH}$)] and [Ni(^{t}BuL$_O{}^{Ph}$)] are shown in Figure 3.9 and 3.10, respectively and selected bond lengths and angles are listed in Table 3.1 and 3.2, respectively. Details of the structure solution and refinement are provided in Appendix 2.

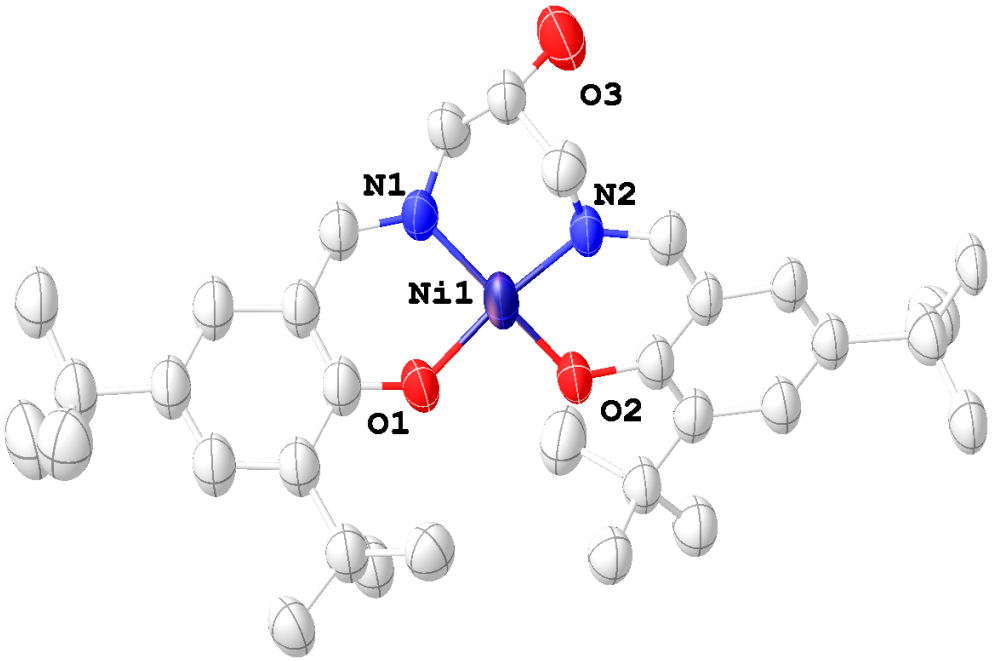


Figure 3.9 View of the X-ray crystal structure of [Ni(^{t}BuL$_O{}^{OH}$)] with H atoms omitted for clarity.

Table 3.1 Selected bond lengths (Å) and angles (°) with e.s.d.s for [Ni(^{t}BuL$_O^{OH}$)].

[Ni(^{t}BuL$_O^{OH}$)]	**Bond lengths / Å**	**[Ni(^{t}BuL$_O^{OH}$)]**	**Bond angles / °**
Ni(1)-N(1)	1.841(11)	N(1)-Ni(1)-N(2)	90.6(5)
Ni(1)-N(2)	1.886(13)	N(1)-Ni(1)-O(1)	164.3(5)
Ni(1)-O(1)	1.863(11)	N(2)-Ni(1)-O(1)	93.8(5)
Ni(1)-O(2)	1.823(11)	N(1)-Ni(1)-O(2)	94.0(5)
N(1)-C(1)	1.320(18)	N(2)-Ni(1)-O(2)	167.0(5)
N(1)-C(3)	1.510 (3)	O(1)-Ni(1)-O(2)	85.0(5)
N(2)-C(2)	1.348(9)	-	-
N(2)-C(4)	1.470(2)	-	-
O(1)-C(16)	1.312(19)	-	-
O(2)-C(15)	1.365(17)	-	-

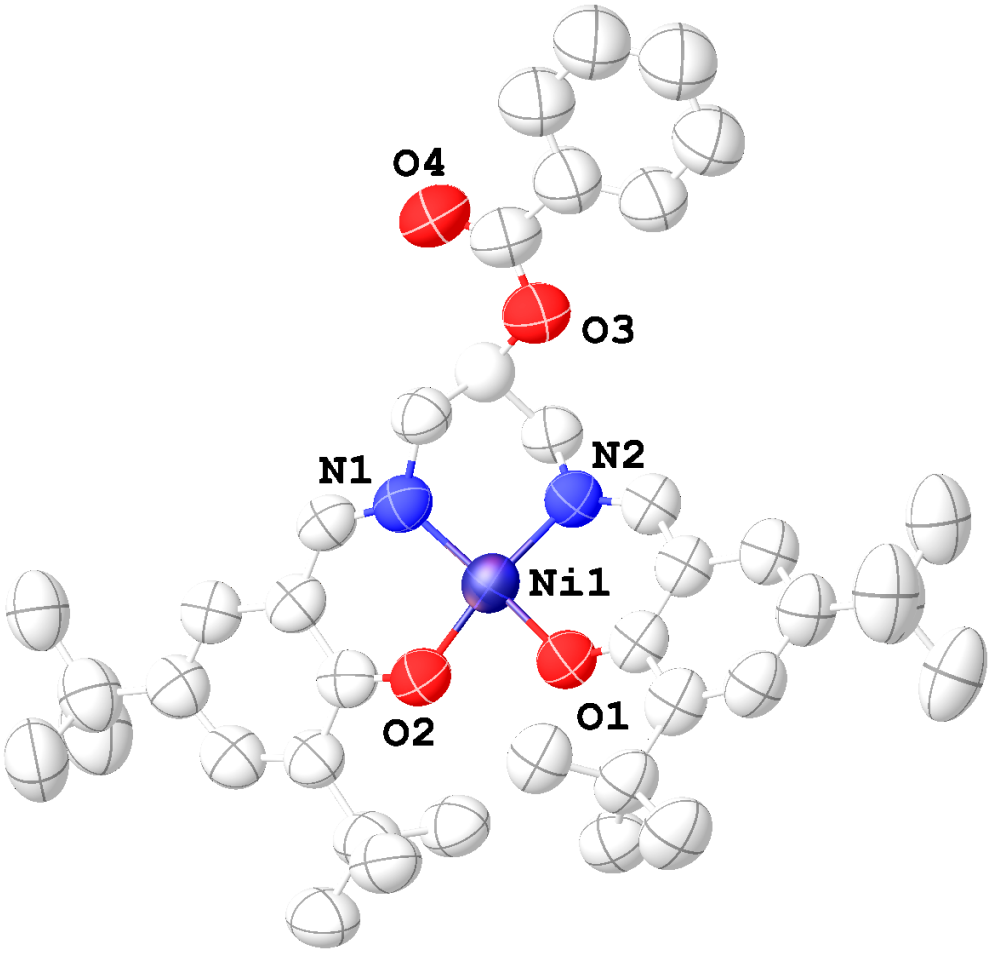


Figure 3.10 View of the X-ray crystal structure of [Ni(^{t}BuLO^{Ph})] with H atoms omitted for clarity.

Table 3.2 Selected bond lengths (Å) and angles (°) with e.s.d.s for [Ni(^{t}BuLO^{OH})].

[Ni(^{t}BuLO^{Ph})]	Bond lengths / Å	[Ni(^{t}BuLO^{Ph})]	Bond angles / °
Ni(1)-N(1)	1.879(7)	N(1)-Ni(1)-N(2)	91.8(3)
Ni(1)-N(2)	1.875(6)	N(1)-Ni(1)-O(1)	163.9(3)
Ni(1)-O(1)	1.858(5)	N(2)-Ni(1)-O(1)	93.2(3)
Ni(1)-O(2)	1.849(6)	N(1)-Ni(1)-O(2)	94.2(3)
N(1)-C(1)	1.300(10)	N(2)-Ni(1)-O(2)	164.4(3)
N(1)-C(3)	1.303(10)	O(1)-Ni(1)-O(2)	85.0(3)
N(2)-C(2)	1.540(10)	-	-
N(2)-C(4)	1.492(9)	-	-
O(1)-C(16)	1.270(9)	-	-
O(2)-C(15)	1.329(10)	-	-

[Ni(^{t}BuL$_{O}^{OH}$)] and [Ni(^{t}BuL$_{O}^{Ph}$)] each contain a four-coordinate monomeric Ni(II) centre bound by a N_2O_2 ligand set derived from two phenolate O-donors and two imine N-donors. The Ni(II)-O(phenolate) (*ca.* 1.82 – 1.86 Å) and Ni(II)-N(imine) (*ca.* 1.84 – 1.87 Å) bond distances are comparable to those in [(talen)Ni$^{II}_{3}$] (talen = 2,4,6-tris[1-(2-salicylaldimino-2-methyl-propylimino)-ethyl]-1,3,5-trihydroxybenzene), [Ni(^{Me}L)] (^{Me}L = *N,N'*-bis(3,5-di-*tert*-butyl-salicylaldene)-4,5-dimethyl-1,2-phenylenediamine) and [Ni^{II}(tbu-salcn)] (tbu-salcn = *N,N'*-bis(3',5'-di-*tert*-butylsalicylidene)-1,2-cyclohexanediamine), which also contain Ni(II) within a tetradentate N_2O_2 coordination sphere with Ni-O and Ni-N distances of *ca.* 1.86 Å and 1.85 Å, respectively.[43–46]

The bond angles (Tables 3.1 and 3.2) show that [Ni(^{t}BuL$_{O}^{OH}$)] and [Ni(^{t}BuL$_{O}^{Ph}$)] adopt distorted square planar coordination geometries. This is confirmed by the dihedral angles between the planes defined by N(1)-Ni(1)-N(2) and O(1)-Ni(1)-O(2) which are 20.92 º and 22.53º , respectively.

3.2.11 Electrochemical Studies of [Ni(^{t}BuLo^{OH})] and [Ni(^{t}BuLo^{Ph})]

The cyclic voltammograms of (1 mM) solutions of [Ni(^{t}BuLo^R)] (R = OH and Ph) in CH_2Cl_2 containing 0.4 M [N^{n}Bu$_4$][BF$_4$] as supporting electrolyte were recorded at 293K under Ar. The complexes show electrochemical activity between the ranges of 0.0 – 1.5 V *vs* Fc^+/Fc (Figure 3.11).

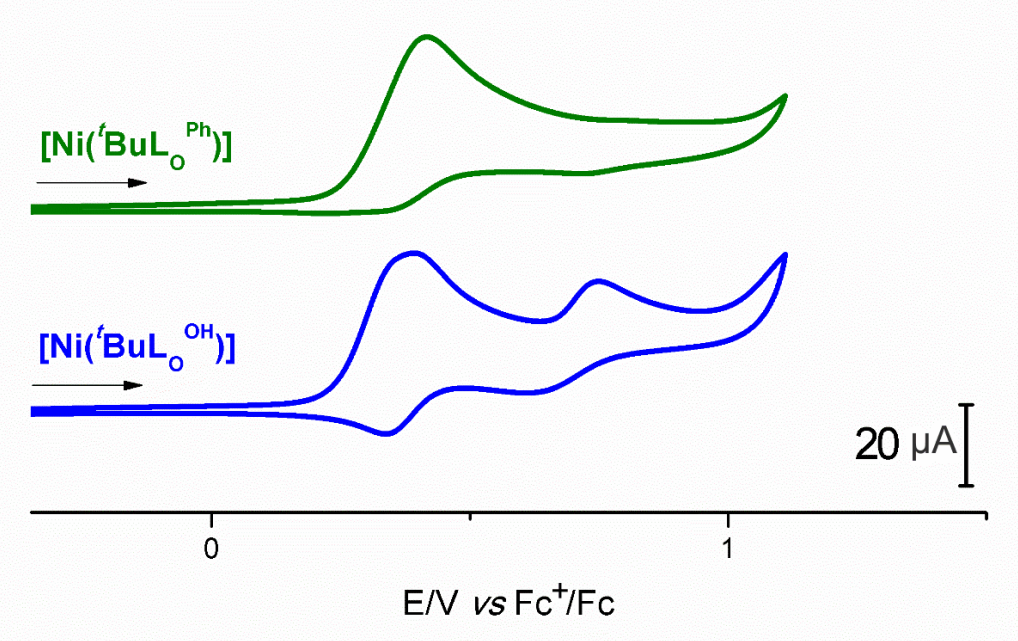


Figure 3.11 CVs [Ni(^{t}BuLo^R)] (R = OH, Ph) (1 mM) at 293 K in CH_2Cl_2 containing 0.4 M [N^{n}Bu$_4$][BF$_4$] as supporting electrolyte at 100 mVs^{-1}.

Table 3.3 Summary of anodic and cathodic peak potentials at scan rate 100mVs-1 for [Ni(^{t}BuLo^R)] (R = OH, Ph, PyN, Fu, Pyr and Imid)

Complex	Epa^1 *vs* Fc^+/Fc (V)	Epc^1 *vs* Fc^+/Fc (V)	Epa^2 *vs* Fc^+/Fc (V)	Epc^2 *vs* Fc^+/Fc (V)
[Ni(^{t}BuLo^{OH})]	0.38	0.33	0.75	0.62
[Ni(^{t}BuLo^{Ph})]	0.41	-	-	-

The cyclic voltammetric data were recorded for of [Ni(^{t}BuLo^R)] (R = OH and Ph), with each process being isolated and investigated for electrochemical

reversibility; however, none of the Ni(II) diphenolate complexes possess reversible electrochemistry.

The cyclic voltammetric data recorded for [Ni(^{t}BuL$_O^{OH}$)] shows two redox processes (Figure 3.11). The first redox process occurs at Ep_a^1 = 0.38 V with an associated return wave observed at Ep_c^1 = 0.33 V *vs* Fc^+/Fc. At slower scan rates (< 100 mVs^{-1}), the cyclic voltammogram for the first redox process of [Ni(^{t}BuL$_O^{OH}$)] shows the loss of the reduction peak at Ep_c^1 = 0.33 V *vs* Fc^+/Fc. This redox behaviour corresponds typically to an EC mechanism where, at slower scan rates, the oxidised form of the compound decomposes before the return sweep is complete. The second redox process for [Ni(^{t}BuL$_O^{OH}$)] occurs at Ep_a^2 = 0.75 V *vs* Fc^+/Fc with an associated return wave observed at Ep_c^2 = 0.62 V *vs* Fc^+/Fc. The cyclic voltammetric data recorded for [Ni(^{t}BuL$_O^{Ph}$)] show one single redox processes at Ep_a^1 = 0.41 and 0.44 V Fc^+/Fc (Figure 3.11).

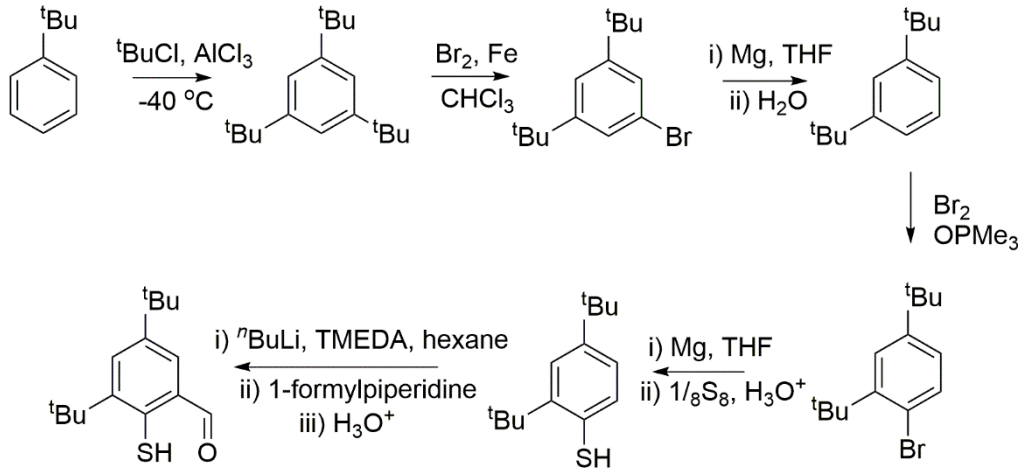
The oxidation processes for [Ni(^{t}BuL$_O^R$)] (R = OH and Ph) (Table 3.3) occur at more negative potentials than those for [Ni(^{t}BuL$_O^{Py1}$)] (Ep_a^1 = 0.49 V *vs* Fc^+/Fc) and [Ni(^{t}BuL$_O^{Py2}$)] (Ep_a^1 = 0.43 V *vs* Fc^+/Fc). However, the irreversibility of the oxidation processes for [Ni(^{t}BuL$_O^R$)] (R = OH and Ph) prevents further spectroscopic investigations which would offer further insight into the effects of the R groups on the structural and electrochemical properties of the Ni(II) diphenolate complexes and would facilitate the assignment of the redox processes as metal or ligand based.

3.3 Synthesis of Dithiolate Ni(II) Complexes

3.3.1 Synthesis of 2,4-di-*tert*-butylthiosalicylaldehyde

The synthesis of 2,4-di-*tert*-butylthiosalicylaldehyde from *tert*-butylbenzene was achieved via the six step synthetic procedure shown in Scheme 3.11.

The first step in the synthesis of 2,4-di-*tert*-butylthiosalicylaldehyde involves the preparation of 1,3,5-tri-*tert*-butylbenzene *via* a Friedel-Crafts alkylation reaction from *tert*-butylbenzene. The desired product was produced in yields in excess of 83 %.[47] This primary intermediate was then brominated to form 1-bromo-2,4-di-*tert*-butylbenzene using a stoichiometric amount of iron powder and excess bromine. The crude product was distilled under reduced pressure to produce a white crystalline solid in a yield of 96 %.[48]



Scheme 3.11 Schematic representation of the synthesis of 2,4-di-*tert*-butylthiosalicylaldehyde from *tert*-butylbenzene.

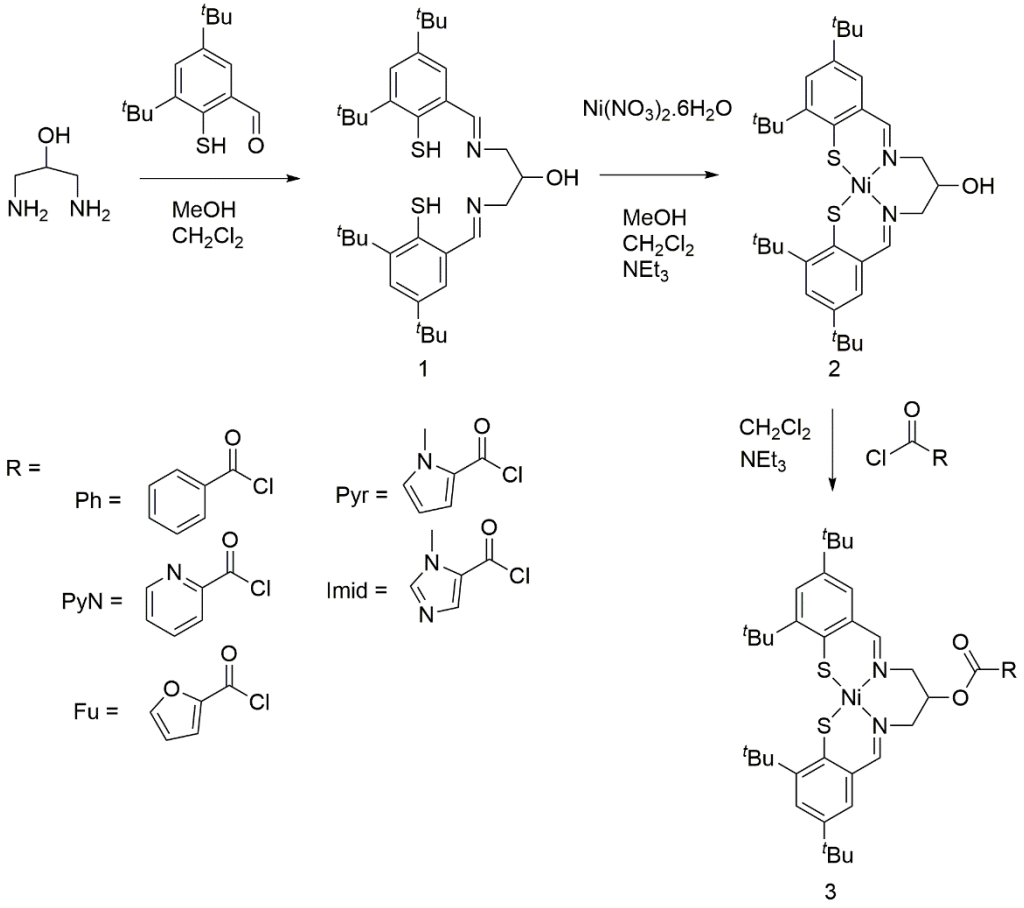
The third step in the synthesis required the production of the Grignard derivative of 1-bromo-3,5-di-*tert*-butylbenzene; this was performed using excess magnesium in tetrahydrofuran. Hydrolysis of this Grignard derivative generated

crude 1,3-di-*tert*-butylbenzene as colourless oil in a yield of 97 %. *ortho*-Bromination of this product was promoted with an excess of bromine at 70 °C in trimethylphosphate. Distillation gave the pure product in 88 % yield.

2,4-Di-*tert*-butylbenzenethiol was prepared via the sulfonation of the Grignard reagent obtained from the reaction of 1-bromo-2,4-di-*tert*-butylbenzene with magnesium. The crude product was purified using Kügelrohr short-path distillation to form colourless oil in a yield of 90 %.

The final step involved the treatment of a solution of 2,4-di-*tert*-butylbenzenethiol in tetrahydrofuran with two equivalents of TMEDA and *n*-butyllithium to produce the *ortho*-lithiated intermediate. The desired product, 2,4-di-*tert*-butylthiosalicylaldehyde, was formed upon quenching the reaction with 1-formylpiperidine.[25,49,50] The crude material was then purified using a short silica column eluted with hexane and the product was isolated as a foamy yellow solid in 82 % yield. This was used immediately for template complexation to avoid oxidative decomposition.

3.3.2 Syntheses of [$H_2{}^tBuL_S{}^{OH}$] and [Ni($^tBuL_S{}^{OH}$)], and the attempted syntheses of [Ni($^tBuL_S{}^{R}$)] (R = Ph, PyN, Fu, Pyr and Imid)



Scheme 3.12 Syntheses of [$H_2{}^tBuL_S{}^{OH}$] and [Ni($^tBuL_S{}^{OH}$)], and the attempted syntheses of [Ni($^tBuL_S{}^{R}$)] (R = Ph, PyN, Fu, Pyr and Imid).

The synthesis of crude [$H_2{}^tBuL_S{}^{OH}$] was achieved by the Schiff-base condensation reaction between di-*tert*-butyl-2-hydroxybenzaldehyde and 1,3-diaminopropan-2-ol in methanol. $Ni(NO_3)_2.6H_2O$ was then added as a solution in methanol to the crude pro-ligand, [$H_2{}^tBuL_S{}^{OH}$], as a solution in dichloromethane and heated to reflux for 24 hours. The product, [Ni($^tBuL_S{}^{OH}$)], was isolated as a dark brown powder which was purified by column

chromatography on silica gel using dichloromethane and pentane (3:2 v/v) as eluent with an overall yield of 62%.

Reactions between [Ni(^{t}BuL$_{S}^{OH}$)] and functionalised acid chlorides were attempted under anhydrous conditions and under an inert atmosphere. Attempts to purify the products of the reactions by column chromatography on silica gel using dichloromethane and pentane (3:2 v/v) as eluent were unsuccessful.

3.3.3 Single Crystal Structure of [Ni(^{t}BuL$_S^{OH}$)]

Crystals of Ni(^{t}BuL$_S^{OH}$)] suitable for X-ray crystallography were grown from dichloromethane and pentane (3:2 v/v) solutions. Details of the structure solution and refinement are provided in Appendix 2.

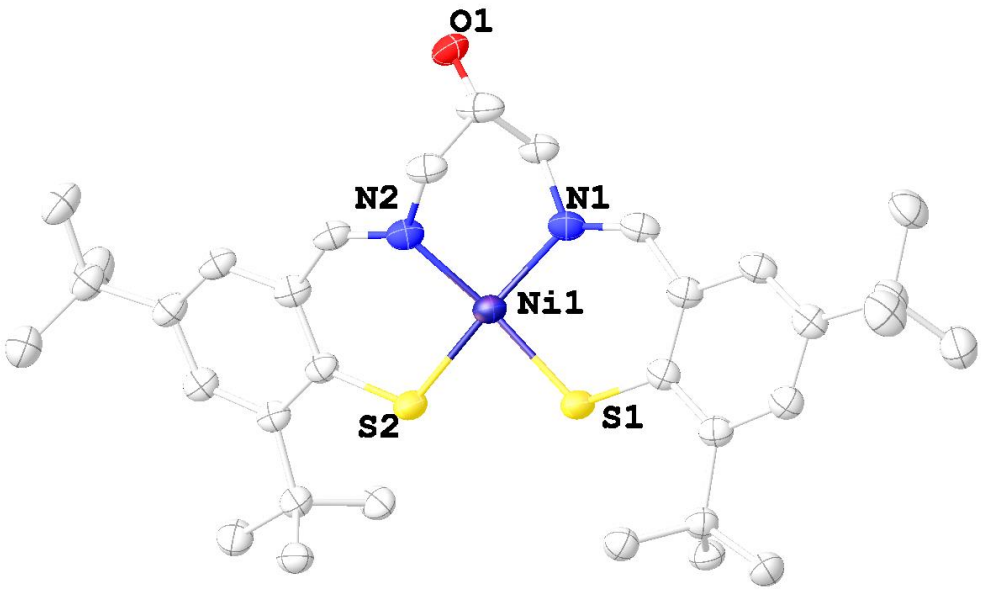


Figure 3.13 View of the X-ray crystal structure of [Ni(^{t}BuL$_S^{Ph}$)] with H atoms omitted for clarity.

Table 3.5 Selected bond lengths (Å) and angles (°) with e.s.d.s for [Ni(^{t}BuL$_S^{OH}$)].

[Ni(^{t}BuL$_S^{OH}$)]	Bond lengths / Å	[Ni(^{t}BuL$_S^{OH}$)]	Bond angles / °
Ni(1)-N(1)	1.8792(19)	N(1)-Ni(1)-N(2)	90.77(8)
Ni(1)-N(2)	1.8961(19)	N(1)-Ni(1)-S(1)	94.23(6)
Ni(1)-S(1)	2.1705(7)	N(2)-Ni(1)-S(1)	166.61(6)
Ni(1)-S(2)	2.1717(6)	N(1)-Ni(1)-S(2)	166.63(6)
N(1)-C(1)	1.282(3)	N(2)-Ni(1)-S(2)	94.14(6)
N(1)-C(3)	1.480(3)	S(1)-Ni(1)-S(2)	83.77(2)
N(2)-C(2)	1.2851(3)	-	-
N(2)-C(4)	1.484(3)	-	-
S(1)-C(16)	1.768(2)	-	-
S(2)-C(15)	1.764(2)	-	-

[Ni(^{t}BuL$_{S}^{OH}$)] contains a monomeric Ni(II) centre coordinated by two thiolate S-donors and two imine N-donors (Figure 3.13, Table 3.5). The Ni(1)-S(1) and Ni(1)-S(2) bond distances (*ca.* 2.17 Å) and Ni(1)-N(1) and Ni(1)-N(2) bond distances (*ca.* 2.89 Å) lie in the range typically observed for previously reported Ni(II) complexes incorporating S-thiolate and N-imine coordination including: [Ni(^{t}BuL$_{S}^{Ph1}$)], [Ni(^{t}BuL$_{S}^{Py1}$)] and [Ni(^{t}BuL$_{S}^{Py2}$)], *N,N'*-bis-(*o*-sulfidobenzylidene)-1,3-diaminopropane nickel(II) (Ni(II)-S(thiolate) = *ca.* 2.17 Å, Ni(II)-N(imine) = *ca.* 1.92 Å).[12,22,23,51–53] The dihedral angle between the planes defined by S(1)-Ni(1)-S(2) and N(1)-Ni(1)-N(2) 18.62° is consistent with a distorted square-planar Ni(II) centre.

3.3.4 Electrochemical Studies of [Ni(^{t}BuL$_S^{OH}$)]

The cyclic voltammogram of a 1 mM solution of [Ni(^{t}BuL$_S^{OH}$)] in CH_2Cl_2 containing 0.4 M [N^{n}Bu$_4$][BF$_4$] as supporting electrolyte was recorded at 293K under Ar (Figure 3.14).

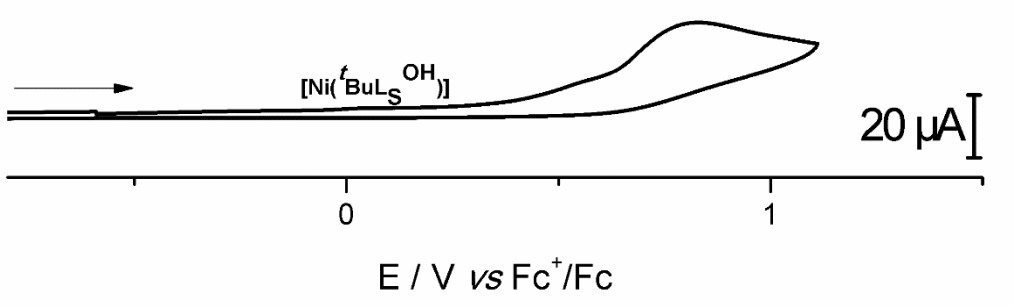


Figure 3.14 Cyclic voltammogram of [Ni(^{t}BuL$_S^{OH}$)] (1 mM) at 293 K in CH_2Cl_2 containing 0.4 M [N^{n}Bu$_4$][BF$_4$] as supporting electrolyte at 100 mVs^{-1}.

[Ni(^{t}BuL$_S^{OH}$)] possesses an irreversible oxidation process at 0.82 V *vs* Fc$^+$/Fc that is at a significantly more positive potential than those of [Ni(^{t}BuL$_S^{Ph}$)] (Ep_a^1 = 0.18 V *vs* Fc$^+$/Fc), [Ni(^{t}BuL$_S^{Py1}$)] (Ep_a^1 = 0.10 V *vs* Fc$^+$/Fc) and [Ni(^{t}BuL$_S^{Py2}$)] (Ep_a^1 = 0.18 V *vs* Fc$^+$/Fc).[23] This suggests that the incorporated OH group does not stabilize the oxidation products. The instability of the oxidised species also precludes further spectroscopic investigations which would offer further insight into the redox processes of [Ni(^{t}BuL$_S^{OH}$)].

3.4 Conclusions

This chapter describes the attempts made to synthesise of a range of diphenolate and dithiolate Ni(II) complexes that builds upon the previous work conducted by Stenson *et al.* and Franks *et al*.[22,23] The aim of the chapter was to focus upon the synthesis of an di-amine bridge that would incorporate an pendant imidazole moiety within the coordination sphere of the Ni(II) complexes in order to replicate the axial imidazole ligation observed in the oxidised form of NiSOD.

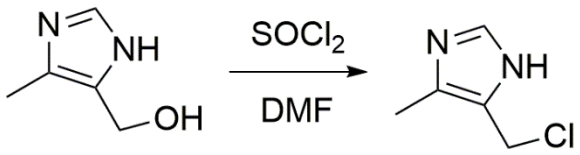
Initial attempts to synthesise a di-amine imidazole bridge followed previous synthetic approaches employed by Franks *et al.*[23] However, these approaches were unsuccessful. Alternative synthetic routes and the use of protecting groups to protect the NH group of the imidazole ring were also unsuccessful at the final step.

Alternative synthetic routes for the incorporation of heterocyclic functionalities onto the ligand bridge were explored. These involved a post complexation step that involved the reaction of a OH moiety pendant to the Ni(II) dipheonolate and dithiophenolate complexes with an aromatic or heterocyclic functionalised acid chloride. [Ni(^{t}BuL$_{O}^{Ph}$)] was isolated but, while mass spectrometric data suggested that [Ni(^{t}BuL$_{O}^{R}$)] (R = PyN, Fu, Pyr and Imid) and [Ni(^{t}BuL$_{S}^{R}$)] (R = Ph, PyN, Fu, Pyr and Imid) had formed, pure products could not be isolated. X-ray crystallographic studies of [Ni(^{t}BuL$_{O}^{R}$)] [Ni(^{t}BuL$_{O}^{R}$)] (R = OH, Ph) and [Ni(^{t}BuL$_{S}^{OH}$)] confirmed their formulation and show that each complex adopts a distorted square planar geometry about the metal centre.

Electrochemical investigations of [Ni(^{t}BuL$_O^R$)] (R = OH, Ph) and [Ni(^{t}BuL$_S^{OH}$)] showed that each exhibit irreversible redox processes. These results demonstrate that the OH and phenyl ester functionalities pendant to the ligand backbone do not stabilize the products formed following the oxidation of [Ni(^{t}BuL$_O^R$)] (R = OH, Ph) and [Ni(^{t}BuL$_S^{OH}$)]. Previous work has shown that the position of a pyridyl N-donor relative to the metal centre is crucial for the stabilisation of oxidised Ni(II) species. The additional carbon atom on the arm of the pyridine moiety in [Ni(^{t}BuL$_S^{Py2}$)] in comparison to [Ni(^{t}BuL$_S^{Py1}$)] prevents the pyridine N-donor from binding to the Ni(II) thiolate metal centre upon oxidation. Thus, in conclusion it appears that the incorporation of a suitable N-donor onto the ligand backbone at an appropriate distance from the Ni-centre is a prerequisite for the stabilization of the oxidation products. Our preliminary results, which have led to the synthesis and structural characterisation of [Ni(^{t}BuL$_O^R$)] (R = OH, Ph) and [Ni(^{t}BuL$_S^{OH}$)], suggest that the functionalisation of the R = OH group in [Ni(^{t}BuL$_O^{OH}$)] and [Ni(^{t}BuL$_S^{OH}$)] could provide a route to the incorporation of pendant N-donors. However, it appears that other routes that do not involve the treatment of [Ni(^{t}BuL$_O^{OH}$)] and [Ni(^{t}BuL$_S^{OH}$)] with functionalised acid chlorides may need to be explored.

3.5 Experimental

3.5.1 Synthesis of 5-(chloromethyl)-4-methyl-1H-imidazole

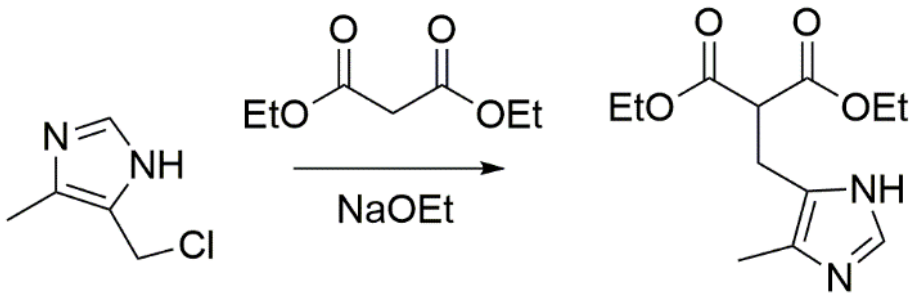


Scheme 3.13 Synthesis of 5-(chloromethyl)-4-methyl-1H-imidazole

(4-Methyl-1H-imidazol-5-yl)methanol hydrochloride (10.0 g, 67.5 mmol) was stirred in $SOCl_2$ (25ml) and DMF (0.01 ml) for 1 h at room temperature. CH_3Cl (50 ml) was added and the resultant white precipitate was collected via filtration. This was further washed with CH_3Cl (2 x 25 ml) and dried *in vacuo* giving the product as a white powder (9.98 g, 76.75 mmol, 87 %).

^{1}H-NMR (400 MHz, $(CD_3)_2SO$), 298 K): δ_H 8.84 (1H, s, Ar<u>H</u>), 4.80 (2H, s, C<u>H</u>$_2$), 2.32 (3H, s, C<u>H</u>$_3$). ^{13}C-NMR (400 MHz, $(CD_3)_2SO$, 298 K): δ_C 134.8 (Ar<u>C</u>), 129.6 (Ar<u>C</u>), 127.0 (Ar<u>C</u>), 34.2 (<u>C</u>H$_2$), 8.93 (<u>C</u>H$_3$). MS (ES+, m/z): 131.0398 [M+H].

3.5.2 Synthesis of diethyl 2-((4-methyl-1H-imidazol-5-yl)methyl)malonate

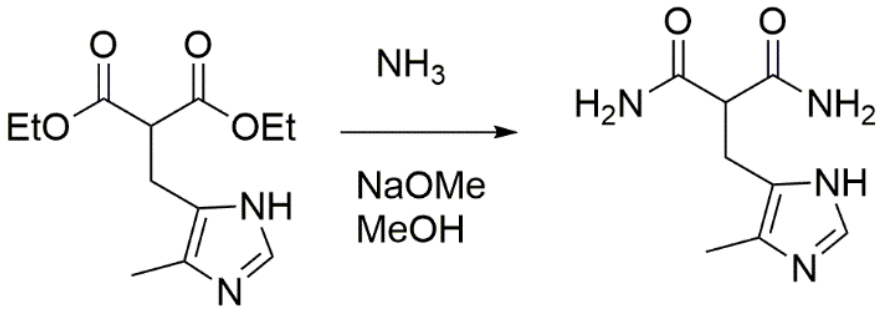


Scheme 3.14 Synthesis of diethyl 2-((4-methyl-1H-imidazol-5-yl)methyl)malonate.

Diethyl malonate (13.82 ml, 91 mmol) was added to a solution of NaOEt (5.41 g of sodium, 100 ml of EtOH) at 0 °C and left to stir for 30 min. 5-(Chloromethyl)-4-methyl-1H-imidazole (11.52 g, 91 mmol) was added at 0 °C. The reaction mixture was then heated to reflux for 24 h. The solvent was removed *in vacuo* and the residue was treated with HCl (4 N) until acidic (pH 1) at 0 °C to produce a red solution. The aqueous layer was then treated with NaOH (6M, 45 ml) at 0 °C and extracted with Et_2O. The Et_2O solution was dried over $MgSO_4$. The solvent was reduced *in vacuo* and the residue distilled under reduced pressure remove excess diethyl malonate to leave a dark red oil (20.1 g, 80 mmol, 88 %).

^{1}H-NMR (400 MHz, $CDCl_3$, 298 K): δ_H 7.63 (1H, d, Ar<u>H</u>), 4.16 – 4.18 (4H, m, C<u>H</u>$_2$), 3.73 (1H, t, *J* 7.0, C<u>H</u>), 3.12 (2H, t, *J* 7.0, C<u>H</u>$_2$), 2.18 (3H, s, C<u>H</u>$_3$), 1.17 (6H, t, *J* 7.2, C<u>H</u>$_3$). ^{13}C-NMR (400 MHz, $CDCl_3$, 298 K): δ_C 169.3 (<u>C</u>=O), 133.1 (Ar<u>C</u>), 128.6 (Ar<u>C</u>), 120.5 (ArC), 61.5 (O<u>C</u>H$_2$) 51.8 (<u>C</u>H), 24.5 (<u>C</u>H$_2$), 13.9 (<u>C</u>H$_3$), 13.8 (<u>C</u>H$_3$). MS (ES+, m/z): 277.1164 [M + Na].

3.5.3 Synthesis of 2-((4-methyl-1H-imidazol-5-yl)methyl)malonamide

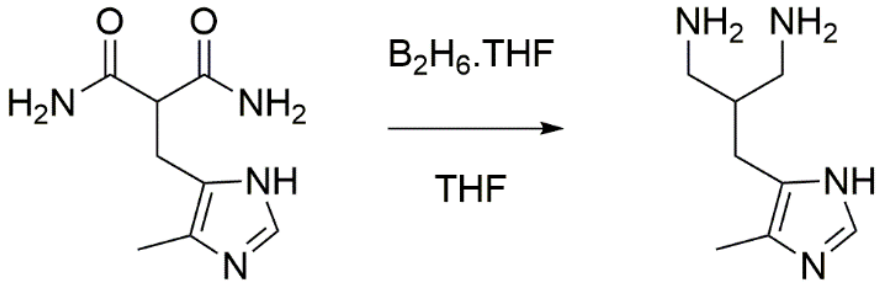


Scheme 3.15 Synthesis of diethyl 2-((4-methyl-1H-imidazol-5-yl)methyl)malonamide.

A solution of diethyl 2-((4-methyl-1H-imidazol-5-yl)methyl)malonate (16 g, 64 mmol) and NaOMe (0.37 g, 6.9 mmol) in anhydrous MeOH (80 ml) was saturated with NH_3. The reaction mixture was cooled for 24 h and the resulting precipitate collected and washed with MeOH and dried under reduced pressure to give a light pink powder (12.0 g, 61.44 mmol, 92%).

^{1}H-NMR (400 MHz, DMSO, 298 K): δH 7.24 (1H, s, ArH), 7.02 (4H, s, NH_2), 3.34 (1H, t, *J* 7.3, CH), 2.86 (2H, d, *J* 7.3, CH_2), 2.10 (3H, s, CH_3). ^{13}C-NMR (400 MHz, DMSO, 298 K): δC 170.7 (C=O), 132.5 (ArC), 128.3 (ArC), 125.0 (ArC), 52.7 (CH), 24.7 (CH_2), 9.59 (CH_3). MS (ES+, m/z): 197.0960 [M + H].

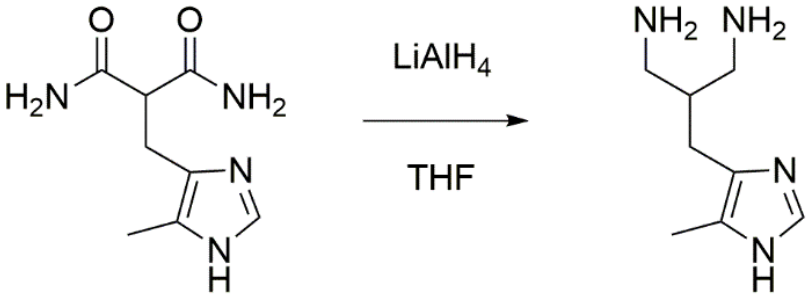
3.5.4 Attempted synthesis of 2-((4-methyl-1H-imidazol-5-yl)methyl)propane-1,3-diamine *via* reduction with B_2H_6.THF



Scheme 3.16 Attempted synthesis of 2-((4-methyl-1H-imidazol-5-yl)methyl)propane-1,3-diamine.

A solution of B_2H_6.THF (1 M, 120 ml) was added to a suspension of 2-((4-methyl-1H-imidazol-5-yl)methyl)malonamide (5 g, 26 mmol) in anhydrous THF (50 ml) at 0 ^oC. The reaction mixture was heated to reflux for 24 h. Excess diborane was destroyed with de-ionised H_2O (40 ml). The reaction mixture was reduced *in* vacuo to give a white solid. The solid was treated with HCl (6 N, 200 ml) and heated to reflux for 1 h. The solvent was removed *in vacuo* and the residue was re- dissolved de-ionised H_2O (100 ml) and treated with NaOH (6 N, 70 ml). The aqueous solution was extracted with Et_2O (4 x 200 ml), dried over $MgSO_4$, and the solvent removed *in vacuo* to produce brown oil. No product could be identified by ^{1}H-NMR, ^{13}C-NMR spectroscopies and mass spectrometry.

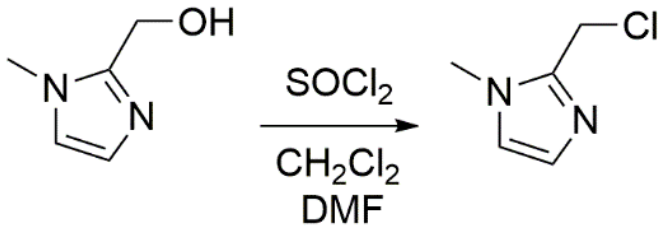
3.5.5 Attempted synthesis of 2-((4-methyl-1H-imidazol-5-yl)methyl)propane-1,3-diamine *via* reduction with $LiAlH_4$



Scheme 3.17 Attempted synthesis of 2-((4-methyl-1H-imidazol-5-yl)methyl)propane-1,3-diamine.

Lithium aluminium hydride in anhydrous and de-gassed THF (0.08g, 2.197 mmol) was added slowly to a suspension of 2-((4-methyl-1H-imidazol-5-yl)methyl)malonamide (0.10g, 0.55 mmol) in de-gassed anhydrous THF. The reaction mixture was then heated to reflux for 3 h and then allowed to cool to room temperature. Excess lithium aluminium hydride was quenched by the drop-wise addition of a saturated solution of Na_2SO_4 (30 ml). The organic layer was separated and dried over $MgSO_4$ and reduced *in vacuo* to produce a brown oil. No product could be identified by ^{1}H-NMR, ^{13}C-NMR spectroscopies and mass spectrometry.

3.5.6 Synthesis of 2-(chloromethyl)-1-methyl-1H-imidazole

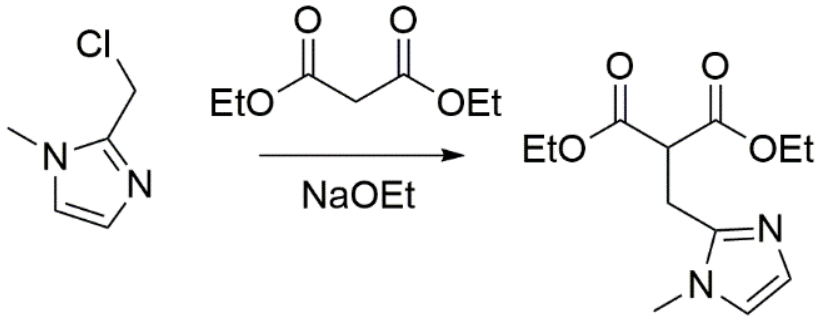


Scheme 3.18 Synthesis of 2-(chloromethyl)-1-methyl-1H-imidazole.

Thionyl chloride (10 ml) was added to 1-methyl-2-hydroxymethyl imidazole (0.20 g, 1.78 mmol) in CH_2Cl_2 (30 ml) and DMF (0.01 ml). The reaction mixture was then heated to reflux for 15 min. The reaction was cooled to room temperature and the solvent removed *in vacuo*. The product was recrystallised from ethanol (25 mL) and dried to give 2-(chloromethy1)-1-methyl-1H-imidazole hydrochloride as brown crystals (0.12 g, 0.96 mmol, 54%).

^{1}H-NMR (400 MHz, $CDCl_3$), 298 K): δ_H 7.45 (1H, d, *J* 6.7, Ar<u>H</u>), 7.44 (1H, d, J 6.7, Ar<u>H</u>), 5.12 (3H, s, C<u>H</u>$_3$), 3.85 (2H, s, C<u>H</u>$_2$). ^{13}C-NMR (400 MHz, $CDCl_3$, 298 K): δ_C 162.8 (Ar<u>C</u>), 125.8 (Ar<u>C</u>), 120.3 (Ar<u>C</u>), 35.8 (<u>C</u>H$_2$), 32.8 (<u>C</u>H$_3$). MS (ES+, m/z): 131.0298 [M+H].

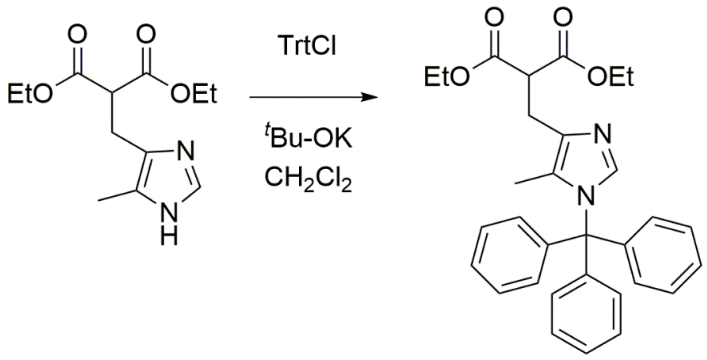
3.5.7 Attempted synthesis of diethyl 2-((1-methyl-1H-imidazol-5-yl)methyl)malonate



Scheme 3.19 Attempted synthesis of 2-((1-methyl-1H-imidazol-5-yl)methyl)malonate.

Diethyl malonate (0.23 ml, 1.53 mmol) was added to a solution of NaOEt (0.2 g of sodium, 50 ml of EtOH) at 0 °C and left to stir for 30 min. 2-(Chloromethyl)-1-methyl-1H-imidazole (0.10 g, 0.76 mmol) was added at 0 °C. The reaction mixture was heated to reflux for 24 h. The solvent was removed *in vacuo* and the residue was treated with HCl (4 M) until acidic (pH 1) whilst at 0 °C to produce a red solution. The aqueous layer was treated with NaOH (6 M, 45 ml) at 0 °C and then extracted with Et_2O (2 x 50 ml). The Et_2O washings were combined and dried over $MgSO_4$. The solvent was reduced *in vacuo* and the residue distilled under reduced pressure (45 °C) to remove excess diethyl malonate to leave a dark red oil. No product could be identified by ^{1}H-NMR, ^{13}C-NMR spectroscopies and mass spectrometry.

3.5.8 Synthesis of diethyl 2-((4-methyl-1-trityl-1H-imidazol-5-yl)methyl)malonate



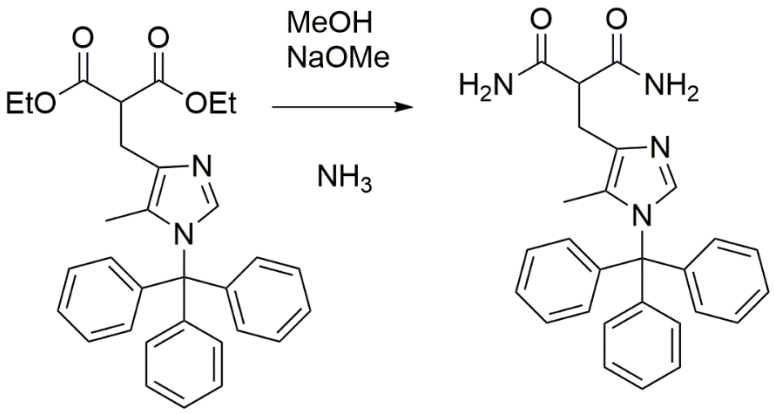
Scheme 3.20 Synthesis of diethyl 2-((4-methyl-1-trityl-1H-imidazol-5-yl)methyl)malonate.

Tritylchloride (0.61 g, 2.17 mmol) was added to a solution of diethyl 2-((4-methyl-1H-imidazol-5-yl)methyl)malonate (0.5 g, 1.97 mmol) and potassium tert-butoxide (0.26g, 2.17 mmol) in CH_2Cl_2 at 0°C. The reaction mixture was stirred at room temperature for 24 h. The solvent was removed *in vacuo* to give a crude oil. The oil was dissolved in acetone and the solution was washed with brine and the organic layer dried over Na_2SO_4. The solvent was removed *in vacuo* to leave an orange oil. The product was purified via column chromatography with CH_2Cl_2 and 10% MeOH as eluent (1.35 g, 80 mmol, 88 %).

^{1}H-NMR (400 MHz, $CDCl_3$, 298 K): δ_H 7.44 (1H, s, Ar<u>H</u>), 7.37 – 7.29 (15H, m, Ar<u>H</u>), 4.12 (4H, m, C<u>H</u>$_2$), 3.78 (1H, *J* 7.0, t, C<u>H</u>), 3.12 (2H, d, *J* 7.0, C<u>H</u>$_2$), 2.18 (3H, s, C<u>H</u>$_3$), 1.41 (6H, t, *J* 7.2, C<u>H</u>$_3$). ^{13}C-NMR (400 MHz, $CDCl_3$, 298 K): δ_C 169.2 (<u>C</u>=O), 141.3 (Ar<u>C</u>), 138.6 (Ar<u>C</u>), 137.7 (Ar<u>C</u>), 131.1 (Ar<u>C</u>), 129.6 (Ar<u>C</u>), 128.3 (Ar<u>C</u>), 126.3 (Ar<u>C</u>), 83.6 (<u>C</u>(Ph)$_3$), 61.5 (O<u>C</u>H$_2$), 51.9 (<u>C</u>H), 20.7 (<u>C</u>H$_2$)

13.9 ($\underline{C}H_3$), 11.5 ($\underline{C}H_3$). MS (ES+, m/z): 497.2362 [M + H].

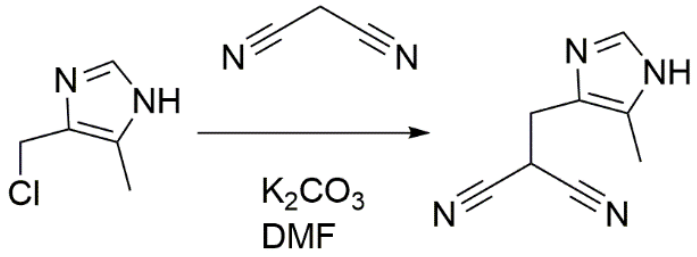
3.5.9 Attempted synthesis of 2-((4-methyl-1-trityl-1H-imidazol-5-yl)methyl)malonamide



Scheme 3.21 Attempted synthesis of 2-((1-methyl-1H-imidazol-5-yl)methyl)malonate.

A solution of diethyl 2-((4-methyl-1-trityl-1H-imidazol-5-yl)methyl)malonate (0.50 g, 1.02 mmol) and NaOMe (0.02 g, 0.40 mmol) in anhydrous MeOH (80 ml) was saturated with NH_3. The reaction mixture was cooled for 24 h and but no precipitate formed. The reaction mixture was reduced *in vacuo* and an orange oil was collected however no product could be identified by ^{1}H-NMR, ^{13}C-NMR spectroscopies and mass spectrometry.

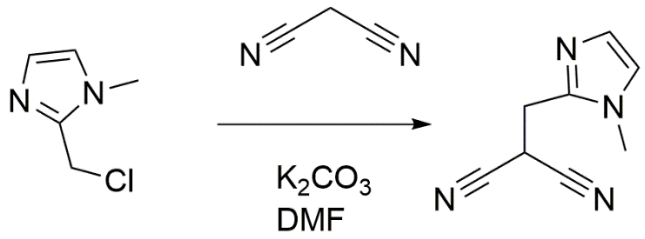
3.5.10 Attempted synthesis of 2-((5-methyl-1H-imidazol-4-yl)methyl)malononitrile



Scheme 3.22 Attempted synthesis of 2-((5-methyl-1H-imidazol-4-yl)methyl)malononitrile.

To a solution of malonitirile (1.12 g, 66.0 mmol) in THF (30 ml) a solution of potassium carbonate (2.34 g, 16.9 mmol) in THF (10 ml) was added. After stirring for 30 min at RT, a solution of 4-(chloromethyl)-5-methyl-1H-imidazole (2.0 g, 15.38 mmol) in THF (10 ml) was added to the reaction mixture. The reaction mixture was left to stir at RT for 24 h. The reaction mixture was quenched with deionised water (30 ml) and extracted with Et_2O (2 x 30 ml). The organic layer was washed with deionised water and reduced *in vacuo* to leave a brown oil. However, no product could be identified by ^{1}H-NMR, ^{13}C-NMR spectroscopies and mass spectrometry.

3.5.11 Synthesis of 2-((1-methyl-1H-imidazol-4-yl)methyl)malononitrile

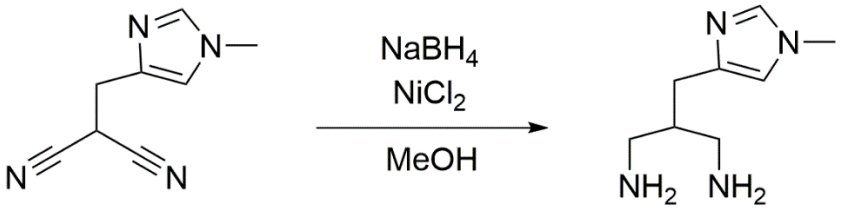


Scheme 3.23 Attempted synthesis of 2-((1-methyl-1H-imidazol-4-yl)methyl)malononitrile.

To a solution of malonitirile (0.05 g, 0.80 mmol) in THF (20 ml) a solution of potassium carbonate (0.10 g, 0.80 mmol) in THF (10 ml) was added drop-wise. After being stirred for 30 min at room temperature a solution of 2-(chloromethyl)-1-methyl-1H-imidazole (0.10 g, 0.80 mmol) in THF (10 ml) was added to the cooled reaction mixture. After this the reaction mixture was left to stir at room temperature for 24 h. The reaction mixture was quenched with deionised water (30 ml) and extracted with Et_2O (2 x 30 ml). The organic layer was washed with deionised water and reduced *in vacuo* to leave a brown oil (0.07 g, 0.53 mmol, 67%).

^{1}H-NMR (400 MHz, CD_3CN, 298 K): δ_H 6.87 (1H, d, *J* 7.2, Ar<u>H</u>), 6.71 (1H, d, *J* 7.2, Ar<u>H</u>), 3.72 (1H, t, *J* 7.0, C<u>H</u>), 3.88 (3H, s, C<u>H</u>$_3$), 3.25 (2H, d, *J* 7.0, C<u>H</u>$_2$). ^{13}C-NMR (400 MHz, CD_3CN, 298 K): δ_C 148.2 (Ar<u>C</u>), 124.3 (Ar<u>C</u>), 121.8 (Ar<u>C</u>), 116.8 (<u>C</u>N), 36.4 (<u>C</u>H$_3$), 25.2 (<u>C</u>H$_2$), 24.2 (<u>C</u>H). MS (ES+, m/z): 161.0749 [M+H].

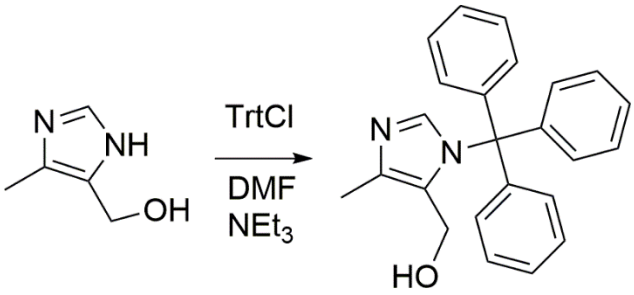
3.5.12 Attempted synthesis of 2-((1-methyl-1H-imidazol-4-yl)methyl)propane-1,3-diamine



Scheme 3.24 Attempted synthesis of 2-((1-methyl-1H-imidazol-4-yl)methyl)propane-1,3-diamine.

To a solution of 2-((1-methyl-1H-imidazol-4-yl)methyl)malononitrile (0.07 g, 0.40 mmol) in MeOH (30 ml) was added $NaBH_4$ (0.18 g, 4.80 mmol) and $NiCl_2$ (0.001 g, 0.04 mmol). The reaction was stirred for 24 h before the solvent was removed *in vacuo* to leave a brown oil. However, no product could be identified by ^{1}H-NMR, ^{13}C-NMR spectroscopies and mass spectrometry.

3.5.13 Synthesis of (4-methyl-1-trityl-1H-imidazol-5-yl)methanol

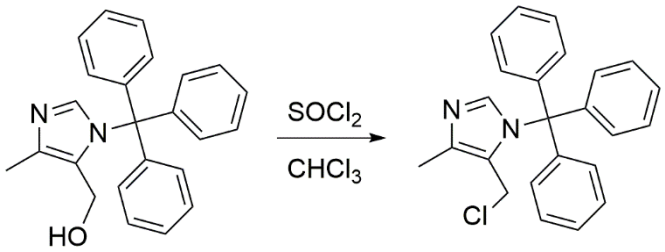


Scheme 3.25 Synthesis of (4-methyl-1-trityl-1H-imidazol-5-yl)methanol

A solution of tritylchloride (2.48 g, 278.77 mmol) in DMF (30 ml) was added drop-wise to a solution of (4-methyl-1H-imidazol-5-yl)methanol (1.0 g, 8.92 mmol) and trimethylamine (2.46 ml, 17.8 mmol) in DMF (30 ml). After stirring for 24 h at RT the solution was filtered to give a white precipitate. The product was washed with water (100 ml) and then acetone (150ml), and dried *in vacuo* as a white powder (1.95 g, 5.53 mmol, 62%).

^{1}H-NMR (400 MHz, $CDCl_3$, 298 K): δ_H 7.34 – 7.29 (15H, m, Ar<u>H</u>), 7.24 (1H, s, Ar<u>H</u>), 5.28 (1H, s, O<u>H</u>), 4.52 (2H, s, C<u>H</u>$_2$), 1.45 (3H, s, C<u>H</u>$_3$). ^{13}C-NMR (400 MHz, $CDCl_3$, 298 K): δ_C 140.5 (Ar<u>C</u>), 139.8 (Ar<u>C</u>), 138.0 (Ar<u>C</u>), 130.1 (Ar<u>C</u>), 128.5 (Ar<u>C</u>), 127.8 (Ar<u>C</u>), 126.3 (Ar<u>C</u>), 85.1 (<u>C</u>(Ph)$_3$), 57.8 (<u>C</u>H$_2$), 11.8 (<u>C</u>H$_3$). MS (ES+, m/z): 355.1732 [M+H].

3.5.14 Synthesis of 4-(chloromethyl)-5-methyl-1-trityl-1H-imidazole (trtityl protection)

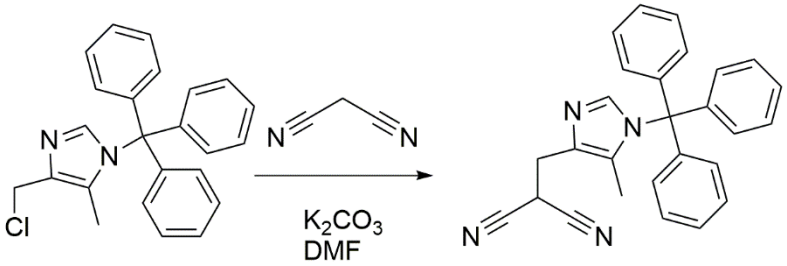


Scheme 3.26 Synthesis of 4-(chloromethyl)-5-methyl-1-trityl-1H-imidazole.

A solution of $SOCl_2$ (0.30 ml, 4.23) in CH_2Cl_2 and DMF (0.01 ml) was added to a solution of (5-methyl-1-trityl-1H-imidazol-4-yl)methanol (1.0 g, 2.82 mmol) in CH_2Cl_2 (20 ml). The reaction mixture was stirred for 4 h and then quenched with a saturated Na_2CO_3 (100 ml) M) solution. The organic layer was washed with water and then dried with $MgSO_4$. The solvent was removed *in vacuo* to reveal a cream powdered product (0.98 g, 2.63 mmol, 98%).

^{1}H-NMR (400 MHz, $CDCl_3$, 298 K): δ_H 7.36 – 7.32 (15H, m, Ar<u>H</u>), 7.29 (1H, s, Ar<u>H</u>), 4.59 (2H, s, C<u>H</u>$_2$), 1.46 (3H, s, C<u>H</u>$_3$). ^{13}C-NMR (400 MHz, $CDCl_3$, 298 K): δ_C 141.3 (Ar<u>C</u>), 139.2 (Ar<u>C</u>), 137.4 (Ar<u>C</u>), 131.2 (Ar<u>C</u>), 129.7 (Ar<u>C</u>), 128.5 (Ar<u>C</u>), 127.7 (Ar<u>C</u>), 83.8 (<u>C</u>(Ph)$_3$), 33.4 (<u>C</u>H$_2$), 11.2 (<u>C</u>H$_3$). MS (ES+, m/z): 373.1393 [M+H].

3.5.15 Synthesis of 2-((5-methyl-1-trityl-1H-imidazol-4-yl)methyl)malononitrile

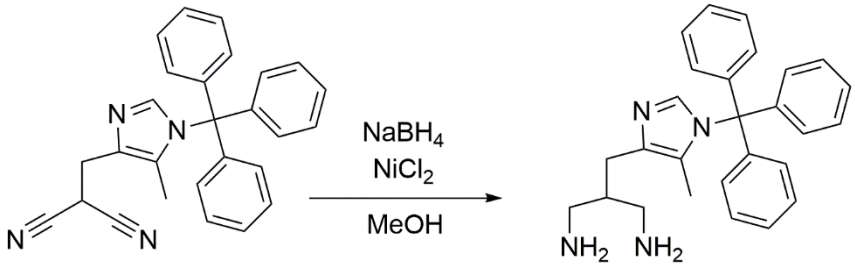


Scheme 3.27 Synthesis of 2-((5-methyl-1-trityl-1H-imidazol-4-yl)methyl)malononitrile

A solution of K_2CO_3 (0.10 g, 0.27 mmol) in THF (10 ml) was added drop-wise to a solution of malonitirile (0.04 g, 0.27 mmol) in THF (20 ml). After being stirred for 30 min at RT, a solution of 24-(chloromethyl)-5-methyl-1-trityl-1H-imidazole (0.10 g, 0.27 mmol) in THF (10 ml) was added to the cooled reaction mixture. The reaction mixture was left to stir at RT for 24 h. The reaction mixture was quenched with deionised water (30 ml) and extracted with Et_2O (2 x 30 ml). The organic layer was washed with deionised water and the solvent removed *in vacuo* to a yield a brown oil (0.05 g, 0.13 mmol, 47%).

^{1}H-NMR (400 MHz, $CDCl_3$, 298 K): δ_H 7.40 – 7.34 (15H, m, Ar<u>H</u>), 7.31 (1H, s, Ar<u>H</u>), 4.42 (1H, t, *J* 7.7, C<u>H</u>), 3.23 (2H, d, *J* 7.7, C<u>H</u>$_2$), 1.45 (3H, s, C<u>H</u>$_3$). ^{13}C-NMR (400 MHz, $CDCl_3$, 298 K): δ_C 140.6 (Ar<u>C</u>), 139.2 (Ar<u>C</u>), 137.7 (Ar<u>C</u>), 131.5 (Ar<u>C</u>), 129.5 (Ar<u>C</u>), 127.9 (Ar<u>C</u>), 126.7 (Ar<u>C</u>), 112.3 (<u>C</u>N), 81.1 (<u>C</u>(Ph)$_3$), 22.6 (CH), 20.6 (<u>C</u>H$_2$), 11.6 (<u>C</u>H$_3$). MS (ES+, m/z): 403.1844 [M+H].

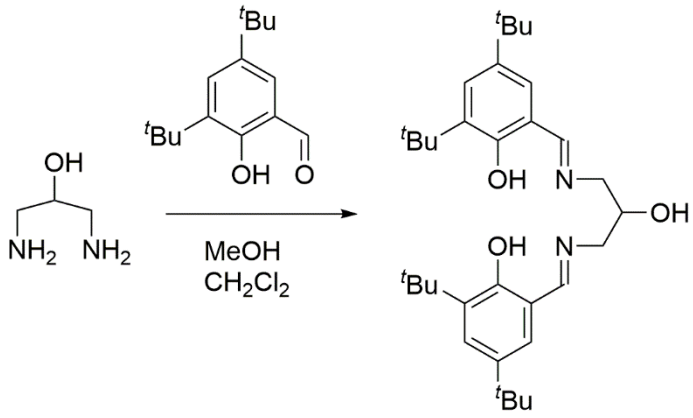
3.5.16 Attempted synthesis of 2-((5-methyl-1-trityl-1H-imidazol-4-yl)methyl)propane-1,3-diamine



Scheme 3.28 Attempted synthesis of 2-((5-methyl-1-trityl-1H-imidazol-4-yl)methyl)propane-1,3-diamine.

$NaBH_4$ (0.13 g, 3.43 mmol) and $NiCl_2$ (0.001 g, 0.04 mmol) were added to a solution of 2-((5-methyl-1-trityl-1H-imidazol-4-yl)methyl)malononitrile (0.20 g, 0.50 mmol) in MeOH (30 ml). The reaction mixture was stirred for 24 after which time the solvent was removed *in vacuo* to yield a brown oil. However, no product could be identified by ^{1}H-NMR, ^{13}C-NMR spectroscopies and mass spectrometry.

3.5.17 Synthesis of [$H_2{}^tBuL_O{}^{OH}$]

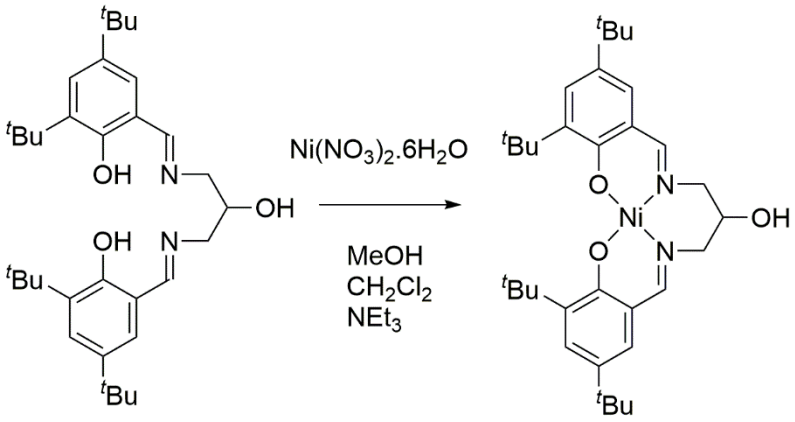


Scheme 3.29 Synthesis of [$H_2{}^tBuL_O{}^{OH}$]

A solution of 1,3-diaminopropan-2-ol (0.19 g, 2.14 mmol) in MeOH (10 ml) was added to a solution of di-*tert*-butyl-2-hydroxybenzaldehyde (1.00 g, 4.27 mmol) in CH_2Cl_2 (20 ml). After 2 h the solvent was removed *in vacuo* to yield a yellow viscous oil.

^{1}H NMR (400 MHz, $CDCl_3$, 298 K): δ_H 8.46 (2H, s, N=C<u>H</u>), 7.42 (2H, d, *J* 2.4, Ar<u>H</u>), 7.15 (2H, d, *J* 2.4, Ar<u>H</u>), 3.49 (1H, s, O<u>H</u>) 4.33 – 4.22 (1H, m, C<u>H</u>) 3.88 (2H, ddd, *J* 12.4, 4.6, 1.0, C<u>H</u>$_2$), 3.75 (2H, ddd, *J* 12.3, 6.4, 1.0, C<u>H</u>$_2$), 1.48 (18H, s, C(C<u>H</u>$_3$)$_3$), 1.33 (18H, s, C(C<u>H</u>$_3$)$_3$). ^{13}C NMR (100 MHz, $CDCl_3$, 298 K): δ_C 168.5 (<u>C</u>=N), 157.9 (Ar<u>C</u>), 140.3 (Ar<u>C</u>), 136.8 (Ar<u>C</u>), 127.2 (Ar<u>C</u>), 126.2 (Ar<u>C</u>), 117.7 (Ar<u>C</u>), 70.7 (<u>C</u>-OH), 63.2 (<u>C</u>H$_2$-N), 35.0 (<u>C</u>(CH$_3$)$_3$), 34.1 (<u>C</u>(CH$_3$)$_3$), 31.5 (<u>C</u>H$_3$), 29.4 (<u>C</u>H$_3$). MS (ES+, m/z): 523.3821 [M+H]. Elemental analysis: found (calculated for $C_{33}H_{50}N_2O_3$): C 75.83 (75.82), H 9.60 (9.64), N 5.38 (5.36). Yield = 2.18 g, 4.19 mmol, 98 %.

3.5.18 Synthesis of [Ni(^{t}BuL$_O^{OH}$)]

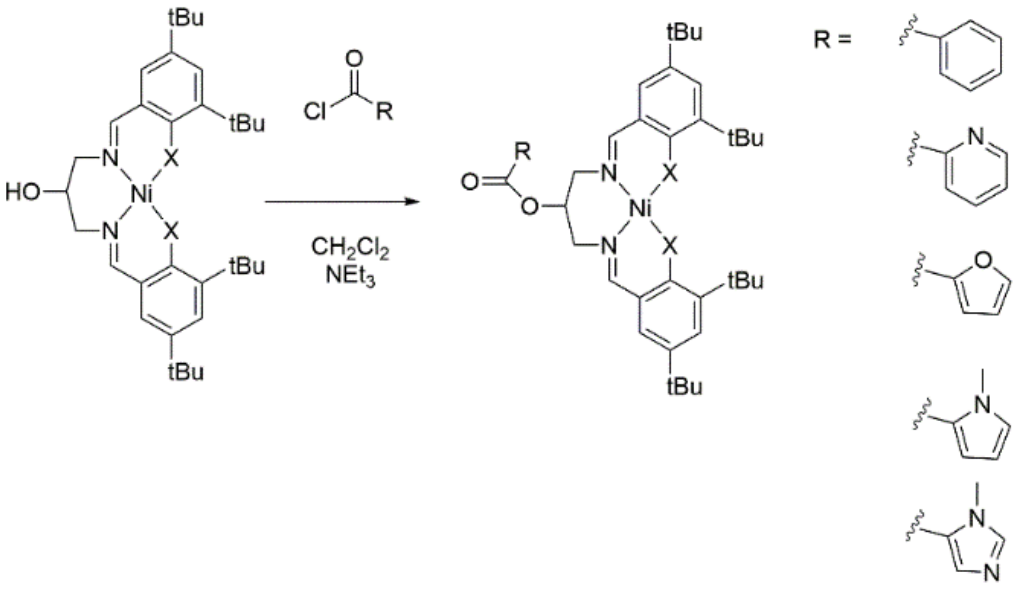


Scheme 3.30 Synthesis of [Ni(^{t}BuL$_O^{OH}$)].

$Ni(NO_3)_2{\cdot}6H_2O$ (0.40 g, 1.92 mmol) in a methanol (10 ml) and NEt_3 (1.21 ml, 8.64 mmol) were added to a solution of crude [$H_2{}^t$BuL$_O^{OH}$] (1.00 g, 1.92 mmol) in CH_2Cl_2 (20 ml). The reaction mixture was heated to reflux for 24 h. The reaction mixture was then reduced *in vacuo* to produce a yellow solid which was further purified by column chromatography on silica gel using dichloromethane and pentane (3:2 v/v) as eluent. The product was recrystallized from a dichloromethane and pentane (3:2 v/v) solution.

The product was recrystallized from dichloromethane and pentane (3:2 v/v) solution. FTIR ν / cm^{-1} (ATR): 2988 (m), 1615 (s), 1547 (s), 1432 (s), 1370 (m), 1238 (m), 1023 (m), 802 (m) 753 (s) 630 (m) 528 (m). MS (ES+, m/z): 579.3018 [M+H]. Elemental analysis: found (calculated for $C_{33}H_{48}NiN_2O_3$): C 68.40 (68.45), H 8.35 (8.31), N 4.83 (4.83). Yield = 1.08 g, 1.87 mmol, 97 %.

3.5.19 Attempted Syntheses of [Ni(^{t}BuL$_O^R$)] (R = Ph, PyN, Fu, Pyr and Imid)



Scheme 3.31 Synthesis of [Ni(^{t}BuL$_O^R$)] and [Ni(^{t}BuL$_S^R$)] (R = Ph, PyN, Fu, Pyr and Imid)

General procedure: Benzoyl chloride (0.12 g, 0.86 mmol) and NEt_3 (0.77 ml, 1.72 mmol) were added to a solution of [Ni(^{t}BuL$_O^{OH}$)] (0.50 g, 0.86 mmol) in anhydrous CH_2Cl_2. The reaction was stirred for 24 h and then the solvent removed under vacuum to produce a yellow powder. Attempts to purify the products were made by column chromatography on silica gel using dichloromethane and pentane (3:2 v/v) as eluent and by recrystallizations of the solid materials isolated from the column fractions.

3.5.20 [Ni(^{t}BuLo^{Ph})]

The product was recrystallized from dichloromethane and pentane (3:2 v/v) solution. FTIR ν / cm^{-1} (ATR): 2978 (m), 1706 (s), 1614 (s), 1548 (s), 1437 (s), 1381 (m), 1259 (s), 1172 (m), 1068 (m), 834 (m) 798 (s) 785 (m), 711 (m) . MS (ES+, m/z): 683.3281 [M+H]. Elemental analysis: found (calculated for $C_{40}H_{52}NiN_2O_4$): C 70.29 (70.30), H 7.67 (7.67), N 4.10 (4.08). Yield = 0.27 g, 0.39 mmol, 46 %.

3.5.21 [Ni(^{t}BuLo^{PyN})]

The mass spectrum of the crude product possesses features that may be assigned to the desired product. However, attempts to purify the product were unsuccessful. MS (ES+, m/z): 684.3233 [M+H].

3.5.22 [Ni(^{t}BuLo^{Fu})]

The mass spectrum of the crude product possesses features that may be assigned to the desired product. However, attempts to purify the product were unsuccessful. MS (ES+, m/z): 673.3073 [M+H].

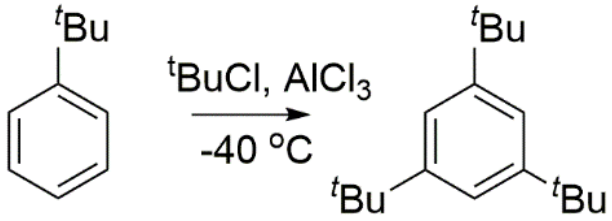
3.5.23 [Ni(^{t}BuLo^{Pyr})]

The mass spectrum of the crude product possesses features that may be assigned to the desired product. However, attempts to purify the product were unsuccessful. MS (ES+, m/z): 686.3390 [M+H].

3.5.24 [Ni(^{t}BuLo^{Imid})]

The mass spectrum of the crude product possesses features that may be assigned to the desired product. However, attempts to purify the product were unsuccessful. MS (ES+, m/z): 687.3342 [M+H].

3.5.25 Synthesis of 1, 3, 5-tri-*tert*-butylbenzene

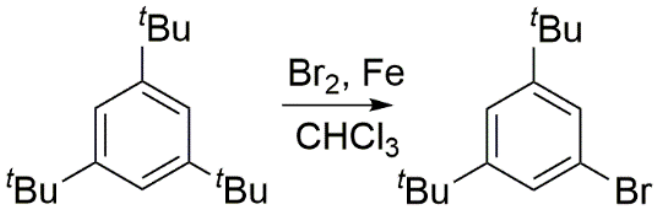


Scheme 3.32 Synthesis of 1, 3, 5-tri-*tert*-butylbenzene.

To a mixture of *tert*-butylbenzene (77.5 ml, 0.5 mol) and *tert*-butyl chloride (500 ml, 4.6 mol), anhydrous aluminum chloride (33 g, 0.25 mol) was added in 2 g portions over a 10 min period to a flask equipped with a paddle stirrer under an inert atmosphere and at temperature of -40°C. The temperature of the reaction was then allowed to rise to -10°C and the reaction stirred for a further 2 h. The yellow reaction mixture was then poured onto ice water (ca. 2 L) and stirred vigorously for 15 min by which time a white solution was obtained. The aqueous mixture was then extracted with Et_2O (3 × 200 ml) and dried over $MgSO_4$ before evaporation to dryness. The partially crystalline product was washed with cold MeOH (2 x 75 ml) and then re-crystallised from MeOH to yield white crystals of 1,3,5-tri-*tert*-butylbenzene.

^{1}H-NMR (300.13 MHz, $CDCl_3$, 298 K): δ_H 7.25 (3H, s, Ar<u>H</u>), 1.33 (27H, s, C<u>H</u>$_3$). ^{13}C-NMR (270 MHz, $CDCl_3$, 298 K): δ_C 150.1 (Ar<u>C</u>), 119.6 (Ar<u>C</u>), 35.1 (<u>C</u>$(CH_3)_3$), 31.7 (<u>C</u>H_3). MS (ES+, m/z): 247.2348 [M+H].Yield = 102.0 g, 0.41 mol, 83 %.

3.5.26 Synthesis of 1-bromo-3, 5-di-*tert*-butylbenzene

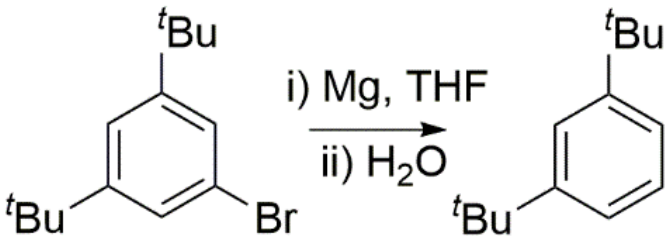


Scheme 3.33 Synthesis of 1-bromo-3, 5-di-*tert*-butylbenzene.

To a cooled (0 ^{o}C) mixture of 1,3,5-tri-*tert*-butylbenzene (78.6 g, 319 mmol) and iron powder (18.6 g, 332 mmol) in $CHCl_3$ (145 ml) a solution of bromine (35 ml, 678 mmol) in $CHCl_3$ (100 ml) was added drop-wise. The addition was controlled so that the temperature remained below 5^{o}C throughout the addition. The reaction mixture was then stirred at room temperature for 16 h before being poured onto ice water. The organic layer was separated and washed with NaOH (10 % in H_2O, 3 × 20 ml) before being dried over $MgSO_4$. The solvent was then removed *in vacuo* and the dark brown residue distilled under reduced pressure (93-95 ^{o}C) to give a white crystalline solid, 1-bromo-3,5-di-*tert*-butylbenzene.

^{1}H-NMR (300.13 MHz, $CDCl_3$, 298 K): δ_H 7.42 (3H, s, Ar<u>H</u>), 1.39 (18H, s, C(C<u>H</u>$_3$)$_3$). ^{13}C-NMR (300.13 MHz, $CDCl_3$, 298 K): δ_C 153.1 (Ar<u>C</u>), 125.6 (Ar<u>C</u>), 123.5 (Ar<u>C</u>), 121.2 (Ar<u>C</u>), 35.1 (<u>C</u>(CH$_3$)$_3$), 31.4 (<u>C</u>H$_3$). MS (ES+, m/z): 269.0827 [M+H]. Yield = 82.4 g, 306 mmol, 96 %.

3.5.27 Synthesis of 1,3-di-*tert*-butylbenzene

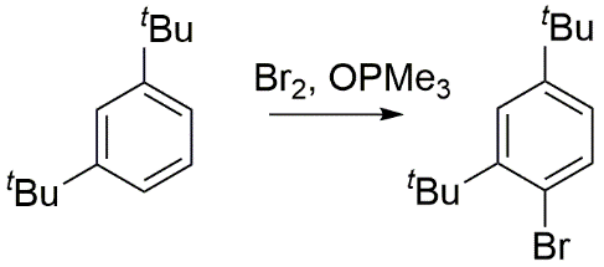


Scheme 3.34 Synthesis of 1,3-di-*tert*-butylbenzene.

A solution of 1-bromo-3,5-di-*tert*-butylbenzene (82.4 g, 306 mmol) in anhydrous THF (100 ml) was added drop-wise to a mixture of magnesium (15.4 g, 630 mmol) and THF (450 ml). The addition of 2 grains of iodine followed by 2 drops of 1,2- dibromoethane initiated the reaction that was then heated at reflux for 16 h. After this the reaction was cooled to room temperature and the reaction mixture was hydrolysed with water and then the solvent was removed *in vacuo* to give a cloudy mixture with a yellow residue. This was filtered and then extracted with Et_2O (3 × 100 ml) and dried over $MgSO_4$. The solvent was removed *in vacuo* and the yellow residue distilled under reduced pressure (48 ^oC) to give clear 1,3-di-*tert*-butylbenzene.

^{1}H-NMR (300.13 MHz, $CDCl_3$, 298 K): δ_H 7.73 (1H, s, Ar<u>H</u>), 7.41 (2H, d, *J* 7.3, Ar<u>H</u>), 7.43 (1H, t, *J* 7.3, Ar<u>H</u>), 1.40 (18H, s, C(C<u>H</u>$_3$)$_3$). ^{13}C-NMR (300.13 MHz, $CDCl_3$, 298 K): δC 150.5 (Ar<u>C</u>), 127.7 (Ar<u>C</u>), 122.4 (Ar<u>C</u>), 122.1 (Ar<u>C</u>), 35.3 (<u>C</u>(CH$_3$)$_3$), 31.3 (<u>C</u>H$_3$). MS (ES+, m/z): 191.3300 [M + H]. Yield = 54.2 g, 297 mmol, 97%.

3.5.28 Synthesis of 1-bromo-2,4-di-*tert*-butylbenzene

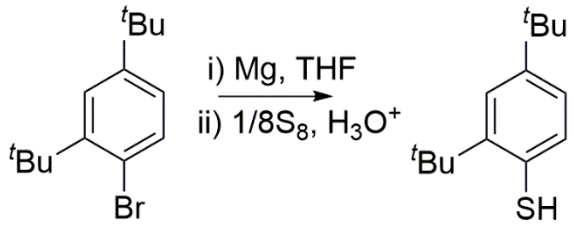


Scheme 3.35 Synthesis of 1-bromo-2,4-di-*tert*-butylbenzene.

A solution of bromine (19.0 ml, 371 mmol) in trimethylphosphate (100 ml) was added drop-wise to a heated (70 ^{o}C) solution of 1,3-di-tert-butylbenzene (58.0 g, 304 mmol) in trimethylphosphate (500 ml). The reaction was stirred at 70^{o}C for 6 h before addition of bromine (1.0 ml, 19.2 mmol) in trimethylphosphate (5 ml), The reaction was then stirred for a further 10 h. The reaction mixture was then extracted with petroleum ether 40-60^{o}C (3 x 100 ml) and washed with Na_2SO_3 solution until the organic layer had de-colourised. The extract was then washed with brine and dried over $MgSO_4$. Petroleum ether was then removed *in vacuo* to give a residual yellow oil which was distilled under reduced pressure (79 ^{o}C) to give pale yellow 1-bromo- 2,4-di-*tert*-butylbenzene.

^{1}H-NMR (300.13 MHz, $CDCl_3$, 298 K): δ_H 7.56 (1H, s, Ar<u>H</u>), 7.54 (1H, d, *J* 7.5, Ar<u>H</u>), 7.11 (1H, d, *J* 7.5, Ar<u>H</u>), 1.57 (9H, s, C(C<u>H</u>$_3$)$_3$), 1.35 (9H, s, C(C<u>H</u>$_3$)$_3$). ^{13}C-NMR (400.13 MHz, $CDCl_3$, 298 K): δ_C 150.4 (Ar<u>C</u>), 147.2 (Ar<u>C</u>), 130.6 (Ar<u>C</u>), 125.5 (Ar<u>C</u>), 124.9 (Ar<u>C</u>), 119.5 (Ar<u>C</u>), 37.1 (<u>C</u>(CH$_3$)$_3$), 35.1 (<u>C</u>(CH$_3$)$_3$), 31.7 (<u>C</u>H$_3$), 30.2 (<u>C</u>H$_3$). MS (ES+, m/z): 269.2260 [M+H]. Yield = 72.0 g, 269 mmol, 88 %.

3.5.29 Synthesis of 2,4-di-*tert*-butylbenzenethiol

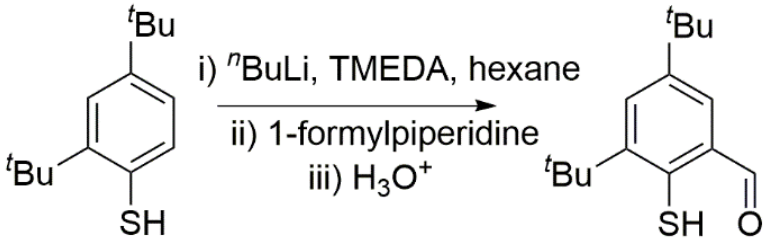


Scheme 3.36 Synthesis of 2,4-di-*tert*-butylbenzenethiol.

An anhydrous THF solution (40 ml) of 1-bromo-2,4-di-*tert*-butylbenzene (35.0g, 131 mmol) was added drop-wise to magnesium (6.0 g, 247 mmol) in THF (280 ml). The reaction was heated at reflux for 45 min before sulfur (4.22 g, 131 mmol) was added at 0 ^{o}C. The reaction was then stirred at 50 ^{o}C for 10 h. After cooling, the liquid was decanted and carefully hydrolysed with excess HCl (5 %, 50 ml). THF was removed *in vacuo* and the crude product extracted with $CHCl_3$, washed with brine and dried over $MgSO_4$. The remaining solvent was then removed *in vacuo* and the product distilled (95 ^{o}C) using short path Kügelruhr apparatus to give colourless 2,4- di-*tert*-butylbenzenethiol.

^{1}H-NMR (300.13 MHz, $CDCl_3$, 298 K): δ_H 7.48 (1H, d, *J* 7.2, ArH), 7.20 (1H, s, ArH), 7.09 (1H, d, *J* 7.2, ArH), 3.56 (1H, s, SH), 1.52 (9H, s, C(CH_3)$_3$), 1.33 (9H, s, C(CH_3)$_3$). ^{13}C-NMR (75.47 MHz, $CDCl_3$, 298 K): δ_C 148.4 (ArC), 146.5 (ArC), 127.6 (ArC), 126.4 (ArC), 123.4 (ArC), 122.3 (ArC), 36.2 (C(CH_3)$_3$), 34.9 (C(CH_3)$_3$), 31.4 (CH_3), 29.8 (CH_3). MS (ES+, m/z): 223.1442 [M+H]. Yield = 26.2 g, 118 mmol, 90 %.

3.5.30 Synthesis of 2,4-di-*tert*-butylthiosalicylaldehyde

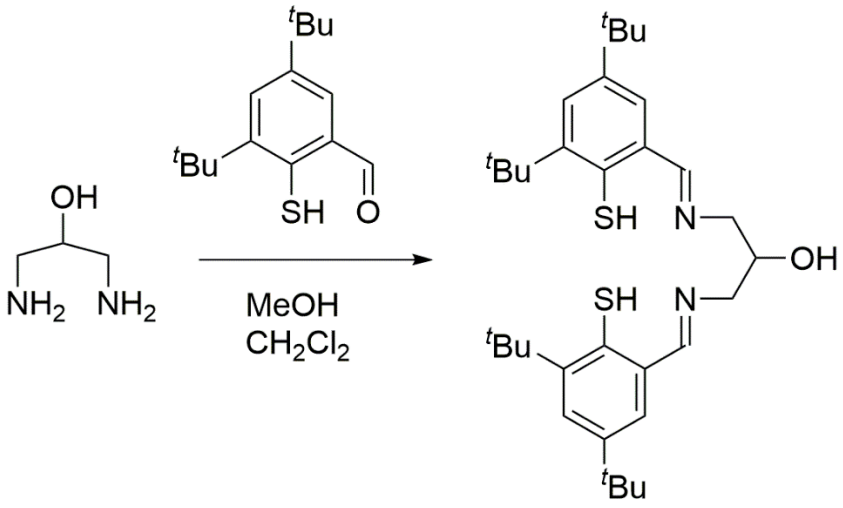


Scheme 3.37 Synthesis of 2,4-di-*tert*-butylthiosalicylaldehyde.

To a solution of TMEDA (3 ml, 19.6 mmol) in anhydrous hexane (30 ml) was added ^{n}BuLi (8.5 ml, 19.6 mmol) at 0 ^{o}C followed by 2,4-di-*tert*-butyl-benzenethiol (2.00 g, 9.00 mmol). The reaction was then stirred at 0 ^{o}C for 30 min before being warmed to room temperature and left to stir for 22 h. 1-formylpiperidine (2.5 ml, 21.9 mmol) was added drop-wise so that the temperature did not exceed 70 ^{o}C. The reaction mixture was then stirred at room temperature for 16 h before the addition of HCl (5 %, 45 ml), after the addition the solution was left to stir for a further 30 min. The aqueous solution was then extracted with diethyl ether (3 × 50 ml). The organic extracts were then combined before being dried over $MgSO_4$. The solvent was then removed *in vacuo* to leave viscous yellow oil, which was dissolved in hexane (5 ml) and passed through a short silica gel chromatographic column containing a silica/hexane slurry. A hexane/CH_2Cl_2 mixture with increasing proportion of CH_2Cl_2 from 100:0 to 50:50 was passed through the column. The second fraction (ca. 75 ml) of solution was collected and the solvent removed *in vacuo* to give a foamy yellow solid, 2,4-di-tert-butylthiosalicylaldehyde which was used without further purification.

^{1}H-NMR (400 MHz, $CDCl_3$, 298 K): δ_H 10.08 (1H, s, S-H), 8.25 (1H, s, O=CH), 7.68 (1H, d, *J* 2.3, ArH), 7.52, (1H, d, *J* 2.3, ArH), 1.58 (9H, s, $C(CH_3)_3$), 1.36 (9H, s, $C(CH_3)_3$). ^{13}C- NMR (400 MHz, $CDCl_3$, 298 K): δ_C 195.7 (C=O), 148.7 (ArC), 147.1 (ArC), 134.9 (ArC), 133.4 (ArC), 130.9 (ArC), 129.6 (ArC), 36.9 ($C(CH_3)$), 34.5 ($C(CH_3)$), 31.2 (CH_3), 29.7 (CH_3). MS (ES+, m/z): 251.1391 [M+H]. Yield = 1.48 g, 5.90 mmol, 59 %,

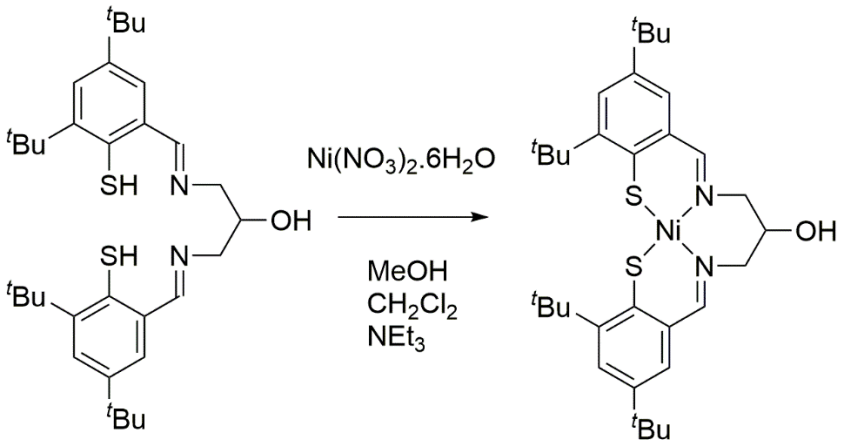
3.5.31 Synthesis of [$H_2{}^tBuL_S{}^{OH}$]



Scheme 3.38 Synthesis of [$H_2{}^tBuL_S{}^{OH}$].

A solution of 1,3-diaminopropan-2-ol (0.19 g, 2.14 mmol) in MeOH (10 ml) was added to a solution of 2,4-di-*tert*-butylthiosalicylaldehyde (1.07 g, 4.28 mmol) in CH_2Cl_2 (20 ml). After 2 h the solvent was removed *in vacuo* to yield a yellow vicious oil. The mass spectrum of the crude product possesses features that may be assigned to the desired product. However, attempts to purify the product were unsuccessful and [$H_2{}^tBuL_S{}^{OH}$] was used without further purification in subsequent reactions. MS (ES+, m/z): 555.3365 [M+H].

3.5.32 Synthesis of [Ni(^{t}BuLs^{OH})]

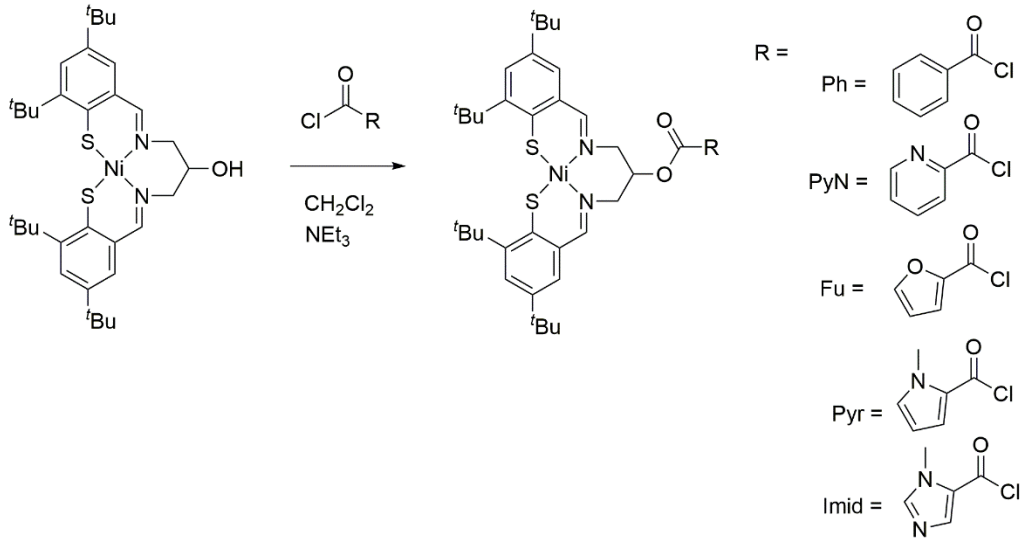


Scheme 3.39 Synthesis of [Ni(^{t}BuLs^{OH})].

$Ni(NO_3)_2.6H_2O$ (0.52 g, 1.82 mmol) in a methanol (10 ml) and NEt_3 (1.21 ml, 8.64 mmol) were added to a solution of crude [H_2^{t}BuLs^{OH}] (1.01 g, 1.82 mmol) in CH_2Cl_2 (20 ml). The reaction mixture was heated to reflux for 24 h. The reaction mixture was then reduced *in vacuo* to produce a brown solid which was further purified by column chromatography on silica gel using dichloromethane and pentane (3:2 v/v) as eluent.

The mass spectrum of the crude product possesses features that may be assigned to the desired product. However, attempts to purify the product were unsuccessful. MS (ES+, m/z): 611.2562 [M+H].

3.5.33 Attempted syntheses of [Ni(^{t}BuLs^R)] (R = Ph, PyN, Fu, Pyr and Imid)



Scheme 3.40 Synthesis of [Ni(^{t}BuLs^R)] (R = Ph, PyN, Fu, Pyr and Imid).

General procedure: Benzoyl chloride (0.12 g, 0.86 mmol) and NEt_3 (0.77 ml, 1.72 mmol) were added to a solution of [Ni(^{t}BuLs^{OH})] (0.53 g, 0.86 mmol) in anhydrous CH_2Cl_2. The reaction was stirred for 24 h and then the solvent removed *in vacuo* to produce a yellow powder that was further purified via column chromatography on silica gel using dichloromethane and pentane (3:2 v/v) as eluent.

3.5.34 [Ni(^{t}BuLs^{Ph})]

The mass spectrum of the crude product possesses features that may be assigned to the desired product. However, attempts to purify the product were unsuccessful. MS (ES+, m/z): 715.2824 [M+H].

3.5.35 [Ni(^{t}BuLs^{PyN})]

The mass spectrum of the crude product possesses features that may be assigned to the desired product. However, attempts to purify the product were unsuccessful. MS (ES+, m/z): 716.2776 [M+H].

3.5.36 [Ni(^{t}BuLs^{Fu})]

The mass spectrum of the crude product possesses features that may be assigned to the desired product. However, attempts to purify the product were unsuccessful. MS (ES+, m/z): 705.2616 [M+H].

3.5.37 [Ni(^{t}BuLs^{Pyr})]

The mass spectrum of the crude product possesses features that may be assigned to the desired product. However, attempts to purify the product were unsuccessful. MS (ES+, m/z): 718.2933 [M+H].

3.5.38 [Ni(^{t}BuLs^{Imid})]

The mass spectrum of the crude product possesses features that may be assigned to the desired product. However, attempts to purify the product were unsuccessful. MS (ES+, m/z): 719.2885 [M+H].

3.6 References

(1) Ermler, U. *Science* **1997**, *278*, 1457–1462.

(2) Drennan, C. L.; Heo, J.; Sintchak, M. D.; Schreiter, E.; Ludden, P. W. *Proc. Natl. Acad. Sci. U. S. A.* **2001**, *98*, 11973–11978.

(3) Dobbek, H.; Svetlitchnyi, V.; Gremer, L.; Huber, R.; Meyer, O. *Science* **2001**, *293*, 1281–1285.

(4) Svetlitchnyi, V.; Dobbek, H.; Meyer-Klaucke, W.; Meins, T.; Thiele, B.; Römer, P.; Huber, R.; Meyer, O. *Proc. Natl. Acad. Sci. U. S. A.* **2004**, *101*, 446–451.

(5) Doukov, T. I.; Iverson, T. M.; Seravalli, J.; Ragsdale, S. W.; Drennan, C. L. *Science* **2002**, *298*, 567–572.

(6) Volbeda, A.; Charon, M. H.; Piras, C.; Hatchikian, E. C.; Frey, M.; Fontecilla-Camps, J. C. *Nature* **1995**, *373*, 580–587.

(7) Higuchi, Y.; Ogata, H.; Miki, K.; Yasuoka, N.; Yagi, T. *Structure* **1999**, *7*, 549–556.

(8) Kieber-Emmons, M. T.; Riordan, C. G. *Acc. Chem. Res.* **2007**, *40*, 618–625.

(9) Neupane, K. P.; Shearer, J. *Inorg. Chem.* **2006**, *45*, 10552–10566.

(10) Wuerges, J.; Lee, J. W.; Yim, Y. I.; Yim, H. S.; Kang, S.-O.; Djinovic Carugo, K. *Proc. Natl. Acad. Sci. U. S. A.* **2004**, *101*, 8569–8574.

(11) Kruger, H. J.; Peng, G.; Holm, R. H. *Inorg. Chem.* **1991**, *30*, 734–742.

(12) Stenson, P. A.; Board, A.; Marin-Becerra, A.; Blake, A. J.; Davies, E. S.; Wilson, C.; McMaster, J.; Schröder, M. *Chemistry* **2008**, *14*, 2564–2576.

(13) Shearer, J.; Zhao, N. *Inorg. Chem.* **2006**, *45*, 9637–9639.

(14) Silva, J. J. R. F. D; Williams, R. J. P. *The Biological Chemistry of the Elements*, 2nd ed.; Oxford University Press: Oxford, 2001.

(15) Fenton, D. E. *Biocoordination Chemistry*; Oxford Chemistry Primers: Oxford, 1995.

(16) Maroney, M. J. *Curr. Opin. Chem. Biol.* **1999**, *3*, 188–199.

(17) Kumar, D. N.; Garg, B. S. *Spectrochim. Acta - Part A Mol. Biomol. Spectrosc.* **2006**, *64*, 141–147.

(18) Ghosh, P.; Begum, A.; Bill, E.; Weyhermüller, T.; Wieghardt, K. *Inorg. Chem.* **2003**, *42*, 3208–3215.

(19) Barondeau, D.; Kassman, C.; Bruns, C.; Tainer, J.; Getzoff, E. *Protein*

Sci. **2004**, *13*, 192–192.

(20) Herbst, R. W.; Guce, A.; Bryngelson, P. A.; Higgins, K. A.; Ryan, K. C.; Cabelli, D. E.; Garman, S. C.; Maroney, M. J. *Biochemistry* **2009**, *48*, 3354–3369.

(21) Shearer, J.; Dehestani, A.; Abanda, F. *Inorg. Chem.* **2008**, *47*, 2649–2660.

(22) Stenson, P. Transition Metal Thiolate Complexes: Modelling the Active Sites of Sulfur-Ligated Metalloenzymes, The University of Nottingham, 2005.

(23) Franks, M. Transition Metal Complexes Containing Phenylthiolate and Phenolate Ligands, University of Nottingham, 2011.

(24) Franks, M.; Gadzhieva, A.; Ghandhi, L.; Murrell, D.; Blake, A. J.; Davies, E. S.; Lewis, W.; Moro, F.; McMaster, J.; Schröder, M. *Inorg. Chem.* **2013**, *52*, 660–670.

(25) Doering, W. E.; Weil, R. A. N. *J. Am. Chem. Soc.* **1947**, *69*, 2461–2466.

(26) Gerli, A.; Sabat, M.; Marzilli, L. G. *J. Am. Chem. Soc.* **1992**, *114*, 6711–6718.

(27) Walker, P. S.; Bergin, P. M.; Grossel, M. C.; Horton, P. N. *Inorg. Chem.* **2004**, *43*, 4145–4153.

(28) Nanjappan, P.; Raju, N.; Ramalingam, K.; Nowotnik, D. P. *Tetrahedron* **1994**, *50*, 8617–8632.

(29) Matziari, M.; Bauer, K.; Dive, V.; Yiotakis, A. *J. Org. Chem.* **2008**, *73*, 8591–8593.

(30) Jacobson, K. A.; Gao, Z.; Tchilibon, S.; Duong, H. T.; Joshi, B. V; Sonin, D. *Society* **2005**, *48*, 24–28.

(31) Clayden, Jonathon; Greeves, Nick; Warren, Stuart; Wothers, P. *Organic Chemistry*, 5th ed.; Oxford University Press, 2006.

(32) Keller, P. C.; Knapp, K. K.; Rund, J. V. *Inorg. Chem.* **1985**, *24*, 2382–2383.

(33) Gautier, F.-M.; Jones, S.; Martin, S. J. *Org. Biomol. Chem.* **2009**, *7*, 229–231.

(34) T. W. Green and P. G. M. Wuts; *Protective Groups in Organic Synthesis, Wiley-Interscience*; Wiley-Interscience: New York, 1999.

(35) Isidro-llobet, A.; Mercedes, A, Fernando, A. *Chem. Rev.* **2009**, No. 109, 2455–2504.

(36) Caddick, S.; Judd, D. B.; Lewis, A. K. d. K.; Reich, M. T.; Williams, M. R. . *Tetrahedron* **2003**, *59*, 5417–5423.

(37) Mitsudera, Hiromasa; Otaka, Ken; Fujiwara, J. Preparation of [(pyrazolyl, isoxazolyl, oxazolyl, oxadiazolyl, or thiadiazolyl)methyl] malononitrile derivatives as pesticides. WO 2005068432, 2005.

(38) Altenburger, J. M.; Lassalle, G. Y.; Matrougui, M.; Galtier, D.; Jetha, J. C.; Bocskei, Z.; Berry, C. N.; Lunven, C.; Lorrain, J.; Herault, J. P.; Schaeffer, P.; O'Connor, S. E.; Herbert, J.-M. *Bioorg. Med. Chem.* **2004**, *12*, 1713–1730.

(39) Peng, H.; Carrico, D.; Thai, V.; Blaskovich, M.; Bucher, C.; Pusateri, E. E.; Sebti, S. M.; Hamilton, A. D. *Org. Biomol. Chem.* **2006**, *4*, 1768–1784.

(40) Chetsanga, C. J. J.; Makaroff, C. *Chem. Biol. Interact.* **1982**, *41*, 235–249.

(41) Dawson, J. Active Models of [NiFe] Hydrogenase Incoporating Functional Proton Relays, The University of Nottingham, 2010.

(42) Board, A. Redox Active Ligands and their Transition Metal Complexes, Univeristy of Nottingham, 2008.

(43) Benisvy, L.; Kannappan, R.; Song, Y. F.; Milikisyants, S.; Huber, M.; Mutikainen, I.; Turpeinen, U.; Gamez, P.; Bernasconi, L.; Baerends, E. J.; Hartl, F.; Reedijk, J. *Eur. J. Inorg. Chem.* **2007**, *2007*, 637–642.

(44) Glaser, T.; Heidemeier, M.; Fröhlich, R.; Hildebrandt, P.; Bothe, E.; Bill, E. *Inorg. Chem.* **2005**, *44*, 5467–5482.

(45) Orio, M.; Philouze, C.; Jarjayes, O.; Neese, F.; Thomas, F. *Inorg. Chem.* **2010**, *49*, 646–658.

(46) Shimazaki, Y.; Yajima, T.; Tani, F.; Karasawa, S.; Fukui, K.; Naruta, Y.; Yamauchi, O. *J. Am. Chem. Soc.* **2007**, *129*, 2559–2568.

(47) Fleischer, E. B.; Stone, A. L.; Dewar, R. B. K.; Wright, J. D.; Keller, C. E.; Pettit, R. *J. Am. Chem. Soc.* **1966**, *88*, 3158–3159.

(48) Komen, C. M. D.; Bickelhaupt, F. *Synth. Commun.* **1996**, *26*, 1693–1697.

(49) Block, E.; Eswarakrishnan, V.; Gernon, M.; Ofori-Okai, G.; Saha, C.; Tang, K.; Zubieta, J. *J. Am. Chem. Soc.* **1989**, *111*, 658–665.

(50) Figuly, G. D.; Loop, C. K.; Martin, J. C. *J. Am. Chem. Soc.* **1989**, *111*, 654–658.

(51) M. K. Taylor, J. Reglinski and D. Wallace, *Acta Crystallogr., Sect. E: Struct. Rep. Online*, **2004**, 60, M850-M851.

(52) Frydendahl, H.; Toftlund, H.; Becher, J.; Dutton, J. C.; Murray, K. S.; Taylor, L. F.; Anderson, O. P.; Tiekink, E. R. T. *Inorg. Chem.* **1995**, *34*, 4467–4476.

(53) Christensen, A.; Jensen, H. S.; McKee, V.; McKenzie, C. J.; Munch, M.

Inorg. Chem. **1997**, *36*, 6080–6085.

Chapter 4: Synthesis and Characterisation of Schiff-Base Zn(II) and Cu(II)-Diphenolate Complexes

4.1 Introduction

Galactose oxidase (GAO)[1–3] is an extracellular Cu(II) containing fungal enzyme that belongs to a group of metalloenzymes that include an organic radical as an integral component of their active site.[4] X-ray crystallography shows that the active site of the active form of GAO is composed of a mononuclear Cu centre in a distorted N_2O_3 square-based pyramidal coordination geometry (Figure 4.1).[1,5,6] Two histidine imidazole donors (His496 and His581), a tyrosine phenolate (Tyr272), and an acetate ion (at the substrate binding position) are located within the equatorial plane, while a second tyrosine phenolate (Tyr495) resides in the axial position (Cu-O = 2.7 Å).[4,6–8] The active site of GAO is responsible for a two-electron oxidation of a broad range of primary alcohols to form the corresponding aldehydes, which is coupled to the reduction of molecular oxygen to form hydrogen peroxide. Considerable progress has been made in the development of chemical analogues of the active site of GAO, including several examples of complexes that contain Cu(II) bound to a phenoxyl radical.[9,10]

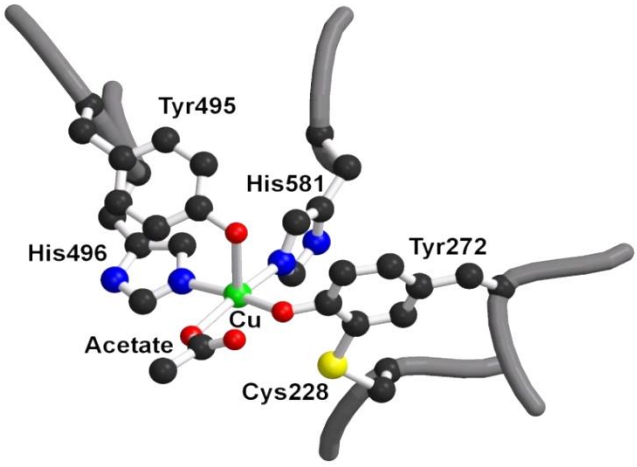


Figure 4.1 (Figure 1.13) The X-ray crystal structure of GAO an extracellular enzyme secreted by the fungus *Dactylium dendroides.*[1]

4.1.2 Previous Work

Benisvy *et al*. reported the synthesis and study of a range of Cu(II) complexes formed from the *N*,*O*-bidentate, Schiff-base phenol-imidazole pro-ligands (Figure 4.2).[9–13] The Cu(II) complexes, [Cu(^{t}BuL$_o^1$)$_2$] (H^{t}BuL$_o^1$ = 2-(4,6-di-*tert*-butylhydroxyphenyl)-4,5-diphenylimidazole)[11,13], [Cu(^{t}BuL$_o^2$)$_2$] (^{t}BuL$_o^2$ = 4,5-di-*p*-methoxyphenylimidazole)[12] and [Cu(^{t}BuL$_o^3$)$_2$] (H ^{t}BuL$_o^3$ = 2-(4,6-di-*tert*-butylydroxyphenyl)benzimidazole)[12], contain CuN_2O_2 centres in distorted square planar coordination geometries. X-band EPR spectra of [Cu(^{t}BuL$_o^1$)$_2$], [Cu(^{t}BuL$_o^2$)$_2$] and [Cu(^{t}BuL$_o^3$)$_2$] in CH_2Cl_2-DMF (9:1) solution at 77 K are typical of d^9 Cu(II) complexes possessing a $(d_{x^2-y^2})^1$ ground state (S = 1/2) with $g_{zz} > g_{yy} \approx g_{xx}$. Electrochemical studies have shown that [Cu(^{t}BuL$_o^1$)$_2$], [Cu(^{t}BuL$_o^2$)$_2$] and [Cu(^{t}BuL$_o^3$)$_2$] possess two reversible one-electron oxidation processes in the region 0.11 – 0.58 V *vs* Fc^+/Fc that are consistent with each process being ligand-based. The UV/vis spectra of the mono cations, [Cu(^{t}BuL$_o^1$)$_2$]$^+$, [Cu(^{t}BuL$_o^2$)$_2$]$^+$ and [Cu(^{t}BuL$_o^3$)$_2$]$^+$, exhibit an intense absorption

feature at *ca.* 410 nm and a less intense, broad absorption between 500 and 900 nm that are assigned to the π-π^* transitions of the coordinated phenoxyl radical ligand. All of the Cu(II)-mono-phenoxyl radical complexes are essentially EPR silent as a result of the antiferromagnetic coupling between the S = 1/2 Cu(II) centre and the S = 1/2 coordinated radical ligand. The nature of $[Cu(^tBuL_o^{1\bullet})(^tBuL_o^1)]^+$ has also been confirmed by X-ray crystallographic studies of $[Cu(^tBuL_o^1)_2][BF_4]$, which identified the cation as one phenoxyl radical and one phenoxide ligand coordinated to a Cu(II) centre.[12,13]

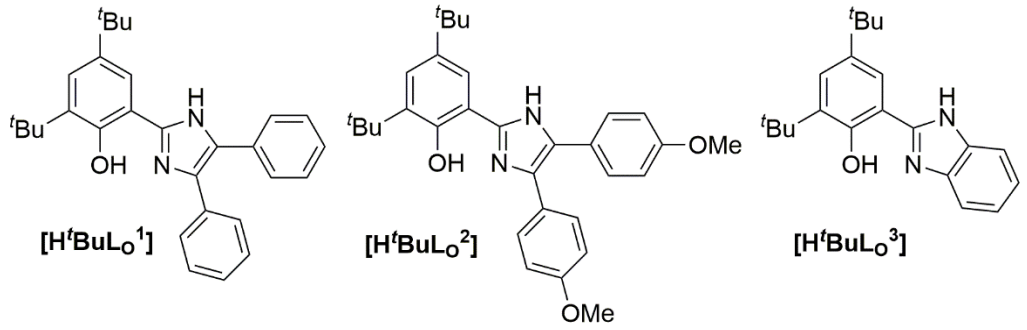


Figure 4.2 *N,O*-bidentate, Schiff-base phenol-imidazole pro-ligands reported by Benvisy *et al.*[11–13]

Franks *et al.*[14] used the ligands derived from $[H_2{}^tBuL_O^{Py2}]$ and $[H_2{}^tBuL_O^{Py2}]$ bind to Cu(II) to afford four coordinate approximate square planar complexes ($[Cu(^tBuL_O^{Py1})]$ and $[Cu(^tBuL_O^{Py2})]$, Figure 4.3). Investigations of the electrochemical properties of $[Cu(^tBuL_O^{Py1})]$ and $[Cu(^tBuL_O^{Py2})]$ in CH_2Cl_2 by cyclic voltammetry show that these complexes support two oxidation processes between 0.45 V and 0.69 V *vs* Fc^+/Fc. Investigation of the first oxidation process of $[Cu(^tBuL_O^{Py1})]$ and $[Cu(^tBuL_O^{Py2})]$ using UV/vis spectroelectrochemistry showed that the species generated by oxidation were unstable under the conditions of the experiment. The chemical irreversibility of the first oxidation

process of [Cu(^{t}BuL$_O^{Py1}$)] and [Cu(^{t}BuL$_O^{Py2}$)] restricted further characterisation of the products formed upon oxidation. However, comparison with previously reported Schiff-base Cu(II) diphenolate complexes (discussed above), together with the potentials at which the oxidation processes of [Cu(^{t}BuL$_O^{Py1}$)] and [Cu(^{t}BuL$_O^{Py2}$)] occur, suggests that the observed redox behaviour is localised on the ligand framework, and is associated with the formation of phenoxyl radical ligands.[11,15,16]

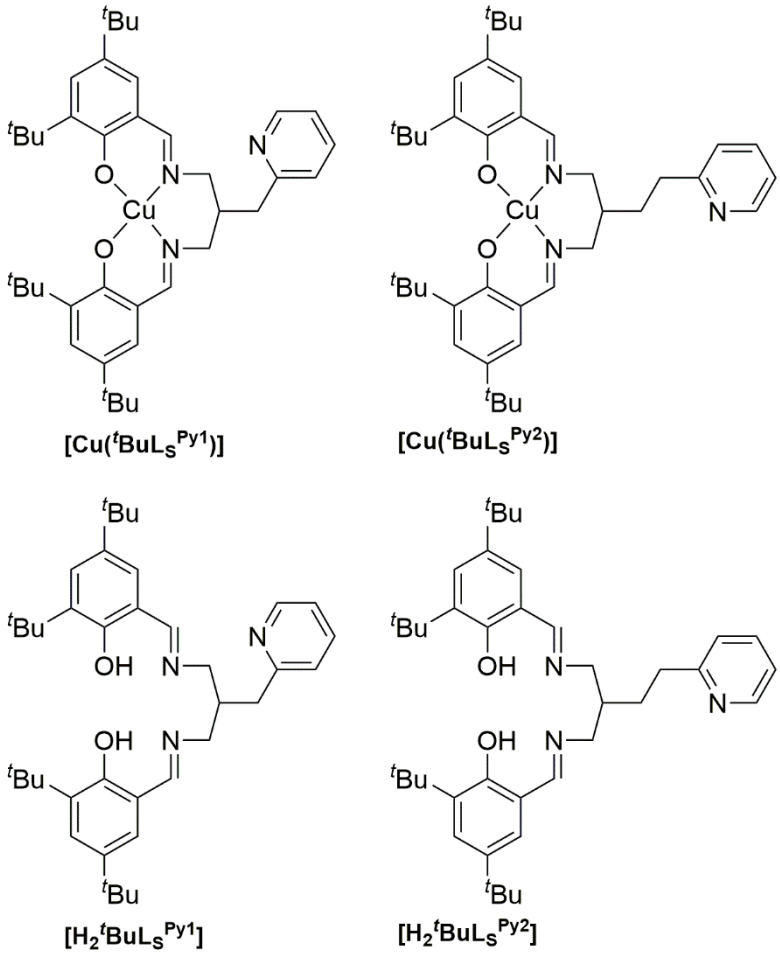


Figure 4.3 Schematic representation of the Cu(II) Schiff-base diphenolate complexes synthesised from the pro-ligands [H$_2$^{t}BuL$_O^{Py1}$] and [H$_2$^{t}BuL$_O^{Py2}$].[14]

4.1.3 Aims

The aims of this chapter are to extend our knowledge of the redox chemistry of transition metal Schiff-base diphenolate complexes through the preparation of a range of Zn(II) and Cu(II) Schiff-base diphenolate complexes that incorporate tetradentate (N_2O_2) ligands.

This chapter will use the ligand framework discussed previously in Chapter 3, [$H_2{}^tBuL_O{}^{OH}$] in order to attempt to synthesise [Zn($^tBuL_O{}^{OH}$)] and [Cu($^tBuL_O{}^{OH}$)] as precursors to [Zn($^tBuL_O{}^{R}$)] and [Cu($^tBuL_O{}^{R}$)] (R = Ph, PyN, Fu, Pyr and Imid) (Figure 4.4). These complexes contain a pendant phenyl (Ph), pyridine (PyN), furan (Fu), pyrrole (Pyr) or imidazole (Imid) group introduced into the metal complex framework to investigate the impact of a fifth donor atom in controlling the redox properties of the Zn(II) and Cu(II) complexes. Since Zn(II) is usually not redox active over the range of potentials used in the electrochemical experiments (-1.60 – 1.70 V *vs* Fc^+/Fc), electrochemical studies on [Zn($^tBuL_O{}^{R}$)] could offer insight into the redox processes associated with the ligand which in turn may offer further insight into the electrochemical behaviour of [Cu($^tBuL_O{}^{R}$)] and [Ni($^tBuL_O{}^{R}$)] (R = Ph, PyN, Fu, Pyr and Imid).

The properties of [Zn($^tBuL_O{}^{OH}$)], [Cu($^tBuL_O{}^{OH}$)], [Zn($^tBuL_O{}^{R}$)] and [Cu($^tBuL_O{}^{R}$)] will be probed using a combination of electrochemical and EPR spectroscopic methods to provide insight into the relative stabilities of the oxidized species and how these vary with the nature of the groups pendant to the ligand framework.

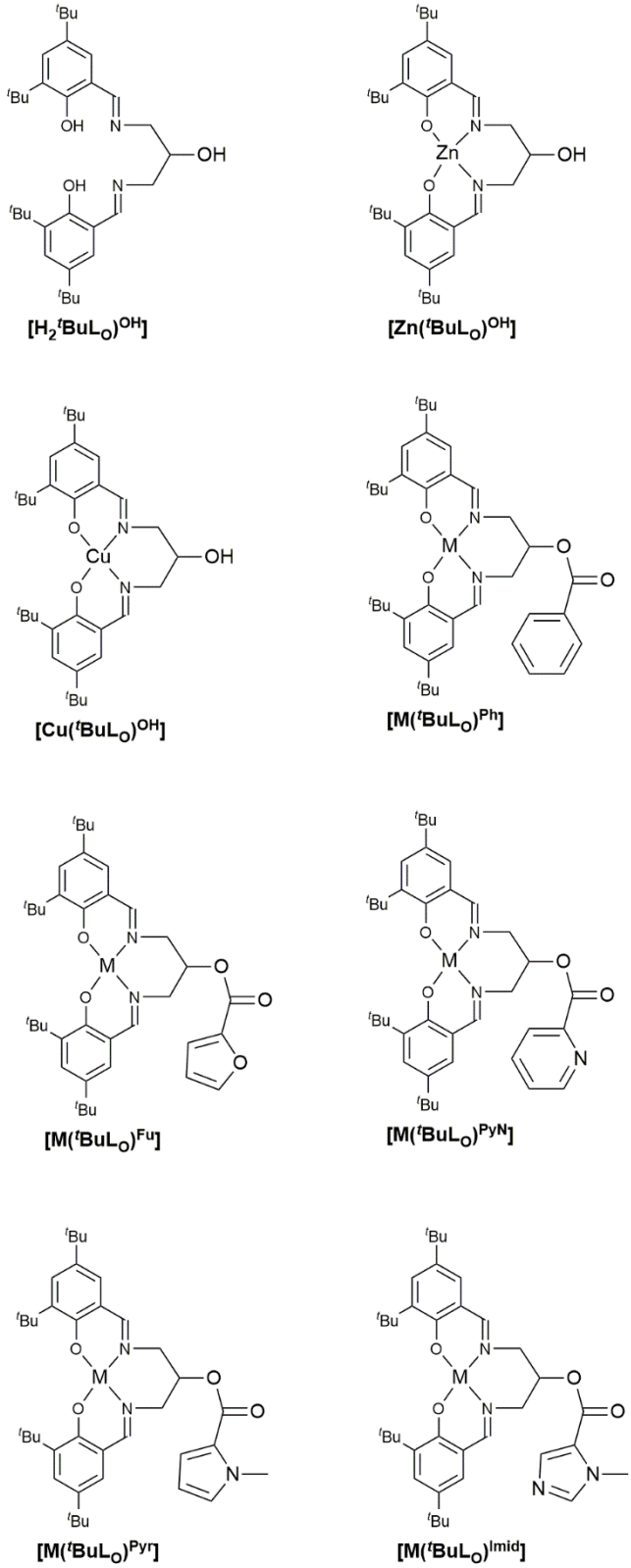
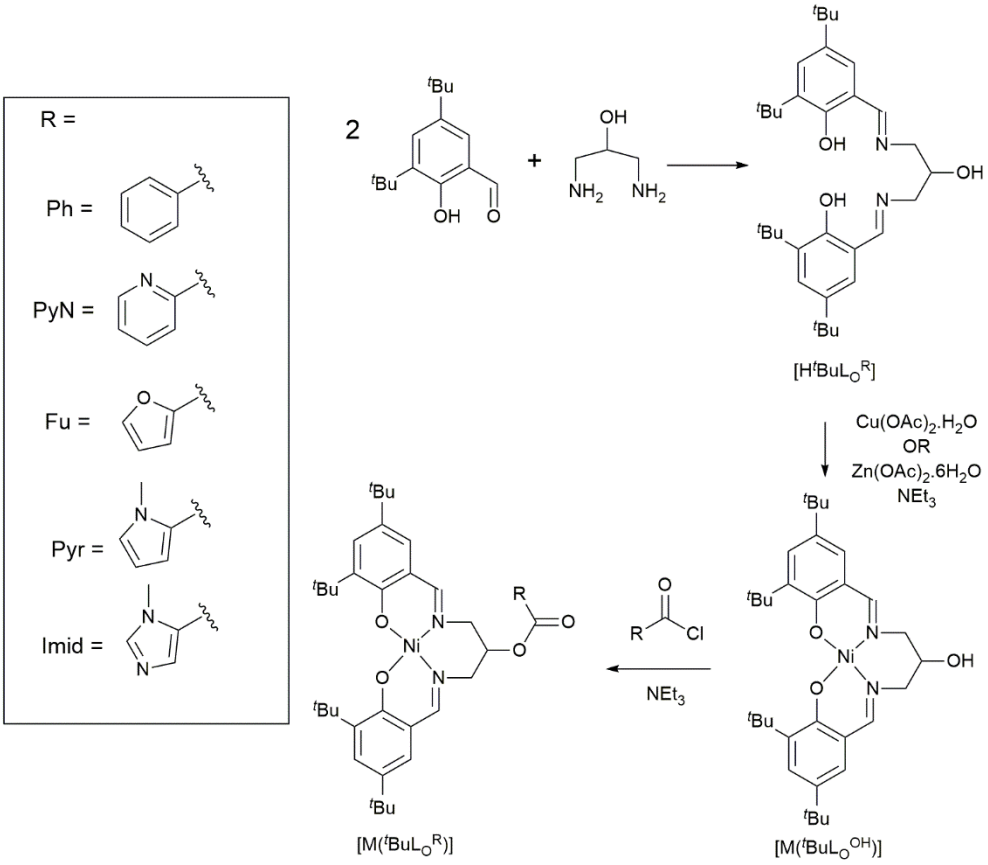


Figure 4.4 Schematic representation of the Zn(II) and Cu(II) Schiff-base diphenolate complexes discussed in this chapter (M = Zn(II) or Cu(II)).

4.2 Results and Discussion

4.2.1 Proposed syntheses of [$H_2{}^tBuL_O{}^{OH}$] and [M($^tBuL_O{}^R$)] (M = Cu(II) and Zn(II) and R = Ph, PyN, Fu, Pyr and Imid)



Scheme 4.1 Syntheses of [$H_2{}^tBuL_O{}^{OH}$], [M($^tBuL_O{}^{OH}$)] and [M($^tBuL_O{}^R$)] (M = Cu(II) and Zn(II), R = Ph, PyN, Fu, Pyr and Imid)

The synthesis of [$H_2{}^tBuL_O{}^{OH}$] was achieved by the Schiff-base condensation reaction between di-*tert*-butyl-2-hydroxybenzaldehyde and 1,3-diaminopropan-2-ol in methanol, as discussed in Chapter 3, Section 3.2.8. The product was isolated as a crude viscous yellow oil in an overall yield of 95%.

The syntheses of [Zn($^tBuL_O{}^{OH}$)] and [Cu($^tBuL_O{}^{OH}$)] involved the addition of a solution of zinc(II) acetate or copper(II) acetate in methanol to a

solution of the pro-ligand, [$H_2{}^tBuL_O{}^{OH}$] in dichloromethane followed by the heating of the reaction mixture to reflux for 24 hours. The crude products were isolated as yellow or dark green powders, respectively. The [Zn($^tBuL_O{}^{OH}$)] or [Cu($^tBuL_O{}^{OH}$)] complexes were purified via column chromatography on silica gel using dichloromethane and pentane (3:2 v/v) as eluent with an overall yield of 96 % and 95 %, respectively.

Attempts were then made to functionalise the hydroxyl moiety of [Zn($^tBuL_O{}^{OH}$)] and [Cu($^tBuL_O{}^{OH}$)] using a range of acid chloride starting materials. The reaction between [Zn($^tBuL_O{}^{OH}$)] and [Cu($^tBuL_O{}^{OH}$)] and the acid chlorides were attempted in anhydrous conditions under an Ar atmosphere. Each reaction mixture was stirred for 24 hours at room temperature and attempts were made to purify the products by column chromatography on silica gel using dichloromethane and pentane (3:2 v/v) as eluent. However, only [Cu($^tBuL_O{}^{Ph}$)], [Cu($^tBuL_O{}^{PyN}$)], [Cu($^tBuL_O{}^{Fu}$)], [Cu($^tBuL_O{}^{Pyr}$)], and [Cu($^tBuL_O{}^{Imid}$)] could be isolated following recrystallization from the column fractions in overall yields of Cu($^tBuL_O{}^{Ph}$)] 45%, [Cu($^tBuL_O{}^{PyN}$)] 36%, [Cu($^tBuL_O{}^{Fu}$)] 42%, [Cu($^tBuL_O{}^{Pyr}$)] 41% and [Cu($^tBuL_O{}^{Imid}$)] 43%. Attempts to purify the products of the reactions involving [Zn($^tBuL_O{}^{OH}$)] by column chromatography on silica gel using dichloromethane and pentane (3:2 v/v) as eluent were unsuccessful.

4.2.2 X-ray Crystallography of [Cu(^{t}BuL$_S^{OH}$)]

The molecular structure of [Cu(^{t}BuL$_O^{OH}$)] is shown in Figure 4.5 and selected bond lengths and angles are listed in Table 4.1. Details of the structure solution and refinement are provided in Appendix 2. Attempts to grow crystals of [Zn(^{t}BuL$_O^R$)] (R = OH, Ph, PyN, Fu, Pyr and Imid) and [Cu(^{t}BuL$_O^R$)] (R = Ph, PyN, Fu, Pyr and Imid) appeared to be successful, however, the crystals only diffracted weakly and data of sufficient quality could not be collected for them.

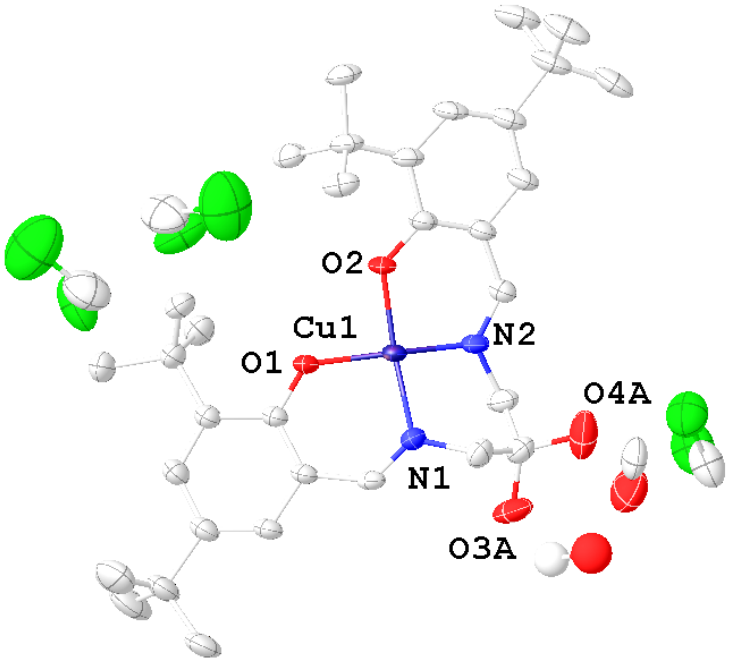


Figure 4.5 View of the X-ray crystal structure of [Cu(^{t}BuL$_S^{OH}$)]·(CH$_2$Cl$_2$)$_3$(CH$_3$OH)$_3$ with H atoms omitted for clarity.

Table 4.1 Selected bond lengths (Å) and angles (°) with e.s.d.s for $[Cu(^{t}BuL_{S}^{OH})]\cdot(CH_2Cl_2)_3(CH_3OH)_3$.

$[Cu(^{t}BuL_{O}^{OH})]$	**Bond lengths / Å**	**$[Cu(^{t}BuL_{O}^{OH})]$**	**Bond angles / °**
Cu(1)-N(1)	1.946(3)	N(1)-Cu(1)-N(2)	91.81(12)
Cu(1)-N(2)	1.936(3)	N(1)- Cu (1)-O(1)	93.85(12)
Cu(1)-O(1)	1.895(3)	N(2)- Cu (1)-O(1)	157.42(14)
Cu(1)-O(2)	1.896(2)	N(1)- Cu (1)-O(2)	156.95(14)
N(1)-C(1)	1.279(5)	N(2)- Cu (1)-O(2)	94.26(12)
N(1)-C(3)	1.467(5)	O(1)- Cu (1)-O(2)	89.02(11)
N(2)-C(2)	1.285(5)	-	-
N(2)-C(4)	1.466(5)	-	-
O(1)-C(16)	1.302(4)	-	-
O(2)-C(15)	1.301(5)	-	-

$[Cu(^{t}BuL_{O}^{OH})]$ contains a monomeric Cu(II) centre coordinated by a N_2O_2 ligand set consisting of two phenolate O-donors and two imine N-donors arranged in a *cis*-conformation with respect to one another. The bond angles (Table 4.1) and the dihedral angle of 32.33º between the N(1)-Cu(1)-N(2) and O(1)-Cu(1)-O(2) planes show that $[Cu(^{t}BuL_{O}^{OH})]$ adopts a distorted square planar coordination geometry. The Cu(II)-O(phenolate) (*ca.* 1.90 Å) and Cu(II)-N(imine) (*ca.* 1.95 Å) bond distances are comparable to those previously reported by Franks *et al.* for $[Cu(^{t}BuL_{O}^{Py1})]$[17] and to those reported for $[CuCu(L)_2]$,[11] $[Cu(^{Bz}L)_2]$ and $[Cu(^{PhOMe}L)_2]$[12,13]: (Cu(II)-O(phenolate) (*ca.* 1.91 Å) and Cu(II)-N(imine) (*ca.* 1.97 Å)).

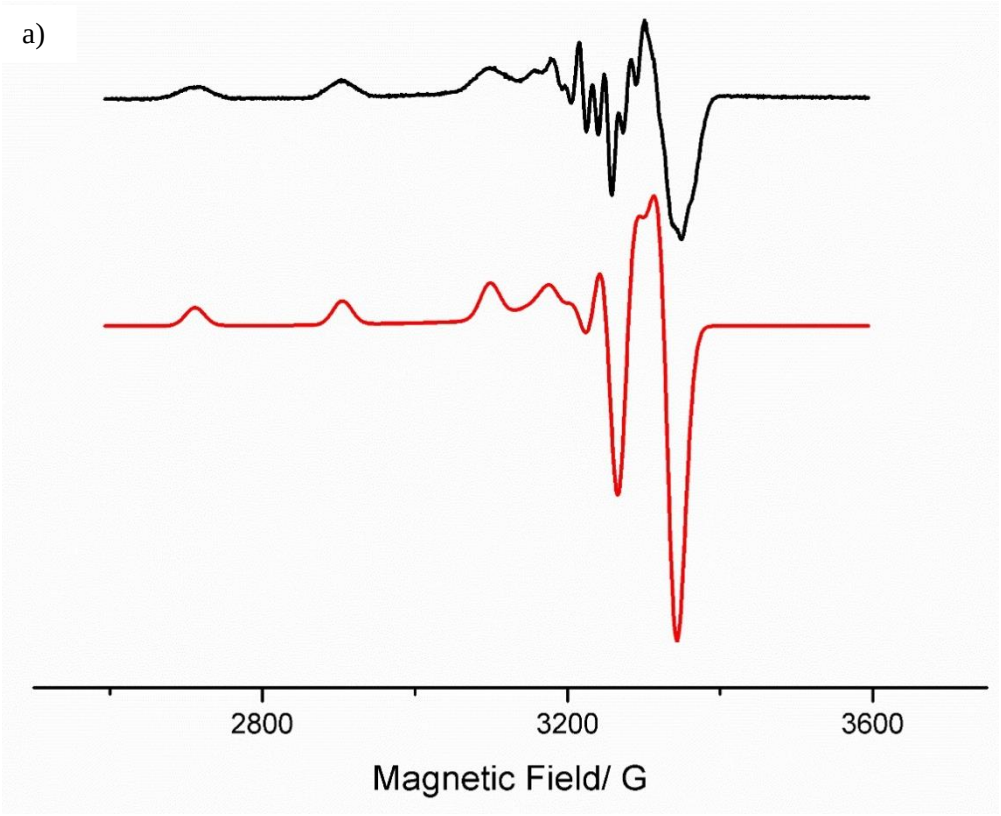
For $[Cu(^{t}BuL_{O}^{OH})]$, the Cu(II)-O(phenolate) (*ca.* 1.90 Å) and Cu(II)-N(imine) (*ca.* 1.95 Å) bond distances are longer than those for $[Ni(^{t}BuL_{O}^{OH})]$ and $[Ni(^{t}BuL_{O}^{Ph})]$ (see Chapter 3) [Ni(II)-O(phenolate) (*ca.* 1.82 – 1.86 Å) and Ni(II)-N(imine) (*ca.* 1.84 – 1.87 Å)]. $[Cu(^{t}BuL_{O}^{OH})]$ also possesses a larger dihedral angle between the planes defined by N(1)-Cu(1)-N(2) and O(1)-Cu(1)-O(2) (32.33º) relative to the dihedral angle between the equivalent planes in

[Ni(^{t}BuL$_{O}^{OH}$)] 20.92^{o} and [Ni(^{t}BuL$_{O}^{Ph}$)] 22.53^{o}, respectively. Thus, [Cu(^{t}BuL$_{O}^{OH}$)] shows a greater deviation away from a square planar geometry towards a tetrahedral geometry.

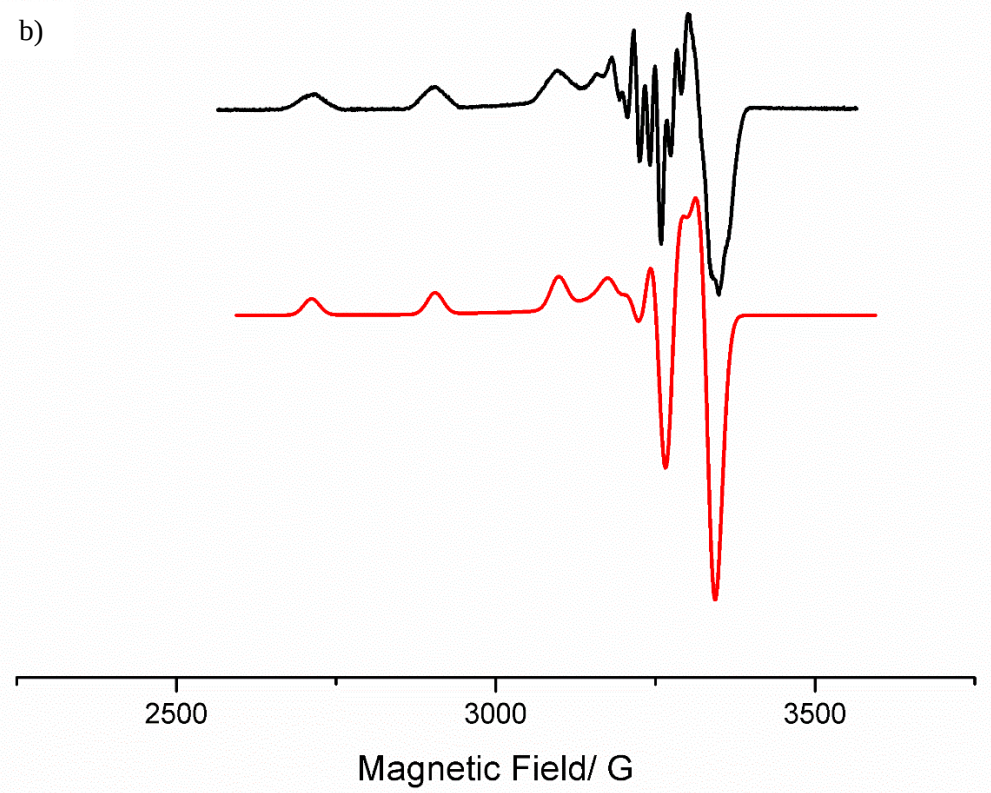
4.2.3 EPR of [Cu(^{t}BuL$_O^R$)] (R = OH, Ph, PyN, Fu, Pyr and Imid)

The X-band EPR spectra of frozen CH_2Cl_2 solutions of [Cu(^{t}BuL$_O^R$)] (R = OH, Ph, PyN, Fu, Pyr, and Imid) containing 0.4 M [N^{n}Bu$_4$][BF$_4$] were recorded at 77 K. The experimental frozen solution X-band EPR spectra of [Cu(^{t}BuL$_O^R$)] (R = OH, Ph, PyN, Fu, Pyr, and Imid) are shown in Figure 4.6 and together with the simulated EPR spectrum of [Cu(^{t}BuL$_O^{OH}$)]. The Cu(II) diphenolate complexes, [Cu(^{t}BuL$_O^R$)] (R = OH, Ph, PyN, Fu, Pyr, and Imid), possess almost identical EPR spectra and are typical of Cu(II) complexes possessing a $(d_{x^2-y^2})^1$ or $(d_{xy})^1$ ground state (S = ½) with $g_{zz} > g_{xx} \approx g_{yy}$.[15] The similarity of the EPR spectra of [Cu(^{t}BuL$_O^R$)] (R = OH, Ph, PyN, Fu, Pyr, and Imid) suggests that the functional group pendant to the backbone of the ligand does not impact the electronic structure of the Cu(II) centre and most likely does not coordinate to the metal in [Cu(^{t}BuL$_O^R$)]. The EPR spectra of [Cu(^{t}BuL$_O^R$)] (R = OH, Ph, PyN, Fu, Pyr, and Imid) display hyperfine and superhyperfine features in the g_{zz} and g_{xx}/g_{yy} regions, respectively, that result from the interaction of the unpaired electron with the nuclear spin of Cu(II) (I = 3/2) and with the nuclear spin of two coordinated ^{14}N atoms (I = 1), respectively. The EPR spectrum of [Cu(^{t}BuL$_O^R$)] (R = OH) may be simulated with the following approximate spin Hamiltonian parameters: g_{xx} = 2.037, g_{yy} = 2.050, g_{zz} = 2.220; $A_{xx}\{^{63,65}Cu\}$ = 21 G, $A_{yy}\{^{63,65}Cu\}$ = 32 G, $A_{zz}\{^{63,65}Cu\}$ = 193 G, and $a_{xx}\{^{14}N\} = a_{yy}\{^{14}N\}$ = 16 G. These parameters are typical of previously reported Cu (II) complexes in an N_2O_2 tetragonal coordination geometry. For example [Cu(^{t}BuL$_O^{Py1}$)]:[14] g_{xx} = 2.038, g_{yy} = 2.050, g_{zz} = 2.210; $A_{xx}\{^{63,65}Cu\}$ = 20 G, $A_{yy}\{^{63,65}Cu\}$ = 32 G, $A_{zz}\{^{63,65}Cu\}$ = 193 G, and $a_{xx}\{^{14}N\} = a_{yy}\{^{14}N\}$ = 16 G; and [Cu(^{t}BuL$_O^{Py2}$)]: g_{xx} = 2.038, g_{yy} = 2.050, g_{zz} =

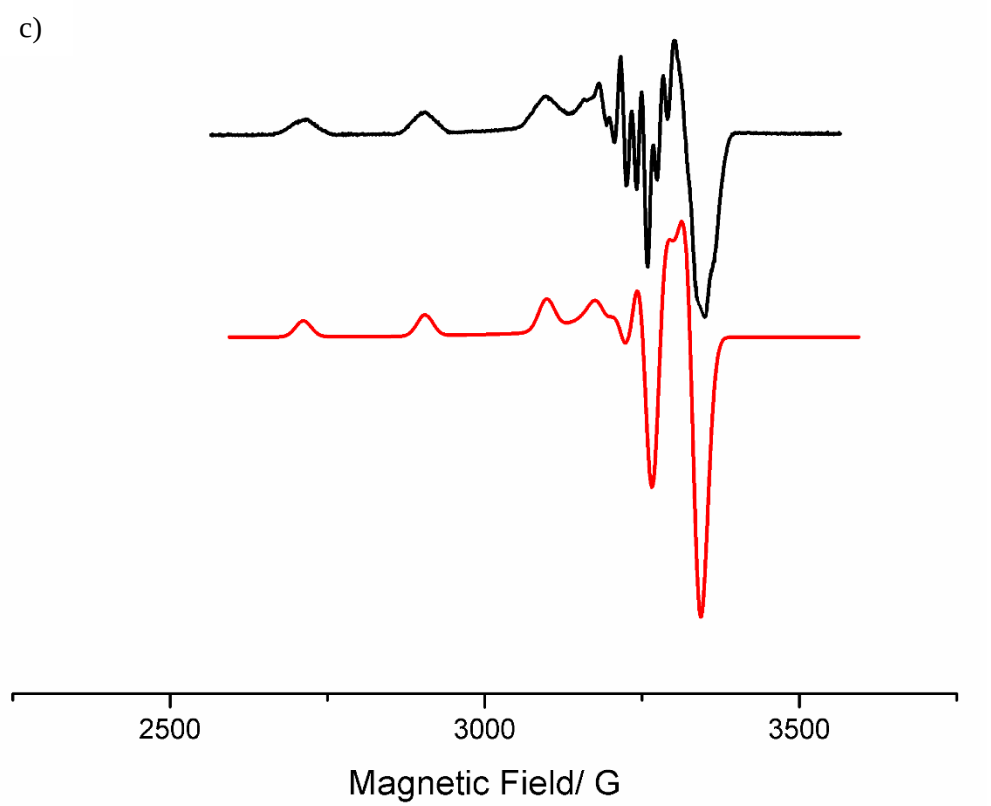
2.211; $A_{xx}\{^{63,65}Cu\}$ = 20 G, $A_{yy}\{^{63,65}Cu\}$ = 32 G, $A_{zz}\{^{63,65}Cu\}$ = 192 G, and $a_{xx}\{^{14}N\} = a_{yy}\{^{14}N\}$ = 16 G.



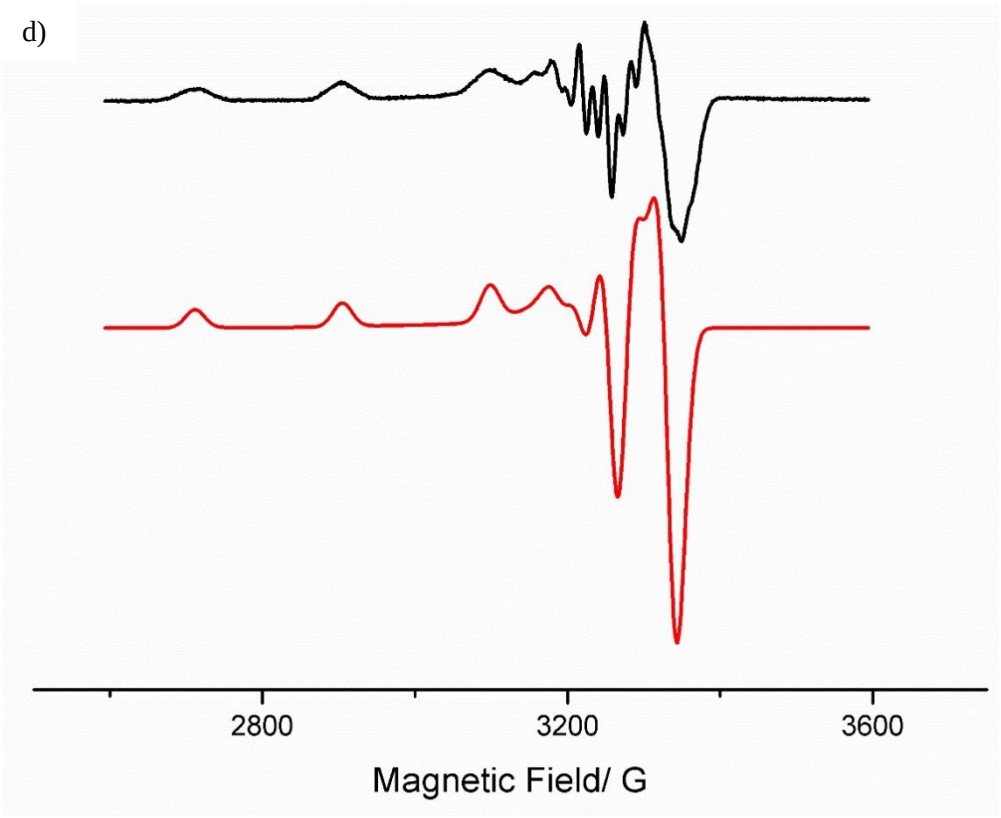
b)


2500
3000
3500
Magnetic Field/ G

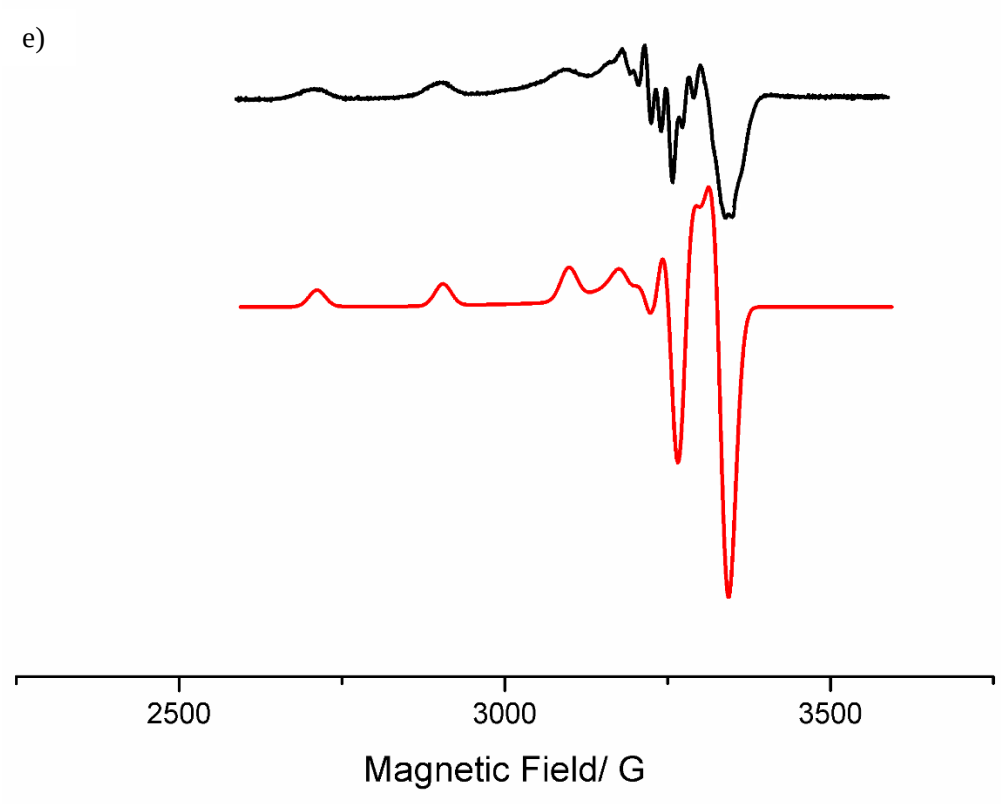
c)


2500
3000
3500
Magnetic Field/ G

d)


2800
3200
3600
Magnetic Field/ G

e)


2500
3000
3500
Magnetic Field/ G

f)

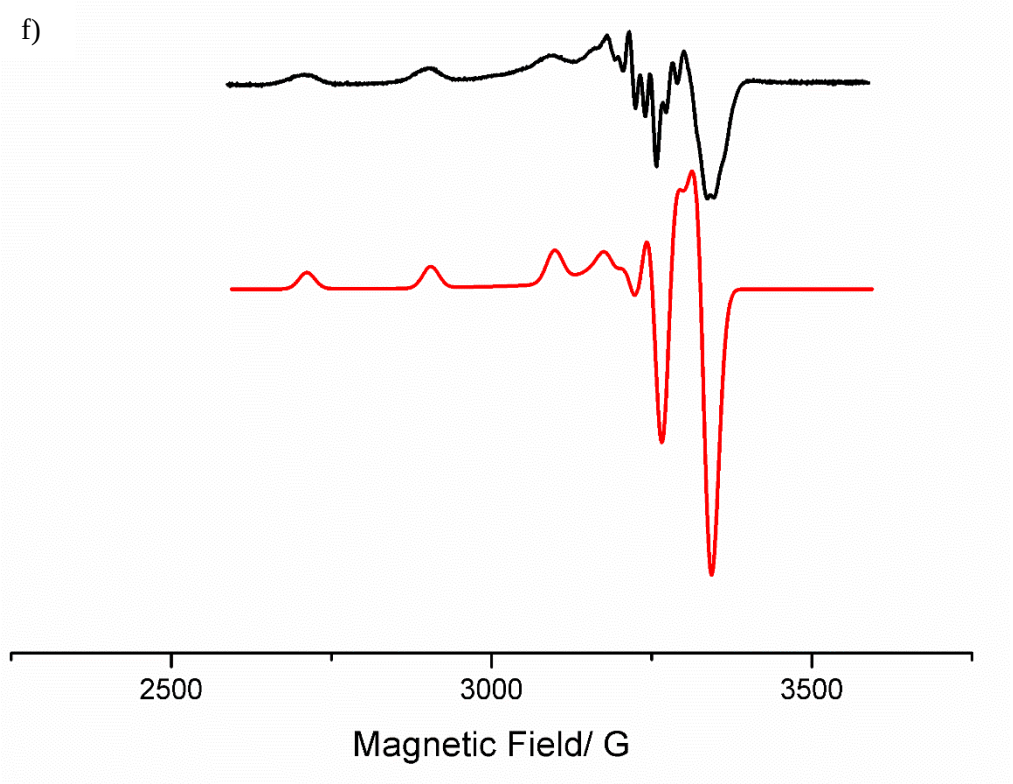


Figure 4.6 The frozen solution EPR spectrum of (a) [Cu(^{t}BuL$_O^{OH}$)] (b) [Cu(^{t}BuL$_O^{Ph}$)] (c) [Cu(^{t}BuL$_O^{PyN}$)] (d) [Cu(^{t}BuL$_O^{Fu}$)] (e) [Cu(^{t}BuL$_O^{Pyr}$)] (f) [Cu(^{t}BuL$_O^{Imid}$)] in CH_2Cl_2 containing 0.4 M [N^{n}Bu$_4$][BF$_4$] at 77 K (black), simulated spectrum of [Cu(^{t}BuL$_O^{OH}$)] (red).

4.2.4 Electrochemical Studies of [Zn(^{t}BuL$_O^{OH}$)], [Cu(^{t}BuL$_O^{OH}$)], and [Cu(^{t}BuL$_O^R$)] and R = OH, Ph, PyN, Fu, Pyr and Imid)

The cyclic voltammograms of [Zn(^{t}BuL$_O^{OH}$)] and [Cu(^{t}BuL$_O^R$)] (R = OH, Ph, PyN, Fu, Pyr and Imid**)** in CH_2Cl_2 solutions (1 mM) containing 0.4 M [N^{n}Bu$_4$][BF$_4$] as supporting electrolyte were recorded at 293K under Ar. [Zn(^{t}BuL$_O^{OH}$)] and [Cu(^{t}BuL$_O^R$)] (R = OH, Ph, PyN, Fu, Pyr and Imid) show electrochemical activity between the ranges of 0.0 – 1.5 V *vs* Fc^+/Fc.

4.2.5 Cyclic Voltammetry of [Zn(^{t}BuL$_O^{OH}$)]

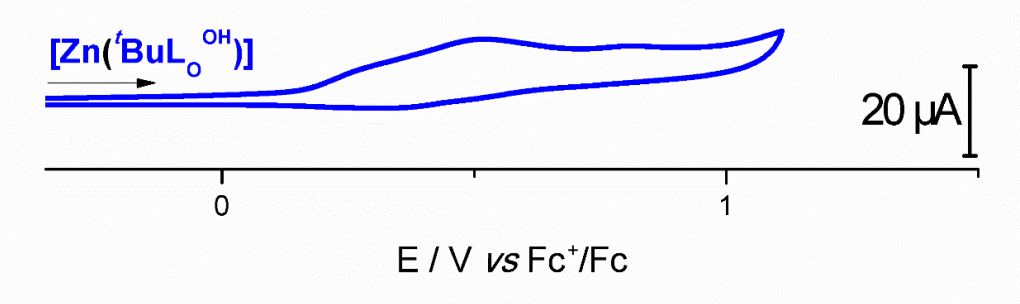


Figure 4.7 Cyclic voltammogram of [Zn(^{t}BuL$_O^{OH}$)] (1 mM) at 293 K in CH_2Cl_2 containing 0.4 M [N^{n}Bu$_4$][BF$_4$] as supporting electrolyte at 100 mVs^{-1}.

Table 4.2 Summary of anodic and cathodic peak potentials at a scan rate of 100mVs^{-1} for [Zn(^{t}BuL$_O^{OH}$)].

Complex	Ep_a^1 *vs* Fc^+/Fc (V)	Ep_c^1 *vs* Fc^+/Fc (V)	Ep_a^2 *vs* Fc^+/Fc (V)	Ep_c^2 *vs* Fc^+/Fc (V)
[Zn(^{t}BuL$_O^{OH}$)]	0.51	0.33	-	-

The cyclic voltammetric data recorded for [Zn(^{t}BuL$_O^{OH}$)] does not demonstrate reversible electrochemistry (Figures 4.7). At slower scan rates (< 100 mVs^{-1}), the cyclic voltammogram of [Zn(^{t}BuL$_O^{OH}$)] showed the loss of the reduction peak at Ep_c^1 = 0.33 V *vs* Fc^+/Fc that re-appears at scan rates > 100

mVs^{-1}. This redox behaviour corresponds typically to an EC mechanism and suggests that the oxidation product decomposes over the timescale of the experiment. The potential for the oxidation process of [Zn($^{t}BuL_{O}^{OH}$)] is significantly higher than those reported previously for the analogous Zn(II) complexes, [Zn($^{t}BuL_{o}^{1}$)$_2$] ($H^{t}BuL_{o}^{1}$ = 2-(4,6-di-*tert*-butylhydroxyphenyl)-4,5-diphenylimidazole)[13], $E_{½}^{1}$ = 0.23 and $E_{½}^{2}$ = 0.49 *vs* Fc^{+}/Fc, [Zn($^{t}BuL_{o}^{2}$)$_2$] ($^{t}BuL_{o}^{2}$ = 2-(4,6-di-*tert*-butylhydroxyphenyl)-4,5-di-*p*-methoxyphenyl-imidazole)[12] and [Zn($^{t}BuL_{o}^{3}$)$_2$] ($H^{t}BuL_{o}^{3}$ = 2-(4,6-di-*tert*-butylhydroxyphenyl)benzimidazole)[12], $E_{½}^{1}$ = 0.41 and $E_{½}^{2}$ = 0.58 V *vs* Fc^{+}/Fc and , $E_{½}^{1}$ = 0.18 and $E_{½}^{2}$ = 0.47 V *vs* Fc^{+}/Fc, respectively.

Since Zn(II) is usually not redox active over the range of potentials employed in the electrochemical experiments, we suggest that the redox process of [Zn($^{t}BuL_{O}^{OH}$)] is associated with the one-electron oxidation of the coordinated ligand, leading to the formation of $[M(L^{\bullet})(L)]^{+}$ which then decomposes before a second oxidation leading to the formation of $[M(L^{\bullet})_2]^{2+}$ occurs.[12,13]

4.2.6 Cyclic Voltametry of [Cu(^{t}BuL$_O^R$)] (R = OH, Ph, PyN, Fu, Pyr and Imid)

The cyclic voltammograms recorded for [Cu(^{t}BuL$_O^R$)] (R = OH, Ph, PyN, Fu, Pyr and Imid) are shown in Figures 4.9 and 4.10, and electrochemical data is presented in Table 4.3.

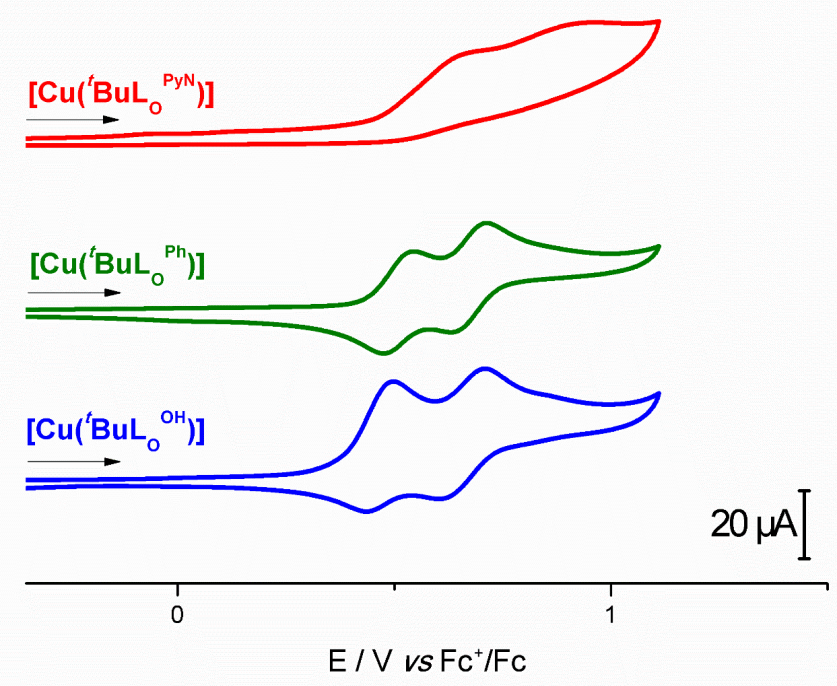


Figure 4.9 Cyclic voltammograms of [Cu(^{t}BuL$_O^{OH}$)] (blue), [Cu(^{t}BuL$_O^{Ph}$)] (green) and [Cu(^{t}BuL$_O^{PyN}$)] (red) (1 mM) at 293 K in CH_2Cl_2 solutions containing 0.4 M [N^{n}Bu$_4$][BF$_4$] as supporting electrolyte at 100 mVs^{-1}.

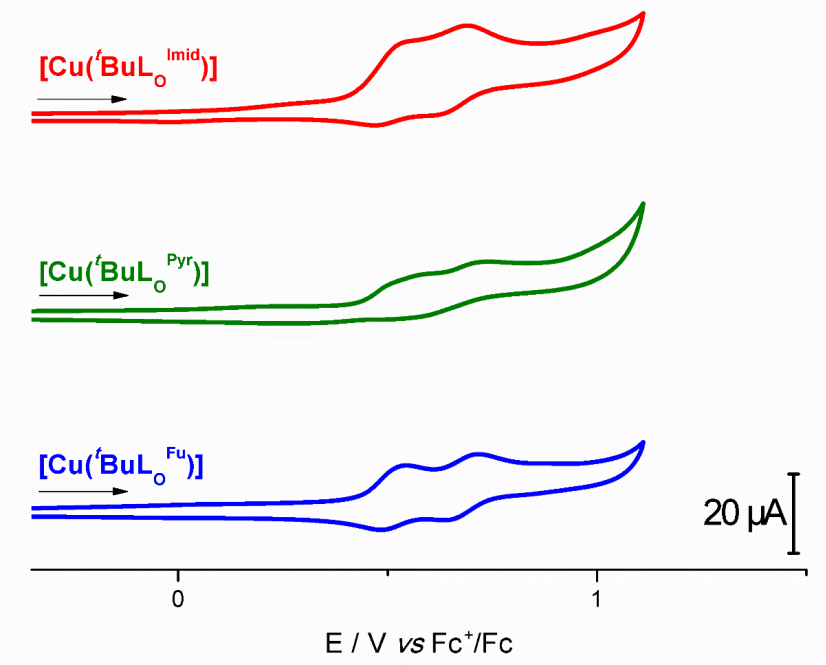


Figure 4.10 Cyclic voltammograms of [Cu(^{t}BuL$_O^{Fu}$)] (blue), [Cu(^{t}BuL$_O^{Pyr}$)] (green) and [Cu(^{t}BuL$_O^{Imid}$)] (red) (1 mM) at 293 K in CH_2Cl_2 solutions containing 0.4 M [N^{n}Bu$_4$][BF$_4$] as supporting electrolyte at 100 mVs^{-1}.

Table 4.3 Summary of anodic and cathodic peak potentials at a scan rate 100mVs^{-1} for [Cu(^{t}BuL$_O^R$)] (R = OH, Ph, PyN, Fu, Pyr and Imid)

Complex	Ep_a^1 *vs* Fc^+/Fc (V)	Ep_c^1 *vs* Fc^+/Fc (V)	Ep_a^2 *vs* Fc^+/Fc (V)	Ep_c^2 *vs* Fc^+/Fc (V)
[Cu(^{t}BuL$_O^{OH}$)]	0.49	0.43	0.70	0.60
[Cu(^{t}BuL$_O^{Ph}$)]	0.54	0.47	0.71	0.63
[Cu(^{t}BuL$_O^{PyN}$)]	0.68	-	0.94	-
[Cu(^{t}BuL$_O^{Fu}$)]	0.54	0.48	0.71	0.63
[Cu(^{t}BuL$_O^{Pyr}$)]	0.54	0.48	0.75	-
[Cu(^{t}BuL$_O^{Imid}$)]	0.54	0.47	0.68	0.62

The cyclic voltammetric data recorded for [Cu(^{t}BuL$_O^R$)] (R = OH, Ph, PyN, Fu, Pyr and Imid) demonstrates that none of the redox processes exhibits reversible electrochemistry. The cyclic voltammograms of [Cu(^{t}BuL$_O^R$)] (R = OH, Ph, Fu, and Imid) each show two redox processes where i_p^c decreases at

slower scan rates (< 100 mVs^{-1}) and show the loss of the reduction peak at Ep_c^1 = 0.43, 0.47, 0.48 and 0.47 V *vs* Fc^+/Fc and Ep_c^2 = 0.60, 0.63, 0.63 and 0.62 V *vs* Fc^+/Fc respectively. These reduction peaks re-emerge at scan rates > 100 mVs^{-1}. This redox behavior corresponds to an EC mechanism where at slower scan rates the oxidised form of the compound decomposes before the return sweep is complete. The cyclic voltammograms of [Cu(^{t}BuL$_O^{PyN}$)] and [Cu(^{t}BuL$_O^{Pyr}$)] appear to be more complex and the two redox processes observed are not well-resolved;[14] [Cu(^{t}BuL$_O^{Pyr}$)] shows a reduction peak for the first redox process, which also disappears at scan rates of < 100 mVs^{-1} and the re-appears at scan rates > 100 mVs^{-1}. [Cu(^{t}BuL$_O^{PyN}$)] shows no corresponding reduction peaks in relation to the two oxidation peaks observed.

The redox processes of [Cu(^{t}BuL$_O^R$)] (R = OH, Ph, PyN, Fu, Pyr and Imid) occur at potentials that are higher than those previously observed for the analogous Cu(II) complexes [Cu(^{t}BuL$_o^1$)$_2$] (H^{t}BuL$_o^1$ = 2-(4,6-di-*tert*-butylhydroxyphenyl)-4,5-diphenylimidazole),[11] $E_{½}^1$ = 0.16 and $E_{½}^2$ = 0.50 *vs* Fc^+/Fc, [Cu(^{t}BuL$_o^2$)$_2$] (H^{t}BuL$_o^2$ = 2-(4,6-di-*tert*-butylhydroxyphenyl)-4,5-di-*p*-methoxyphenylimidazole)[12] and [Cu(^{t}BuL$_o^3$)$_2$] (H^{t}BuL$_o^3$ = 2-(4,6-di-*tert*-butylhydroxyphenyl)benzimidazole)[12] $E_{½}^1$ = 0.36 and $E_{½}^2$ = 0.58 V *vs* Fc^+/Fc and , $E_{½}^1$ = 0.11 and $E_{½}^2$ = 0.44 V *vs* Fc^+/Fc, respectively. However, they are very similar to the redox potentials observed for [Cu(^{t}BuL$_O^{Py1}$)], $E_{½}^1$ = 0.47 and Ep_a^2 = 0.69 and Ep_c^2 = 0.62 *vs* Fc^+/Fc and [Cu(^{t}BuL$_O^{Py2}$)], $E_{½}^1$ = 0.48 and Ep_a^2 = 0.69 and Ep_c^2 = 0.62 *vs* Fc^+/Fc, respectively.[14] The values of redox potentials for of [Cu(^{t}BuL$_O^R$)] (R = OH, Ph, PyN, Fu, Pyr and Imid) are consistent with the range observed for oxidation processes that are ligand-based and associated with

the generation of $[Cu(^{R}L)(^{R}L^{\bullet})]^{+}$ and $[Cu(^{R}L^{\bullet})_2]^{2+}$ species.[11–15,18] An irreversible reduction process was also observed for $[Cu(^{t}BuL_{O}^{R})]$ (R = OH, Ph, PyN, Fu, Pyr and Imid) between -1.45 and -1.85 V *vs* Fc^{+}/Fc, which may be tentatively assigned to a metal-based Cu(II)/Cu(I) reduction process.[13]

4.3 Conclusions

This chapter describes the attempts made to synthesise a novel Zn(II) diphenolate, [Zn(^{t}BuL$_{O}^{OH}$)], complex and a range of diphenolate Cu(II) complexes, [Cu(^{t}BuL$_{O}^{R}$)] (R = OH, Ph, PyN, Fu, Pyr and Imid), and builds on the research into the related [Ni(^{t}BuL$_{O}^{R}$)] complexes discussed in Chapter 3. X-ray crystallographic studies showed that the monomeric complex, [Cu(^{t}BuL$_{O}^{OH}$)], possesses an approximately square planar coordination geometry with the metal centre bound by diimine and diphenolate donors. The frozen solution X-band EPR spectra of [Cu(^{t}BuL$_{O}^{R}$)] are similar to one another and confirm that each complex possesses a paramagnetic Cu(II) S = ½ d^{9} metal centre. The similarity between each EPR spectrum as R is varied suggests that the functional group pendant to the ligand backbone does not interact greatly with Cu(II) centre in [Cu(^{t}BuL$_{O}^{R}$)].

[Zn(^{t}BuL$_{O}^{OH}$)] was isolated and mass spectrometric data suggested that [Zn(^{t}BuL$_{O}^{R}$)] (R = Ph, PyN, Fu, Pyr and Imid) had formed, however pure products could not be isolated. Although, the functionalisation of the R = OH group in [Zn(^{t}BuL$_{O}^{OH}$)] could provide a route to the incorporation of pendant N-donors and offer insight into the redox processes in these centres, it appears that other routes that do not involve the treatment of [Zn(^{t}BuL$_{O}^{OH}$)] with functionalised acid chlorides may need to be explored in order to achieve this.

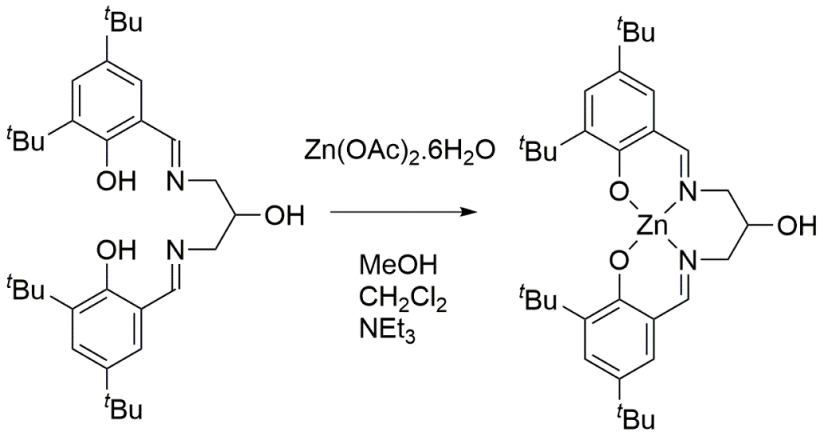
Electrochemical studies demonstrated that the redox processes for [Zn(^{t}BuL$_{O}^{OH}$)] were irreversible suggesting that the redox products were unstable. In addition, these oxidation processes occurred at higher oxidation potentials than had been previously reported for analogous Zn(II) complexes by Benisvy

et al.[11–13,19] and Franks *et al*.[17] The instability of the oxidation products of [Zn(^{t}BuL$_{O}^{OH}$)] prevented further spectroscopic studies.

[Cu(^{t}BuL$_{O}^{R}$)] (R = OH, Ph, PyN, Fu, Pyr and Imid) each possess two irreversible redox processes. The irreversibility of these processes prevented further spectroscopic studies to probe the nature of the oxidized species. The potentials of the redox processes for [Cu(^{t}BuL$_{O}^{R}$)] (R = OH, Ph, Fu, Pyr and Imid) are similar to those for the analogous Cu(II) complexes reported previously by Franks *et al.*[14] and, based upon the potentials at which these oxidation processes occur, they may be tentatively assigned to the successive oxidation of the two phenolate groups within each complex to generate phenoxyl radical ligands.[11–14] The potentials of the redox processes for [Cu(^{t}BuL$_{O}^{R}$)] (R = OH, Ph, Fu, Pyr and Imid) are all relatively similar despite the difference in the pendant group in each Cu(II) complex. This suggests that the differing pendant groups (R = OH, Ph, Fu, Pyr and Imid) have little impact upon the stabilisation of the species generated on the oxidation of [Cu(^{t}BuL$_{O}^{R}$)] (R = OH, Ph, Fu, Pyr and Imid). In contrast [Cu(^{t}BuL$_{O}^{PyN}$)] possesses first and second redox processes that are *ca.* 0.14 V and 0.23 V more positive than their [Cu(^{t}BuL$_{O}^{R}$)] (R = OH, Ph, Fu, Pyr and Imid) counterparts. This suggests that the pyridyl functionalization of the pendant arm in [Cu(^{t}BuL$_{O}^{PyN}$)] may stabilize its oxidation product.

4.4 Experimental

4.4.1 Synthesis of [Zn(^{t}BuL$_O^{OH}$)]



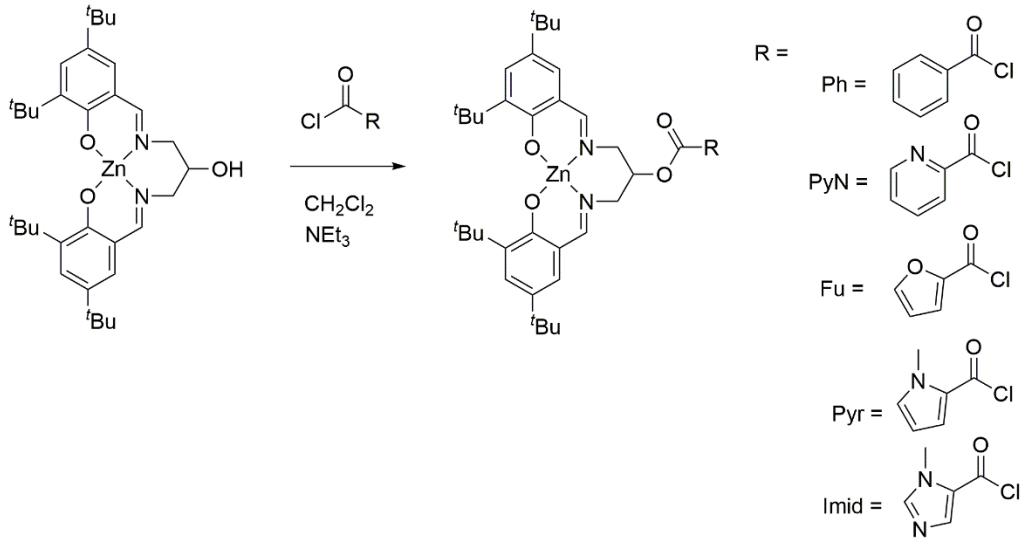
Scheme 4.3 Synthesis of [Zn(^{t}BuL$_O^{OH}$)]

Zn.(OAc)$_2$.6H$_2$O (0.40 g, 1.92 mmol) in a methanol (10 ml) and NEt$_3$ (1.21 ml, 8.64 mmol) were added to a solution of [H$_2$^{t}BuL$_O^{OH}$] (1.00 g, 1.92 mmol) in CH$_2$Cl$_2$ (20 ml). The reaction mixture was heated to reflux for 24 h. The reaction mixture was then reduced under vacuum to produce a yellow solid which was further purified by column chromatography on silica gel using dichloromethane and pentane (3:2 v/v) as eluent.

^{1}H NMR (400 MHz, CDCl$_3$, 298 K): δ_H 8.45 (2H, s, N=C<u>H</u>), 7.41 (2H, d, *J* 2.5, Ar<u>H</u>), 7.13 (2H, d, *J* 2.5, Ar<u>H</u>), 4.27 – 4.33 (1H, m, C<u>H</u>), 3.91 (2H, ddd, *J* 13.5, 4.5, 1.0, C<u>H</u>$_2$), 3.77 (2H, ddd, *J* 12.5, 6.0, 0.9, C<u>H</u>$_2$), 1.46 (18H, s, C(C<u>H</u>$_3$)$_3$), 1.32 (18H, s, C(C<u>H</u>$_3$)$_3$). ^{13}C NMR (100 MHz, CDCl$_3$, 298 K): δ_C 168.5 (<u>C</u>=N), 157.9 (Ar<u>C</u>), 140.2 (Ar<u>C</u>), 136.7 (Ar<u>C</u>), 127.2 (Ar<u>C</u>), 126.1 (Ar<u>C</u>), 117.7 (Ar<u>C</u>), 70.1 (<u>C</u>-OH), 63.2 (<u>C</u>H$_2$-N), 35.1 (<u>C</u>(CH$_3$)$_3$), 34.1 (<u>C</u>(CH$_3$)$_3$), 31.4 (<u>C</u>H$_3$), 29.4 (<u>C</u>H$_3$). FTIR ν / cm^{-1} (ATR): 2958 (m), 1556 (s), 1437 (s), 1391 (m), 1235 (m), 1023 (m), 803 (m) 744 (s) 673 (m). MS (ES+, m/z): 585.2956 [M+H]. Elemental

analysis: found (calculated for $C_{33}H_{48}ZnN_2O_3$): C 67.55 (67.62), H 8.27 (8.25), N 4.79 (4.78). Yield 1.10 g, 1.83 mmol, 96 %.

4.4.2 Attempted syntheses of [Zn(^{t}BuLO^R)] (R = Ph, PyN, Fu, Pyr and Imid)



Scheme 4.4 Synthesis of [Zn(^{t}BuLO^R)] (R = Ph, PyN, Fu, Pyr and Imid)

General procedure: Benzoyl chloride (0.12 g, 0.86 mmol) and NEt_3 (0.77 ml, 1.72 mmol) were added to a solution of [Zn(^{t}BuLO^{OH})] (0.50 g, 0.86 mmol) in anhydrous CH_2Cl_2. The reaction was stirred for 24 h and then the solvent removed under vacuum to produce a yellow powder that was further purified via column chromatography on silica gel using dichloromethane and pentane (6/4 v/v) as eluent.

4.4.3 [Zn(^{t}BuLO^{Ph})]

The mass spectrum of the crude product possesses features that may be assigned to the desired product. However, attempts to purify the product were unsuccessful. MS (ES+, m/z): 689.3219 [M+H].

4.4.4 [Zn(^{t}BuL$_{O}^{PyN}$)]

The mass spectrum of the crude product possesses features that may be assigned to the desired product. However, attempts to purify the product were unsuccessful. MS (ES+, m/z): 690.3171 [M+H].

4.4.5 [Zn(^{t}BuL$_{O}^{Fu}$)]

The mass spectrum of the crude product possesses features that may be assigned to the desired product. However, attempts to purify the product were unsuccessful. MS (ES+, m/z): 679.3011 [M+H].

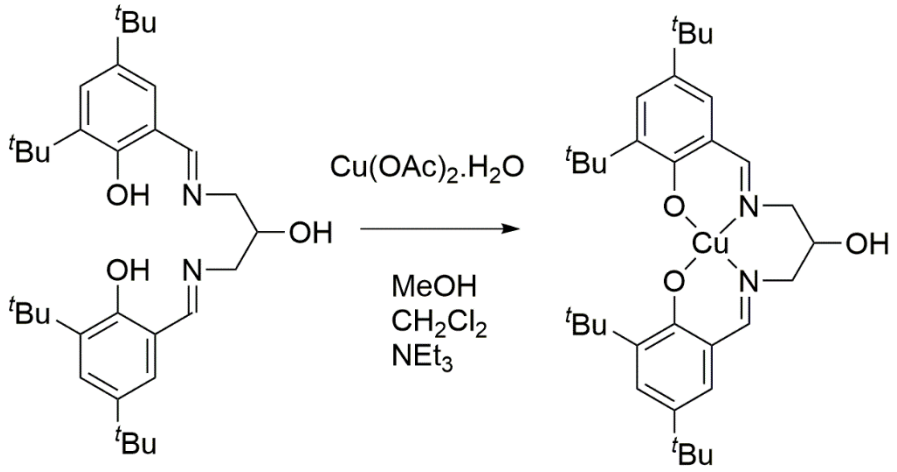
4.4.6 [Zn(^{t}BuL$_{O}^{Pyr}$)]

The mass spectrum of the crude product possesses features that may be assigned to the desired product. However, attempts to purify the product were unsuccessful. MS (ES+, m/z): 692.3328 [M+H].

4.4.7 [Zn(^{t}BuL$_{O}^{Imid}$)]

The mass spectrum of the crude product possesses features that may be assigned to the desired product. However, attempts to purify the product were unsuccessful. MS (ES+, m/z): 693.3280 [M+H].

4.4.8 Synthesis of [Cu(^{t}BuL$_O^{OH}$)]

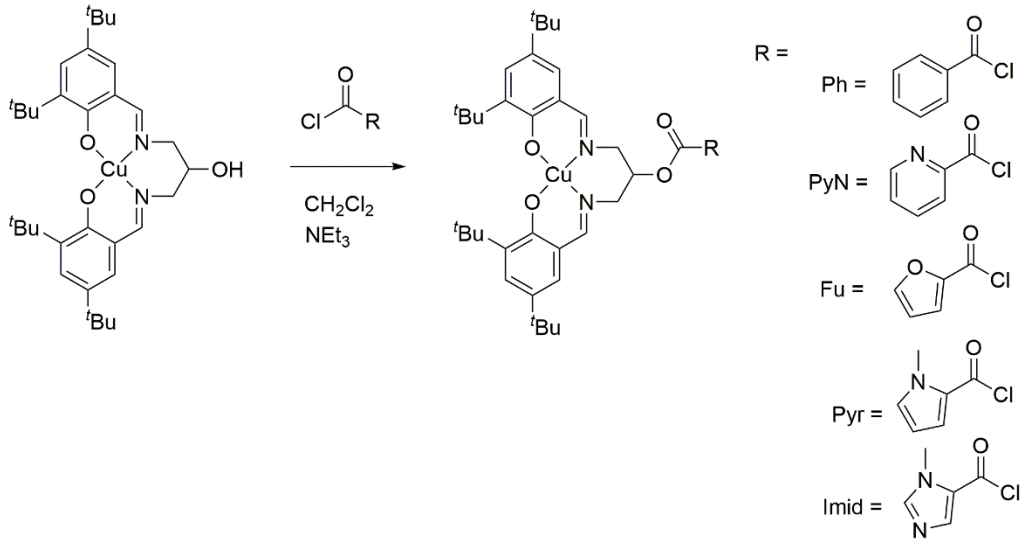


Scheme 4.5 Synthesis of [Cu(^{t}BuL$_O^{OH}$)]

Cu.(OAc)$_2$.H$_2$O (0.40 g, 1.92 mmol) in a methanol (10 ml) and NEt$_3$ (1.21 ml, 8.64 mmol) were added to a solution of [H$_2$^{t}BuL$_O^{OH}$] (1.00 g, 1.92 mmol) in CH$_2$Cl$_2$ (20 ml). The reaction mixture was heated to reflux for 24 h. The reaction mixture was then reduced under vacuum to produce a green solid which was further purified by column chromatography on silica gel using dichloromethane and pentance (3:2 v/v) as eluent.

MS (ES+, m/z): 584.2961 [M+H]. Elemental analysis: found (calculated for C$_{33}$H$_{48}$CuN$_2$O$_3$): C 67.55 (67.62), H 8.27 (8.25), N 4.79 (4.78). FTIR ν / cm^{-1} (ATR): 2957 (m), 1614 (s), 1531 (s), 1434 (s), 1359 (s), 1209 (m), 1072 (m), 1064 (s), 877 (m) 788 (s) 637 (m). Yield 1.06 g, 1.81 mmol, 95 %.

4.4.9 Syntheses of [Cu(^{t}BuL$_O^R$)] (R = Ph, PyN, Fu, Pyr and Imid)



Scheme 4.6 Synthesis of [Cu(^{t}BuL$_O^R$)] (R = Ph, PyN, Fu, Pyr and Imid)

General procedure: Benzoyl chloride (0.12 g, 0.86 mmol) and NEt_3 (0.77 ml, 1.72 mmol) were added to a solution of [Cu(^{t}BuL$_O^{OH}$)] (0.50 g, 0.86 mmol) in anhydrous CH_2Cl_2. The reaction was stirred for 24 h and then the solvent removed *in vacuo* to produce a green powder that was further purified via column chromatography on silica gel using dichloromethane and pentane (3:2 v/v) as eluent.

4.4.10[Cu(^{t}BuL$_O^{Ph}$)]

MS (ES+, m/z): 688.3223 [M+H]. Elemental analysis: found (calculated for $C_{40}H_{52}CuN_2O_4$): C 69.80 (69.79), H 7.76 (7.61), N 4.05 (4.07). FTIR ν / cm^{-1} (ATR): 2955 (m), 1748 (s), 1619 (m), 1530 (s), 1434 (s), 1322 (m), 1223 (m), 1069 (s), 912 (m), 877 (m), 835 (s), 789 (s), 744 (m).Yield 0.27 g, 0.39 mmol, 45 %.

4.4.11 [Cu(^{t}BuLO^{PyN})]

MS (ES+, m/z): 689.3176 [M+H]. Elemental analysis: found (calculated for $C_{39}H_{51}CuN_3O_4$): C 67.88 (67.75), H 7.46 (7.45), N 6.09 (6.10). FTIR ν / cm^{-1} (ATR): 2962 (m), 1629 (m), 1474 (s), 1391 (m), 1360 (m), 1252 (m), 1093 (m), 1016 (s), 802 (m) 743 (s). Yield 0.21 g, 0.31 mmol, 36 %.

4.4.12 [Cu(^{t}BuLO^{Fu})]

MS (ES+, m/z): 678.3016 [M+H]. Elemental analysis: found (calculated for $C_{38}H_{50}CuN_2O_5$): C 67.39 (67.28), H 7.43 (7.51), N 4.10 (4.13). FTIR ν / cm^{-1} (ATR): 2965 (m), 1702 (s), 1582 (s), 1473 (m), 1409 (m), 1384 (s), 1360 (m), 1322 (m), 1226 (s), 1170 (m), 1061 (m), 997 (m), 867 (m), 834 (s), 789 (s), 744 (m), 615 (m). Yield 0.24 g, 0.36 mmol, 42 %.

4.4.13 [Cu(^{t}BuLO^{Pyr})]

MS (ES+, m/z): 691.3332 [M+H]. Elemental analysis: found (calculated for $C_{39}H_{53}CuN_3O_4$): C 67.83 (67.75), H 7.65 (7.73), N 6.03 (6.08). FTIR ν / cm^{-1} (ATR): 2947 (s), 1756 (s), 1697 (m), 1620 (m), 1467 (s), 1381 (s), 1317 (m), 1236 (m), 1201 (s), 1169 (m), 997 (m), 865 (s) 685 (s) 606 (m). Yield 0.24 g, 0.36 mmol, 42 %.

4.4.14 [Cu(^{t}BuLO^{Imid})]

MS (ES+, m/z): 691.3385 [M+H]. Elemental analysis: found (calculated for $C_{38}H_{52}CuN_4O_4$): C 65.92 (65.74), H 7.57 (7.60), N 8.05 (8.09). FTIR ν / cm^{-1} (ATR): 2968 (m), 1749 (m), 1617 (s), 1530 (s), 1360 (s), 1322 (m), 1258 (m), 1225 (s), 1169 (m), 1015 (s), 798 (s) 637 (m). Yield 0.22 g, 0.31 mmol, 37 %.

4.5 References

(1) Ito, N.; Phillips, S. E.; Stevens, C.; Ogel, Z. B.; McPherson, M. J.; Keen, J. N.; Yadav, K. D.; Knowles, P. F. *Nature* **1991**, *350*, 87–90.

(2) Whittaker, J.W. *Metal Ions in Biological Systems*; And, H. S., Sigel, M. D., Eds.; Taylor & Francis Inc: New York, 1994.

(3) Klinman, J. P. *Chem. Rev.* **1996**, *96*, 2541–2562.

(4) Stubbe, J.; van der Donk, W. A. *Chem. Rev.* **1998**, *98*, 705–762.

(5) Whittaker, J. W. *Arch. Biochem. Biophys.* **2005**, *433*, 227–239.

(6) Ito, N.; Phillips, S.; Yadav, K.; Knowles, P. *J. Mol. Biol.* **1994**, *238*, 794–814.

(7) Whittaker, M. M.; Ekberg, C. A.; Peterson, J.; Sendova, M. S.; Day, E. P.; Whittaker, J. W. *J. Mol. Catal. B Enzym.* **2000**, *8*, 3–15.

(8) Whittaker, M.; Whittaker, J. *J. Biol. Chem.* **1988**, *263*, 6074–6080.

(9) Itoh, S.; Taki, M.; Fukuzumi, S. *Coord. Chem. Rev.* **2000**, *198*, 3–20.

(10) Jazdzewski, B. a.; Tolman, W. B. *Coord. Chem. Rev.* **2000**, *200-202*, 633–685.

(11) Benisvy, L.; Blake, A. J.; Collison, D.; Davies, E. S.; Garner, C. D.; McInnes, E. J.; McMaster, J.; Whittaker, G.; Wilson, C. *Chem. Commun.* **2001**, No. 18, 1824–1825.

(12) Benisvy, L.; Bill, E.; Blake, A. J.; Collison, D.; Davies, E. S.; Garner, C. D.; McArdle, G.; McInnes, E. J. L.; McMaster, J.; Ross, S. H. K.; Wilson, C. *Dalton Trans.* **2006**, No. 1, 258–267.

(13) Benisvy, L.; Blake, A. J.; Collison, D.; Davies, E. S.; Garner, C. D.; McInnes, E. J. L.; McMaster, J.; Whittaker, G.; Wilson, C. *Dalton Trans.* **2003**, No. 5, 1975–1985.

(14) Franks, M. Transition Metal Complexes Containing Phenylthiolate and Phenolate Ligands, University of Nottingham, 2011.

(15) Parker, D.; Stephen Davies, E.; Wilson, C.; McMaster, J. *Inorg. Chim. Acta* **2007**, *360*, 203–211.

(16) Wang, Y.; Stack, T. D. P. *J. Am. Chem. Soc.* **1996**, *118*, 13097–13098.

(17) Franks, M.; Gadzhieva, A.; Ghandhi, L.; Murrell, D.; Blake, A. J.; Davies, E. S.; Lewis, W.; Moro, F.; McMaster, J.; Schröder, M. *Inorg. Chem.* **2013**, *52*, 660–670.

(18) Rotthaus, O.; Jarjayes, O.; Thomas, F.; Philouze, C.; Saint-Aman, E.; Pierre, J.-L. *Dalton Trans.* **2007**, No. 8, 889–895.

(19) Figuly, G. D.; Loop, C. K.; Martin, J. C. *J. Am. Chem. Soc.* **1989**, *111*, 654–658.

Chapter 5: Conclusions and Future Work

Conclusions and Future Work

5.1 Conclusions

The work described in this thesis has attempted to provide insight into the chemistry of the active sites of GAO and NiSOD through the synthesis, and electro- and spectroelectrochemical characterisation of Zn(II), Ni(II) and Cu(II)-containing complexes as analogues of these centres.

Attempts to prepare a range of Zn(II), Ni(II) and Cu(II) Schiff-base diphenolate complexes [M(^{t}BuL$_O^R$)] (M = Zn(II), Ni(II) and Cu(II); R = H, OMe, ^{t}Bu and Cl)) (Figure 5.1, Chapter 2) were made using four novel N_3O_2 pro-ligands that incorporate a bridging aryl group in which each aryl ring is functionalised with a different R group at the *para*-position of the ring.

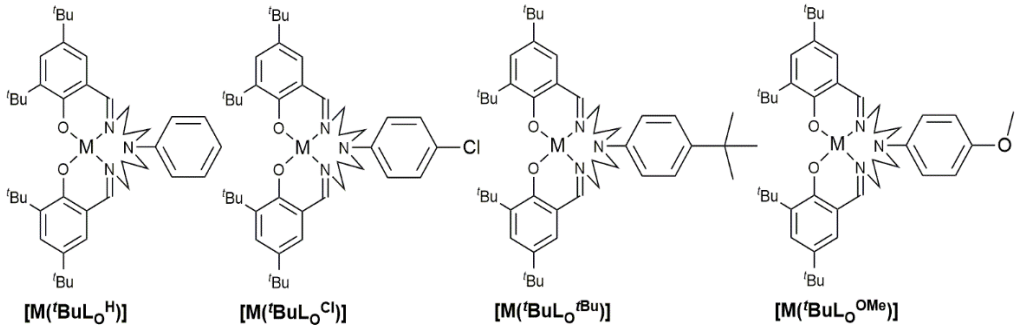


Figure 5.1 Schematic representation of the Schiff-base diphenolate complexes presented in Chapter 2 - [M(^{t}BuL$_O^R$)] (M = Zn(II), Ni(II) and Cu(II); R = H, OMe, ^{t}Bu and Cl)

X-ray crystallography shows that the metal centres in [Cu(^{t}BuL$_O^H$)], [Cu(^{t}BuL$_O^{OMe}$)] and [Ni(^{t}BuL$_O^{OMe}$)] adopt five-coordinate distorted square-based pyramidal coordination geometries. [Cu(^{t}BuL$_O^{OMe}$)] possesses a metal to amine N-donor distance, M(1)-N(3) = 2.4511(17) Å, that is significantly shorter than that for [Cu(^{t}BuL$_O^H$)] (2.579(2) Å). This observation is consistent with the

differences in basicity of the amine *N*-donor in each complex (the pK_a of 4-methoxyphenylamine = 5.36 and the pK_a of phenylamine = 4.87). Thus, this difference in basicity may modulate the electronic structure of the metal centre in [M(^{t}BuL$_O^R$)]. In addition, the M-N(3) distance in [Ni(^{t}BuL$_O^{OMe}$)] (2.19(11) Å) is shorter than that in [Cu(^{t}BuL$_O^H$)] and [Cu(^{t}BuL$_O^{OMe}$)]. This difference in the M-N(3) (M = Ni(II) and Cu(II)) distance may be attributed to the Jahn-Teller distortion associated with Cu(II) centres.[1,2]

Electrochemical investigations of crude [Zn(^{t}BuL$_O^R$)] (R = H, ^{t}Bu), [Zn(^{t}BuL$_O^R$)] (R = Cl, OMe) and [M(^{t}BuL$_O^R$)] (M = Ni(II) and Cu(II), R = H, Cl, ^{t}Bu and OMe) show that each complex possesses two oxidation processes between 0.11 V and 0.61 V *vs* Fc^+/Fc. The first oxidation process of [M(^{t}BuL$_O^{OMe}$)] (M = Zn(II), Ni(II) and Cu(II)) and the second oxidation process of [Cu(^{t}BuL$_O^{OMe}$)] are electrochemically reversible. UV/vis spectroelectrochemical studies also confirm the chemical reversibility of the first oxidation process of [M(^{t}BuL$_O^{OMe}$)] (M = Zn(II), Ni(II) and Cu(II). EPR spectroscopic studies on [Zn(^{t}BuL$_O^{OMe}$)]$^+$ and [Cu(^{t}BuL$_O^{OMe}$)]$^+$ suggest that this process is associated with the oxidation of a bound phenolate ligand to generate a bound phenoxyl radical ligand. In this respect, [Cu(^{t}BuL$_O^{OMe}$)]$^+$ serves as an analogue of the oxidised Cu(II)-tyrosyl radical form of the active site of GAO.[3] In contrast, EPR spectroscopic studies of [Ni(^{t}BuL$_O^{OMe}$)]$^+$ are consistent with the generation of a formal Ni(III) centre,[4] which serves as an analogue of the oxidised form of the active site of NiSOD.[5] Furthermore our results suggest that the increased electron donating ability of the aryl amine donor, associated with the incorporation of an OMe substituent in the *para*-position, is necessary to support the reversible redox chemistry exhibited by these systems.

The oxidation of the Ni(II) form of NiSOD to Ni(III) is associated with the reversible, axial binding of an imidazole donor derived from a histidine residue.[5] The research described in Chapter 2 demonstrates that a the binding of fifth N-donor in [Ni(^{t}BuL$_{O}^{OMe}$)] appears to support a reversible Ni(III)/Ni(II) couple. X-ray crystallography shows that the fifth N-donor in [Ni(^{t}BuL$_{O}^{OMe}$)] is bound to the Ni(II) centre and it appears that the ligand is pre-organised to favour this coordination mode; it is likely that this mode is retained in the Ni(III) form. In Chapters 3 and 4 we focussed on the attempted syntheses of Schiff-base diphenolate and dithiolate complexes incorporating a pendant imidazole moiety that has the potential to bind reversibly to the metal centre. This reversible binding has the potential to render the Ni(II) form four coordinate and the Ni(III) form five coordinate and would more closely replicate the chemistry at the active site of NiSOD.[5]

Initial attempts to synthesise a di-amine bridge fuctionalised with an imidazole group followed previous synthetic approaches employed by Franks *et al.*[4] and the use of protecting groups to protect the NH group of the imidazole ring. However, these approaches were unsuccessful. Alternative synthetic routes for the incorporation of aromatic and heterocyclic functionalities onto the ligand bridge involved reactions of metal-bound Schiff-base diphenolate and dithiophenolate ligands, functionalised with an OH group, with aromatic or heterocyclic functionalised acid chlorides.

Attempts were made to synthesise a range of Zn(II), Ni(II) and Cu(II) Schiff-base diphenolate and dithiolate complexes (Figure 5.2) however, only [Ni(^{t}BuL$_{O}^{Ph}$)] and [Cu(^{t}BuL$_{O}^{R}$)] (R = Ph, PyN, Fu, Pyr and Imid) were isolated. Mass spectrometric data suggested that [Zn(^{t}BuL$_{O}^{R}$)] (R = Ph, PyN, Fu, Pyr and

Imid), [Ni(^{t}BuL$_O^R$)] (R = PyN, Fu, Pyr and Imid) and [Ni(^{t}BuL$_S^R$)] (R = Ph, PyN, Fu, Pyr and Imid) had formed, however pure products could not be isolated. X-ray crystallographic studies of [Ni(^{t}BuL$_O^R$)] [Ni(^{t}BuL$_O^R$)] (R = OH, Ph), [Cu(^{t}BuL$_O^{OH}$)] and [Ni(^{t}BuL$_S^{OH}$)] confirmed their formulation and demonstrated that each complex adopts a distorted square planar geometry about the metal centre.

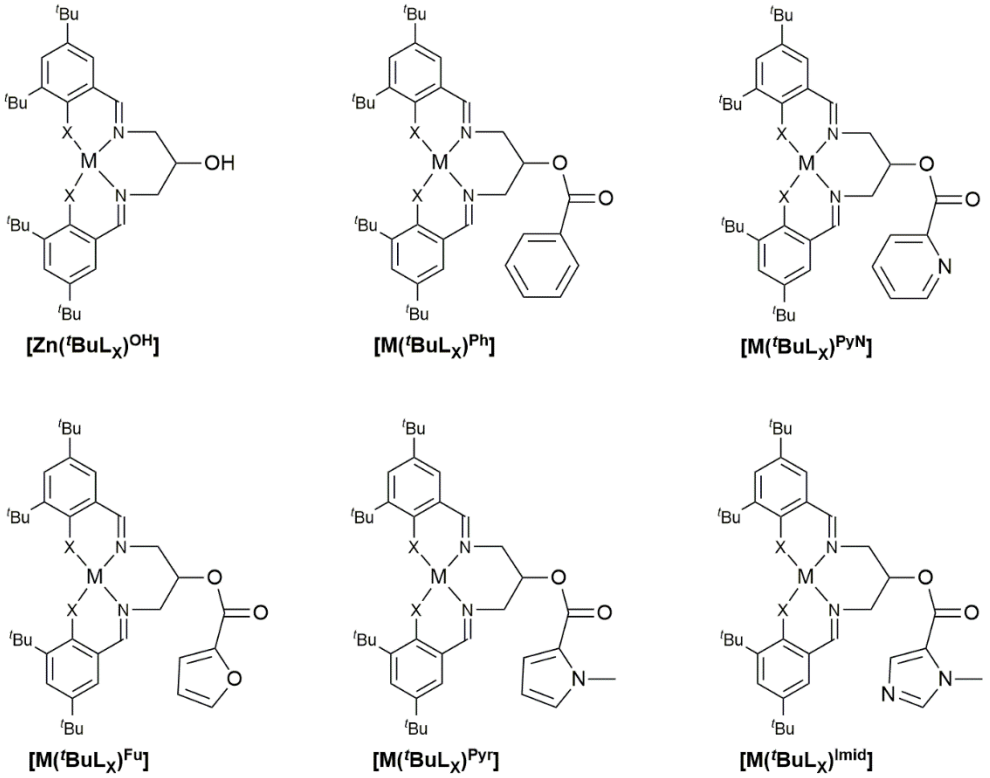


Figure 5.2 Schematic representation of the Schiff-base diphenolate complexes [M(^{t}BuL$_O^R$)] (where M = Zn(II), Ni(II), and Cu(II), R = OH, Ph, PyN, Fu, Pyr and Imid nd X = S or O).

Electrochemical investigations of [Ni(^{t}BuL$_O^R$)] (R = OH, Ph), [Ni(^{t}BuL$_S^{OH}$)] and [Cu(^{t}BuL$_O^R$)] (R = OH, Ph, PyN, Fu, Pyr and Imid) show that each complex exhibits irreversible redox processes. These results demonstrate that the OH and phenyl ester functionalities pendant to the ligand backbone do not stabilize the oxidation products of [Ni(^{t}BuL$_O^R$)] (R = OH, Ph), [Ni(^{t}BuL$_S^{OH}$)]

and [Cu(^{t}BuL$_O^R$)] (R = OH, Ph, PyN, Fu, Pyr and Imid). Previous work by Franks *et al*.[4] demonstrate that the position of a N-donor relative to the metal centre is crucial for the stabilisation of oxidised Ni(II) species in Schiff-base diphenolate and dithiolate complexes. It appears that the incorporation of a suitable N-donor onto the ligand backbone at an appropriate distance from the metal centre is a prerequisite for the stabilization of the oxidation products of [M(^{t}BuL$_O^R$)]-type complexes.

5.2 Future work

5.2.1 The development of routes to [M(^{t}BuL$_O^R$)] (M = Zn(II), Ni(II) and Cu(II)) and [Ni(^{t}BuL$_S^R$)] (R = Ph, PyN, Fu, Pyr and Imid)

Our isolation of [Ni(^{t}BuL$_O^R$)] (R = Ph), and [Cu(^{t}BuL$_O^R$)] (R = Ph, PyN, Fu, Pyr and Imid) suggests that the functionalisation of the R = OH group in [M(^{t}BuL$_O^{OH}$)] (M = Zn(II), Ni(II) and Cu(II)) and [Ni(^{t}BuL$_S^{OH}$)] may be achieved, and could provide a route to the incorporation of pendant N-donors. However, it appears that other routes that do not involve the treatment of [M(^{t}BuL$_O^{OH}$)] (M = Zn(II), Ni(II) and Cu(II)) and [Ni(^{t}BuL$_S^{OH}$)] with functionalised acid chlorides should be explored. These routes could employ carbodiimides, *e.g. N*, *N*'-dicyclohexylcarbodiimide (DCC), and 4-dimethylaminopyridine (DMAP) together with an appropriately functionalised carboxylic acid.[6]

5.2.2 Towards analogues of the active sites of the [NiFe] hydrogenases

The [NiFe] hydrogenases catalyse either H_2 uptake or production and this catalytic function has encouraged research towards understanding the mechanism(s) by which these processes occur.[7]

The structure of the active site of [NiFe] hydrogenase as revealed by X-ray crystallography is shown Figure 5.3.[8, 9] The Ni centre is coordinated by four cysteine thiolate donors in a non-planar geometry; two of which bridge the Ni and Fe metal centres and the Fe centre is coordinated by one CO and two CN^- ligands.[10, 11] The isolated oxidised form of the active site also incorporates an additional exogenous species, X, which has been assigned to peroxide or hydroxide species.[12-14] The nature of the active site of the [NiFe] hydrogenases has inspired attempts to synthesise small molecule analogues containing Ni and Fe centres coordinated by biologically relevant ligand sets.[7]

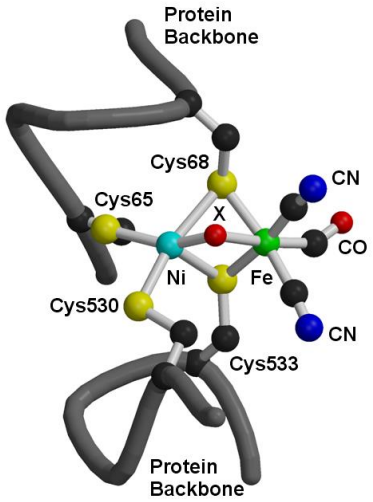


Figure 4.3 Structure of the active site of the as isolated, inactive form of [NiFe] hydrogenase from *Desulfovibrio gigas.*[8, 9]

Binuclear and trinuclear $[Ni(L_S^{Py1})\{Fe(CO)_3\}_2]$, $[Ni(L_S^{Ph1})\{Fe(CO)_3\}_2]$, $[Ni(L_S^{Py1})Fe(CO)_3]$, $[Ni(L_S^{Ph1})Fe(CO)_3]$ (Figure 5.3) have been prepared and characterised by Franks *et al.*[4] as analogues of the active site of the [NiFe] hydrogenases from the reaction between the Ni(tsalen)-type complexes $[Ni(L_S^R)]$ (R = Py1 or Ph1) and excess $Fe_2(CO)_9$ in toluene.

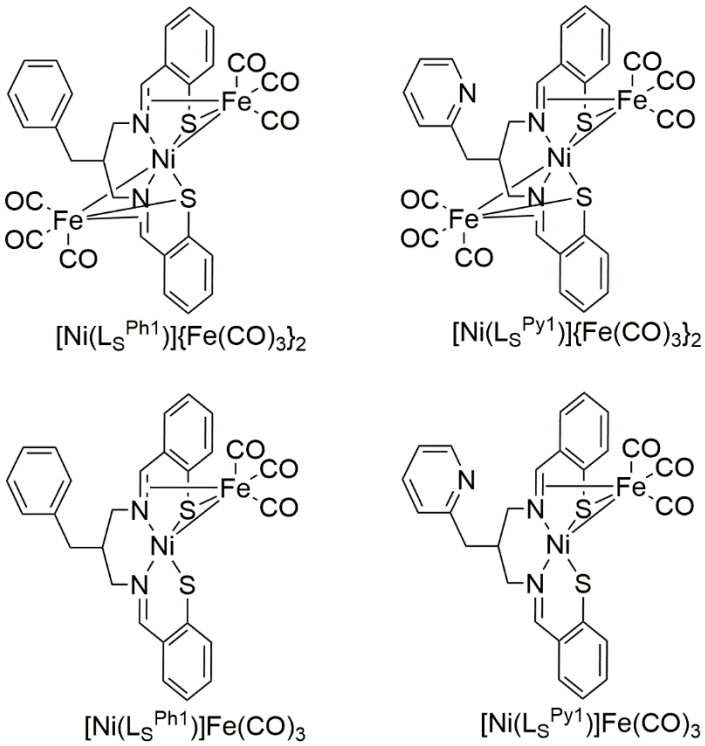


Figure 5.4 Schematic representation of the [Ni(μ_2-S){Fe(CO)$_3$}$_n$] (n = 1 or 2) complexes prepared by Franks *et al.*[4]

Each complex incorporates biologically relevant structural elements reminiscent of the active site of the inactive form of [NiFe] hydrogenase (*D. gigas*),[1] including a binuclear Ni(μ_2-S)Fe core with a separation between the Ni and Fe centres of approximately 2.9 Å.[4] Preliminary electrochemical studies of these complexes suggest that they do not support reversible redox processes. Future work would seek to expand the range of [NiFe] Schiff-base complexes by employing [Ni(^{t}BuL$_S^R$)] (R = OH, Ph, PyN, Fu, Pyr and Imid, Chapter 3) to prepare [Ni(L$_S^R$)Fe(CO)$_3$] and [Ni(L$_S^R$){Fe(CO)$_3$}$_2$] (R = OH, Ph, PyN, Fu, Pyr and Imid) for direct comparison with [Ni(L$_S^{Py1}$){Fe(CO)$_3$}$_2$], [Ni(L$_S^{Ph1}$){Fe(CO)$_3$}$_2$], [Ni(L$_S^{Py1}$)Fe(CO)$_3$], [Ni(L$_S^{Ph1}$)Fe(CO)$_3$]. The structural characterisation, electrochemical and spectroscopic studies of these low

molecular weight complexes could provide insight into the nature and chemistry of the active site of [NiFe] hydrogenases.

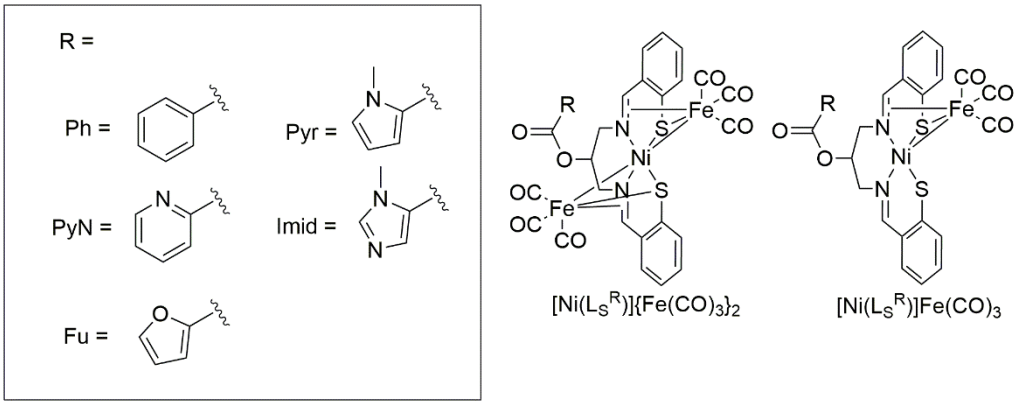


Figure 5.5 Schematic representations of $[Ni(\mu_2\text{-}S)\{Fe(CO)_3\}_n]$ (n = 1 or 2) complexes to be prepared from $Ni(^tBuL_S^R)]$ (R = OH, Ph, PyN, Fu, Pyr and Imid).

References

(1) Yilmaz, V. T.; Degirmencioglu, I.; Andac, O.; Karabocek, S.; Slawin, A. M. Z. *J. Mol. Struct.* **2003**, *654*, 125–129.

(2) Franks, M.; Gadzhieva, A.; Ghandhi, L.; Murrell, D.; Blake, A. J.; Davies, E. S.; Lewis, W.; Moro, F.; McMaster, J.; Schröder, M. *Inorg. Chem.* **2013**, *52*a, 660–670.

(3) Jazdzewski, B. A.; Tolman, W. B. *Coord. Chem. Rev.*, **2000**, *200*, 633-685.

(4) Franks, M. Transition Metal Complexes Containing Phenylthiolate and Phenolate Ligands, University of Nottingham, 2011.

(5) Barondeau, D. P.; Kassman, C. J.; Bruns, C. K.; Tainer, J. A.; Getzoff, E. D. *Protein Sci.*, **2004**, *13*, 192-192.

(6) Neises, B.; Steglich, W. *Angew. Chem., Int. Ed. Engl.*, **1978,** *17*, 522–524

(7) Dawson, J; Perotto, C.; McMaster, J.; Schröder, M.; *Bioinspired Catalysis*, eds. W. Weigand and P. Schollhammer, Wiley-VCH Verlag GmbH & Co., 2014, pp. 79-104.

(8) Volbeda, A.; Charon, M. H.; Piras, C.; Hatchikian, E. C.; Frey, M.; Fontecillacamps, J. C. *Nature*, **1995**, *373*, 580-587.

(9) Volbeda, A.; Fontecilla-Camps, J. C.; *Coord. Chem. Rev.*, **2005**, *249*, 1609-1619.

(10) deLacey, A. L.; Hatchikian, E. C.; Volbeda, A.; Frey, M.; FontecillaCamps, J. C.; Fernandez, V. M. *J. Am. Chem. Soc.*, **1997**, *119*, 7181-7189.

(11) Pierik, A. J.; Roseboom, W.; Happe, R. P.; Bagley, K. A.; Albracht, S. P. J. *J. Biol. Chem.*, **1999**, *274*, 3331-3337.

(12) Ogata, H.; Hirota, S.; Nakahara, A.; Komori, H.; Shibata, N.; Kato, T.; Kano, K.; Higuchi, Y. *Structure*, **2005**, *13*, 1635-1642.

(13) Volbeda, A.; Martin, L.; Cavazza, C.; Matho, M.; Faber, B. W.; Roseboom, W.; Albracht, S. P. J.; Garcin, E.; Rousset M.; Fontecilla-Camps, J. C. *J. Biol. Inorg. Chem.*, **2005**, *10*, 239-249.

(14) Volbeda, A.; Fontecilla-Camps, J. C. *Coord. Chem. Rev.*, **2005**, 249, 1609-1619.

Appendices

Appendix 1: Reagents, Experimental Techniques and Physical Measurements

All reagents purchased from the suppliers (including Aldrich, Acros, Lancaster and Fluka) were used as received. N_2 and Ar were obtained as high-purity gases from BOC gases.

Unless otherwise stated all manipulations, reactions and transfers of samples were conducted under pure Ar or N_2 atmospheres using standard Schlenk techniques. Where required, all solvents were purchased pre-dried stored under Ar or N_2 in Young's ampoules.

Elemental analyses were carried out by the Microanalysis Service at the University of Nottingham (Exeter Analytical Inc. CE-440 Elemental Analyser) or at the London Metropolitan University (Carlo Erba CE1108 Elemental Analyser). NMR spectra were recorded on either a Bruker DPX 300, DPX 400 or AV(III) 400 spectrometer. Mass spectrometric data was recorded by the Mass Spectrometry Service at the University of Nottingham. X-band EPR spectra were recorded on a Bruker EMX spectrometer at the University of Nottingham. The simulations of EPR spectra were performed using the Bruker WINEPR SimFonia package.

Cyclic voltammetric studies were made using an Eco Chemie Autolab PGSTAT20 potentiostat. All solutions were purged with a stream of Ar prior to use. Cyclic voltammetry was performed in a single compartment cell using a three-electrode system; a glassy carbon working electrode, a Pt wire secondary electrode and a saturated calomel reference electrode (SCE). Cyclic voltammetry was carried out in CH_2Cl_2 containing 1 mM of test sample and 0.4 M $[N^nBu_4][BF_4]$ as supporting electrolyte using standard Schlenk techniques under an atmosphere of Ar. All cyclic voltammograms were recorded at a series of scan-rates (ν) (typically ν = 0.02 - 0.3 V s^{-1}) and the potentials of these measurements were referenced to the Fc^+/Fc couple by internal calibration.

Coulometric measurements were performed with a two compartment H-cell in CH_2Cl_2 containing 0.4 M $[N^nBu_4][BF_4]$. The cell consisted of a Pt/Rh gauze basket working electrode which was separated from the Pt/Rh gauze secondary electrode by a glass frit. The SCE reference electrode was sited at the

centre of the working electrode. The working electrode compartment was fitted with a magnetic stirrer bar and the test solution was stirred rapidly during electrolysis.

All UV/vis spectra were recorded on a Perkin Elmer Lambda 16 spectrometer in an optically transparent electrochemical (OTE) cell. Potentials at the working electrode were controlled by a Sycopel Scientific Ltd. DD10M potentiostat. The OTE cell consisted of a modified quartz cuvette (pathlength 0.05 mm) fitted with an optically transparent Rh/Pt gauze working electrode, a Pt wire secondary electrode and a SCE reference electrode. Both reference and secondary electrodes were connected to the cell *via* salt bridge tubes. Experimental temperature was controlled by purging a stream of cooled N_2 gas over the cell surface.

Appendix 2: Single Crystal X-ray Crystallographic Data

Single crystal X-ray diffraction data were collected using three different instruments: (1) Oxford SuperNova CCD area detector diffractometer using graphite-monochromated Cu-*K*α radiation from a sealed X-ray tube source; (2) Beamline I19 of the Diamond Light Source Synchrotron Radiation using a Rigaku Saturn 724+ area detector diffractometer; and (3) Agilent SuperNova diffractometer, Atlas CCD area detector, Cu/Mo microfocus X-ray sources.

Temperatures were regulated with an Oxford Cryosystems openflow cryostat.[1] Empirical absorption corrections were applied using either Gaussian or Multi-scan CrysAlis *PRO*, Agilent Technologies. Structures were solved by direct methods using SHELXT (Sheldrick 2015) and refined with SHELXL (Sheldrick 2015). When necessary crystallographic data was treated using the PLATON program SQUEEZE routine.[2] All cif files were checked using checkCIF.[3]

Computer programs used: CrysAlis PRO 1.171.38.41 (Rigaku OD, 2015),[4] SIR2004 (Burla et al., 2007),[5] Olex2 (Dolomanov et al., 2009).[6]

Appendix 2.1: Crystallographic Data

	[Cu(^{t}BuLO^H)]	**[Cu(^{t}BuLO^{OMe})]**	**[Ni(^{t}BuLO^{OMe})]**
Crystal data			
Identification code	CUFNCC2	CUFNCG	NIFNCF
Chemical formula	$C_{46}H_{65}CuN_5O_2 \cdot 2(CH_3CN)$	$C_{43}H_{61}CuN_3O_3$	$C_{43}H_{61}N_3NiO_3$
M_r	783.57	731.48	726.65
Crystal system, space group	Monoclinic, $P2_1$	Orthorhombic, *Pbca*	Orthorhombic, *Pbca*
Temperature (K)	120	120	120
a, *b*, *c* (Å)	14.3756(2), 9.97895(12), 16.6058(3)	11.59377(17), 25.5747(4), 27.1189(4)	11.5504(3), 25.5904(6), 27.1422(6)
α, β, γ (°)	90, 114.868(2), 90	90, 90, 90	90, 90, 90
V (Å^3)	2161.29(6)	8041.0(2)	8022.7(3)
Z	2	8	8
Radiation type	Cu *K*α	Cu *K*α	Cu *K*α
μ (mm^{-1})	1.029	1.075	1.007
Crystal form, colour	Plate, brown	Plate, brown	Plate, green
Crystal size (mm)	n/a	0.1868 × 0.1398 × 0.0566	0.4452 × 0.161 × 0.0822
Data collection			
Diffractometer	GV1000, Atlas diffractometer	GV1000, Atlas diffractometer	SuperNova, Single source at offset, Atlas diffractometer
Absorption correction	Multi-scan *CrysAlis PRO*, Agilent Technologies, Version 1.171.37.33	Multi-scan *CrysAlis PRO*, Agilent Technologies, Version 1.171.37.33	Multi-scan *CrysAlis PRO*, Agilent Technologies, Version 1.171.37.33
T_{min}, T_{max}	0.903, 1.000	0.889, 1.000	0.861, 1.000
No. of measured, independent and observed [$I > 2\sigma(I)$] reflections	8778, 6128, 5957	20106, 7989, 6521	22248, 8021, 7126
R_{int}	0.023	0.030	0.019
Refinement			
$R[F^2 > 2\sigma(F^2)]$, $wR(F^2)$, *S*	0.030, 0.079, 1.03	0.043, 0.122, 1.05	0.034, 0.091, 1.03
No. of reflections	6128	7989	8021
No. of parameters	532	464	495
No. of restraints	1	0	480
Weighting scheme	$w = 1/[\sigma^2(F_o^2) + (0.0517P)^2 + 0.1150P]$ where $P = (F_o^2 + 2F_c^2)/3$	$w = 1/[\sigma^2(F_o^2) + 0.0682P)^2 + 3.0684P]$ where $P = (F_o^2 + 2F_c^2)/3$	$w = 1/[\sigma^2(F_o^2) + (0.0457P)^2 + 3.7671P]$ where $P = (F_o^2 + 2F_c^2)/3$
$\Delta\rho_{max}$, $\Delta\rho_{min}$ (e Å^{-3})	0.45, -0.23	0.82, -0.47	0.85, -0.40

	[Ni(^{t}BuLo^{OH})]	**[Ni(^{t}BuLo^{Ph})]**	**[Ni(^{t}BuLs^{OH})]**
Crystal data			
Identification code	NIFNCH	NIFNCS	NIFNCL
Chemical formula	$C_{33}H_{48}N_2NiO_3$	$C_{40}H_{52}N_2NiO_4$	$C_{33}H_{48}N_2NiOS_2$
M_r	603.91	683.54	611.56
Crystal system, space group	Triclinic, $P\bar{1}$	Monoclinic, $P2_1/n$	Triclinic, $P\bar{1}$
Temperature (K)	120	293	120
a, *b*, *c* (Å)	11.223(2), 13.452(4), 14.305(3)	15.4297(17), 11.1186(10), 26.024(2)	9.2921(5), 12.2573(8), 14.6054(11)
α, β, γ (°)	111.10(2), 103.240(19), 105.77(2)	90, 97.245(9), 90	96.489(6), 108.538(6), 90.042(5)
V (Å^3)	1806.0(8)	4429.0(8)	1565.90(19)
Z	2	4	2
Radiation type	Cu *K*α	Synchrotron, λ = 0.6889Å	Cu *K*α
μ (mm^{-1})	1.416	0.436	2.343
Crystal form, colour	Plate, brown	Plate, brown	Plate, brown
Crystal size (mm)	0.4873 × 0.1157 × 0.0663	n/a	0.3786 × 0.1721 × 0.0969
Data collection			
Diffractometer	GV1000, Atlas diffractometer	Kappa Rigaku Saturn724+ diffractometer	GV1000, Atlas diffractometer
Absorption correction	Gaussian *CrysAlis PRO*, Agilent Technologies, Version 1.171.37.35	Multi-scan *CrysAlis PRO*, Agilent Technologies, Version 1.171.37.33	Gaussian *CrysAlis PRO*, Agilent Technologies, Version 1.171.37.35
T_{min}, T_{max}	0.857, 0.7965	0.250, 1.000	0.724, 0.895
No. of measured, independent and observed [$I > 2\sigma(I)$] reflections	6144, 4310, 2254	51351, 15046, 4222	13320, 6191, 5345
R_{int}	0.078	0.140	0.043
Refinement			
$R[F^2 > 2\sigma(F^2)]$, $wR(F^2)$, S	0.206, 0.542, 1.68	0.177, 0.534, 1.23	0.112, 0.343, 2.54
No. of reflections	4310	16180	6161
No. of parameters	362	436	374
No. of restraints	432	520	0
Weighting scheme	$w = 1/[\sigma^2(F_o^2) + (0.2000P)^2]$ where $P = (F_o^2 + 2F_c^2)/3$	$w = 1/[\sigma^2(F_o^2) + (0.2000P)^2]$ where $P = (F_o^2 + 2F_c^2)/3$	$w = 1/[\sigma^2(F_o^2) + (0.1000P)^2]$ where $P = (F_o^2 + 2F_c^2)/3$
$\Delta\rho_{max}$, $\Delta\rho_{min}$ (e Å^{-3})	1.91, -0.82	0.62, -0.79	1.99, -1.25

	[Cu(^{t}BuLO^{OH})]	**[Zn(^{t}BuLO^{Br})]**	**[Ni(^{t}BuLO^{Br})]**
Crystal data			
Identification code	CUFNCJ	ZNFNCF	NIFNCD
Chemical formula	$C_{33.81}H_{48}CuN_2O_{3.81}\cdot C_{33.42}H_{48}CuN_2O_{3.42}\cdot 1.54(CH_2Cl_2)\cdot 0.39(CO)$	$C_{48}H_{64}Br_2N_4O_2Zn$	$C_{48}H_{64}Br_2N_4NiO_2$
M_r	1352.44	954.22	947.56
Crystal system, space group	Triclinic, $P\bar{1}$	Orthorhombic, *Fdd2*	Orthorhombic, *Fdd2*
Temperature (K)	120	120	120
a, *b*, *c* (Å)	10.6108(4), 14.5924(3), 24.8559 (8)	33.3678(9), 31.0266(13), 9.0614 (4)	34.1245(14), 32.1790(14), 8.3701 (4)
α, β, γ (°)	89.963 (2), 89.955 (3), 78.879 (2)	90, 90, 90	90, 90, 90
V (Å^3)	3776.33 (19)	9381.2 (6)	9191.1 (7)
Z	2	8	8
Radiation type	Cu *K*α	Cu *K*α	Mo *K*α
μ (mm^{-1})	2.08	3.03	2.96
Crystal form, colour	Plate, green	Plate, yellow	Plate, green
Crystal size (mm)	0.62 × 0.11 × 0.07	0.42 × 0.12 × 0.09	0.26 × 0.08 × 0.04
Data collection			
Diffractometer	GV1000, Atlas diffractometer	GV1000, Atlas diffractometer	GV1000, Atlas diffractometer
Absorption correction	Gaussian *CrysAlis PRO*, Agilent Technologies, Version 1.171.37.35	Gaussian *CrysAlis PRO*, Agilent Technologies, Version 1.171.37.35	Gaussian *CrysAlis PRO*, Agilent Technologies, Version 1.171.36.28
T_{min}, T_{max}	0.922, 0.987	1.026, 1.313	1.024, 1.119
No. of measured, independent and observed [$I > 2\sigma(I)$] reflections	22236, 13251, 10640	265, 3848, 3755	9124, 3650, 3516
R_{int}	0.045	0.029	0.023
Refinement			
$R[F^2 > 2\sigma(F^2)]$, $wR(F^2)$, *S*	0.077, 0.235, 1.07	0.027, 0.063, 1.04	0.024, 0.061, 1.06
No. of reflections	13251	3848	3650
No. of parameters	919	264	264
No. of restraints	1378	1	1
Weighting scheme	$w = 1/[\sigma^2(F_o^2) + (0.1405P)^2 + 3.0275P]$ where $P = (F_o^2 + 2F_c^2)/3$	$w = 1/[\sigma^2(F_o^2) + (0.0236P)^2]$ where $P = (F_o^2 + 2F_c^2)/3$	$w = 1/[\sigma^2(F_o^2) + (0.0343P)^2 + 8.6181P]$ where $P = (F_o^2 + 2F_c^2)/3$
$\Delta\rho_{max}$, $\Delta\rho_{min}$ (e Å^{-3})	1.31, −0.54	0.57, −0.28	0.52, −0.26

	[Cu(^{t}BuLo^{Br})]
Crystal data	
Identification code	CUFNCB
Chemical formula	$C_{48}H_{64}Br_2N_4CuO_2$
M_r	947.56
Crystal system, space group	Orthorhombic, *Fdd2*
Temperature (K)	120
a, *b*, *c* (Å)	34.1234(4), 32.1941(5), 8.38667 (11)
α, β, γ (°)	90, 90, 90
V (Å^3)	2396.2(4)
Z	8
Radiation type	Cu *K*α
μ (mm^{-1})	2.95
Crystal form, colour	Plate, brown
Crystal size (mm)	0.23 × 0.12 × 0.07
Data collection	
Diffractometer	GV1000, Atlas diffractometer
Absorption correction	Gaussian *CrysAlis PRO*, Agilent Technologies, Version 1.171.36.28a
T_{min}, T_{max}	0.998, 1.088
No. of measured, independent and observed [$I > 2\sigma(I)$] reflections	30305, 4657, 4609
R_{int}	0.025
Refinement	
$R[F^2 > 2\sigma(F^2)]$, $wR(F^2)$, S	0.019, 0.053, 1.05
No. of reflections	4657
No. of parameters	264
No. of restraints	1
Weighting scheme	$w = 1/[\sigma^2(F_o^2) + (0.0346P)^2 + 7.2044P]$ where $P = (F_o^2 + 2F_c^2)/3$
$\Delta\rho_{max}$, $\Delta\rho_{min}$ (e Å^{-3})	0.68, -0.65

2.2 References

(1) Cosier, J.; Glaser, A. M. *J. Appl. Crystallogr*., **1986**, 19, 105.

(2) Spek, A. *Acta Crystallogr. Sect. D*, **2009**, 65, 148.

(3) International Union of Crystallography, http://checkcif.iucr.org/.

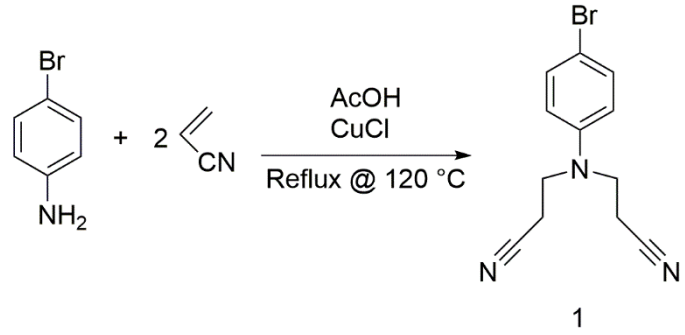
(4) Dolomanov, O.V., Bourhis, L.J., Gildea, R.J, Howard, J.A.K. Puschmann, H., *J. Appl. Cryst*. **2009**, 42, 339.

(5) Burla, M.C.; Caliandro, R.; Camalli, M.; Carrozzini, B.; Cascarano, G.L.; De Caro, L.; Giacovazzo, C.; Polidori, G.; Siliqi, D.; Spagna, R. *J. Appl. Cryst.* **2007**, 40, 609.

(6) Sheldrick, G.M. *Acta Cryst.* 2015, C71, 3.

Appendix 3: Attempted synthesis of the Schiff-base diphenolate ligand [$H_2{}^tBuL_O{}^{Br}$] and [M($^tBuL_O{}^{Br}$)] (M = Zn, Ni, Cu)

A3.1 Attempted synthesis of 3,3'-((4-bromophenyl)azanediyl)-dipropanenitrile



1

Scheme 1 Attempted synthesis of 3,3'-((4-bromophenyl)azanediyl)-dipropanenitrile.

The synthetic methodology for the attempted synthesis of *para*-functionalised 3,3'-((4-bromophenyl)azanediyl)dipropanenitrile (**1**) (Scheme 1) was similar to that employed for the synthesis of 3,3'-(phenylazanediyl)dipropanenitrile (Chapter 2 Section 2.4.1)[1] except for use of 4-bromoaniline instead of aniline. The progress of the reaction was monitored by thin layer chromatography, which showed a mixture of products present after 48 hours of reaction time consistent with the formation of singly and doubly substituted products and confirmed by mass spectrometry.

An increase in the acrylonitrile: 4-bromoaniline ratio to 3:1[1] and longer reaction times did not drive the formation of the target doubly substituted product (**1**), 3,3'-((4-bromophenyl)azanediyl)dipropanenitrile. The singly substituted product (**2**), 3-((4-bromophenyl)amino)propanenitrile (Figure 1) and (**1**) were found consistently in the reaction mixture.

Appendix 3: Attempted synthesis of Schiff-base diphenolate ligand [$H_2{}^tBuL_O{}^{Br}$] and [M($^tBuL_O{}^{Br}$)]

Attempts to purify and isolate 3,3'-((4-bromophenyl)azanediyl)dipropanenitrile (**1**) via column chromatography and by crystallisation of the crude material were unsuccessful. We therefore attempted the reduction of the mixture of nitrile species to their corresponding amines with a view to isolating the mono and di-substituted products following reduction.

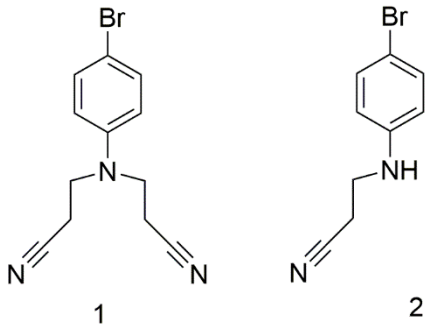
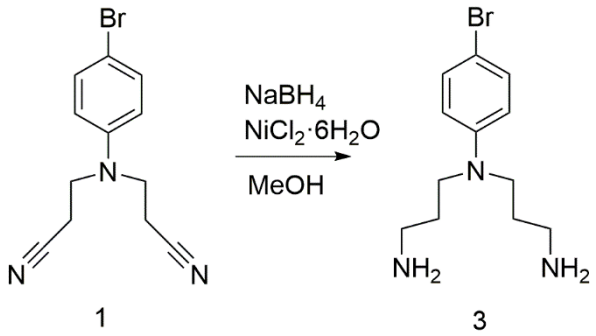


Figure 1 3,3'-((4-bromophenyl)azanediyl)dipropanenitrile (**1**) and 3-((4-bromophenyl)amino)propanenitrile (**2**).

A3.2 Attempted synthesis of N1-(3-aminopropyl)-N1-(4-bromophenyl)propane-1,3-diamine



Scheme 2 Attempted synthesis of N1-(3-aminopropyl)-N1-(4-bromophenyl)propane-1,3-diamine (**3**) from (**1**).

The synthetic methodology for the attempted synthesis of *para*-functionalised N1-(3-aminopropyl)-N1-(4-bromophenyl)propane-1,3-diamine (**3**) (Scheme 2) was similar to that employed for the synthesis of N1-(3-aminopropyl)-N1-phenylpropane-1,3-diamine (Chapter 2 Section 2.4.5)[2] except for use of the crude mixture of 3,3'-((4-bromophenyl)azanediyl)dipropanenitrile (**1**) and 3-((4-bromophenyl)amino)propanenitrile (**2**) instead of 3,3'-(phenylazanediyl)dipropanenitrile as the starting material.[2] The progress of the reaction was followed by thin layer chromatography, which once again showed the presence of two products. This observation is consistent with the formation of the doubly and singly substituted amines: N1-(3-aminopropyl)-N1-(4-bromophenyl)propane-1,3-diamine (**3**) and N1-(4-bromophenyl)propane-1,3-diamine (**4**) (Figure 2). Features that could be assigned to these products could be observed in the ^{1}H-NMR, and ^{13}C-NMR spectra, and mass spectrum of the crude reaction mixture. Attempts to purify and isolate (**3**) and (**4**) by column

chromatography and by crystallisation were unsuccessful. The crude material was taken forward to attempt the syntheses of [$H_2{}^tBuL_O{}^{Br}$] and [M($^tBuL_O{}^{Br}$)] (M = Zn(II), Ni(II), or Cu(II)).

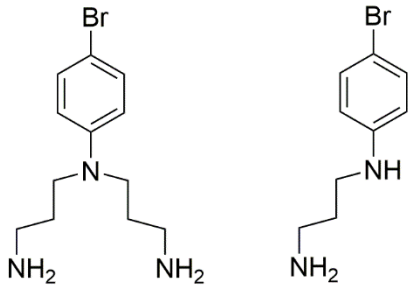
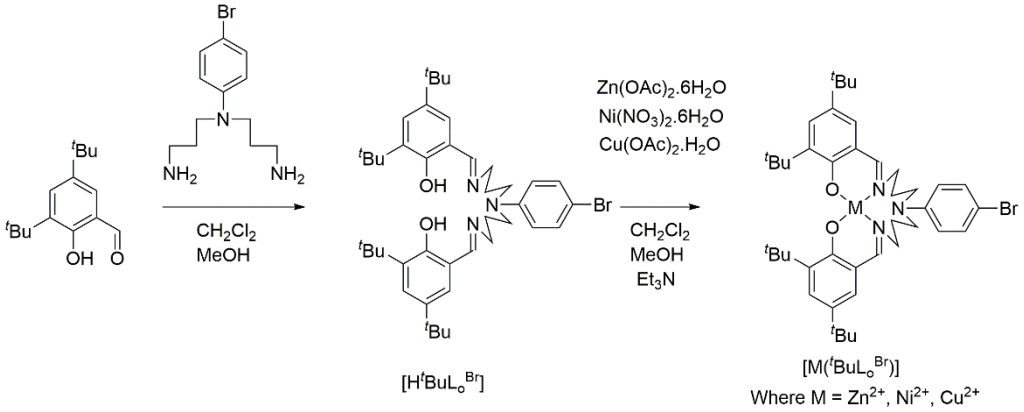


Figure 2 N1-(3-aminopropyl)-N1-(4-bromophenyl)propane-1,3-diamine (**3**) and N1-(4-bromophenyl)propane-1,3-diamine (**4**).

A3.3 Attempted synthesis [$H_2{}^tBuL_O{}^{Br}$] and [M($^tBuL_O{}^{Br}$)] (M = Zn, Ni, Cu)



Scheme 3 Attempted synthesis [$H_2{}^tBuL_O{}^{Br}$] and [M($^tBuL_O{}^{Br}$)] (M = Zn, Ni, Cu)

The synthetic methodology for the attempted synthesis of [$H_2{}^tBuL_O{}^{Br}$] and [M($^tBuL_O{}^{Br}$)] (M = Zn, Ni, Cu) followed the same protocols employed for the attempted syntheses of [$H_2{}^tBuL_O{}^{R}$] and [M($^tBuL_O{}^{Br}$)] (R = H, Cl, ^{t}Bu, OMe) and (M = Zn, Ni, Cu) (Chapter 2, Section 2.4). The attempted synthesis of crude [$H_2{}^tBuL_O{}^{Br}$] led to a mixture of products [$H_2{}^tBuL_O{}^{Br}$] and [$H^tBuL_O{}^{Br1}$] (Figure 3) that could not be separated. This crude mixture was taken forward in attempts for the syntheses of [M($^tBuL_O{}^{Br}$)] (M = Zn, Ni, Cu) via direct metallation. These attempts also led to a crude product mixture that contained a mixture of [M($^tBuL_O{}^{Br}$)] and [M($^tBuL_O{}^{Br1}$)$_2$] (M = Zn, Ni, Cu) (Figure 4), as identified by mass spectrometry. Attempts to separate the two products via column chromatography and by crystallisation were unsuccessful.

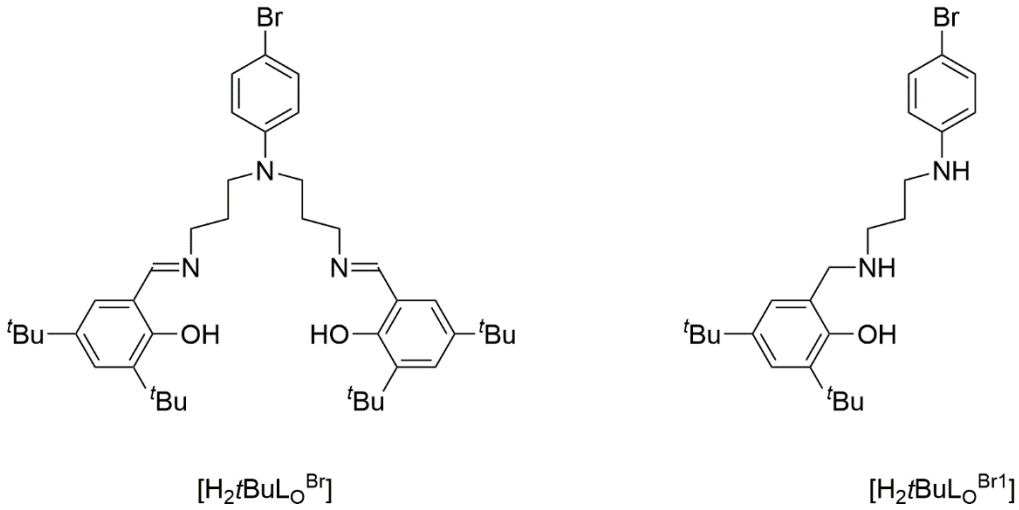


Figure 3 [$H_2{}^tBuL_O{}^{Br1}$] (left) and [$H_2{}^tBuL_O{}^{Br}$] (right) respectively.

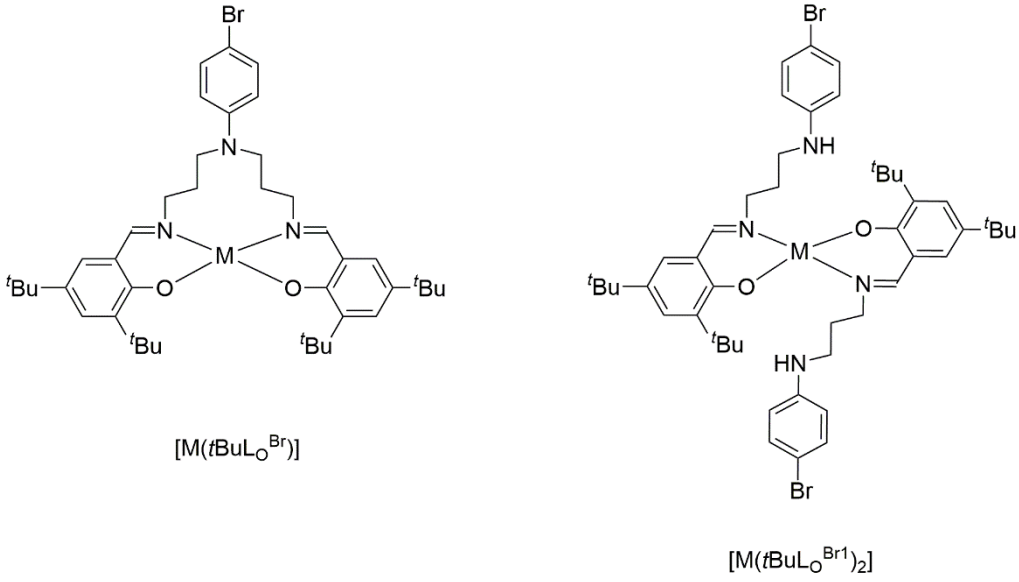


Figure 4 [M($^tBuL_O{}^{Br}$)] (left) and [M($^tBuL_O{}^{Br1}$)$_2$] (right) (M = Zn, Ni, Cu).

A3.4 X-ray Crystallography of [M($^tBuL_O{}^{Br1}$)$_2$] (M = Zn, Ni, Cu)

Crystals of [M($^tBuL_O{}^{Br1}$)$_2$] (M = Zn, Ni, Cu) that were suitable for X-ray crystallography were grown from solutions of the crude reaction products in dichloromethane and methanol (1:10). The structures of [M($^tBuL_O{}^{Br1}$)$_2$] (M =

Zn, Ni, Cu) are shown in Figures 5 - 7 and selected bond distances and angles are shown in Tables 1 – 3.

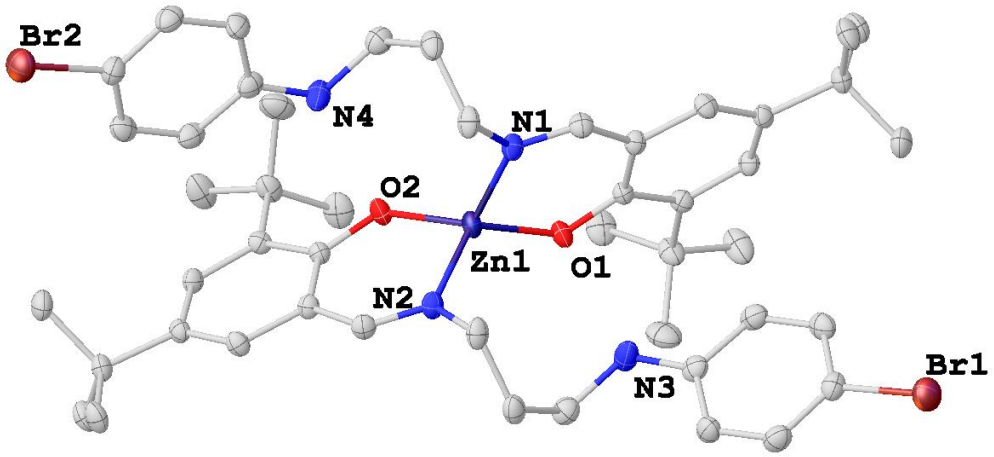


Figure 5 View of the X-ray crystal structure of [Zn($^tBuL_O{}^{Br1}$)$_2$] with H atoms omitted for clarity.

Table 1 Selected bond lengths (Å) and angles (°) with e.s.ds for [Zn($^tBuL_O{}^{Br1}$)$_2$].

[Zn($^tBuL_O{}^{Br1}$)$_2$]	Bond lengths / Å	[Cu($^tBuL_O{}^{H}$)]	Bond angles / °
Zn(1)-N(1)	2.010(3)	N(1)-Zn(1)-N(2)	103.02(15)
Zn(1)-N(2)	2.008(3)	N(1)-Zn(1)-O(1)	96.10(10)
Zn(1)-O(1)	1.916(2)	N(2)-Zn(1)-O(1)	123.71(10)
Zn(1)-O(2)	1.915(2)	N(1)-Zn(1)-O(2)	123.66(10)
N(1)-C(1)	1.374(4)	N(2)-Zn(1)-O(2)	96.10(10)
N(1)-C(3)	1.449(4)	O(1)-Zn(1)-O(2)	115.87(13)
N(2)-C(2)	1.475(4)	-	-
N(2)-C(4)	1.282(4)	-	-
O(1)-C(16)	1.313(4)	-	-
O(2)-C(17)	1.313(4)	-	-

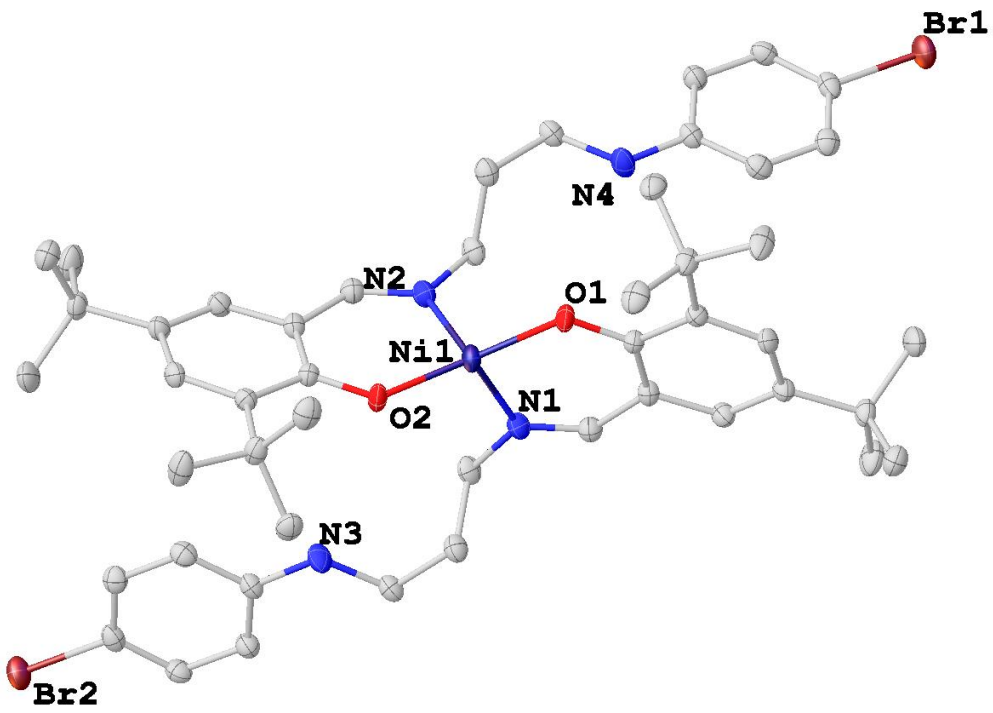


Figure 7 View of the X-ray crystal structure of [Ni($^tBuL_O{}^{Br1}$)$_2$] with H atoms omitted for clarity.

Table 2 Selected bond lengths (Å) and angles (°) with e.s.ds for [Ni($^tBuL_O{}^{Br1}$)$_2$].

[Cu($^tBuL_O{}^{Br1}$)$_2$]	Bond lengths / Å	[Cu($^tBuL_O{}^{H}$)]	Bond angles / °
Ni(1)-N(1)	1.961(3)	N(1)-Ni(1)-N(2)	94.69(16)
Ni(1)-N(2)	1.961(3)	N(1)-Ni(1)-O(1)	93.55(9)
Ni(1)-O(1)	1.908(2)	N(2)-Ni(1)-O(1)	111.66(10)
Ni(1)-O(2)	1.908(2)	N(1)-Ni(1)-O(2)	111.66(10)
N(1)-C(1)	1.292(4)	N(2)-Ni(1)-O(2)	93.55(9)
N(1)-C(3)	1.468(4)	O(1)-Ni(1)-O(2)	142.91(14)
N(2)-C(2)	1.447(4)	-	-
N(2)-C(4)	1.379(4)	-	-
O(1)-C(16)	1.323(3)	-	-
O(2)-C(17)	1.323(3)	-	-

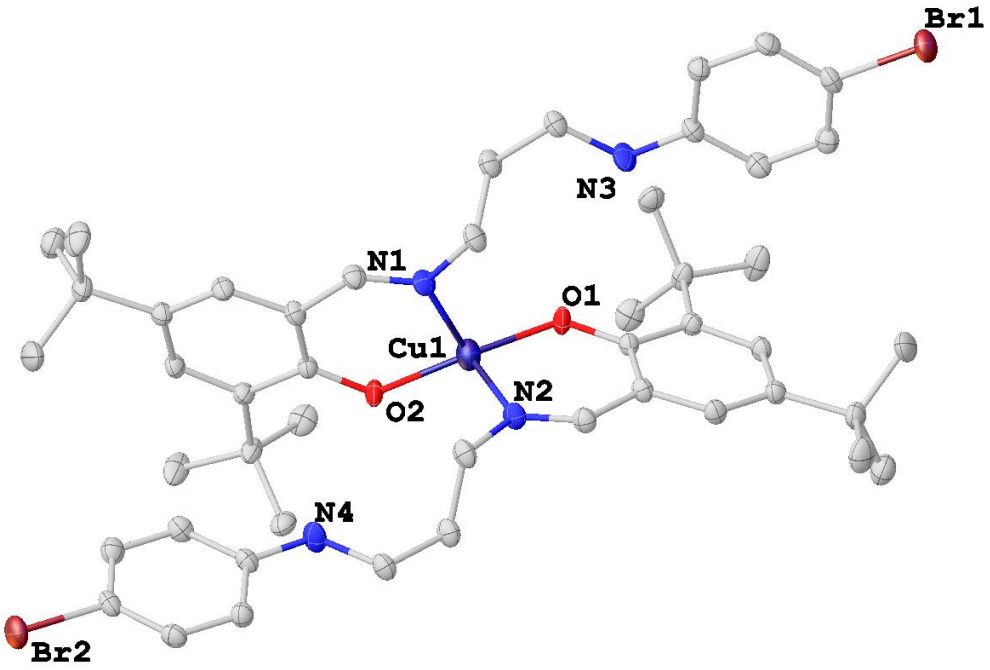


Figure 7 View of the X-ray crystal structure of [Cu(^{t}BuL$_O$^{Br1})$_2$] with H atoms omitted for clarity.

Table 3 Selected bond lengths (Å) and angles (°) with e.s.ds for [Cu(^{t}BuL$_O$^{Br1})$_2$].

[Cu(^{t}BuL$_O$^{Br1})$_2$]	Bond lengths / Å	[Cu(^{t}BuL$_O$^{H})]	Bond angles / °
Cu(1)-N(1)	1.967(4)	N(1)-Cu(1)-N(2)	94.9(2)
Cu(1)-N(2)	1.967(4)	N(1)-Cu(1)-O(1)	93.25(15)
Cu(1)-O(1)	1.912(3)	N(2)-Cu(1)-O(1)	111.82(15)
Cu(1)-O(2)	1.912(3)	N(1)-Cu(1)-O(2)	111.82(15)
N(1)-C(1)	1.285(6)	N(2)-Cu(1)-O(2)	93.25(15)
N(1)-C(3)	1.404(6)	O(1)-Cu(1)-O(2)	143.1(2)
N(2)-C(2)	1.448(6)	-	-
N(2)-C(4)	1.408(6)	-	-
O(1)-C(16)	1.312(5)	-	-
O(2)-C(17)	1.312(5)	-	-

[M($^tBuL_O{}^{Br1}$)$_2$] (M = Zn, Ni, Cu) each contain a four-coordinate monomeric M(II) centre bound by a N_2O_2 ligand set derived from two phenolate O-donors and two imine N-donors. The M(II)-O(phenolate) (*ca.* 1.96 – 2.00 Å) and M(II)-N(imine) (*ca.* 1.96 – 2.00 Å) bond distances are comparable to those in [Cu($^tBuL_O{}^{H}$)], [Cu($^tBuL_O{}^{OMe}$)] and [Ni($^tBuL_O{}^{OMe}$)] synthesised in Chapter 2

The bond angles (Table 1 - 3) show that [M($^tBuL_O{}^{Br1}$)$_2$] (M = Zn, Ni, Cu) adopt approximate tetrahedral coordination geometries, in which the dihedral angles between the planes defined by N(1)-M(1)-N(2) and O(1)-M(1)-O(2) are 77.78 º, 85.91 º and 85.90 º, respectively.

A3.5 Experimental

A3.5.1 Attempted synthesis of 3,3'-((4-bromophenyl)azanediyl)-dipropanenitrile

Aniline (17.90 g, 0.10 mol) was added to a solution of CuCl (1.00 g, 0.01 mol) in glacial acetic acid (20.0 ml) after which acrylonitrile (20.0 ml, 3.10 mol) was added to the reaction mixture drop-wise over a period of 10 mins. The solution was then heated to reflux at 120 °C for 24 h. After cooling to room temperature the reaction mixture was extracted with CH_2Cl_2 (2 x 100 ml), the organic phase was washed with 2 M NaOH (2 x 75.0 ml) and dried over $MgSO_4$. The mixture was filtered and the solvent removed *in vacuo.* The crude product was re-crystallised twice from hot ethanol to give crystalline solid.

Crude yield = 18 % based on using 17.90 g bromoaniline, to give a brown crystalline solid (4.95 g, 1.7 mmol, 18 %). MS (ES+, m/z): 278.0215 [M+H] and 224.9949 [M+H].

A3.5.2 Attempted synthesis of N1-(3-aminopropyl)-N1-(4-bromophenyl)propane-1,3-diamine

To a solution of crude 3,3'-((4-bromophenyl)azanediyl)dipropanenitrile (0.50 g, 1.80 mmol) in anhydrous methanol (100 ml), $NiCl_2{\cdot}6H_2O$ (0.48 g, 0.20 mmol) was added. $NaBH_4$ (0.53 g, 14.0 mmol) was added in small portions to the reaction mixture over a period of 30 min. After the addition was complete the reaction mixture was stirred for 48 h at room temperature. After this time diethylenetriamine (1.00 ml, 8.72 mmol) was added to the reaction mixture. The mixture was stirred for a further 30 min and the solvent removed *in vacuo.* The resulting residue was dissolved in EtOAc and washed with a saturated $NaHCO_3$

solution (2 x 50.0 ml). The mixture was then dried with $MgSO_4$ and the solvent removed *in vacuo* to give a brown oil.

Crude yield = 68 % based on using 0.50 g of 3,3'-(4-bromophenylazanediyl)dipropanenitrile, to give a brown oil (0.17 g, 0.33 mmol, 68 %). 285.0841 [M+H] and 229.0262 [M+H].

A3.5.3 Attempted synthesis [$H_2{}^tBuL_O{}^{Br}$] and [M($^tBuL_O{}^{Br}$)] (M = Zn, Ni, Cu)

A solution of crude N1-(3-aminopropyl)-N1-(4-bromophenyl)propane-1,3-diamine (1.50 g, 5.26 mmol) in CH_2Cl_2 (25.0 ml) was added drop-wise to a solution of 3,5-di-*tert*-butyl-2-hydroxybenzaldehyde (2.46 g, 10.52 mmol) in CH_2Cl_2 (25.0 ml). The reaction mixture was stirred at room temperature for 2 h. The solvent was removed *in vacuo* to give a yellow oil which was used without further purification.

Crude yield = 68 % based on using 0.50 g of 3,3'-(4-bromophenylazanediyl)dipropanenitrile, to give a brown oil (0.17 g, 0.33 mmol, 68 %). 285.0841 [M+H] and 229.0262 [M+H].

A3.5.4 Attempted synthesis [Zn($^tBuL_O{}^{Br}$)]

Typical procedure: $Zn(OAc)_2{\cdot}2H_2O$ (0.17 g, 0.78 mmol) in methanol (3.00 ml) was added drop-wise to a solution of crude [$H^tBuL_O{}^{Br}$] (0.56 g, 0.78 mmol) in CH_2Cl_2 (20.0 ml). The mixture was left to stir for 5 min before Et_3N (0.11 ml, 0.78 mmol) was added. After this time the reaction mixture was left to stir for 24 h at reflux. The volume of the solvent was then reduced to *ca.* 5 ml *in vacuo* and a yellow solid was precipitated following the addition of hexane (30 ml) and collected by filtration.

The mass spectrum of the crude product possesses features that may be assigned to the desired product. However, attempts to purify the product in bulk were unsuccessful. MS (ES+, m/z): 780.3004 [M+H] and 951.2687 [M+H].

A3.5.5 Attempted synthesis of [Ni(^{t}BuL$_O{}^{Br}$)]

[Ni(^{t}BuL$_O{}^{Br}$)] was prepared using the general procedure above from crude [H^{t}BuL$_O{}^{Br}$] (0.56 g, 0.78 mmol). The mass spectrum of the crude product possesses features that may be assigned to the desired product. However, attempts to purify the product in bulk were unsuccessful. MS (ES+, m/z): 774.3006 [M+H] and 945.2750 [M+H].

A3.5.6 Attempted synthesis of [Cu(^{t}BuL$_O{}^{Br}$)]

[Cu(^{t}BuL$_O{}^{Br}$)] was prepared using the general procedure above from crude [H^{t}BuL$_O{}^{Br}$] (0.56 g, 0.78 mmol). The mass spectrum of the crude product possesses features that may be assigned to the desired product. However, attempts to purify the product in bulk were unsuccessful. MS (ES+, m/z): 779.3008 [M+H] and 950.2692 [M+H].

A3.6 References

(1) Pittelkow, M.; Nielsen, C. B.; Kadziola, A.; Christensen, J. B. *J. Incl. Phenom. Macrocycl. Chem.* **2008**, *63*, 257–266.

(2) Caddick, S.; Judd, D. B.; Lewis, A. K. d. K.; Reich, M. T.; Williams, M. R. . *Tetrahedron* **2003**, *59*, 5417–5423.